

Univerza  
v Ljubljani

Fakulteta  
*za gradbeništvo  
in geodezijo*



Jamova cesta 2  
1000 Ljubljana, Slovenija  
<http://www3.fgg.uni-lj.si/>

**DRUGG** – Digitalni repozitorij UL FGG  
<http://drugg.fgg.uni-lj.si/>

To je izvirna različica zaključnega dela.

Prosimo, da se pri navajanju sklicujete na bibliografske podatke, kot je navedeno:

Oset, U. 2012. Laboratorijsko testiranje prelivanja valov čez valobrane v pristaniščih. Diplomaska naloga. Ljubljana, Univerza v Ljubljani, Fakulteta za gradbeništvo in geodezijo. (mentor Četina, M., somentor Cappietti, L.): 157 str.

University  
of Ljubljana

Faculty of  
*Civil and Geodetic  
Engineering*



Jamova cesta 2  
SI – 1000 Ljubljana, Slovenia  
<http://www3.fgg.uni-lj.si/en/>

**DRUGG** – The Digital Repository  
<http://drugg.fgg.uni-lj.si/>

This is original version of final thesis.

When citing, please refer to the publisher's bibliographic information as follows:

Oset, U. 2012. Laboratorijsko testiranje prelivanja valov čez valobrane v pristaniščih. B.Sc. Thesis. Ljubljana, University of Ljubljana, Faculty of civil and geodetic engineering. (supervisor Četina, M., co-supervisor Cappietti, L.): 157 pp.

Univerza  
v Ljubljani

Fakulteta za  
*gradbeništvo in  
geodezijo*



Jamova 2  
1000 Ljubljana, Slovenija  
telefon (01) 47 68 500  
faks (01) 42 50 681  
fgg@fgg.uni-lj.si

UNIVERZITETNI ŠTUDIJ  
GRADBENIŠTVA  
HIDROTEHNIČNA SMER

Kandidatka:

**URŠKA OSET**

**LABORATORIJSKO TESTIRANJE PRELIVANJA  
VALOV ČEZ VALOBRANE V PRISTANIŠČIH**

Diplomska naloga št.: 3251/HS

**LABORATORY EXPERIMENTS ON WAVE  
OVERTOPPING AT HARBOUR BREAKWATERS**

Graduation thesis No.: 3251/HS

**Mentor:**

prof. dr. Matjaž Četina

**Predsednik komisije:**

izr. prof. dr. Janko Logar

**Somentor:**

prof. dr. Lorenzo Cappiatti

**Člani komisije:**

prof. dr. Bogdan Zgonc

Ljubljana, 27. 09. 2012

## **ERRATA, STRAN ZA POPRAVKE**

<b>Page</b>	<b>Line</b>	<b>Error</b>	<b>Correction</b>
-------------	-------------	--------------	-------------------

---



## BIBLIOGRAPHIC-DOCUMENTALISTIC INFORMATION AND ABSTRACT

**UDK:** 627.223.6:627.235(043.2)  
**Author:** Urška Oset  
**Supervisor:** prof. Matjaž Četina, Ph.D  
**Co-advisor:** prof. Lorenzo Cappiotti, Ph.D  
**Document type:** Graduation Thesis – University studies  
**Title:** Laboratory experiments on wave overtopping at harbour breakwaters  
**Notes:** 157 pg., 53 tab., 75 fig., 32 graph., 9 att., 114 eq.  
**Key words:** wave overtopping, wave-by-wave overtopping volume, wave pressure, breakwater, wavewall, Matlab

### Abstract

Each year in Italy approximately 2-5 people are killed due to wave action on wave wall and similar constructions. Wave overtopping occurs because of wave running up the face of a wave wall and is affected by many factors. Small modification of geometry of the structure may drastically change the amount of overtopping. Generally, most of the overtopping waves are fairly small, but a small number can give significantly larger wave-by-wave overtopping volumes. More accurate estimation of overtopping rates should be determined by hydraulic model tests. This thesis is part of the international ERASMUS exchange between University of Ljubljana and University of Florence aimed to study the process of wave overtopping and wave pressure of impact at harbour breakwater models in the wave flume. This research gives an overview of the main topic wave overtopping discharges, for a large number of wave and design conditions. Due to this fact two level analysis was deployed. I. level analysis estimated whether working of measuring instruments was properly and investigated the wave performance, by calculating its characteristic parameters, wave-by-wave overtopping volumes and pressure stresses. Furthermore, II. level analysis made a comparison between mean overtopping discharges and maximum wave-by-wave overtopping volumes and continued by analysing maximum pressures of impact and reflection parameters for each wave attack and design of construction. The analysis and results were obtained by Matlab program. After eight wave types were executed on six different model constructions the most effective harbour breakwater was assessed.

**BIBLIOGRAFSKO-DOKUMENTACIJSKA STRAN IN IZVLEČEK**

<b>UDK:</b>	<b>627.223.6:627.235(043.2)</b>
<b>Avtor:</b>	<b>Urška Oset</b>
<b>Mentor:</b>	<b>prof. dr. Matjaž Četina</b>
<b>Somentor:</b>	<b>prof. dr. Lorenzo Cappietti</b>
<b>Naslov:</b>	<b>Laboratorijsko testiranje prelivanja valov čez valobrane v pristaniščih</b>
<b>Tip dokumenta:</b>	<b>Diplomska naloga – univerzitetni študij</b>
<b>Obseg in oprema:</b>	<b>157 str., 53 pregl., 75 sl., 32 graf., 9 pril., 114 en.</b>
<b>Ključne besede:</b>	<b>prelivanje valov, volumen posameznega pljuska, valovni tlaki, valobran, vgrajena betonska stena v valobranu, Matlab</b>

**Izvelek**

Pojav prelivanja valov preko valobranov v pristaniščih predstavlja enega izmed glavnih vzrokov pri povzročanju škode na privezanih plovilih v pristaniščih. Vsako leto v Italiji umre približno 2 do 5 ljudi zaradi nevarnih prelivanj valov čez stene valobranov in druge konstrukcije. Proces prelivanja valov je odvisen od številnih dejavnikov in že majhne spremembe geometrije konstrukcije močno spremenijo obnašanje in količino prelitih valov. V splošnem je količina prelitih valov majhna, nekaj valov pa lahko povzroči izdatnejše prelive. Laboratorijski eksperimenti na fizičnem hidravličnem modelu so nujno potrebni za natančnejšo oceno obnašanja prelivajočih se valov, saj je proces slučajen. Ta diplomska naloga je bila narejena v sodelovanju med Univerzo v Ljubljani in Univerzo v Firencah v okviru mednarodne študijske izmenjave ERASMUS, z namenom preučevanja procesa prelivanja in tlakov valov na hidravličnem modelu pristaniškega valobrana. S preizkušanjem velikega števila valovnih in geometrijskih pogojev smo dobili širok pregled nad obnašanjem prelivanja valov. V ta namen smo razvili dvostopenjsko analizo. Z analizo I. stopnje smo ocenili ali so merilni instrumenti delovali pravilno in izračunali karakteristike valov, velikost pljuskov in tlakov. V drugostopenjski analizi pa smo primerjali rezultate med srednjimi pretoki prelivanja in maksimalnimi volumni pljuskov, nato pa analizirali še maksimalne tlake in odboj valov na vgrajeno steno za posamezen tip konstrukcije in valovanja. Obdelava podatkov iz meritev na hidravličnem modelu se je izvedla s pomočjo računalniškega programa Matlab. Po testiranju šestih različnih konstrukcij modela valobrana z osmimi nevihtnimi stanji morja smo določili najvarnejšo konstrukcijo valobrana.

## ACKNOWLEDGEMENT

First of all, I would like to thank prof. dr. Lorenzo Cappiotti for being a great advisor. Thanks for all the help and guidance in the time I was writing my thesis. I learned a lot while being in your company in Florence. Thanks also to prof. dr. Pier Luigi Aminti for giving me the chance to listen lectures, visit some interesting conferences and get to know Italian coast and ports better.

Iskreno hvala prof. dr. Matjažu Četini za mentorstvo in vse koristne informacije pri nastajanju te diplomske naloge. Hvala tudi prof. dr. Rudiju Rajarju za svetovanje in zaključni pregled te naloge.

Posebna hvala moji družini za zaupanje in podporo tekom celega študijskega obdobja.

Grazie di cuore a Francesco, con il tuo supporto così forte non mi hai mai fatto sentire che delle volte siamo così distanti.

Un ringraziamento speciale va anche ad Andrea e Deniz per l'aiuto, l'amicizia e la voglia di trascorrere le serate in laboratorio a risolvere problemi di ogni tipo.

Hvala tudi podjetju DRI upravljanje investicij d.o.o., ki me je v letih študija s kadrovske štipendije finančno podprl.

Na koncu en velik hvala vsem študijskim kolegom in prijateljem, z vami so vse študijske ure in izpiti postali veliko lažje premagljivi.

## **IZJAVA O AVTORSTVU, STATEMENTS**

Skladno s 27. členom Pravilnika o diplomskem delu UL Fakultete za gradbeništvo in geodezijo,

podpisana Urška Oset izjavljam, da sem avtorica diplomske naloge z naslovom: »Laboratorijsko testiranje prelivanja valov čez valobrane v pristaniščih«.

Izjavljam, da prenašam vse materialne avtorske pravice v zvezi z diplomsko nalogo na UL, Fakulteto za gradbeništvo in geodezijo.

Noben del tega zaključnega dela ni bil uporabljen za pridobitev strokovnega naziva ali druge strokovne kvalifikacije na tej ali na drugi univerzi ali izobraževalni inštituciji.

## **STATEMENTS**

I, the undersigned Urška Oset, hereby declare that I am the author of graduation thesis entitled: »Laboratory experiments on wave overtopping at harbour breakwaters«.

I declare that electronic version is exactly the same as printed version.

I declare that I allow the publication of the electronic version of my graduation thesis in the repository of UL FGG.

Ljubljana, 10. 09. 2012

---

(podpis kandidatke/signature)

## TABLE OF CONTENTS

<b>ERRATA, STRAN ZA POPRAVKE .....</b>	<b>I</b>
<b>BIBLIOGRAPHIC-DOCUMENTALISTIC INFORMATION AND ABSTRACT .....</b>	<b>III</b>
<b>BIBLIOGRAFSKO-DOKUMENTACIJSKA STRAN IN IZVLEČEK .....</b>	<b>IV</b>
<b>ACKNOWLEDGEMENT .....</b>	<b>III</b>
<b>IZJAVA O AVTORSTVU, STATEMENTS .....</b>	<b>VI</b>
<b>TABLE OF CONTENTS.....</b>	<b>XIII</b>
<b>LIST OF TABLES .....</b>	<b>XIII</b>
<b>LIST OF FIGURES .....</b>	<b>XV</b>
<b>LIST OF GRAPHS .....</b>	<b>XVII</b>
<b>ABBREVIATIONS AND SYMBOLS .....</b>	<b>XVIII</b>
<b>1 INTRODUCTION.....</b>	<b>1</b>
<b>2 THEORETICAL BACKGROUNDS.....</b>	<b>3</b>
2.1 Basic definition of wave and wave parameters .....	3
2.1.1 Monochromatic waves .....	3
2.1.1.1 Linear wave theory.....	4
2.1.2 Irregular (random) waves .....	5
2.1.2.1 Observation techniques .....	6
2.2 Types of the waves.....	7
2.2.1 Types of scales .....	9
2.3 Standard techniques for defining random waves .....	10
2.3.1 Zero-crossing method.....	10
2.3.2 Wave height distribution .....	11
2.3.2.1 Relations between representative wave heights .....	12
2.3.3 Distribution of wave period.....	13
2.3.4 Wave spectrum.....	14
2.3.4.1 Introduction .....	14
2.3.5 Random – phase/amplitude model (RPAM) .....	15
2.3.6 The variance density spectrum.....	17
2.3.6.1 Interpretation of the variance density spectrum .....	17

2.3.6.2 Relationship between wave spectra and wave heights .....	18
2.3.6.3 Relationship between wave spectra and wave periods .....	19
2.3.7 Analytical parametric frequency spectra functions .....	20
2.4 Harbour hydrodynamics .....	21
2.4.1 Definition of harbour .....	21
2.4.2 Wave transmission, reflection and breaking waves.....	23
2.4.2.1 Wave transmission.....	23
2.4.2.2 Wave reflection.....	23
2.5 Breakwaters .....	25
2.5.1 Rubble mound breakwaters .....	27
2.5.1.1 Cross section design .....	27
2.5.2 Construction materials.....	28
2.5.2.1 Rock and concrete armour.....	28
2.5.2.1.1 Armour unit density.....	30
2.5.2.2 Primary armour layer.....	30
2.5.2.3 Breakwater crest .....	31
2.6 Overtopping.....	32
2.6.1 Introduction of the phenomena.....	32
2.6.2 Overtopping parameters .....	34
2.6.2.1 The wave height.....	34
2.6.2.2 The wave period .....	34
2.6.2.3 Permeability, porosity and roughness.....	34
2.6.2.4 Toe of structure.....	35
2.6.2.5 The foreshore.....	36
2.6.2.6 Slope.....	36
2.6.2.7 Berm .....	36
2.6.2.8 Crest freeboard and armour freeboard and width .....	37
2.6.3 Wave overtopping discharge .....	37
2.6.4 Wave overtopping volumes .....	38
2.6.5 Tolerable discharges .....	38
2.6.5.1 Wave overtopping processes and hazards .....	39
2.6.5.2 Return periods of overtopping hazards.....	39
2.6.5.3 Tolerable mean discharges of overtopping.....	40

2.6.6 Prediction of overtopping.....	42
2.6.6.1 Analytical models.....	43
2.6.6.2 Wave-by-wave overtopping volumes.....	46
2.6.6.2.1 Wave run-up and number of overtopping waves .....	46
2.6.6.2.2 Wave-by-wave overtopping volume and $V_{\max}$ .....	48
<b>3 PHYSICAL MODEL .....</b>	<b>50</b>
3.1 Overview of hydraulic physical models.....	50
3.1.1 What is a physical model?.....	50
3.1.2 Types of physical models.....	50
3.1.3 Advantages and disadvantages of physical models.....	53
3.2 Scaling requirements (for short-wave models) .....	54
3.2.1 Scaling laws.....	54
3.2.1.1 Scaling laws for rubble mound breakwaters .....	57
3.2.1.2 Permeability scaling .....	57
3.2.1.3 Relative densities.....	58
3.2.1.4 Stability scaling.....	58
3.2.1.5 Wave overtopping .....	59
3.2.1.6 Modelling limits .....	59
3.3 Scale effects in laboratory .....	59
3.3.1 Wave reflection .....	60
3.3.2 Wave separation, wave transmission.....	60
3.3.3 Wave breaking.....	60
3.4 Model set-up and model operation.....	60
3.4.1 Layout of model .....	60
3.4.2 Bathymetry (fixed bed) .....	61
3.4.3 Structure .....	61
3.4.3.1 Crown walls.....	61
3.4.4 Waves condition.....	62
3.4.4.1 Long and short crested waves .....	62
3.5 Used materials.....	62
3.6 Measurement equipment and measurement procedure .....	63
3.6.1 Instrumentation.....	63

3.6.2 Assessment techniques .....	63
3.7 Analysis procedures.....	65
3.7.1 Data handling.....	65
3.7.2 Removal of spurious data .....	65
3.7.3 Damage assessment .....	66
3.7.4 Overtopping and wave transmission.....	66
<b>4 LABORATORY TESTING PROCEDURES .....</b>	<b>67</b>
4.1 Introduction and Motivations .....	67
4.1.1 Main objectives.....	67
4.2 Laboratory description.....	67
4.2.1 Wave flume .....	68
4.2.2 Wave generator.....	69
4.2.3 Recirculation pump.....	70
4.2.4 Back paddle pump .....	70
4.2.5 Wave flume refilling pump.....	71
4.3 Used instruments .....	71
4.3.1 Wave gauges (WG) .....	71
4.3.2 Load cells.....	73
4.3.3 Pressure transducers .....	74
4.3.4 Hydrometric tip at nonius .....	75
4.3.5 Overtopping tank .....	76
4.3.6 Photo, video.....	76
4.4 Scaling requirements .....	78
4.4.1 Froude similarity.....	78
4.4.2 Dimensioning breakwater layers .....	78
4.4.2.1 Selection parameters.....	79
4.4.2.2 Recommended scaling procedure of core material in rubble mound breakwater model test.....	82
4.4.3 Used materials .....	86
4.4.3.1 Armour layer.....	86
4.4.3.2 Filter layer .....	88
4.4.3.3 Core .....	90

4.4.3.4	Overspill basin (OB) .....	92
4.4.3.5	Wave wall.....	93
4.5	Harbour breakwater design and construction.....	93
4.5.1	Slope angle.....	94
4.5.2	Layer thickness.....	94
4.5.3	Configuration of cross sections .....	94
4.6	Water levels and wave conditions.....	99
4.6.1	Water levels.....	99
4.6.2	Wave conditions.....	99
4.6.2.1	Preliminary tests.....	100
4.7	Instrument placement.....	102
4.8	Test conditions .....	103
4.8.1	Definition of wave attacks.....	103
4.8.2	Test methodology.....	104
4.8.3	Test nomenclature .....	104
<b>5</b>	<b>ANALYSIS AND RESULTS.....</b>	<b>106</b>
5.1	Analysis structure.....	106
5.2	I. level analysis.....	108
5.2.1	Calibration procedure.....	109
5.2.2	Wave gauges registration .....	110
5.2.2.1	Time level series.....	110
5.2.2.2	Amplitude spectrum .....	111
5.2.2.3	Wave heights zero crossing distribution .....	112
5.2.2.4	Reflection analysis .....	113
5.2.2.5	Wave characteristic parameters.....	114
5.2.3	Wave overtopping analysis .....	115
5.2.4	Wave pressure of impact .....	117
5.2.5	Effective and target values of wave parameters.....	119
5.2.6	Problems at I. level analysis.....	120
5.3	II. Level analysis .....	120
5.3.1	Overtopping analysis.....	121
5.3.1.1	Mean overtopping discharges.....	123

5.3.1.2 Maximum overtopping discharge .....	126
5.3.2 Maximum wave pressure of impact.....	127
5.3.3 Reflection analysis.....	134
<b>6 CONCLUSIONS.....</b>	<b>137</b>
<b>7 SLOVENSKI POVZETEK.....</b>	<b>140</b>
<b>BIBLIOGRAPHY.....</b>	<b>155</b>
<b>APPENDIX</b>	

## LIST OF TABLES

Table 1: Classification of water waves based on the relative depth criterion $d/L$ .....	5
Table 2: Published damage coefficients $K_D$ .....	28
Table 3: Damage coefficients concrete units, zero damage .....	29
Table 4: Van der Meer's coefficients .....	30
Table 5: Shape factor and porosity .....	30
Table 6: Shape factor and porosity .....	31
Table 7: Hazard type .....	40
Table 8: Limits for overtopping for pedestrians .....	40
Table 9: Limits for overtopping for vehicle .....	41
Table 10: Limits for overtopping for property behind the defence .....	41
Table 11: Typically used scaling relationships .....	57
Table 12 : Correspondence between WG and channel.....	73
Table 13: Scales used for reducing the model.....	78
Table 14: Average of $\rho_s$ for all rocks.....	81
Table 15: Prototype data of the model.....	82
Table 16: Vertical distances from MWL.....	83
Table 17: Characteristic pore velocity in the prototype .....	84
Table 18: Results from iterative method to obtain the characteristic core diameter .....	86
Table 19: Calculations for granulometric analysis - Armour Layer.....	87
Table 20: Characteristic parameters determined by granulometric analysis - Armour layer...	87
Table 21: Calculations for granulometric analysis - Filter Layer.....	89
Table 22: Characteristic parameters determined by granulometric analysis – Filter layer .....	89
Table 23: Calculations for granulometric analysis – Core .....	91
Table 24: Characteristic parameters determined by granulometric analysis – Core.....	91
Table 25: Layer thickness in the model.....	94
Table 26: Cross section heights at all configurations.....	95
Table 27: Water levels in the wave flume at back blade pump on or off.....	99
Table 28: Assumed and generated parameters of preliminary wave attacks.....	101
Table 29: Assumed wave attacks for definitive tests .....	102
Table 30: Distances of single tools from the wave maker.....	102
Table 31: Definition of wave attacks.....	103
Table 32: Analysis procedure .....	106
Table 33: Scheme of wave attacks performed in laboratory from 03.04. – 02.05.2012 .....	108
Table 34: Calibration parameters for each wave gauge [cm] = [Volt] A + B .....	109
Table 35: Reflection coefficients analysis according to Goda and Suzuki .....	113
Table 36: Characteristic wave parameters for wave attack H1T105G2CF1C3 .....	114
Table 37: Accumulated overtopping volume for H1T105G2F1C3 .....	116
Table 38: Overtopping discharges with mean values measured directly from o.tank.....	116
Table 39: Effective values of $H_{m0}$ and $T_p$ for configurations C0, C1 and C3 .....	119
Table 40: Effective values of $H_{m0}$ and $T_p$ for configurations C4, C5 and C6 .....	120
Table 41: Mean overtopping discharges $q_m$ .....	123
Table 42: Mean wave-by-wave overtopping volumes calculated by Matlab program .....	124
Table 43: Max wave-by-wave overtopping volume calculated by Matlab program.....	126
Table 44: Maximum pressures for each wave attack at all configurations .....	128

Table 45: Maximum pressure values for wave attack H1T085G2F1 .....	129
Table 46: Maximum pressure values for wave attack H1T085G5F1 .....	129
Table 47: Maximum pressure values for wave attack H1T105G2F1 .....	130
Table 48: Maximum pressure values for wave attack H1T105G5F1 .....	131
Table 49: Maximum pressure values for wave attack H1T125G2F1 .....	131
Table 50: Maximum pressure values for wave attack H1T125G5F1 .....	132
Table 51: Maximum pressure values for wave attack H2T115G2F1 .....	133
Table 52: Maximum pressure values for wave attack H2T115G5F1 .....	133
Table 53: Results from reflection analysis.....	134

## LIST OF FIGURES

Figure 1: Violent wave overtopping .....	1
Figure 2: Definition of terms of the wave. ....	3
Figure 3: Water particle displacements from mean position in deep water. ....	5
Figure 4: A bird's eye view of ocean waves .....	6
Figure 5: Left: The WAVERIDER buoy at sea.....	7
Figure 6: Frequencies and periods of the vertical motions of the ocean surface.....	9
Figure 7: The definition of wave parameters for a random sea state. ....	10
Figure 8: Left: Example of a histogram of wave heights. Right: Normalized histogram .....	12
Figure 9: The relationship between estimated significant wave height and period.....	14
Figure 10: The observed surface elevation and its amplitude and phase spectrum.....	15
Figure 11: The summation of many harmonic waves. ....	16
Figure 12: The RPAM .....	16
Figure 13: The transformation of the discrete amplitude spectrum of the RPAM .....	17
Figure 14: The (ir)regular character of the waves for three different widths of the spectrum .	18
Figure 15: Comparison of the PM and JONSWAP spectrum .....	21
Figure 16: Harbour of Rotterdam .....	22
Figure 17: Harbour sitting classifications.....	22
Figure 18: Parameters involved in wave transmission .....	23
Figure 19: Complete and partial reflection and effects on overtopping .....	24
Figure 20: The four main types of breaking waves .....	25
Figure 21: Plunging waves and spilling waves on a beach .....	25
Figure 22: Detached and attached breakwaters .....	26
Figure 23: Rubble mound breakwater in deep water (left) and in shallow water (right) .....	28
Figure 24: Sample concrete armour units.....	29
Figure 25: Artificial armour units with concrete cap .....	31
Figure 26: Examples of overtopping in Italy.....	33
Figure 27: Effect of permeability .....	35
Figure 28: Toe of structure .....	36
Figure 29: Definition of freeboard for different constructions.....	37
Figure 30: Example of wave overtopping measurements .....	37
Figure 31: Harbour Rapallo during and after wave attack on the 6th Nov 2000. ....	39
Figure 32: Criteria for critical overtopping discharges .....	42
Figure 33: Comparison of wave overtopping formulae for various kinds of structures .....	44
Figure 34: Comparison of wave overtopping as function of slope angle.....	44
Figure 35: Waves characterized by $H_s$ and $T_p$ .....	45
Figure 36: Run-up level and location for overtopping differ .....	46
Figure 37: Percentage of overtopping waves for rubble mound breakwaters .....	47
Figure 38: Mean overtopping discharge for 1:15 smooth and rubble mound slopes .....	47
Figure 39: Various distributions of overtopping volumes on a Rayleigh scale graph. ....	48
Figure 40: Relationship between mean discharge $q$ and $V_{max}$ .....	49
Figure 41: Typical laboratory wave tank.....	52
Figure 42: Typical two-dimensional coastal structure model .....	52
Figure 43: Typical three-dimensional coastal structure model in wave basin .....	53
Figure 44: Bathymetry layout.....	61

Figure 45: Measurement of wave overtopping using an overtopping tank.....	64
Figure 46: Pressure sensors installed inside the wave wall .....	65
Figure 47: Left: Firenze situated on a map. Right: Top view at the Faculty of Engineering. .	68
Figure 48: CoastLab wave flume at the Maritime Engineering Laboratory .....	68
Figure 49: Left: Diffuser at the bottom of the flume. Right: The bottom of the channel. ....	69
Figure 50: Front prospective of the mechanical part of the wave maker.....	70
Figure 51: Recirculation pump .....	70
Figure 52: Back paddle pump effects .....	71
Figure 53: Wave gauges and their electric scheme .....	73
Figure 54: Load cell .....	74
Figure 55: Pressure transducer .....	74
Figure 56: Disposition of the pressure transducers on the wave wall (in model scale, cm). ...	74
Figure 57: Hydrometric tip at the nonius .....	75
Figure 58: Overtopping tank for overtopping measurement.....	76
Figure 59: a) Camera (left); b) Video camera (right).....	77
Figure 60: Location for characteristic velocity in the core .....	82
Figure 61: Rocks used for armour layer.....	87
Figure 62: Rocks used for filter layer. ....	89
Figure 63: Rocks used for core .....	90
Figure 64: Placing tetrapods into the model .....	92
Figure 65: Raising the wave wall in configurations C4 and C5 .....	93
Figure 66: Side view of the wave flume with locations of analysed structures.....	93
Figure 67: Schematic illustration of experiment (in model scale) .....	94
Figure 68: Construction phases of the harbour breakwater in the wave flume.....	96
Figure 69: Configuration C0 .....	96
Figure 70: Configuration C1 .....	97
Figure 71: Configuration C2 .....	97
Figure 72: Configuration C3 .....	98
Figure 73: Configuration C4 .....	98
Figure 74: Configuration C5 .....	99
Figure 75: Maximum pressure stresses for each pressure transducer. ....	128

## LIST OF GRAPHS

Graph 1: Granulometric analysis for the material constructing the armour layer.....	88
Graph 2: Granulometric analysis for material constructing the filter.....	90
Graph 3: Granulometric analysis for the material constructing core.....	92
Graph 4: Results for WG1, WG2 and WG3 calibrations on 18 <sup>th</sup> of April 2012.....	110
Graph 5: Results for WG4 and WG5 calibrations on 18 <sup>th</sup> of April 2012.....	110
Graph 6: Time level series at WG1, WG2 and WG3 for the test H1T105G2CF1C3.....	111
Graph 7: Time level series at WG4 and WG5 for the test H1T105G2CF1C3.....	111
Graph 8: Amplitude spectrum at WG1, WG2 and WG3 for the test H1T105G2CF1C3.....	112
Graph 9: Wave heights distribution at WG1, WG2 and WG3.....	112
Graph 10: Wave heights distribution at WG4 and WG5.....	113
Graph 11: Graphs for total effective spectrum, incident spectrum.....	114
Graph 12: Graph Overtopping time history.....	115
Graph 13: Mean overtopping discharges for all tests depending on configuration type.....	117
Graph 14: Wave pressures acquired by pressure transducer.....	118
Graph 15: Wave pressure stresses acquired by pressure transducer.....	118
Graph 16: Different types of malfunctioning of pressure transducers offset.....	119
Graph 17: Typical output of overtopping analysis.....	122
Graph 18: Mean overtopping discharge $q_m$ for all wave attacks in relation to config.....	123
Graph 19: Ground plan of mean overtopping discharge graph.....	124
Graph 20: Mean wave-by-wave overtopping volume.....	125
Graph 21: Max wave-by-wave overtopping volume.....	126
Graph 22: Typical output results after joining all sub tests of wave pressures.....	127
Graph 23: Maximum pressures for each wave attack.....	128
Graph 24: Max pressures for wave attack H1T085G2F1.....	129
Graph 25: Max pressures for wave attack H1T085G5F1.....	130
Graph 26: Max pressures for wave attack H1T105G2F1.....	130
Graph 27: Max pressures for wave attack H1T105G5F1.....	131
Graph 28: Max pressures for wave attack H1T125G2F1.....	132
Graph 29: Max pressures for wave attack H1T125G5F1.....	132
Graph 30: Max pressures for wave attack H2T115G2F1.....	133
Graph 31: Max pressures for wave attack H2T115G5F1.....	134
Graph 32: Typical output results for reflection analysis.....	136

**ABBREVIATIONS AND SYMBOLS**

2D	Two dimensional
3D	Three dimensional
ACCROPODETM	Artificial concrete armour units
BS 6349	The British Standards
CEM	Coastal Engineering Manual
CIRIA, CUR, CETMEF	The Rock Manual
CLASH	Crest Level Assessment of coastal Structures by full
scale monitoring	
CoastLab	Maritime Engineering Laboratory of Florence University
CORE-LOCTM	Artificial concrete armour units
Dolosse	Artificial concrete armour units
GANIMEDE	Personal computer in CoastLab
JONSWAP	Joint North Sea Wave Project spectrum
LDV	Velocity meter
MMD, $D_{50}$	Mass-median-diameter
MWL	Mean water level
OB	Personal computer in the laboratory for
PC GENERATORE	Personal computer in CoastLab
PM formula, spectrum	Pierson and Moskowitz formula, spectrum
PSD	The particle-size distribution
Rms	Root-mean-square
RPAM	Random-phase/amplitude model
SHEDs or COBS	Hollow cube blocks
SWL	Still water level
TAW	Guidelines for overtopping
TCA	Load cells model
Tetrapods	Artificial concrete armour units
Tribars	Artificial concrete armour units
UK	United Kingdom
WG	Wave gauges
WO	Wave overtopping
Xbloc®	Artificial concrete armour units

## 1 INTRODUCTION

Wave overtopping is of principal concern for structures constructed primarily to defend against flooding or against coastal erosion, sometimes termed coast protection. Such structures may be built also to protect areas of water for ship navigation or mooring: ports, harbours or marinas; these are often formed as breakwaters or moles. On average, approximately 2-5 people are killed each year of Italy and UK through wave action, chiefly on seawalls and similar structures. Overtopping discharge occurs because of waves running up the face of a seawall (Pullen et al., 2007).



Figure 1: Violent wave overtopping occurs when waves break against sea walls throwing water and spray over the top.

Source: <http://www.vows.ac.uk/>, 12. 07. 2012.

Overtopping is not a continuous process but an intermittent occurrence at times of attack of individual high waves varying from one wave to another. Wave overtopping is affected by many factors which will be studied in this research; even a small modification of the geometry of a structure may change the amount of overtopping (Wai et al. 2003). Longer storm duration gives more overtopping waves, but statistically, also a larger maximum volume. Many small overtopping waves (like for river dikes or embankments) may create the same mean overtopping discharge as a few large waves for rough sea conditions. The maximum volume are however, much larger for rough sea conditions with large waves (Pullen et al., 2007). Generally, most of the overtopping waves are fairly small, but a small number can give significantly larger overtopping volumes. More accurate estimate of the overtopping rate should be determined through hydraulic model tests (Wai et al., 2003) as in this research was done.

This thesis is part of the international exchange ERASMUS between University of Ljubljana and University of Florence aimed to study the process of wave overtopping and wave pressure of impact at harbour breakwaters on physical model in the wave flume.

An overview of the main thesis topic wave overtopping for a large number of wave conditions (in Ligurian Sea) and geometries tested will be presented. The main objective of this research is to study the differences between various constructions and to find the most effective harbour breakwater construction with no or less possible harmful consequences of overtopping waves. The analysis and results will be obtained with Matlab program. Activities conducted in this laboratory research will be design of experiments, realization of a physical model with its configurations, conducting experiments (with measurements) and post processing of analysis.

The thesis is organized in 7 chapters, as follows: In Chapter 2, important theoretical backgrounds on wave and wave parameters, standard techniques for defining random waves, harbour hydrodynamics, breakwaters and overtopping phenomenon are presented. In Chapter 3 overview of hydraulic physical models, scale effects in laboratory, used materials and measurement equipment is described. In Chapter 4 testing procedure with laboratory description, design of harbour breakwater and wave condition is presented and continues in Chapter 5, where analysis and results are found. Finally, Chapter 6 concludes the thesis research about wave overtopping and is followed by Slovenian summary of thesis research.

## 2 THEORETICAL BACKGROUNDS

### 2.1 Basic definition of wave and wave parameters

#### 2.1.1 Monochromatic waves

Monochromatic waves may be generated in the laboratory but are rare in nature. These are the waves, which has the same wave length and period. The model is of certain help for definition of basic wave parameters and, as such is introduced as follow while the random nature of wind generated waves and the related wave characteristic parameters are discussed in the next paragraph.

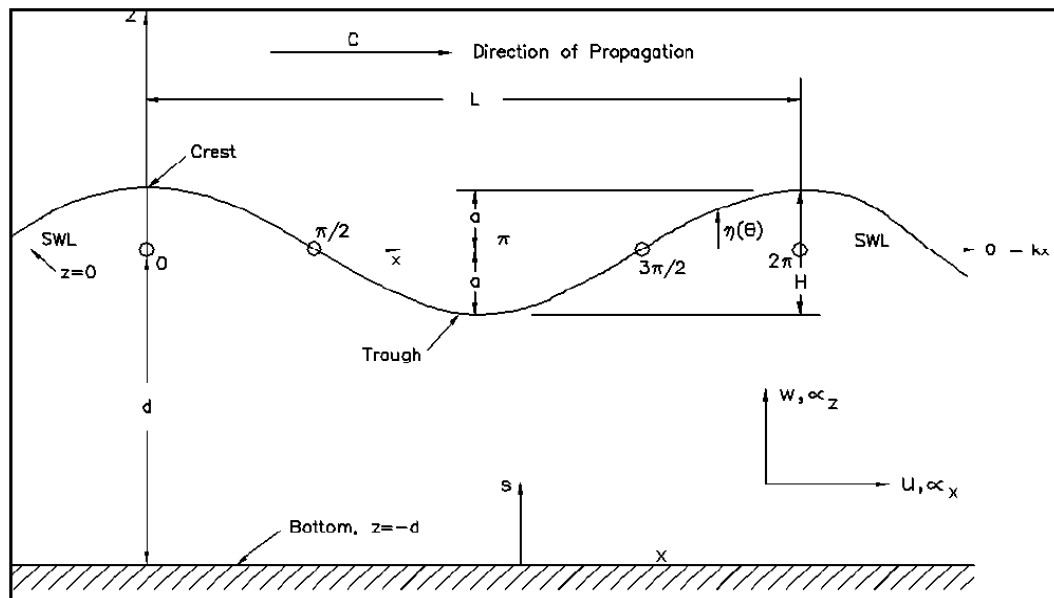


Figure 2: Definition of terms of the wave.  
 Source: Coastal Engineering Manual, 2002.

As shown in Fig. 2, the highest point of the wave is the crest and the lowest point is the trough. For regular waves, the height of the crest above the still-water level (SWL) and the distance of the trough below the SWL are each equal to the wave amplitude  $a$ . Therefore  $a = H/2$ , where  $H$  = the wave height. The time interval between the passage of two successive wave crests or troughs at a given point is the wave period  $T$ . The wavelength  $L$  is the horizontal distance between two identical points on two successive wave crests or two successive wave troughs.

Other wave parameters include:

- $\omega = 2\pi/T$  the angular or radian frequency,

- $k = 2\pi / L$  the wave number,
- $C = L/T = \omega / k$  the phase velocity or wave celerity,
- $\epsilon = H/L$  the wave steepness,
- $d/L$  the relative depth,
- and  $H/d$  the relative wave height.

These are the most common parameters encountered in coastal practice. Wave motion can be defined in terms of dimensionless parameters  $H/L$ ,  $H/d$ , and  $d/L$ ; these are often used in practice (Coastal Engineering Manual, 2002).

### 2.1.1.1 Linear wave theory

The most elementary wave theory for monochromatic waves is the small-amplitude or linear wave theory. This theory, is easy to apply, and gives a reasonable approximation of wave characteristics for a wide range of wave parameters. A more complete theoretical description of waves may be obtained as the sum of many successive approximations, where each additional term in the series is a correction to preceding terms. For some situations, waves are better described by these higher-order theories, which are usually referred to as finite-amplitude wave theories. Although there are limitations to its applicability, linear theory can still be useful provided the assumptions made in developing this simple theory are not grossly violated.

The assumptions made in developing the linear wave theory are:

- The fluid is homogeneous and incompressible; therefore, the density  $D$  is a constant.
- Surface tension can be neglected.
- Coriolis effect due to the earth's rotation can be neglected.
- Pressure at the free surface is uniform and constant.
- The fluid is ideal or inviscid (lacks viscosity).
- The particular wave being considered does not interact with any other water motions. The flow is irrotational (only normal forces are important and shearing forces are negligible).
- The bed is a horizontal, fixed, impermeable boundary, which implies that the vertical velocity at the bed is zero.

- The wave amplitude is infinitesimal and the waveform is invariant in time and space.
- Waves are plane or long-crested (two-dimensional) (Coastal Engineering Manual, 2002).

Another important aspect of linear wave theory deals with the displacement of individual water particles within the wave. Water particles generally move in elliptical paths in shallow or transitional depth water and in circular paths in deep water.

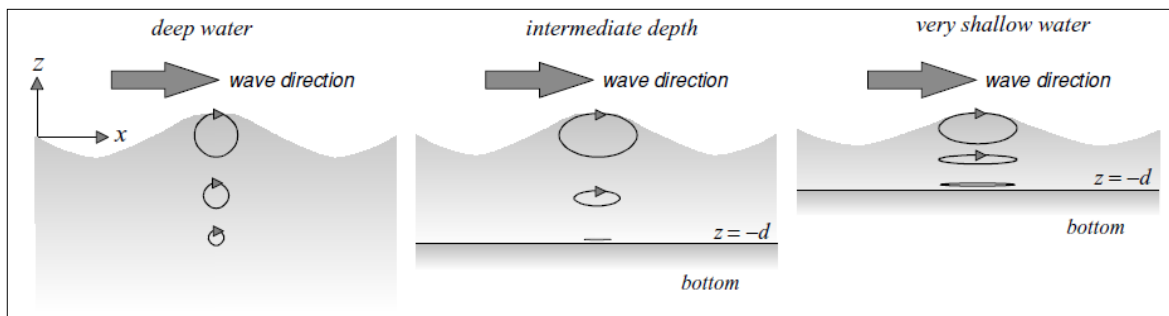


Figure 3: Water particle displacements from mean position in deep water, intermediate-depth water and very shallow-water.

Source: Holthuijsen, 2007.

Table 1: Classification of water waves based on the relative depth criterion  $d/L$  after Coastal Engineering Manual, 2002.

Classification of Water Waves			
Classification	$d/L$	$kd$	$\tanh(kd)$
Deep water	$1/2$ to $\infty$	$\pi$ to $\infty$	$\approx 1$
Transitional	$1/20$ to $1/2$	$\pi/10$ to $\pi$	$\tanh(kd)$
Shallow water	$0$ to $1/20$	$0$ to $\pi/10$	$\approx kd$

### 2.1.2 Irregular (random) waves

The term irregular waves is used to denote natural sea states in which the wave characteristics are expected to have a statistical variability in contrast to monochromatic waves, where the properties may be assumed constant.

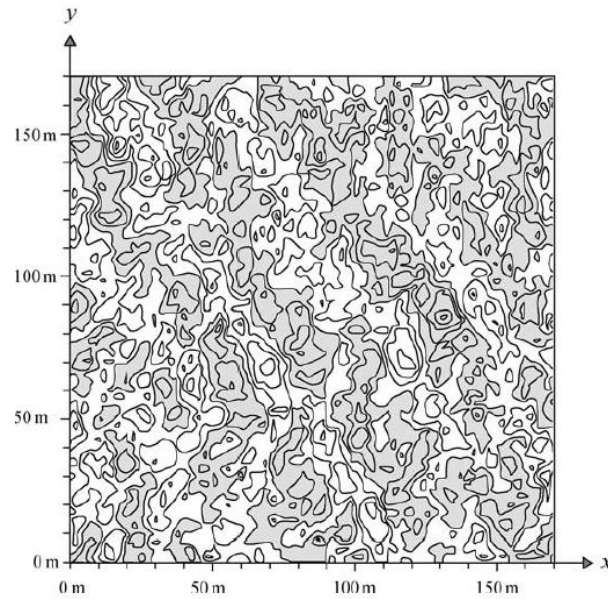


Figure 4: A bird's eye view of ocean waves, as recorded with stereo-photography with cameras looking down from two helicopters, i.e., the sea-surface elevation as a function of horizontal co-ordinates at one moment in time (the contour line interval is 0.20 m, shaded areas are below mean sea level).

Source: Holthuijsen, 2007.

### 2.1.2.1 Observation techniques

#### 1) Visual observations

They are often the only source of information and can be subjective

#### 2) Measurement techniques

##### a) In situ techniques

Instrument may be located at the sea surface (e.g., a floating surface buoy), or below the sea surface (e.g., a pressure transducer mounted on a frame at the sea bottom), or it may be surface-piercing (e.g., a wire mounted on a platform from above the sea surface, extending to some point below the sea surface). Most of these instruments are used to acquire time records of the up-and-down motion of the surface at one (horizontal) location.

##### — Wave buoys

They follow the 3-dimensional motion of the water particles at the sea surface. It measures its vertical acceleration with an onboard accelerometer. The buoys are usually provided with radio communication to send their signals to a land- or platform-based receiving station, new

buoys are often supplemented with satellite communication and position detection by the Global Positioning System (GPS).

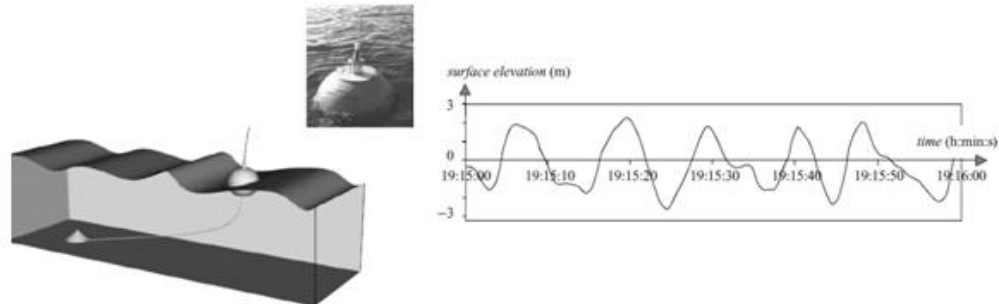


Figure 5: Left: The WAVERIDER buoy at sea. The buoy measures its own vertical acceleration to estimate the sea-surface motion. Right: The up-and-down motion of the sea surface in a storm by a buoy, i.e., the sea-surface elevation at one location as a function of time.

Source: Holthuijsen, 2007.

#### b) Remote – sensing techniques

They are usually better, because they are objective, but the instruments have their own peculiarities too. The two most important are (a) limitations of the basic principle of the instrument (e.g., a buoy floating at the sea surface may swerve around or capsize in a very steep wave) and (b) sensitivity to the aggressive marine environment (e.g., mechanical impacts, marine fouling and corrosion).

The alternative of remote sensing, which relies on instruments that are positioned above the water, is generally not sensitive to the marine environment but it may be sensitive to the atmospheric environment (e.g., rain, clouds, water vapour) (Holthuijsen, 2007).

### 2.2 Types of the waves

- Trans – tidal waves

Are the longest waves. Are generated by low-frequency fluctuations in the Earth's crust and atmosphere.

- Tides

Are slightly shorter waves than the first ones. Are being generated by the interaction between the oceans on the one hand and the Moon and the Sun on the other. Their periods range from a few hours to somewhat more than a day, wave lengths vary between a few hundred and a few thousand kilometres.

- Storm surges

The wave length and period are slightly shorter from that ones from the tides. They are large-scale elevation of the ocean surface in a severe storm, being generated by the (low) atmospheric pressure and the high wind speeds in the storm. The space and time scales are roughly equal to those of the generating storm (typically a few hundred kilometres and one or two days). It can cause severe flooding when it approaches to the coast and the water piles up (e.g., the flooding in New Orleans by hurricane Katrina in August 2005, or the annual flooding in Bangladesh by cyclones).

- Tsunamis

Are generated by a submarine 'land' slide or earthquake. They are difficult to predict and barely noticeable in the open ocean (due to their low amplitude there) but they wreak havoc on unsuspecting coastal regions as they increase their amplitude considerably on approaching the coast.

- Seiches

Are even more difficult to predict in comparison to tsunamis. These are standing waves, with a frequency equal to the resonance frequency of the basin in which they occur (in harbours and bays or even at sea, for instance in the Adriatic Sea). Usually are generated from the open sea (storms).

- Infra-gravity waves

They are being generated by groups of wind-generated waves, for instance in the surf zone at the beach (surf beat), with periods of typically a few minutes.

- Wind-generated waves

Their period is shorter than 30 s.

- Surface gravity waves

Are waves dominated by gravity, periods longer than  $\frac{1}{4}$  s.

- Wind sea

Are waves generated by local wind, irregular and short crested.

- Swell

Are regular, long – crested appearance, and are generated when they leave the generation area. Swell describes the natural waves that appear most like monochromatic waves in deep water, but swell, too, is fundamentally irregular in nature.

- Capillary waves

Their periods are shorter than  $\frac{1}{4}$  s, wave lengths shorter than 10 cm and affected by surface tension.

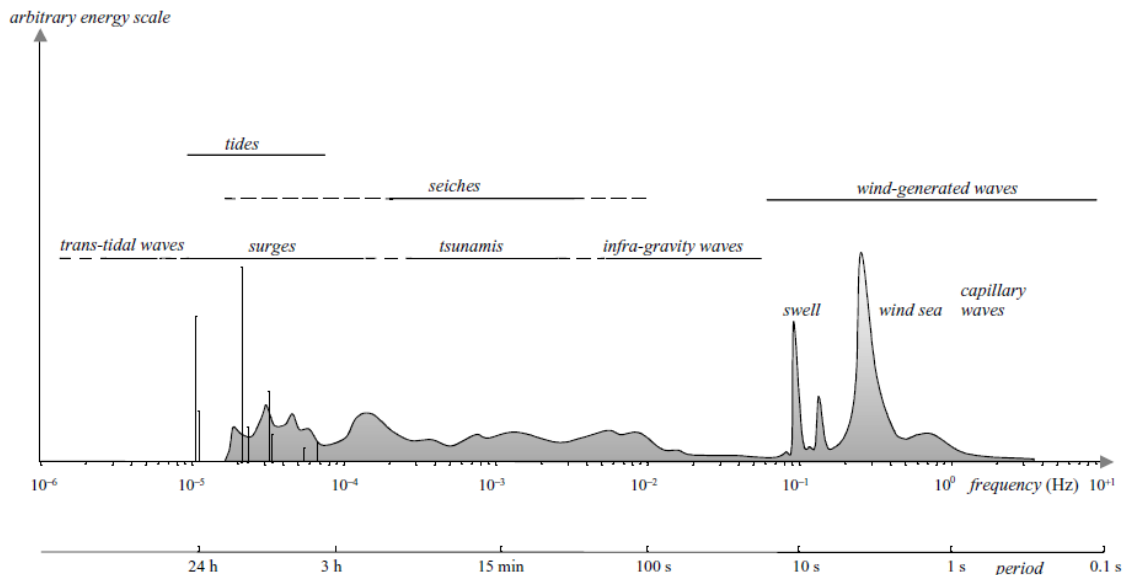


Figure 6: Frequencies and periods of the vertical motions of the ocean surface.  
Source: Holthuijsen, 2007.

### 2.2.1 Types of scales

Ocean waves are wind-generated surface gravity waves. We can describe them:

- At several spatial scales (ranging from hundreds of meters or less to thousands of kilometres).
- Several time scales (ranging from seconds (i.e. one wave period) to thousands of years).

Scales are used for describing variation in space and time of these waves.

- Small scales have dimensions about 10 – 100 s and 10 – 1000 m,
- Larger scales have dimensions of about 100 – 1000 s and 100 – 10 000 m,
- Scales of coastal waters.

We can easily describe waves with the variance density spectrum of the waves, which is followed by the linear theory of surface gravity waves. This theory gives the interrelation

amongst physical characteristics as the surface motion, the wave-induced pressure in the water and the motion of water particles. Although several theories for these processes have been developed, the actual formulations in numerical wave models are still very much empirical and therefore relatively simple and descriptive (Holthuijsen, 2007).

### 2.3 Standard techniques for defining random waves

#### 2.3.1 Zero-crossing method

This is method defines a wave when the surface elevation crosses the zero-line or the mean water level (MWL) upward and continues until the next crossing point. This is the zero-upcrossing method. When a wave is defined by the downward crossing of the zero-line by the surface elevation, the method is the zero-downcrossing. There can be differences between the definitions of wave parameters obtained by the zero up- and down-crossing methods for description of irregular sea states (Goda, 2000).

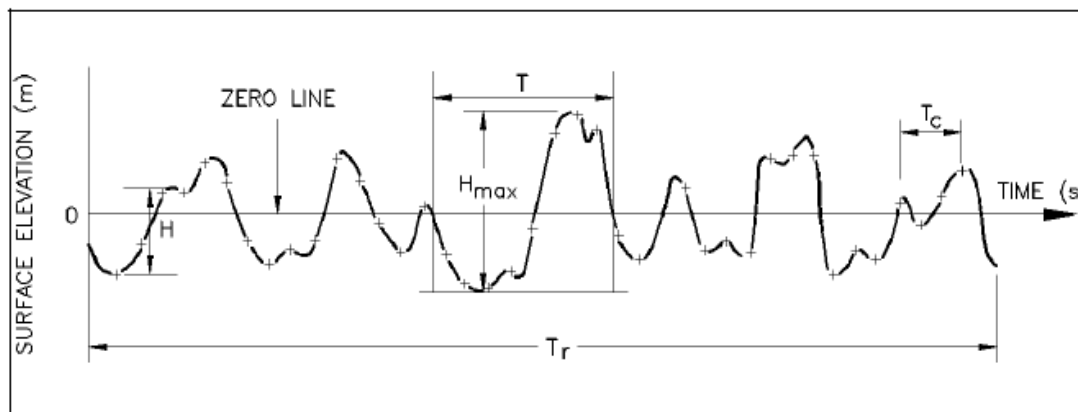


Figure 7: The definition of wave parameters for a random sea state.

Source: Coastal Engineering Manual, 2002.

In coastal projects, engineers are faced with designing for the maximum expected, the highest possible waves, or some other equivalent wave height. From one wave record measured at a point, these heights may be estimated by ordering waves from the largest to the smallest and assigning to them a number from 1 to N. Wave period is the time interval between successive crossings of the MWL by the water surface in a downward direction called zero down-crossing period or zero up-crossing period for the period deduced from successive up-crossings (see Fig. 7). Wave height is the vertical distance between the highest and lowest surface elevation in wave (see Fig. 7). Even though there are so many heights the wave will thus have only one wave height.

Nowadays almost all data are recorded in digital form, based on this we can get:

- 1) Highest wave is wave with the maximum wave height and largest wave period in the record  $H_{\max}$ ,  $T_{\max}$ .
- 2) Highest one - tenth wave is the mean height of the highest one-tenth waves. Waves in the record are counted and selected in descending order of wave height from the highest wave, until one-tenth of total number of waves is reached  $T_{1/10}$ ,  $H_{1/10}$ .

$$H_{1/10} = \frac{1}{N/10} \sum_{j=1}^{N/10} H_j \quad (2.1)$$

$$T_{1/10} = \frac{1}{N/10} \sum_{j=1}^{N/10} T_j \quad (2.2)$$

- 3) Significant wave or highest one - third wave with  $T_{1/3}$ ,  $H_{1/3}$  is the average of the first (highest) one-third ( $N/3$ ) waves.

$$H_{1/3} = \frac{1}{N/3} \sum_{j=1}^{N/3} H_j \quad (2.3)$$

$$T_{1/3} = \frac{1}{N/3} \sum_{j=1}^{N/3} T_{0,j} \quad (2.4)$$

- 4) Mean wave is the wave specified by the means  $\bar{T}$ ,  $\bar{H}$  of the heights and periods of all waves in a record.

$$\bar{H}_0 = \frac{1}{N} \sum_{i=1}^N H_{0,i} \quad (2.5)$$

$$T_0 = \frac{1}{N} \sum_{i=1}^N T_{0,i} \quad (2.6)$$

The most frequently used is the significant wave with  $T_{1/3}$  and  $H_{1/3}$ .

### 2.3.2 Wave height distribution

The histogram of wave heights containing about 100 waves, usually exhibits a rather jagged shape, because of the relatively small sample size. We can obtain smoother distribution of wave heights by assembly many wave records and by counting the relative frequencies of the normalized wave heights in their respective classes.

In Fig. 8 ordinate the relative frequency  $n/N_0$  ( $N_0$  is the total number of the waves) is divided by the class interval of the normalized wave height  $\Delta(H/\bar{H})$ , so that the area under the histogram is equal to unity. Relative frequency tells us how often each value occurs (Goda, 2000).

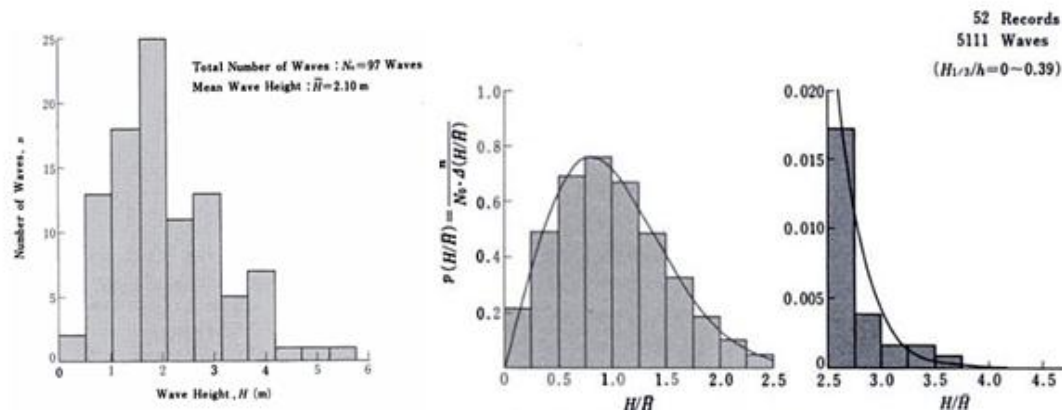


Figure 8: Left: Example of a histogram of wave heights. Right: Normalized histogram of wave heights.

Source: Goda, 2000.

Rayleigh distribution (The middle graph in Fig. 8) is proposed for the distribution of individual wave heights, which is given by the Eq. 2.7:

$$p(x) = \frac{\pi}{2} x \exp\left[-\frac{\pi}{2} x^2\right]; x = \frac{H}{\bar{H}} \quad (2.7)$$

Function  $p(x)$  represents the probability density; that is, the probability of a normalized wave height taking an arbitrary value between  $x$  and  $x+dx$  is given by the product  $p(x)dx$ . The ordinate of the middle plot in Fig. 8 is an approximation to  $p(x)$ .

The function  $P(x)$  gives the probability of a particular wave height exceeding a prescribed value.

$$P(x) = \int_0^{\infty} p(\xi) d\xi = \exp\left[-\frac{\pi}{4} x^2\right] \quad (2.8)$$

Rayleigh distribution provides a good approximation to the distribution of individual wave heights which are defined by the zero-upcrossing and zero-downcrossing wave methods.

### 2.3.2.1 Relations between representative wave heights

$H_{1/3}$  and  $H_{1/10}$  can be evaluated by manipulating of the probability density function. Thus we have (theoretical prediction):

$$H_{1/10} = 1,27H_{1/3} = 2,03\bar{H}, H_{1/3} = 1,60\bar{H} \quad (2.9)$$

These results represent the mean values of a number of wave records ensembled together. Individual wave records containing only 100 waves or so may give noticeable departures from these mean relations. The most probable value, or the mode of distribution, is a function of the number of waves in a wave train or a wave record, which is given by (Goda, 2000):

$$(H_{max}/H_{1/3})_{mode} \cong 0,706\sqrt{\ln N_0} \quad (2.10)$$

The arithmetic mean of is greater than the most probable value, as seen from the skewed shape of the curves:

$$(H_{max}/H_{1/3})_{mode} \cong 0,706[\sqrt{\ln N_0} + \gamma/(2\sqrt{\ln N_0})] \quad (2.11)$$

The height  $(H_{max})_\mu$  is given by:

$$(H_{max})_\mu/H_{\frac{1}{3}} \cong 0,706 \sqrt{\ln \left[ \frac{N_0}{\ln(1/(1-\mu))} \right]} \quad (2.12)$$

The value  $H_{max}$  should be estimated based upon consideration of the duration of storm waves and the number of waves, and by allowing some tolerance for a range of deviation. The prediction generally employed falls within the range:

$$H_{max} = (1,6 \sim 2,0)H_{1/3} \quad (2.13)$$

$$H_{max} = 1,8H_{1/3} \text{ (for vertical breakwaters)} \quad (2.14)$$

$$H_{max} = 2,0H_{1/3} \text{ (for offshore structures)} \quad (2.15)$$

The particular final value is chosen by consideration of the reliability of the estimation of the design storm waves, the accuracy of the design formula, the importance of the structure, the type and nature of the possible structural failure, and others factors.

### 2.3.3 Distribution of wave period

A distribution of wave period is narrower than that of wave heights; the spread lies mainly in the range of 0.5 to 2.0 times the mean wave period. When wind waves and swell coexists, the period distribution becomes broader, sometimes can be also bi-modal (with 2 peaks). The wave period does not exhibit a universal distribution law such as the Rayleigh distribution in the case of wave heights. The average values for many wave records can be summarized as:

$$T_{max} \cong T_{1/10} \cong T_{1/3} \cong 1,2T \quad (2.16)$$

Waves of smaller heights often have shorter periods in a wave record, whereas waves of greater heights than the mean height do not show a correlation with the wave period. Visual estimated significant wave heights  $H_v$  and periods  $T_v$  VS measures values.

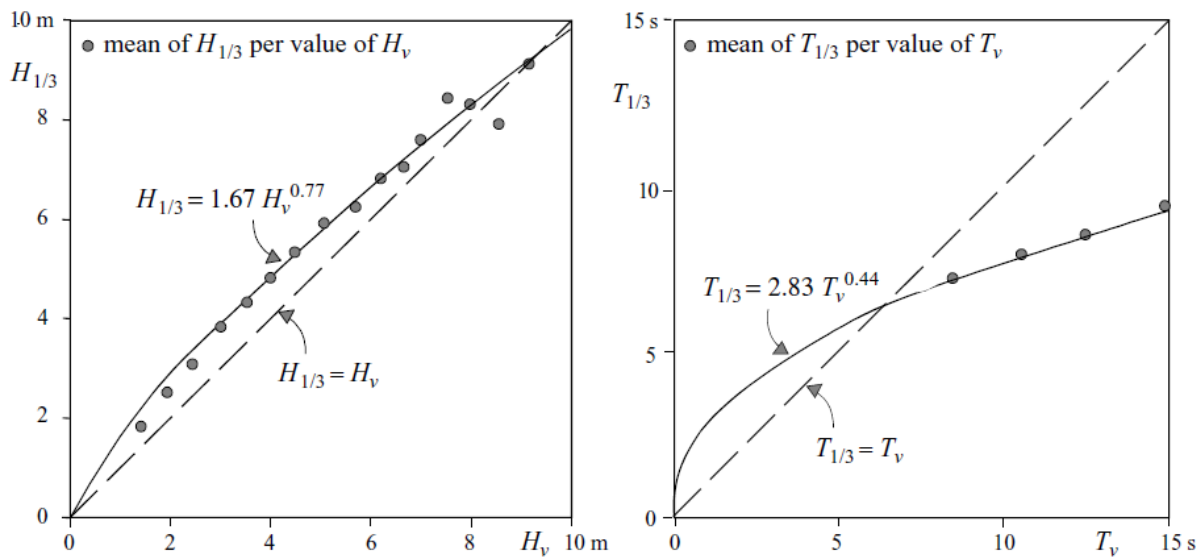


Figure 9: The relationship between the visually estimated significant wave height and period and the measured significant wave height and period. The standard deviation of the measured values is about 15% of the mean of the measurements at every value of  $H_v$  or  $T_v$ .

Source: Holthuijsen, 2007.

Fig. 9 represents relationship between the visually estimated significant wave height  $H_v$  and the measured significant wave height  $H_{1/3}$ . The best-fit power law for these data:

$$H_{1/3} = 1,67H_v^{0,77} \text{ (in m) so that } H_{1/3} \approx H_v \quad (2.17)$$

In contrast to this, the visually estimated significant wave period does not agree well with the instrumental measurements. The best-fit power-law relationship in the same study is:

$$T_{1/3} = 2,83T_v^{0,44}, \text{ so that } T_{1/3} \neq T_v \text{ (Holthuijsen, 2007)}. \quad (2.18)$$

## 2.3.4 Wave spectrum

### 2.3.4.1 Introduction

Wave spectrum serves to describe sea surface as a stochastic process (i.e. to characterise all possible observations, like time records, etc.). Wave spectrum is the most important form in which ocean waves are described and random-phase/amplitude model, which leads us to the final result. Basic concept of the wave spectrum can be explained on the essence on a wave record. Amplitude spectrum characterise the wave record.

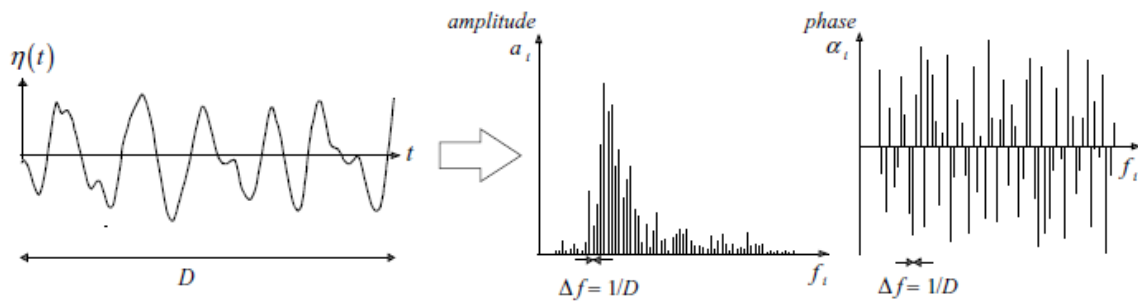


Figure 10: The observed surface elevation and its amplitude and phase spectrum.

Source: Holthuijsen, 2007.

The basic concept of the wave spectrum is simple and can be explained on a wave record, i.e., the surface elevation  $\eta(t)$  at one location as a function of time, with duration  $D$ , obtained at sea with a wave buoy or a wave pole. We can exactly reproduce that record as the sum of a large number of harmonic wave components (a Fourier series):

$$\eta(t) = \sum_{i=1}^N a_i \cos(2\pi f_i t + \alpha_i) \quad (2.19)$$

Where  $a_i$  and  $\alpha_i$  are the amplitude and phase, respectively, of each frequency  $f_i = i/D$  ( $i = 1, 2, 3, \dots$ ; the frequency interval is therefore  $\Delta f = 1/D$ ). With a Fourier analysis, we can determine the values of the amplitude and phase for each frequency and this would give us the amplitude and phase spectrum for this record as seen in Figure 2.9. Average amplitude spectrum:

$$\bar{a}_i = \sum_{m=1}^M a_{i,m} \quad (2.20)$$

For all frequencies  $f_i$ , where  $a_{i,m}$  is the value of  $a_i$  in the experiment with sequence number  $m$ . For large values of  $M$  the value of  $\bar{a}_i$  converges (approaches a constant value as we increase  $M$ ), thus solving the sampling problem. It is more meaningful to distribute the variance of each wave component  $\frac{1}{2} a_i^2$ . There are two reasons; first, the variance is a more relevant (statistical) quantity than the amplitude. Second, the linear theory for surface gravity waves shows that the energy of the waves is proportional to the variance. This implies that, through the variance, a link is available to such physical properties as wave energy, but also wave-induced particle velocity and pressure variations. The variance spectrum  $\frac{1}{2} a_i^2$  is discrete, i.e., only the frequencies  $f_i = i/D$  are present, whereas in fact all frequencies are present at sea. The definition of the variance density spectrum thus becomes (Holthuijsen, 2007):

$$E(f) = \lim_{\Delta f \rightarrow 0} \frac{1}{\Delta f} \frac{1}{2} \bar{a}^2 \text{ or } E(f) = \lim_{\Delta f \rightarrow 0} \frac{1}{\Delta f} E\left\{\frac{1}{2} \bar{a}^2\right\} \quad (2.21)$$

### 2.3.5 Random – phase/amplitude model (RPAM)

Is the basic model for describing the moving surface elevation  $\eta(t)$ . Surface elevation in that case is considered to be the sum of a large number of harmonic waves (each with constant amplitude and a phase randomly chosen for each realisation).

$$\eta(t) = \sum_{i=1}^N a_i \cos(2\pi f_i t + \alpha_i), \tag{2.22}$$

Where  $N$  is large number of frequencies,  $a_i$  amplitude and  $\alpha_i$  is a phase. In this model phase at each frequency  $f_i$  (in this model) is uniformly distributed between 0 and  $2\pi$ .

$$p(\alpha_i) = \frac{1}{2\pi} \text{ for } 0 < \alpha_i < 2\pi \tag{2.23}$$

And amplitude  $a_i$  is at each frequency Rayleigh distributed.

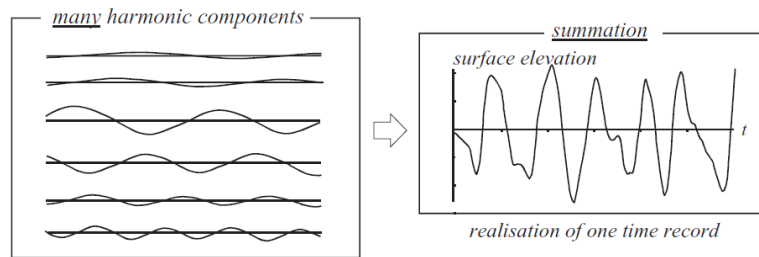


Figure 11: The summation of many harmonic waves, with constant but randomly chosen amplitudes and phases, creates a random sea surface.

Source: Holthuijsen, 2007.

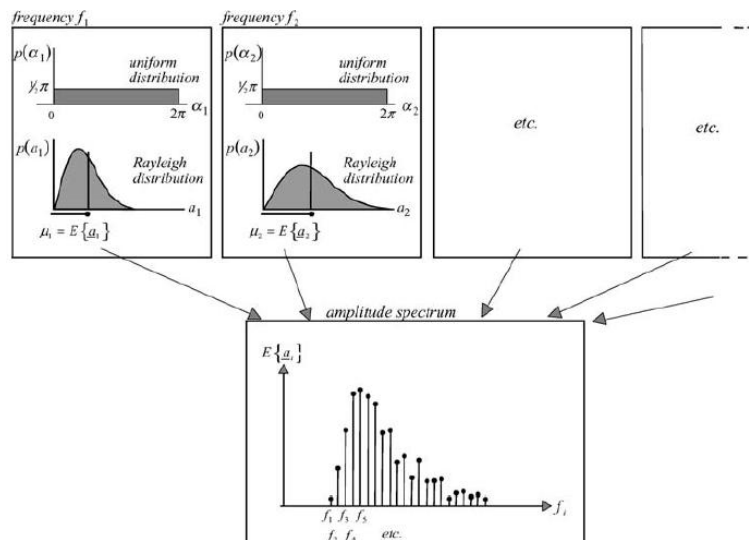


Figure 12: The RPAM: at every frequency there is one uniform distribution for the random phase and one Rayleigh distribution for the random amplitude (characterized by the expected value  $E\{ a_i \}$ ). Top panels: for a series of frequencies,  $f_i$  ( $i = 1, 2, 3, 4, 5$  etc.). Bottom panel: the expected value of the amplitude as a function of frequency, i.e., the amplitude spectrum.

Source: Holthuijsen, 2007.

A wave record at sea can be seen as one such realisation. For each new realisation of  $\eta(t)$ , the sample values of  $a_i$  and  $\alpha_i$  are again randomly drawn from these probability density functions.

It is thus (hypothetically) possible to create a (large) set of realisations of the sea surface (this is called an ensemble).

The following remarks should be made in applicability of the RPAM to real ocean waves:

- Because conditions at sea are never really stationary, a wave record needs to be divided into segments that are each deemed to be approximately stationary (a duration of 15–30 min is commonly used for wave records obtained at sea);
- The RPAM is a summation of wave components at discrete frequencies  $f_i$ , whereas, in fact, a continuum of frequencies is present at sea.

### 2.3.6 The variance density spectrum

The amplitude spectrum provides enough information to describe the sea-surface elevation realistically as a stationary, Gaussian process. The variance density spectrum gives a complete description of the surface elevation of ocean waves in a statistical sense (all statistical characteristics of the wave field can be expressed in terms of this spectrum). Both the amplitude and the variance spectrum are based on discrete frequencies. All frequencies are present at sea.

The RPMA needs therefore to be modified. This is done by distributing the variance  $E\{1/2 \cdot \bar{a}^2\}$  over the frequency interval  $\Delta f_i$  at frequency  $f_i$ . The resulting variance density spectrum  $E^*(f_i)$  is then:

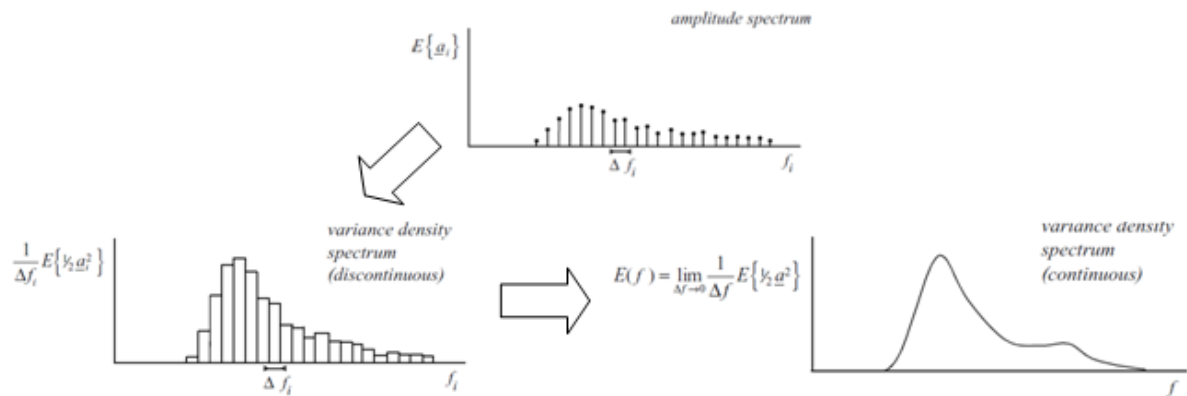


Figure 13: The transformation of the discrete amplitude spectrum of the RPAM to the final function  $E(f)$  which is called the (continuous) variance density spectrum.

Source: Holthuijsen, 2007.

#### 2.3.6.1 Interpretation of the variance density spectrum

If we multiply the spectrum by  $g\rho$  we obtain the energy density spectrum. This spectrum shows how the wave energy is distributed over the frequencies, which seems to be easier to comprehend. Energy density spectrum is used to describe the physical aspects of waves

(within the limitations of the stationary, Gaussian model and the linear theory of surface gravity waves). The overall appearance of the waves can be inferred from the shape of the spectrum: the narrower the spectrum, the more regular the waves are.

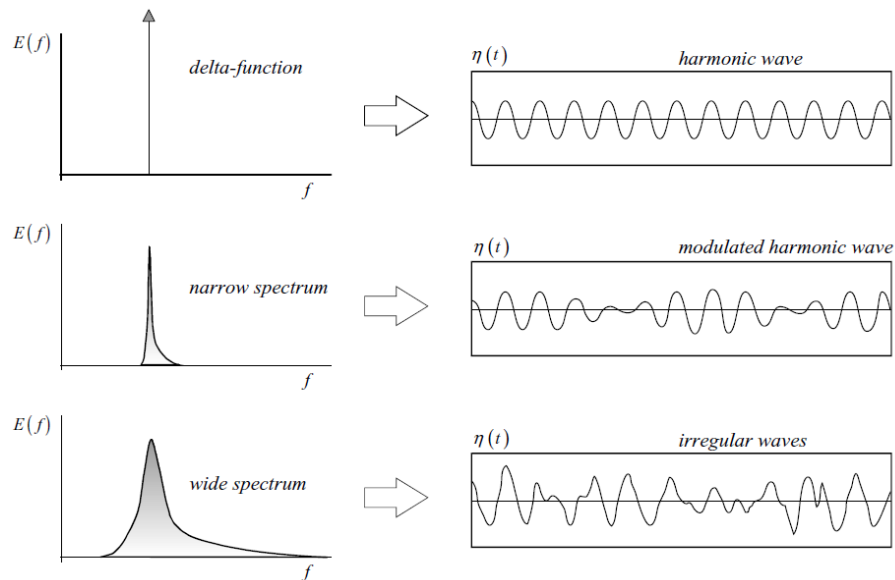


Figure 14: The (ir)regular character of the waves for three different widths of the spectrum.  
Source: Holthuijsen, 2007.

The total energy (i.e. summed over all components; per unit horizontal ocean surface area) is:

$$E_{total} = \rho g \eta^2 \quad (2.24)$$

Energy density spectrum is:

$$E_{energy}(f) = \rho g E_{variance}(f) \quad (2.25)$$

### 2.3.6.2 Relationship between wave spectra and wave heights

Estimation of the heights of representative waves from the wave spectrum is possible, first by obtaining representative value of the total wave energy  $m_0$  and integrating the directional wave spectrum in the full frequency from (Goda, 2000):

$$m_0 = \int_0^\infty \int_{-\pi/2}^{\pi/2} S(f, \theta) df d\theta \quad (2.26)$$

This integral is by definition of the wave spectrum equal to the variance of the surface elevation. Thus,

$$m_0 = \bar{\eta}^2 = \lim_{t_0 \rightarrow \infty} \frac{1}{t_0} \int_0^{t_0} \eta^2 dt \quad (2.27)$$

Where:  $m_0$  is zeroth-order moment of the variance density spectrum  $E(f)$  or total wave energy in  $[m^2, cm^2]$ . Value  $\eta_{rms}$  bears relationship to the heights of the representative waves when the wave height follows the Rayleigh distribution.

$$\eta_{rms} = \sqrt{\overline{\eta^2}} = \sqrt{m_0} \quad (2.28)$$

Where: root-mean-square (rms) is value of the surface elevation.  
 In particular:

$$H_{1/3} = 4,004\eta_{rms} = 4,004\sqrt{m_0} \quad (2.29)$$

$$H_{m0} \approx 4,0\sqrt{m_0} \text{ in deep water} \quad (2.30)$$

Wave heights observed in the sea tend to indicate a distribution slightly narrower than Rayleighan.

In the case of JONSWAP-type spectrum, the wave height ratios gradually increase toward those of the Rayleigh distribution as the peak enhancement factor  $\gamma$  becomes large.

Inversely, the estimation of significant wave height based on a given wave spectrum is always possible by evaluating the integral  $m_0$  with Eq. 2.26. Such operations for the wave height estimation from spectral information become necessary in the analysis of wave refraction, diffraction, etc., in which the transformation of the directional wave spectrum is principally computed (Goda, 2000).

### 2.3.6.3 Relationship between wave spectra and wave periods

The mean wave period defined by the zero-upcrossing method is given by the zeroth and second moments of the frequency spectrum as follows (Goda, 2000):

$$T = \sqrt{\frac{m_0}{m_2}}, \quad (2.31)$$

$$\text{Where: } m_2 = \int_0^\infty f^2 S(f) df \quad (2.32)$$

This relation is used when period is required from data of the wave spectrum. The main period parameter obtainable from a spectrum is the peak period  $T_p$  defined as the inverse of the peak frequency  $f_p$ . The period parameters defined by the zero-upcrossing (or zero-downcrossing) method such as  $T_{1/3}$  cannot be derived from a wave spectrum theoretically. Their relationship with  $T_p$  must be established on the basis of many field data or by means of numerical simulations. Spectral peak becomes sharper, the differences between various wave period parameters become small and these period approach the peak period  $T_p$  (Goda, 2000).

### 2.3.7 Analytical parametric frequency spectra functions

The characteristics of the frequency spectra of sea waves have been well established through analysis of a large number of wave records taken into various waters of the world. The spectra of fully developed wind waves, for example, can be approximated by the following standard formula:

$$S(f) = 0,257H_{1/3}^2 T_{1/3}^{-4} f^{-5} \exp [-1,03(T_{1/3}f)^{-4}] \quad (2.33)$$

Other formula of frequency spectrum is for example Pierson and Moskowitz (PM) formula. The PM spectrum describes a fully-developed sea with one principal parameter, the wind speed, and assumes that both the fetch and duration are infinite. This idealization is justified when wind blows over a large area at a constant speed without substantial change in its direction for tens of hours (Coastal Engineering Manual, 2002).

$$S(f) = 0,205H_{1/3}^2 T_{1/3}^{-4} f^{-5} \exp [-0,75(T_{1/3}f)^{-4}] \quad (2.34)$$

Eq. 2.33 and 2.34 are applied for the wind waves fully developed in the ocean.

Spectrum, which we used in the wave flume is called the JONSWAP spectrum. It is for fetch-limited seas and was obtained from the Joint North Sea Wave Project - JONSWAP (Hasselmann et al. 1973) and includes the wind speed as the parameter for the purpose of wave forecasting, but it can be rewritten in approximate form in terms of the parameters of wave height and period as follows:

$$S(f) = \beta_j H_{1/3}^2 T_p^{-4} f^{-5} \exp [-1,25(T_p f)^{-4}] \gamma^{\exp \left[ \frac{(T_p f - 1)^2}{2\sigma^2} \right]} \quad (2.35)$$

In which:

$$\beta_j = \frac{0,0624}{0,230 + 0,0336\gamma - 0,185(1,9 + \gamma)^{-1}} [1,094 - 0,01915 \ln] \quad (2.36)$$

$$T_p \cong \frac{T_{1/3}}{[1 - 0,132(\gamma + 0,2)^{-0,559}]} \quad (2.37)$$

$$\sigma = \begin{cases} \sigma_a: f \leq f_p \\ \sigma_b: f \geq f_p \end{cases} \quad (2.38)$$

$$\gamma = 1 \sim 7 \text{ (mean of 3,3)}, \sigma_a \cong 0,07, \sigma_b \cong 0,09 \quad (2.39)$$

The JONSWAP spectrum is characterized by a parameter  $\gamma$  which is called the peak enhancement factor; this controls the sharpness of the spectral peak. For  $\gamma=3.3$ , (this is the mean value determined for the North Sea), the peak value of the spectral density function becomes 2.1 times higher than of Eq. 2.34 for the same significant wave height and period.

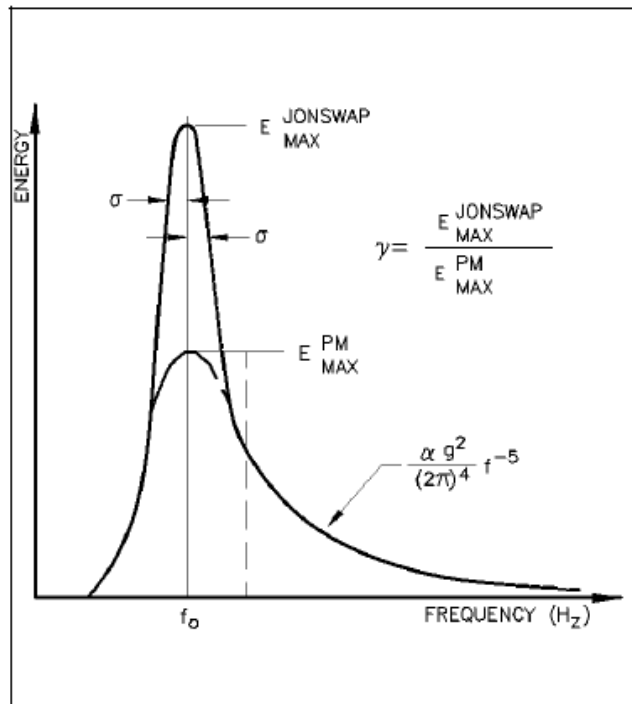


Figure 15: Comparison of the PM and JONSWAP spectrum.  
 Source: Coastal Engineering Manual, 2002.

JONSWAP spectrum is an extension of the PM spectra (Hasselmann et al., 1973), because PM did not consider the influence of nonlinear interactions between waves in their formula. The sea surface is never definitely formed, even if we say the wind is blowing steadily.

Actual wave spectra usually exhibit some deviations from these standard forms. In particular, when swell coexists with wind waves, a secondary peak appears at the frequency corresponding to the representative period of swell or wind waves, depending on their relative magnitudes. In some cases, not only bi-modal but also tri-modal frequency spectra can be observed.

## 2.4 Harbour hydrodynamics

### 2.4.1 Definition of harbour

Harbour is a sheltered part of a body of water deep enough to provide anchorage for ships or a place of shelter; refuge. The purpose of a harbour is to provide safety for boats and ships at mooring or anchor and to provide a place where upland activities can interface with waterborne activities. Harbours range in complexity from the basic harbour of refuge, consisting of minimal or no upland support and only moderate protective anchorage from storm waves to the most complex, consisting of commercial port facilities, recreational marinas, and fuel docks linked to the sea through extensive navigation channels and protective navigation structures (Coastal Engineering Manual, 2002).

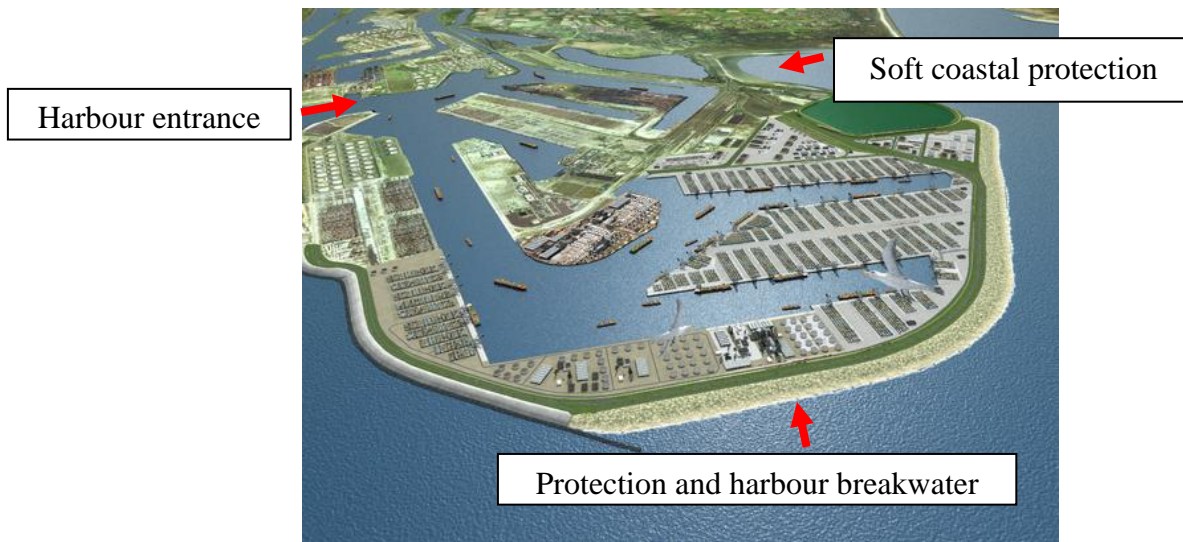


Figure 16: Harbour of Rotterdam.

Source: <http://www.rnw.nl/africa/bulletin/new-rotterdam-docks-change-dutch-coastline>, 16.06. 2012.

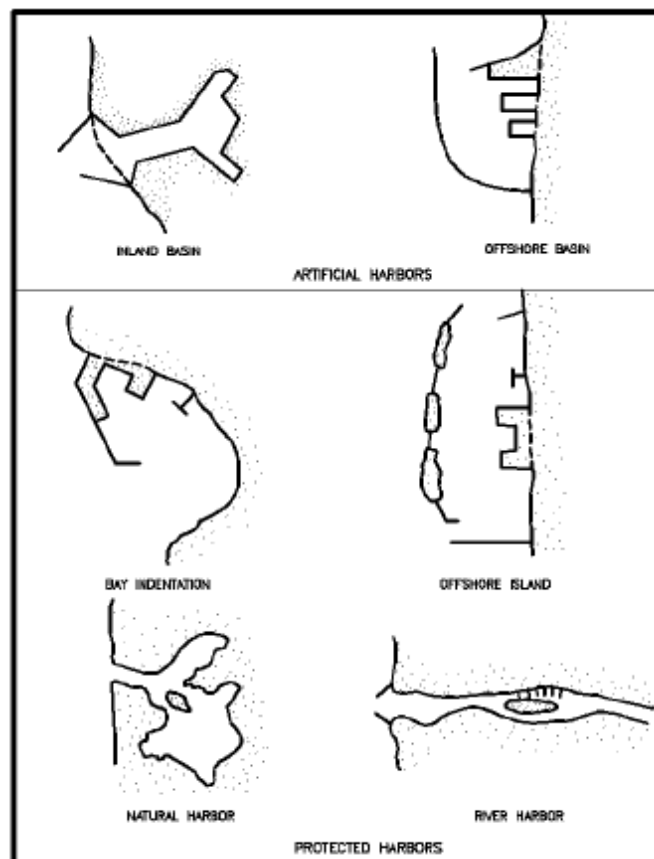


Figure 17: Harbour sitting classifications.  
 Source: Coastal Engineering Manual, 2002.

## 2.4.2 Wave transmission, reflection and breaking waves

### 2.4.2.1 Wave transmission

When waves interact with a structure, a portion of their energy will be dissipated, a portion will be reflected and, depending on the geometry of the structure, a portion of the energy may be transmitted past the structure.

In case of wave overtopping, large overtopping waves cause new waves behind the structure. It is usual for breakwaters and low-crested structures along the shore, where water is behind the structure and it is defined by the wave transmission coefficient:

$$K_t = \frac{H_t}{H_i} \quad (2.40)$$

Where  $H_t$  and  $H_i$  are the transmitted and incident wave heights. The limits of wave transmission are  $K_t = 0$  (no transmission, high crest and impermeable breakwater) and 1 (no reduction in wave height, conditions of missing breakwater). If a structure has its crest above water the transmission coefficient will never be larger than about 0.4 - 0.5.  $K_t$  represents the amount of incident wave energy transferred above and through the breakwater.

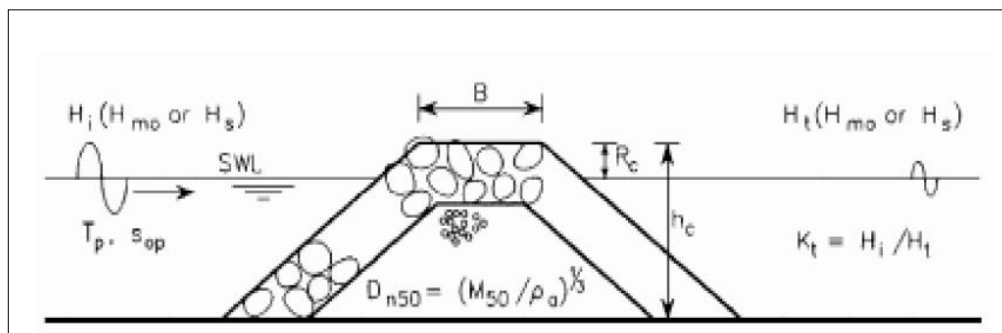


Figure 18: Parameters involved in wave transmission.

### 2.4.2.2 Wave reflection

If there is a change in water depth as a wave propagates forward, a portion of the wave's energy will be reflected. When a wave hits a vertical, impermeable, rigid surface-piercing wall, essentially all of the wave energy will reflect from the wall. On the other hand, when a wave propagates over a small bottom slope, only a very small portion of the energy will be reflected. The degree of wave reflection is defined by the reflection coefficient:

$$C_r = \frac{H_r}{H_i} \quad (2.41)$$

Where  $H_r$  and  $H_i$  are the reflected and incident wave heights.

Wave energy that enters a harbour must eventually be dissipated. This dissipation primarily occurs at the harbour interior boundaries (Coastal Engineering Manual, 2002).

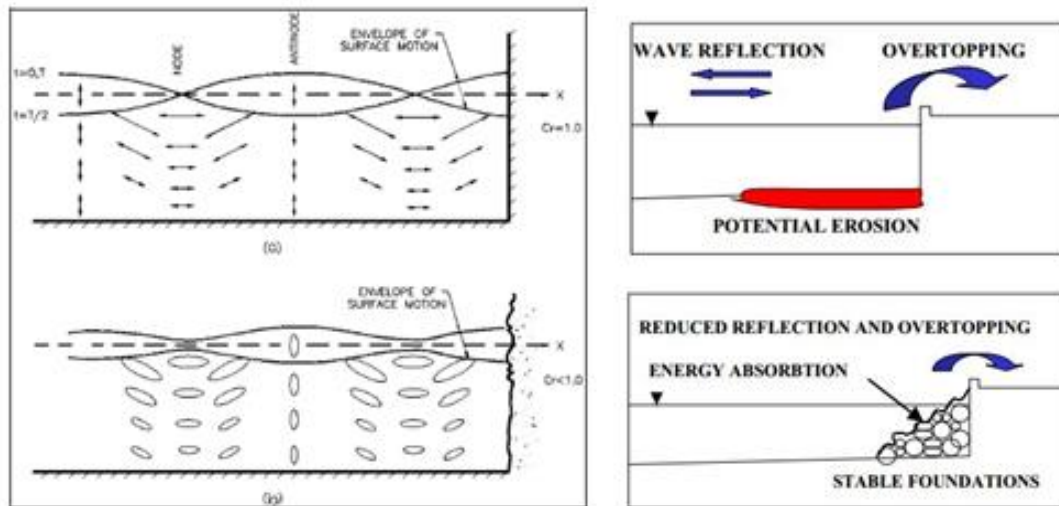


Figure 19: Complete and partial reflection and effects on overtopping.  
Source: Coastal Engineering Manual, 2002.

Figure 19 is a profile view of the water surface envelope positions for a wave reflecting from a wall that has a reflection coefficient equal to unity (i.e.,  $H_i = H_r$ ). The figure also shows the water particle paths at key points. At nodal points, water particle motions are horizontal and at antinodes, water particle motions are vertical.

### 2.4.2.3 Wave steepness and breaker parameter

Wave steepness is defined as the ratio of wave height  $H_{m0}$  to wave length  $L_0$ :

$$s_0 = \frac{H_{m0}}{L_0} \quad (2.42)$$

This will tell us something about the wave's history and characteristics. Generally a steepness of  $s_0=0.01$  indicates a typical swell sea and a steepness of  $s_0=0.04$  to  $0.06$  a typical wind sea. Swell sea are often associated with long period waves, where it is the period that becomes the main parameter that affects overtopping. The breaker parameter, Surf Similarity Parameter or Iribarren Number is defined as:

$$\xi_{m-1,0} = \frac{\tan \alpha}{(L_{m-1,0})^{1/2}} \quad (2.43)$$

Where  $\alpha$  is the slope of the front face of the structure and  $L_{m-1,0}$  being the deep water wave length  $gT_{m-1,0}^2/2\pi$  and  $H_{m0}$  is wave height. The combination of structure slope and wave steepness gives a certain type of wave breaking.

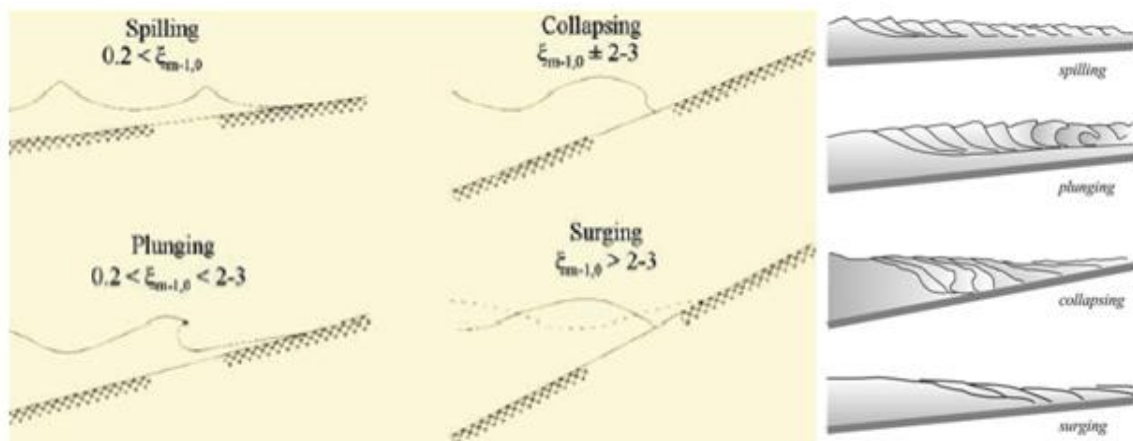


Figure 20: The four main types of breaking waves.  
Source: Pullen et al., 2007.

For  $\xi_{m-1,0} > 2 - 3$  waves are considered not to be breaking (surging waves), although they there may still be some breaking, and for  $\xi_{m-1,0} < 2 - 3$  waves are breaking. Waves on a gentle foreshore break as spilling waves and more than one breaker line can be found on such a foreshore. Plunging waves break with steep and overhanging fronts and the wave tongue will hit the structure or back washing water; an example is shown in Fig. 21 (left).



Figure 21: Plunging waves; for  $\xi_{m-1,0} < 2.0$  (left) and spilling waves on a beach; for  $\xi_{m-1,0} < 0.2$  (right).  
Source: Pullen et al., 2007.

The transition between plunging waves and surging waves is known as collapsing. The wave front becomes almost vertical and the water excursion on the slope (wave run-up + run down) is often largest for this kind of breaking.

## 2.5 Breakwaters

Breakwater is a structure that protects the area in its lee from wave attack.

Purpose of breakwaters:

- To provide shelter from the waves;
- Through this shelter, to manipulate the littoral transport conditions and thereby to trap some sand.

Types of breakwaters:

- Detached breakwaters

Breakwaters are completely isolated from the shoreline.

- Headland breakwaters
- Nearshore breakwaters

- Attached Breakwaters

Breakwaters can be connected to the shoreline.

- Low crested structure
- High crested structure
- Rubble mound structure
- Composite structure

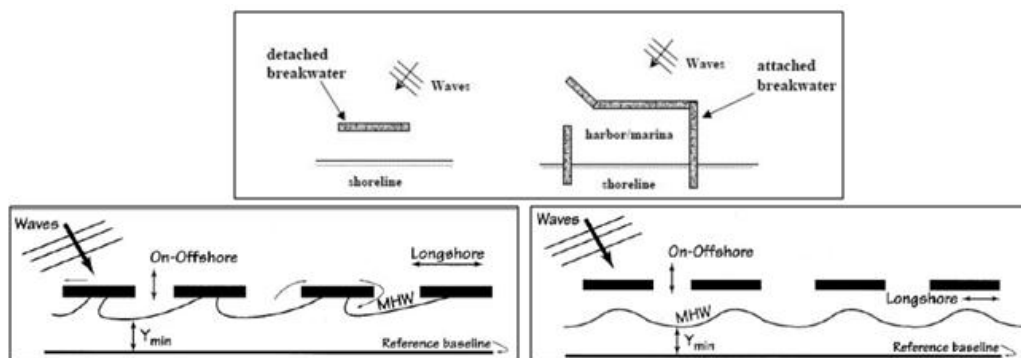


Figure 22: Detached and attached breakwaters (up), headland breakwaters (left) and nearshore breakwaters (right).

Source: [http://coastal.wru.edu.vn/Thu\\_vien/Mon\\_hoc/CTBVB/Chuong12%20-%20de%20chan%20song.pdf](http://coastal.wru.edu.vn/Thu_vien/Mon_hoc/CTBVB/Chuong12%20-%20de%20chan%20song.pdf), 20. 08. 2012.

- Using mass (caissons)
- Using a revetment slope (e.g. with rock or concrete armour units)
- Emerged breakwaters
- Submerged breakwaters
- Floating breakwaters.

## 2.5.1 Rubble mound breakwaters

The principal function of a rubble mound breakwater is to protect a coastal area from excessive wave action. The term “rubble” as used here includes rock, riprap and precast concrete armour units. Similarly, “armour unit” includes both rock and precast concrete units.

### 2.5.1.1 Cross section design

Rubble mound breakwaters are built up like filters. They consist of layers of stone. The center core of the breakwater is made up of quarry run rock of the most economically available size. The outside layer consists of large armour units that can be either rock or specially designed concrete units. This primary armour layer is intended to be statically stable with respect to the environmental conditions imposed on it (the waves and currents do not move the armour stones under design conditions). It is usual to build the primary armour layer roughly two unit diameters thick and to place the units randomly, meaning that they are not especially fitted together. If the armour units were placed directly over the core, the finer core material would be removed by the waves through the openings of the armour layer. It is therefore necessary to construct the breakwater as a filter of three or four layers so that the material from any layer is not removed through the layer above it. A typical example filter relationship to prevent removal of the lower material through the upper layer is:

$$D_{15} \text{ (upper layer)} < 5D_{85} \text{ (lower layer)} \quad (2.44)$$

Where  $D$  is the nominal size and  $D_{85}$  means that the nominal size of the sample is less than  $D_{85}$ .

For rock, the nominal armour unit diameter is defined as:

$$D_a = D_{50} = \left(\frac{M_a}{\rho_a}\right)^{1/3} \quad (2.45)$$

Where  $M_a$  is the armour unit mass and  $\rho_a$  is the armour density.

When a breakwater is built on erodible material, the toe filter is of particular interest. It is located where the largest stone (the primary armour) and the base on which the breakwater is built (often fine material such as sand) are adjacent to each other. To prevent removal of the base material through the armour, this toe filter also needs to be built up to several layers, but the layers must be compact so that the total depth of the filter remains small.

The toe filter is crucial to the operation of the breakwater. If it fails, the base material will be removed and the lowest armour stones will drop down into the resulting cavity and endanger the stability of the whole primary armour layer. If the breakwater is located in shallow water under breaking waves, the toe filter must be completely protected by the primary armour. It is also customary to use geotextiles in the toe filter and to dig down into the base material to make room for a toe filter of appropriate thickness.

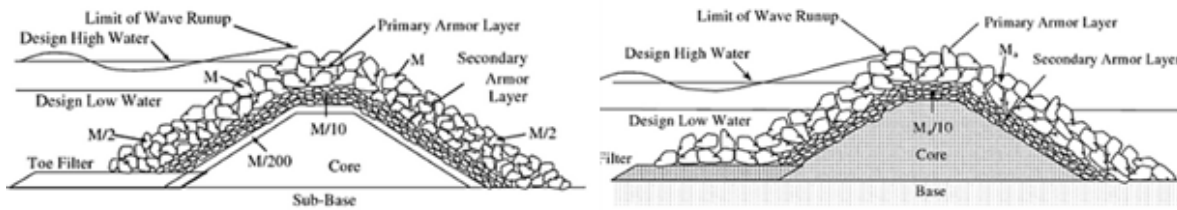


Figure 23: Rubble mound breakwater in deep water (left) and in shallow water (right).  
Source: Kamphuis, 2000.

## 2.5.2 Construction materials

### 2.5.2.1 Rock and concrete armour

Stable rock armour mass has traditionally been calculated with the Hudson formula (Kamphuis, 2000).

$$M_a = \frac{\rho_a H_{des}^3}{K_D \left(\frac{\rho_a}{\rho} - 1\right)^3 \cot \theta} = \frac{\rho_a H_{des}^3}{K_D \Delta_a^3 \cot \theta} \quad (2.46)$$

Where  $\rho_a$  is armour unit density,  $\rho$  is the fluid density,  $\theta$  is the angle of the front slope of the structure with respect to horizontal and  $\Delta_a$  is the relative underwater density of the armour.

$$\Delta_a = \frac{\rho_a - \rho}{\rho} = \frac{\rho_a}{\rho} - 1 \quad (2.47)$$

$K_D$  is an empirically determined damage coefficient. It is a function of all the variables involved in armour stability that are not included in Eq. 2.46, but primarily, it is a function of the type of armour, its shape, its location along the breakwater and the amount of damage considered to be acceptable.

Table 2: Published damage coefficients  $K_D$  (for rough angular armour stone rock, zero damage (Kamphuis, 2000)).

	Non-Breaking Waves	Breaking Waves
Structure Trunk	4,0	2,0
Structure Head	3,2	1,9

The term »zero damage« means that there is nominally no removal of the armour units from the face of the breakwater. We use  $K_D = 4$  for armour stone on a breakwater trunk. The same stone will be less stable on the head of a breakwater than on its trunk that is why we use the 20% decrease in  $K_D$  shown in Table 2. The uncertainties and hence the final construction costs, particularly for large and costly projects are usually reduced through physical model studies. Equation (2.46) can be rearranged as (Kamphuis, 2000):

$$N_s = \frac{H_{des}}{\Delta_a D_a} = (K_D \cot \theta)^3 \quad (2.48)$$

Where  $N_s$  is known as the stability number.

Armour units need not be rock. They can be manufactured out of concrete and a whole gallery of different units is available.

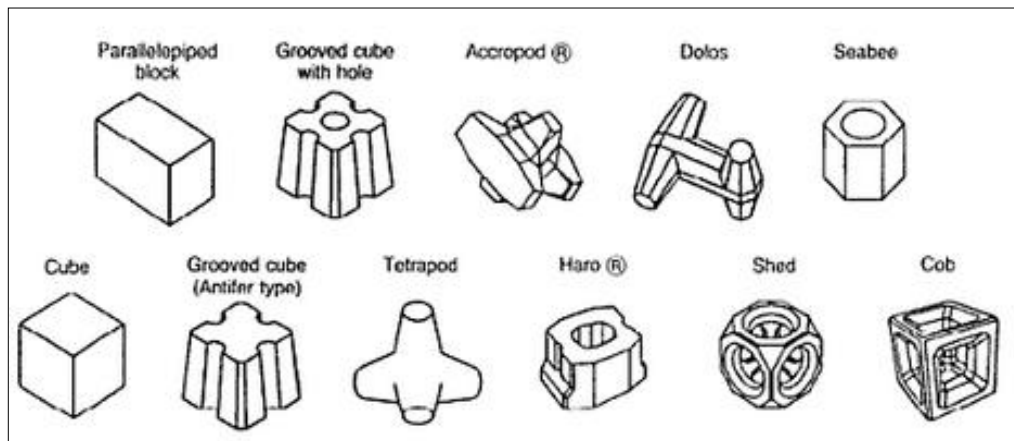


Figure 24: Sample concrete armour units.

Source: Kamphuis, 2000.

Sample published values of  $K_D$  for zero damage on a breakwater trunk are given in Table 2. The units still must primarily depend on their mass for stability. Prototype units with relatively thin members (such as Dolos) can break under the stresses imposed upon them. Armour unit strength was initially not simulated in hydraulic model tests and results showed Dolos to be very stable ( $K_D=32$ ) because of their interlocking. Conservative practice, based on field experience and additional model testing with Dolos that were scaled for strength, now recommended  $K_D= 16$  for Dolos.

Table 3: Damage coefficients concrete units, zero damage (Kamphuis, 2000).

Armour unit	$K_D$
Rock	4
Tetrapods	8
Tribars	10
Dolos	32(16)
Modified Cubes	7,5

Van der Meer presents a different expression for concrete units that he tested. For tests, which were limited to  $\theta = 1,5$  and for zero damage:

$$N_s = c_1 s_m^{c_2} \quad (2.49)$$

Where  $c_1$  and  $c_2$  are constants that depend on the type of unit as shown in Table 4.

Table 4: Van der Meer's coefficients (Kamphuis, 2000).

	$c_1$	$c_2$
Cubes	1	-0.1
Tetrapods	0.85	-0.2
Accropods	3.7	0

Table 5: Shape factor and porosity (Kamphuis, 2000).

	$k_a$	$e$
Rock	1	0.37
Modified Cubes	1.1	0.47
Tetrapods	1.04	0.50
Tribars	1.02	0.54
Dolos	0.94	0.56

### 2.5.2.1.1 Armour unit density

Armour unit size  $D_a$  varies inversely with underwater relative armour density  $\Delta_a$  in both the Hudson equation and the Van Meer equations. If concrete is used, it is possible to increase  $\rho_a$  substantially through to use of heavy aggregate, such as blast furnace slag. This is an effective method to reduce the required armour unit mass. For example, a relatively small increase in concrete density from a normal concrete ( $\rho_{a1}=2200 \text{ kg/m}^3$ ) to a heavier concrete ( $\rho_{a2}=2600 \text{ kg/m}^3$ ) results in a  $\Delta_{a1}=1.2$ , and therefore  $D_{a2}=0.75 D_{a1}$  or  $M_{a2}=0.42 M_{a1}$ , a reduction in armour mass of more than 50%.

### 2.5.2.2 Primary armour layer

On the seaward side, it is customary to extend the armour layer from the breakwater crest down to about  $1.5 H_s$  below the lowest water level. Because the wave action is less at greater depth, smaller armour units can be placed below  $-1.5 H_s$ . Figure 23 (left) indicates a preliminary size ( $M_a/2$ ). Preliminary armour is placed on the back of the structure down to the lowest water level, because overtopping waves will put severe down-slope stress on any armour covers the complete structure, including the toe filter.

The primary armour layer is usually placed in a double layer. Since the nominal armour unit size as defined in Eq. 2.45 is the size of a cube, a shape factor  $k_a$  is introduced to account for the shape of the unit as well as for its random placement. The armour layer thickness is therefore:

$$r_a = n_a k_a D_a \quad (2.50)$$

Usually  $n_a=2$ . Typical values of  $k_a$  are given in Table 6. The number of armour units required per unit length of the structure is:

$$N_a = \frac{A_a n_a k_a (1-e)}{D_a^2} \quad (2.51)$$

Where  $A_a$  is the surface area (per unit length of the breakwater) to be covered by the armour units and  $e$  is the porosity of the armour layer. The values in Eq. 2.51 are approximate. They depend heavily on the rock that comes out of the quarry and the methods and care of placement. Their values have a major influence on both the armour layer thickness and the number of units required (the cost of the armour layer). As a result it is virtually impossible to estimate numbers of armour units accurately, and this can cause major differences between estimated and real costs of armour in a design.

Table 6: Shape factor and porosity.

	$k_a$	E
<b>Rock</b>	1	0,37
<b>Modified Cubes</b>	1,1	0,47
<b>Tetrapods</b>	1,04	0,5
<b>Tribars</b>	1,02	0,54
<b>Dolos</b>	0,94	0,56

### 2.5.2.3 Breakwater crest

The crest of a rock armour breakwater is usually made up of the same rock as the rest of the armour layer and it is normally about three stones wide. The crest of a breakwater with concrete units is usually a monolithic cap unit, which provides support for the armour units (Fig. 25). This cap can carry traffic and infrastructure. Because the cap is impermeable, there is often concentrated damage at the interface between the cap and the concrete armour units. Since the uprush of the water cannot pass through the cap, it can only go up through the topmost primary armour units. The resulting high vertical fluid velocities will decrease the stability of the units near the cap so that they are easily displaced or broken.

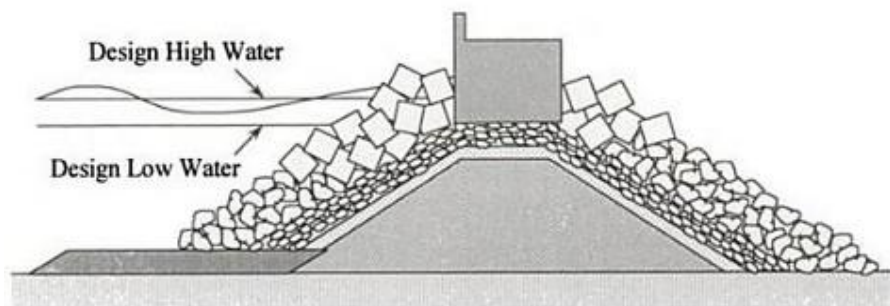


Figure 25: Artificial armour units with concrete cap.  
 Source: Kamphuis, 2000.

The first estimate of the design crest elevation of a rubble mound breakwater is the limit of run-up of the largest waves, superimposed on the highest water level. Such a crest height

would prevent all wave overtopping and as a result prevent any generation of waves behind the structure by overtopping and as a result prevent any generation of waves behind the structure by overtopping waves. The combination of safety in the harbour, negative esthetical impact and cost of the structure combine to determine the actual breakwater crest elevation. Wave run-up is the vertical distance above SWL reached by the waves. A relatively simple estimate of run-up (Kamphuis, 2000) is:

$$\frac{R_{2\%}}{H_s} = 1,5r_f\xi_p \text{ for } \xi_p < 2; \quad (2.52)$$

$$\frac{R_{2\%}}{H_s} = 3r_f \text{ for } \xi_p \geq 2; \quad (2.53)$$

Where  $R_{2\%}$  is the runup exceeded by 2% of the waves,  $r_f$  is a factor which takes into account friction, any horizontal berm sections in the front face, the angle of approach and whether the waves are short crested. The surf similarity parameter  $\xi_p$ , is based on the peak period of the wave spectrum. For a simple rock breakwater and with waves coming normal to the front face,  $r_f=0.5$ . For Dolos  $r_f=0.45$  and for a smooth slope,  $r_f=1.0$ . This factor  $r_f$  is reduced by incident wave angle. For the usual short crested waves  $r_f$  may be multiplied by a factor, which reduces linearly with a wave angle from  $0^\circ$  to 0.8 at  $90^\circ$ . A rubble mound breakwater will settle after its construction. If the base under the structure is solid (sand, gravel or rock), it is usual to add 0.3 m to the design crest elevation. For softer bases, the breakwater base is sometimes widened to decrease the stresses in the soil. Sometimes the soil directly below is expected to settle substantially, accurate settlement calculations are necessary to determine the design crest elevation with a little damage. Generally,  $N_s$  is less than 4.

## 2.6 Overtopping

### 2.6.1 Introduction of the phenomena

Wave overtopping is of principal concern for structures constructed primarily to defend against flooding or providing against coastal erosion, sometimes termed coast protection. Such structures may be built also to protect areas of water for ship navigation or mooring: ports, harbours or marinas; these are often formed as breakwaters or moles (Pullen et al., 2007).

Overtopping discharge occurs because of waves running up the face of a seawall. There are:

— “Green water” overtopping

In this case the wave run-up levels are high enough and water will reach and pass continuously over the crest of the wall. In cases where the structure is vertical, the wave impact against the wall and send a vertical plume of water over the crest.

— “White water” overtopping or spray

Occurs when waves break on the seaward face of the structure and produce non-continuous significant volumes of splash. These droplets may then be carried over the wall either under their own momentum or as a consequence of an onshore wind. It reduces visibility for driving, important on coastal highways, and will extend the spatial extent of salt spray effects such as damage to crops/vegetation, or deterioration of the building.

— “Light spray” is third less important form of overtopping

Is a method by which water may be carried over the crest in the form of spray generated by the action of wind on the wave crests immediately offshore of the wall. Even with strong wind the volume is not large and this spray will not contribute to any significant overtopping volume, however onshore winds may increase discharges under 1 l/s/m.

Defending against overtopping by rubble mound structures tend to be more common in areas where harder rock is available. Along urban frontages, especially close to ports, erosion or flooding defence structures may include vertical (or battered/steep) walls. Such walls may be composed of stone or concrete blocks, mass concrete, or sheet steel piles.

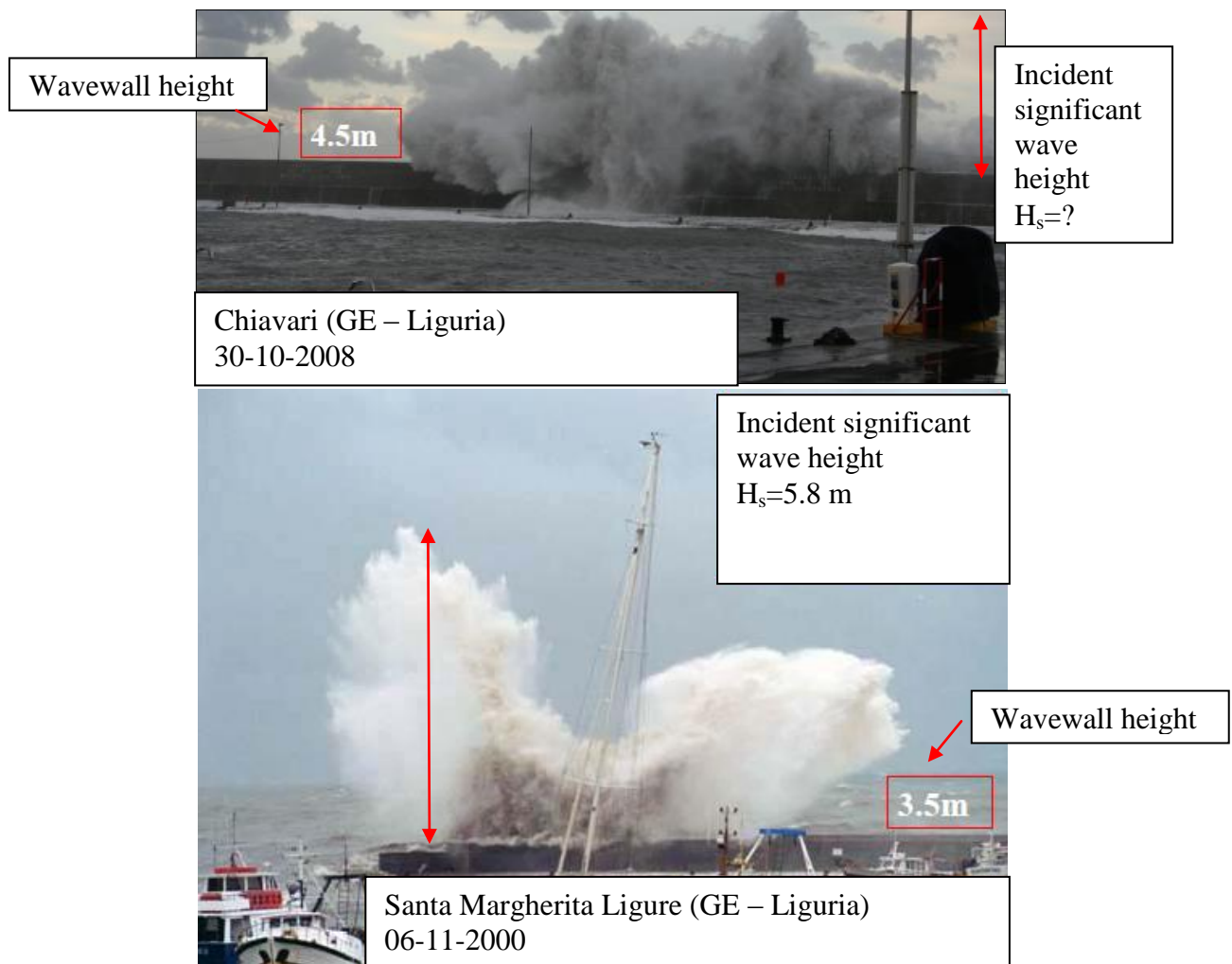


Figure 26: Examples of overtopping in Italy.  
Source: Cappiotti, 2011.

## 2.6.2 Overtopping parameters

Wave overtopping is affected by many factors; even a small modification of the geometry of a structure may change the amount of overtopping. Although there is no reliable conclusion, the increase of wave overtopping by an onshore wind is large when the quantity of overtopping is small and the wind effect decreases gradually as the overtopping rates increases. More accurate estimate of the overtopping rate should be determined through hydraulic model tests.

### 2.6.2.1 The wave height

The wave height in the wave run-up and wave overtopping formulae is the incident significant wave height  $H_{m0}$  at the toe of the structure, calls the spectral wave height:

$$H_{m0} = 4(m_0)^{1/2} \quad (2.54)$$

### 2.6.2.2 The wave period

The wave period used for some wave run-up and overtopping formulae is the spectral period:

$$T_{m-1.0} (=m_{-1}/m_0) \quad (2.55)$$

This period gives more weight to the longer periods in the spectrum than an average period and, independent of the type of spectrum, gives similar wave run-up or overtopping for the same values of  $T_{m-1.0}$  and the same wave heights. In this way, wave run-up and overtopping can be easily determined for double-peaked and ‘flattened’ spectra, without the need for other difficult procedures. Vertical and steep seawalls often use the  $T_{m0,1}$  or  $T_m$  wave period.

### 2.6.2.3 Permeability, porosity and roughness

— Roughness,

on the slope dissipates wave energy during wave run-up and will therefore reduce wave overtopping. Roughness is created by irregularly shaped block revetments or artificial ribs or blocks on a smooth slope.

— Porosity,

is defined as the percentage of voids between the units or particles. For rock, concrete armour an also sand the porosity may range roughly between 30 – 55%. But regarding this, still the behaviour of waves on a sand beach or a rubble mound slope is different.

— Permeability,

Run-up and wave overtopping are dependent on the permeability of the core. The armour of rubble mound slopes is very permeable and waves will easily penetrate between the armour

units and dissipate energy. This becomes more difficult for the underlayer and certainly for the core of the structure. Difference is made between “impermeable under layers or core” and a “permeable core”. In both cases the same armour layer is present, but the structure and underlayers differ. A structure with a “permeable core” has an under layer or large rock (about one tenth of the weight of the armour), sometimes a second under layer of smaller rock and then the core of still smaller rock. Here the up-rushing waves can penetrate into armour layer and will then sink into the under layers and core. A structure with an “impermeable core” can be covered by armour layer of rock. The under layer is often small and thin and placed on a geotextile. Underneath the geotextile sand or clay may be present, which is impermeable for up-rushing waves.

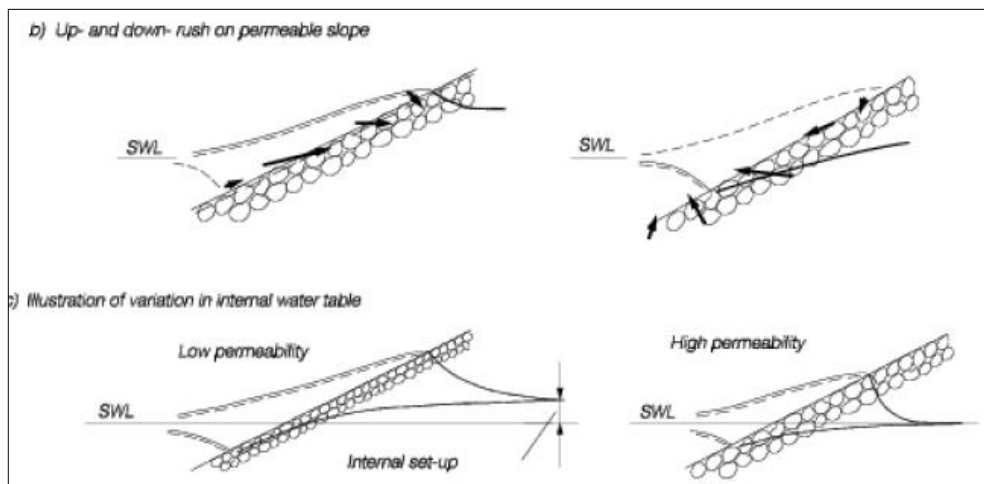


Figure 27: Effect of permeability.  
Source: Hughes, 2002.

#### 2.6.2.4 Toe of structure

Mostly, the toe of structure lies where the foreshore meets the front slope of the structure or if present, at the rubble mound toe in front of it.

It is possible that a sandy foreshore varies with season and even under severe wave attack. Toe levels may therefore vary during a storm, with maximum levels of erosion occurring during the peak of the tidal/surge cycle. The wave height that is always used in wave overtopping calculations is the incident wave height at the toe.

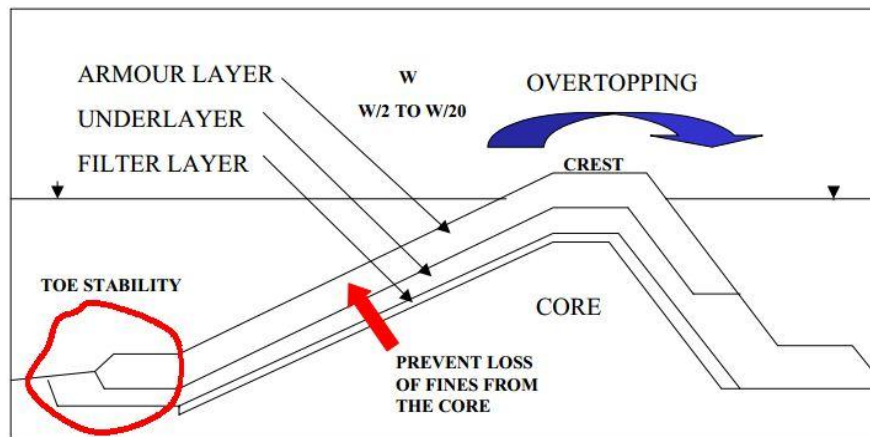


Figure 28: Toe of structure.  
Source: Hughes, 2002.

### 2.6.2.5 The foreshore

The foreshore is the section in front of the dike and can be horizontal or up to a maximum slope of 1:10. The foreshore can be deep, shallow or very shallow. If the water is shallow or very shallow then shoaling and depth limiting effects will need to be considered so that the wave height at the toe; or end of the foreshore; can be considered. A foreshore is defined as having a minimum length of one wavelength  $L_o$ . In cases where a foreshore lies in very shallow depths and is relatively short, then the methods outlined should be used. Waves break and the wave height decreases (by 50 % or more) at the shallow foreshore, but the wave spectrum retain more or less the shape of the incident wave spectrum. At a very shallow foreshore the spectral shape changes drastically and hardly any peak can be detected (flat spectrum). As the waves become very small due to breaking many different wave periods arise.

### 2.6.2.6 Slope

Part of a structure is defined as a slope if the slope of that part lies between 1:1 and 1:8. These limits are also valid for an average slope, which is the slope that occurs when a line is drawn between  $-1.5 H_{m0}$  and  $+Ru_{2\%}$  in relation to the still water line and berms are not included.

### 2.6.2.7 Berm

A berm is a part of a structure profile in which the slope varies between horizontal and 1:15. The position of the berm in relation to the SWL is determined by the depth,  $dh$ , the vertical distance between the middle of the berm and the SWL. The width of a berm,  $B$ , may not be greater than one-quarter of a wavelength, i.e.,  $B < 0,25 L_o$ .

### 2.6.2.8 Crest freeboard and armour freeboard and width

The crest height of a structure is defined as the crest freeboard,  $R_c$ , and has to be used for wave overtopping calculations. It is actually the point on the structure where overtopping water can no longer flow back to the seaside. The height (freeboard) is related to SWL. For rubble mound structures, it is often the top of a crest element and not the height of the rubble mound armour.

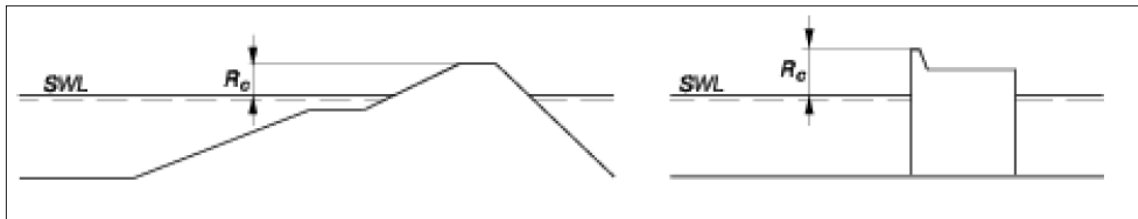


Figure 29: Definition of freeboard for different constructions.  
 Source: Hughes, 2002.

### 2.6.3 Wave overtopping discharge

Wave overtopping is the mean discharge per linear meter of width,  $q$ , for example in  $\text{m}^3/\text{s}/\text{m}$  or in  $\text{l}/\text{s}/\text{m}$ . Usually overtopping discharges are calculated in  $\text{m}^3/\text{s}/\text{m}$ , unless otherwise stated; it is more convenient to multiply by 1000 and quote the discharge in  $\text{l}/\text{s}/\text{m}$ . In reality, there is no constant discharge over the crest of a structure during overtopping. The process of wave overtopping is very random in time and volume. The highest wall will push a large amount of water over the crest in a short period of time, less than a wave period. Lower waves will not produce any overtopping.

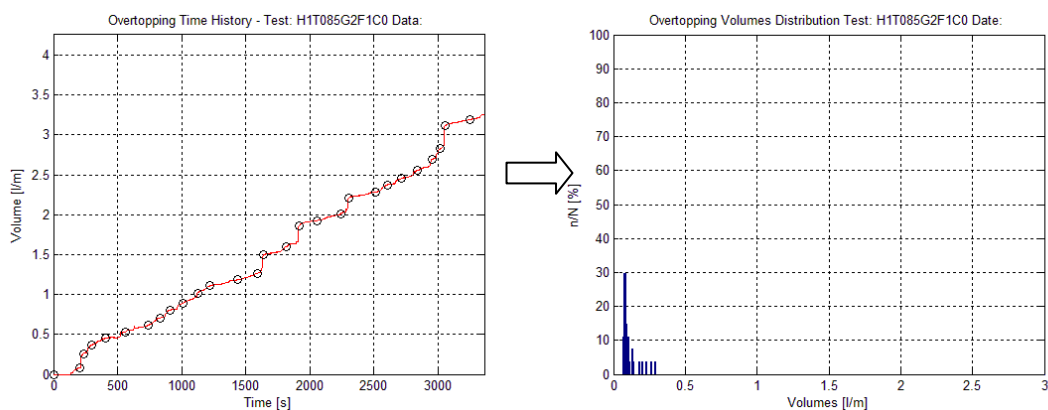


Figure 30: Example of wave overtopping measurements (left: Cumulative overtopping in time history (l/m), right: Overtopping volumes distribution), showing the random behavior.

Fig. 30 shows an example of our wave overtopping measurements. The graph shows 1 hour (55.5 min for tests with wave height H1 and 51 min for tests with H2) long measurements. The graph on the right clearly shows the irregularity of wave overtopping volumes. The right

graph gives the cumulative overtopping as it was measured in the overtopping tank. Individual overtopping volumes can be distinguished, unless a few overtopping waves come in one wave group.

Still a mean overtopping discharge is widely used as it can easily be measured and also classified:

$q < 0,11$  l/s per m: Insignificant with respect to strength of crest and rear of structure.

$q = 1$  l/s per m: On crest and inner slopes grass and/or clay may start to erode.

$q = 10$  l/s per m: Significant overtopping for dikes and embankments. Some overtoppings for rubble mound breakwaters.

$q = 100$  l/s per m: Crest and inner slopes of dikes have to be protected by asphalt or concrete; for rubble mound breakwaters transmitted waves may be generated.

#### 2.6.4 Wave overtopping volumes

A mean discharge does not yet describe how many waves will overtop and how much water will be overtopped in each wave. The volume of water,  $V$ , which comes over the crest of a structure, is given in  $m^3$  per wave per m width. Generally, most of the overtopping waves are fairly small, but a small number gives significantly larger overtopping volumes (see Fig. 30). The maximum volume overtopped in a sea state depends on the mean discharge  $q$ , on the storm duration and the percentage of overtopping waves. Longer storm duration gives more overtopping waves, but statistically, also a larger maximum volume. Many small overtopping waves (like for river dikes or embankments) may create the same mean overtopping discharge as a few large waves for rough sea conditions. The maximum volume are however, much larger for rough sea conditions with large waves. Traditionally, for a designing, it is used "Average capacity overflow" [ $m^3/s/m$ ] and its tolerable limits. More recently, in research, the interest is on "Single volumes overflow or wave-by-wave overtopping volume" [ $m^3/m$ ] and its tolerable limits.

#### 2.6.5 Tolerable discharges

Most sea defence structures are constructed primarily to limit overtopping volumes that might cause flooding. But there are also sea defences that protect people living, working or enjoying themselves, designers and owners of these defences must, however, also deal with potential hazards from overtopping. On average, approximately 2-5 people are killed each year of Italy and UK through wave action, chiefly on seawalls and similar structures. It is often helpful to analyse direct wave and overtopping effects, and their consequences under four general categories:

- a) Direct hazard of injury or death to people immediately behind the defence;
- b) Damage to property, operation and/or infrastructure in the area defended, including loss of economic, environmental or other resource, or disruption to an economic activity or process.

c) Damage to defence structure(s), either short-term or longer-term, with the possibility of breaching and flooding.

d) Low depth flooding (inconvenient but not dangerous).

The character of overtopping flows or jets, and the hazards they cause, also depend upon the geometry of the structure and of the immediate hinterland behind the seawall crest, and the form of overtopping.

### 2.6.5.1 Wave overtopping processes and hazards

Under most forms of wave attack, waves tend to break before or onto sloping embankments with the overtopping process being relatively gentle. Relatively few water levels and wave conditions may cause “impulsive” breaking where the overtopping flows are sudden and violent. Conversely, steeper, vertical or compound structures are more likely to experience intense local impulsive breaking, and may overtop violently and with greater velocities. The form of breaking will therefore influence the distribution of overtopping volumes and their velocities, both of which will impact on the hazards that they cause.



Figure 31: Left: Harbour Rapallo during wave attack on the 6th Nov 2000. Right: Damaged harbour Rapallo after the wave attack.

Source: Cappiotti, 2000.

### 2.6.5.2 Return periods of overtopping hazards

Return periods at which overtopping hazards are analysed, and against which a defence might be designed, may be set by national regulation or guidelines. As with any area of risk management, different levels of hazard are likely to be tolerated at inverse levels of probability or return period. Guidance on example return periods used in evaluating levels of protection suggest example protection levels versus return periods as shown in Table 7. In practice, some of these return periods may be regarded as too short. National guidelines have recommended lower risk, e.g. a low probability of flooding in UK is now taken as <0.1 % probability (1:1000 year return) and medium probability of sea flooding as between 0.5 and 0.1 % (1:200 to 1:1000 year return). Many existing sea defences in the UK however offer levels of protection far lower than these.

Table 7: Hazard type (Pullen et al., 2007).

Hazard type and reason	Design life	Level of Protection <sup>(1)</sup>
	(years)	(years)
Temporary or short term measures	1–20	5–50
Majority of coast protection or sea defence walls	30–70	50–100
Flood defences protecting large areas at risk	50–100	100–10,000
Special structure, high capital cost	200	Up to 10,000
Nuclear power stations etc.	–	10,000

<sup>(1)</sup> Note: Total probability return period

### 2.6.5.3 Tolerable mean discharges of overtopping

Tests on the effects of overtopping on people suggest that information on mean discharges alone may not give reliable indicators of safety for some circumstances, and that maximum individual volumes may be better indicators of hazard than average discharges.

The volume (and velocity) of the largest overtopping event can vary significantly with wave condition and structure type, even for a given mean discharge. Hazardous effect on overtopping waters reduces with the distance away from the defence line, so effective overtopping discharge at  $x$  (over a range 5–25 m),  $q_{effective}$  is given by:

$$q_{effective} = q_{seawall} x \quad (2.56)$$

The overtopping limits suggested in Table 8 to Table 11 therefore derive from a generally precautionary principle informed by previous guidance and by observations and measurements made by the CLASH partners and other researchers.

Table 8: Limits for overtopping for pedestrians (Pullen et al., 2007).

Hazard type and reason	Mean discharge	Max volume <sup>(1)</sup>
	$q$ (l/s/m)	$V_{max}$ (l/m)
Trained staff, well shod and protected, expecting to get wet, overtopping flows at lower levels only, no falling jet, low danger of fall from walkway	1–10	500 at low level
Aware pedestrian, clear view of the sea, not easily upset or frightened, able to tolerate getting wet, wider walkway <sup>(2)</sup> .	0.1	20–50 at high level or velocity

<sup>(1)</sup> Note: These limits relate to overtopping velocities well below  $v_c \approx 10$  m/s. Lower volumes may be required if the overtopping process is violent and/or overtopping velocities are higher.

<sup>(2)</sup> Note: Not all of these conditions are required, nor should failure of one condition on its own require the use of a more severe limit.

Limits for pedestrians in Table 8 show a logical sequence, with allowable discharges reducing steadily as the recipient's ability or willingness to anticipate or receive the hazard reduces.

Table 9: Limits for overtopping for vehicle (Pullen et al., 2007).

Hazard type and reason	Mean discharge	Max volume
	q (l/s/m)	V <sub>max</sub> (l/m)
Driving at low speed, overtopping by pulsating flows at low flow depths, no falling jets, vehicle not immersed	10–50 <sup>(1)</sup>	100–1,000
Driving at moderate or high speed, impulsive overtopping giving falling or high velocity jets	0.01–0.05 <sup>(2)</sup>	5–50 <sup>(2)</sup> at high level or velocity

<sup>(1)</sup> Note: These limits probably relate to overtopping defined at highway.

<sup>(2)</sup> Note: These limits relate to overtopping defined at the defence, but assumes the highway to be immediately behind the defence.

Table 10: Limits for overtopping for property behind the defence (Pullen et al., 2007).

Hazard type and reason	Mean discharge	Max volume
	q (l/s/m)	V <sub>max</sub> (l/m)
Significant damage or sinking of larger yachts	50	5,000–50,000
Sinking small boats set 5–10 m from wall. Damage to larger yachts	10 <sup>(1)</sup>	1,000–10,000
Building structure elements	1 <sup>(2)</sup>	~
Damage to equipment set back 5–10 m	0.4 <sup>(1)</sup>	~

<sup>(1)</sup> Note: These limits relate to overtopping defined at the defence.

<sup>(2)</sup> Note: This limit relates to the effective overtopping defined at the building.

Table 11: Limits for overtopping for damage to the defence crest or rear slope (Pullen et al., 2007).

Hazard type and reason	Mean discharge
	q (l/s/m)
<b>Embankment seawalls/sea dikes</b>	
No damage if crest and rear slope are well protected	50–200
No damage to crest and rear face of grass covered embankment of clay	1–10
No damage to crest and rear face of embankment if not protected	0.1
<b>Promenade or revetment seawalls</b>	
Damage to paved or armoured promenade behind seawall	200
Damage to grassed or lightly protected promenade or reclamation cover	50

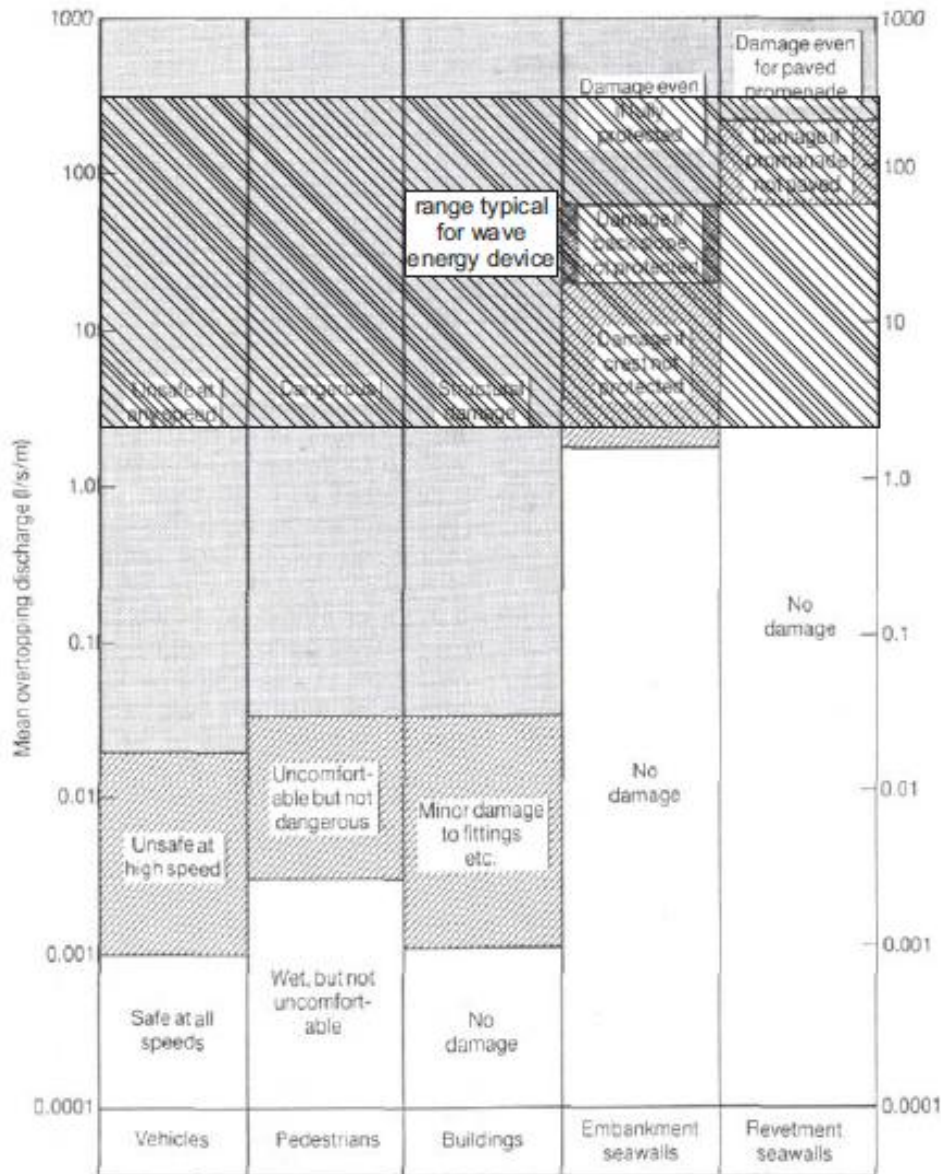


Figure 32: Criteria for critical overtopping discharges. Source: Kofoed, 2002.

### 2.6.6 Prediction of overtopping

Prediction of water levels is extremely important for prediction of wave run-up levels or wave overtopping, which are often used to design the required crest level of a flood defence structure or breakwater. Moreover, in shallow areas the extreme water level often determines the water depth and thereby the upper limit for wave heights.

Extreme water levels in design or assessment of structures may have the following components:

- Mean sea level (increasing due to global warming + 0.2 m to more than + 1.0 m by 2050),
- Astronomical tide,
- Surges related to (extreme) weather conditions and
- High river discharges (Pullen et al., 2007).

### 2.6.6.1 Analytical models

Analytical methods use a simplified representation of the physics of the process presented in (usually dimensionless) equations to relate the main response parameters (overtopping discharge etc.) to key wave and structure parameters. The form and coefficients of the equations are adjusted to reproduce results from physical model (or field) measurements of waves and overtopping (Pullen et al., 2007).

The main parameter in the overtopping process is the mean overtopping discharge  $q$  ( $\text{m}^3/\text{s}$  per m width or in practical applications l/s per m width), which is easy to measure in a laboratory wave flume or basin. Most of the other parameters are in some way related to this overtopping discharge. Very often the empirical methods or formulae are applicable for typical structures only, like smooth slopes (dikes, sloping seawalls), rubble mound structures or vertical structures (caissons) or walls.

The principal formula used for wave overtopping is (Pullen et al., 2007):

$$\frac{q}{\sqrt{gH_{m0}^3}} = a \exp\left(-\frac{bR_c}{H_{m0}}\right) \quad (2.57)$$

It is an exponential function with the dimensionless overtopping discharge  $q/(H_{m0}^3)^{1/2}$  and the relative crest freeboard  $R_c/H_{m0}$ . This type of equation shown in a log-linear graph gives a straight line, which makes it easy to compare the formulae for various structures. For easy comparison of different structures, like smooth and rubble mound sloping structures and vertical structures for pulsating and impulsive waves, some simplifications will be assumed.

In order to simplify the smooth structure no berm is considered ( $\gamma_b=1$ ), only perpendicular wave attack is present ( $\gamma_\beta=1$ ), and no vertical wall on top of the structure is present ( $\gamma_v=1$ ). As a smooth structure is considered also,  $\gamma_f = 1$ . This limits the structure to a smooth and straight slope with a perpendicular wave attack. The slope angles considered for a smooth slopes are  $\cot\alpha = 1$  to 8, which means from very steep to very gentle. If relevant a wave steepness of  $s_o = 0.04$  (steep storm waves) and 0.01 (long waves due to swell or wave beraking) will be considered. The same equation as for smooth sloping structures is applicable for rubble mound slopes, but now with a roughness factor of  $\gamma_f = 0.5$ , simulating a rock structure. Rubble mound structures are often steep, but rock slopes may also be gentle. Therefore slope angles with  $\cot\alpha = 1.5$  and 4.0 are considered.

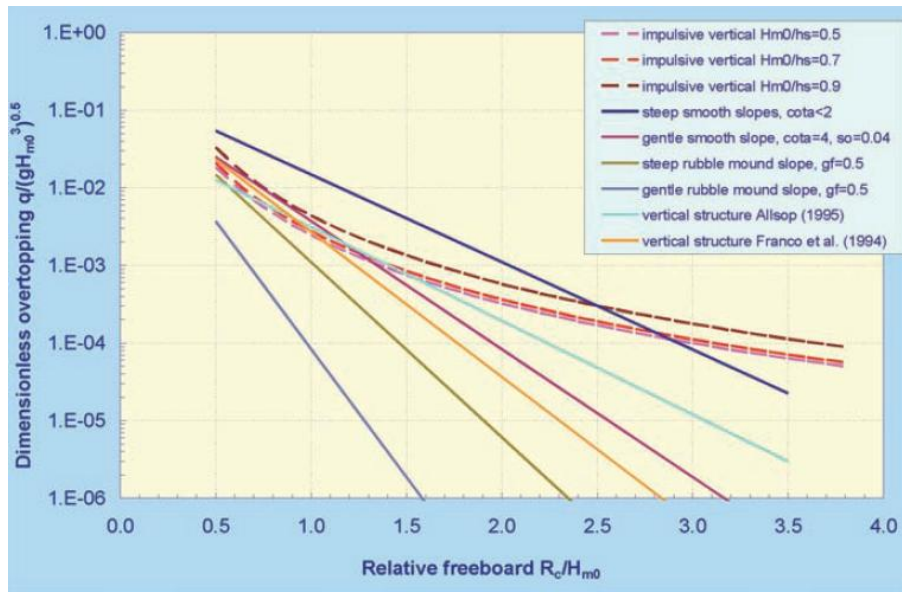


Figure 33: Comparison of wave overtopping formulae for various kinds of structures. Source: Pullen et al., 2007.

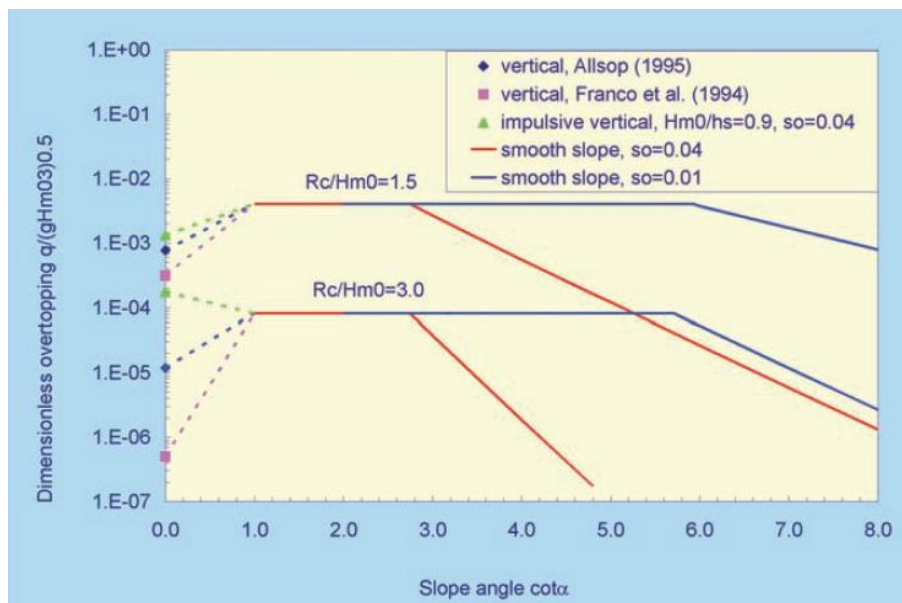


Figure 34: Comparison of wave overtopping as function of slope angle. Source: Pullen et al., 2007.

Fig. 34 shows the influence of the slope angle on wave overtopping by comparing various structures. A vertical structure means  $\cot\alpha = 0$ . Steep smooth structures can roughly be described by  $1 \leq \cot\alpha \leq 3$ . Battered walls have freeboards  $0 \leq \cot\alpha \leq 1$ . Gentle slopes have roughly  $\cot\alpha \geq 2$  or 3. Fig. 34 shows curves for two relative freeboards:  $R_c/H_{m0} = 1.5$  &  $3.0$ . Steep slopes give the largest overtopping, which reduces for gentler slopes; for a given wave condition and water level. Vertical slopes give less overtopping than steep smooth slopes, except for a high vertical structure under impulsive conditions.

A number of different methods may be available to predict of particular structures (usually simplified sections) under given wave conditions and water levels. In theory, an analytical method can be used to relate the driving process (waves) and the structure to the response through equations based directly on a knowledge of the physics of the process. It is however extremely rare for the structure, the waves and the overtopping process to all be so simple and well-controlled that an analytical method on its own can give reliable predictions. The primary predictions methods are therefore based in empirical methods that relate the overtopping response (usually mean overtopping discharge) to the main wave and structure parameters.

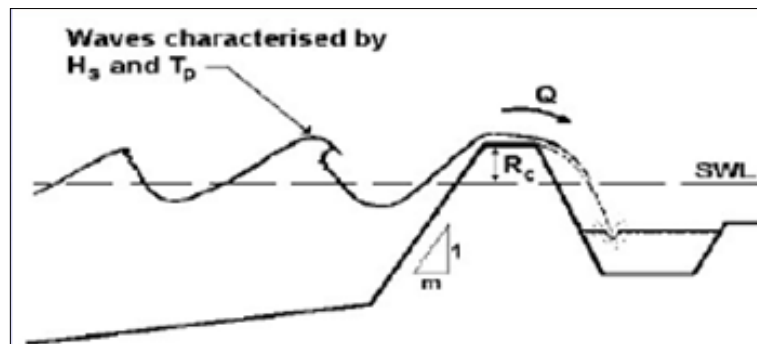


Figure 35: Waves characterized by  $H_s$  and  $T_p$ .  
 Source: Pullen et al., 2007.

Experimental evidence has led to the definition of two different "analytical models" one for surging and one for plunging waves.

$$\frac{q}{\sqrt{gH_{m0}^3}} = \frac{0,067}{\sqrt{\tan\alpha}} \gamma_b \xi_{m-1,0} \exp\left(-4,3 \frac{R_c}{\xi_{m-1,0} H_{m0} \gamma_b \gamma_f \gamma_\beta \gamma_v}\right) : \text{plunging} \quad (2.58)$$

With a maximum of:

$$\frac{q}{\sqrt{gH_{m0}^3}} = 0,2 \exp\left(-2,3 \frac{R_c}{H_{m0} \gamma_f \gamma_\beta}\right) : \text{surging} \quad (2.59)$$

$\gamma_b$ =influence factor for a berm [-],

$\gamma_f$ =influence factor for a roughness elements on a slope [-],

$\gamma_\beta$ =influence factor for oblique wave attack [-].

Furthermore it was observed a dependence of intensity of overtopping depending on the conditions of wave breaking on the seabed in front of the breakwater. Two formulations are applicable only to  $\xi_{m-1,0} < 5$ .

In case of very intense breaking in the seabed in front of the breakwater, wave spectrum is relatively flat and without a significant peak. In this case the long waves influence the breaking parameter, which is calculated as  $\xi_{m-1,0}$ . Overtopping is much more abundant and the formula changes as following:

For very shallow seabed:  $\xi_{m-1,0} > 5-7$

$$\frac{q}{\sqrt{gH_{m0}^3}} = 0,21 \exp\left(-\frac{R_c}{\gamma_f \gamma_\beta H_{m0} (0,33 + 0,22 \xi_{m-1,0})}\right) \quad (2.60)$$

### 2.6.6.2 Wave-by-wave overtopping volumes

#### 2.6.6.2.1 Wave run-up and number of overtopping waves

This method gives a formula for the run-up distribution as a function of wave conditions, slope angle and permeability of the structure. The easiest way to calculate run-up (or overtopping percentage) different from 2 % is to take the 2 %-value and assume a Rayleigh distribution. The probability of overtopping  $P_{ov} = N_{ow}/N_w$  (the percentage is simply 100 times larger) can be calculated by:

$$P_{ov} = \frac{N_{ow}}{N_w} = \exp\left[-\left(\sqrt{-\ln 0,02} \frac{R_c}{R_{u,2\%}}\right)^2\right] \quad (2.61)$$

Equation 2.61 can be used to calculate the probability of overtopping, given a crest freeboard  $R_c$  or to calculate the required crest freeboard, given an allowable probability or percentage of overtopping waves. The percentage is not the same as the number of overtopping waves or overtopping percentage. The run-up is always a point on a straight slope, where for a rock slope or armoured mound the overtopping is measured some distance away from the seaward slope and on the crest, often behind a crown wall, Fig. 36 gives the difference. This means that Equation 2.61 gives an over estimation of the number of overtopping waves.

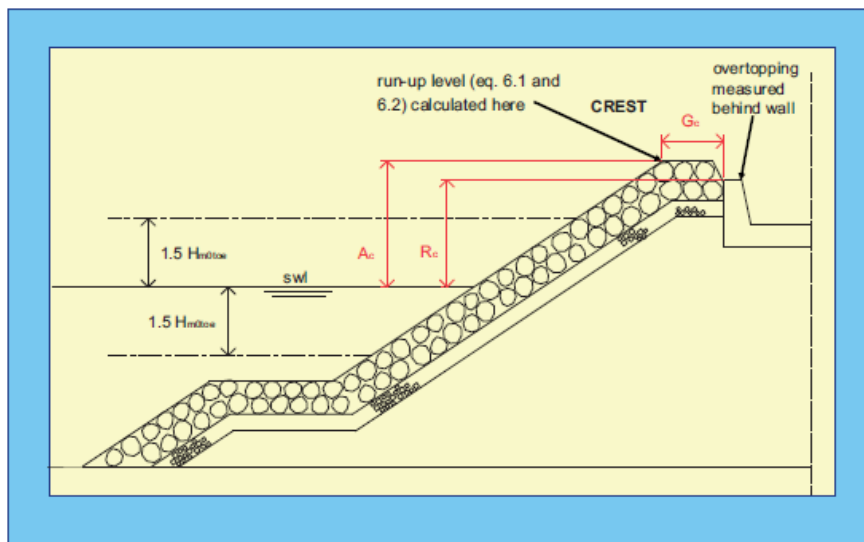


Figure 36: Run-up level and location for overtopping differ.  
Source: Pullen et al., 2007.

Fig. 36 shows measured data for rubble mound breakwaters armoured with Terapods, Acropode™ or a single layer of cubes (Pullen et al., 2007) for tests performed at Delft Hydraulics. Equation 2.61 can be used to predict the number or percentage of overtopping waves or to establish the armour crest level for an allowable percentage of overtopping waves.

$$P_{0v} = \frac{N_{0w}}{N_w} = \exp \left[ - \left( \frac{A_c D_n}{0,19 H_{m0}^2} \right)^{1,4} \right] \quad (2.62)$$

Equation 2.61 will come to more overtopping waves than 2.62. Both estimations together give a designer enough information to establish the required crest height of a structure given an allowable overtopping percentage.

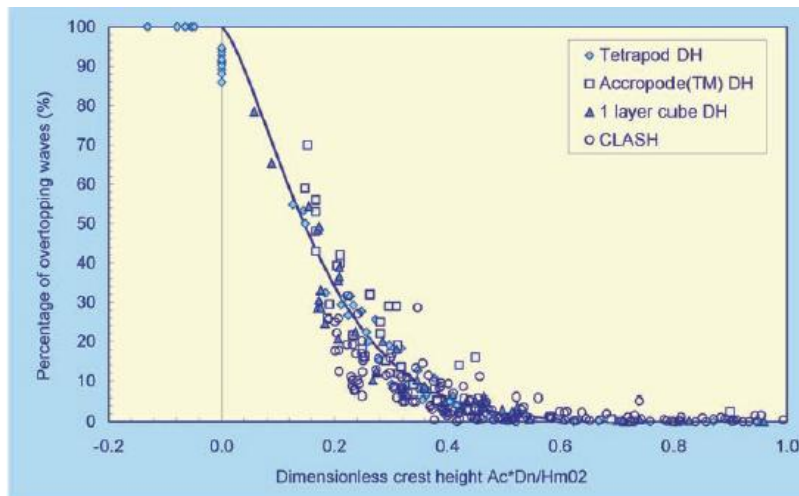


Figure 37: Percentage of overtopping waves for rubble mound breakwaters as a function of relative (Armour) crest height and armour size ( $R_c \leq A_c$ ).  
 Source: Pullen et al., 2007.

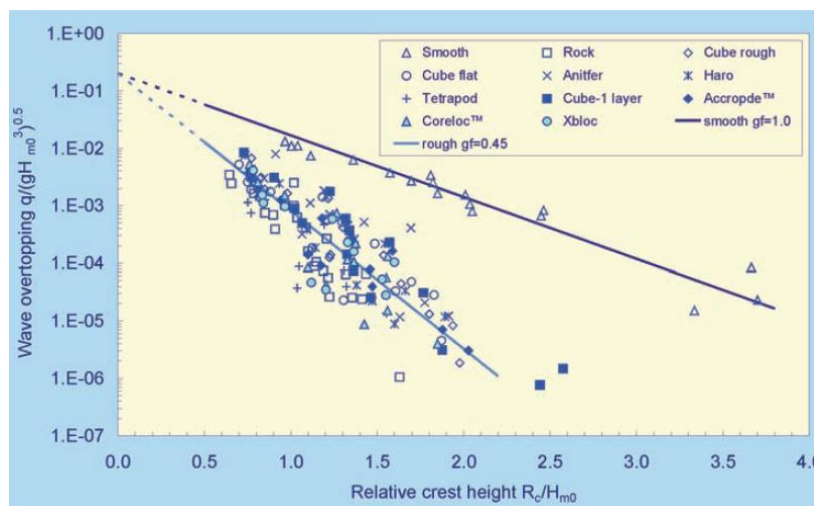


Figure 38: Mean overtopping discharge for 1:15 smooth and rubble mound slopes.  
 Source: Pullen et al., 2007.

### 2.6.6.2.2 Wave-by-wave overtopping volume and $V_{max}$

Wave overtopping is a dynamic and irregular process and the mean overtopping discharge,  $q$ , does not cover this aspect. But by knowing the storm duration,  $t$ , and the number of overtopping waves in that period,  $N_{ow}$ , it is easy to describe this irregular and dynamic overtopping, if the overtopping discharge,  $q$ , is known.

Each overtopping wave gives a certain overtopping volume of water,  $V$  and this can be given as a distribution (see Fig. 30). Equation with two-parameter Weibull distribution describes the behaviour quite well. It has shape parameter,  $b$  (based on different and limited data sets), and a scale parameter,  $a$ . The shape parameter gives a lot of information on the type of distributions. Figure 39 gives an overall view of some well-known distributions. The horizontal axis gives the probability of exceedance and has been plotted according to the Rayleigh distribution. The reason for this is that waves at deep water have Rayleigh distribution and every parameter related to the deep water wave conditions, like shallow water waves or wave overtopping, directly show the deviation from such a Rayleigh distribution in the graph. A Rayleigh distribution should be a straight line in Fig. 39 and a deviation from a straight line means a deviation from the Rayleigh distribution.

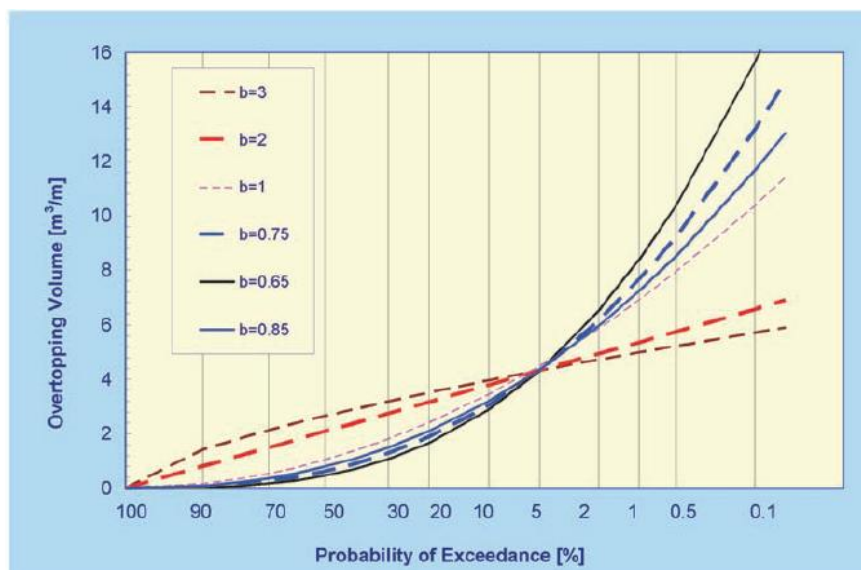


Figure 39: Various distributions of overtopping volumes on a Rayleigh scale graph. A straight line ( $b=2$ ) is a Rayleigh distribution.

Source: Pullen et al., 2007.

The wave distribution can change in Weibull distribution with  $b > 2$ , when waves approach shallow water and the highest waves break. If  $b = 3$  this indicates that there are more large waves of similar height. The exponential distribution (often found for extreme wave climates) has  $b = 1$  and shows that extremes become larger compared to most of the data. Such an exponential distribution would give a straight line in a log-linear graph. The average value  $b$  is equal to 0.75 and has been used for rubble mound structures, which make smooth and rubble mound structures easy comparable and distribution very steep. This characterizes the process with a lot of small wave-by-wave overtopping events and few overflows of large

amount (in contrast in physical model we need long measurements, otherwise the measurement are underestimate!).

The exceedance probability,  $P_V$  of an overtopping volume per wave is then similar to:

$$P_V = PV(V \leq V) = 1 - \exp \left[ -\left(\frac{V}{a}\right)^{0,75} \right] \quad (2.63)$$

with:

$$a = 0,84T_m \frac{q}{P_{ov}} = 0,84T_m q \frac{N_w}{N_{ow}} = 0,84q \frac{t}{N_{ow}} \quad (2.64)$$

Equation 2.62 shows that the scale parameter  $a$ , depends on the overtopping discharge,  $q$ , but also on the mean period,  $T_m$ , and probability of overtopping,  $N_{ow}/N_w$ , or which is similar, on the storm duration,  $t$ , and the actual number of overtopping waves  $N_w$ .

Equations for calculating the overtopping volume per wave for a given probability of exceedance, is given by Eq. 2.63. The maximum overtopping during a certain event is fairly uncertain, as most maximum, but depends on the duration of the event. In a 6 hours period one may expect a larger maximum than only during 15 minutes.

The maximum overtopping volume  $V_{max}$  by only one wave during an event depends on the actual number of overtopping waves,  $N_{ow}$ , and can be calculated by:

$$V_{max} = a[\ln(N_{ow})]^{4/3} \quad (2.65)$$

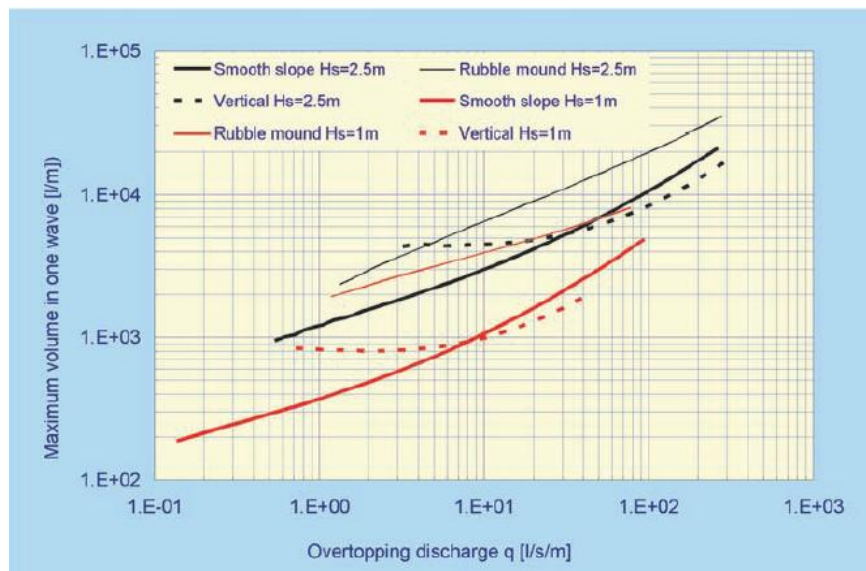


Figure 40: Relationship between mean discharge  $q$  and maximum overtopping volume  $V_{max}$  in one wave for smooth, rubble mound and vertical structures for wave heights of 1.0 and 2.5 m.

Source: Pullen et al., 2007.

### 3 PHYSICAL MODEL

#### 3.1 Overview of hydraulic physical models

##### 3.1.1 What is a physical model?

“A physical model is a physical system reproduced (usually at a reduced size) so that the major dominant forces acting on the system are represented in the model in correct proportion to the actual physical system”. (Hughes, 1993, 10)

Physical model tests are required where the importance of the assets or the structure is being defended is high or when the stability of the structure is not assured by analytical models/semi empirical formulas and numerical models.

They are also employed when:

- Designs have to be optimised.
- Overtopping is a major parameter of the study (in case of our study).
- Complex phenomena such as wave breaking and wave transmission are analyzed.
- The bathymetry or the structure geometry is complex.
- Transitions between structures / structure sections are to be studied.
- Concrete armour units are employed as primary armour (especially those with potentially more brittle failure mechanisms and if a reliable quantification of small armour movements is important).

In practice physical modelling procedures in various laboratories vary so far e.g. in wave generation techniques, typically used model storm sequences, wave calibration techniques, scaling of short duration loadings, scaling of permeable materials, monitoring of damage, quantifying of small armour movements and damage, overtopping analysis, analysis and verification procedures, factors of safety etc. That is why the comparison of model results between varying laboratories is very difficult (Wolters, 2007).

##### 3.1.2 Types of physical models

There are two fundamental types of physical models used in coastal engineering practice to study near shore coastal processes:

- 1) Fixed - bed models

Have solid boundaries that cannot be modified by the hydrodynamic processes outgoing in the model. Fixed-bed models are used to study waves, currents or similar hydrodynamic phenomena in the laboratory under controlled circumstances. The scaling effects associated with fixed-bed models are reasonably well understood and much confidence can be given to the results of carefully-conducted fixed-bed model studies.

## 2) Movable – bed models

Have a bed composed of material that can react to the applied hydrodynamic forces (hopefully in a similar manner as the prototype response). The scaling effects inherent in movable-bed physical models used for studying sedimentary problems are not as well understood as they are for fixed-bed models.

Both fixed-bed and movable-bed can be whether “short-term” or “long-term”. Short-term models examine response of the project or physical system to short duration (hours to days), high intensity events, such as storms. Those are far more practical to conduct. Long-term models determine system changes that occur over extended time periods (days to years) (Hughes, 1993.)

Wave motions can be separated into two logical divisions of physical model:

### a) Short- wave models

Short waves have wave period between 1 - 20 seconds. Are used to study wind wave and swell effects on coastal projects, beaches, and navigation. Gravity waves are defined as short waves when:

$$kh > \frac{\pi}{10} \text{ or } \frac{h}{L} > \frac{1}{20} \quad (3.1)$$

k is a wave number, h is a water depth, L is a wave length, and k and L are related by the expression  $k = \frac{2\pi}{L}$ .

Physical models of short waves are considered to be non-dissipative or fully turbulent. That means that wave experience negligible loss due to friction prior to wave breaking; and when energy is lost, it is lost entirely through turbulent dissipation processes, such as associated with the breaking mechanism. Studies of such wave models can be conducted in laboratory wave tanks with the understanding that the model presents a two-dimensional (2D) viewpoint of the wave process, or they can be conducted in wave basins where width is large enough that wave can have an oblique approach to the beach and three-dimensional (3D) processes can be studied. One of the most important uses of short-wave physical models is in support of harbour design (Hughes, 1993).

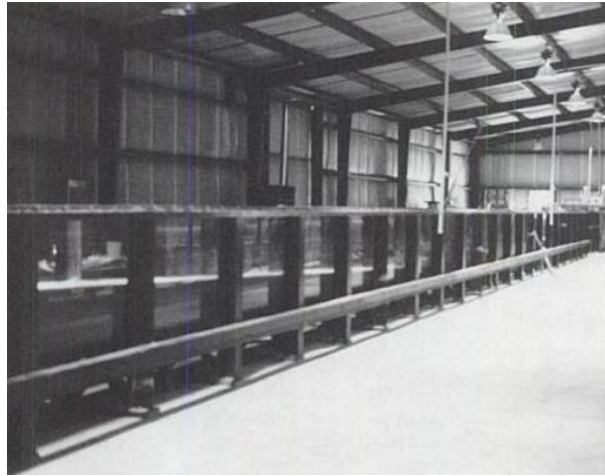


Figure 41: Typical laboratory wave tank, which enables less expensive examination of problems.

Source: Hughes, 1993.

#### b) Long-wave models

Long waves have periods ranging between minutes and days and are used to study the effects of tides, tsunamis, and other long-period waves on harbours, ports, estuaries and tidal inlets. Some coastal engineering projects such as design of a harbour, must evaluate both short and long-wave impacts. Generally, both types of wave motion cannot be investigated in the same physical model unless the harbour is quite small.

We can divide physical models also by dimensional optimizing:

##### 1) 2D models

Are used to optimize breakwater cross section(s), usually a typical cross section of the investigated structure at the point of maximum wave exposure respectively for the most important wave direction. These models are sufficient for the analysis of the interaction between waves and the trunk of structures.

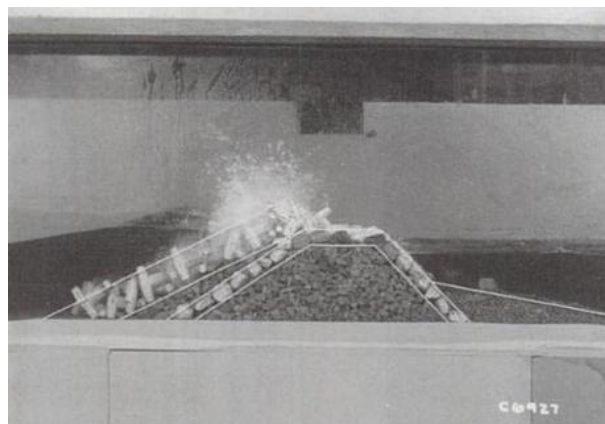


Figure 42: Typical two-dimensional coastal structure model.

Source: Hughes, 1993.

## 2) 3D models

This model is used to verify/optimize the roundhead and other 3D features of the breakwater. 3D physical models are required whenever the structure is three-dimensional or the wave action at the structure is significantly oblique (say  $\beta > 30^\circ$ , where  $\beta$  is the angle from the perpendicular), short-crested or focussed and in situations with very irregular seaward bathymetry.



Figure 43: Typical three-dimensional coastal structure model in wave basin.

Source: <http://www.wrl.unsw.edu.au/site/projects/3d-physical-modelling-of-dalrymple-bay-coal-terminal-apron-widening-queensland/>, 20. 06. 2012.

2D and 3D models are often also combined so that the weak interactions (refraction, diffraction) are modelled with the 3D model and the strong interactions between waves and structure with a 2D model at a larger scale (Wolters, 2007).

### 3.1.3 Advantages and disadvantages of physical models

In general the advantages of physical models are that they:

- Allow insight into phenomena not yet described or understood.
- Integrate the governing physical processes without simplifying assumptions that have to be made for analytical or numerical models.
- Can be used to obtain measurements to verify or disprove theoretical results.
- Can be used to obtain measurements for phenomena so complicated that so far they have not been accessible for theoretical approaches.
- Can be used to obtain measurements for extreme conditions not measured in the field.

- High degree of experimental control that allows simulation of varied or sometimes rare environmental conditions at the convenience of the researcher.
- Ability to get a visual feedback from the model.

The physical model provides an immediate qualitative impression of the physical processes which in turn can help to focus the study and reduce the planned testing (Hughes, 1993).

Disadvantages of physical model testing:

- Scale effects occur in models that are smaller than the prototype if it is not possible to simulate all relevant variables in correct relationship to each other.
- Laboratory effects induced by model boundaries and unrealistic forcing conditions can influence the process being simulated (Wolters, 2007).
- Sometimes all forcing functions and boundary conditions acting in nature are not included in the physical model, and the missing functions and conditions need to be assessed and accounted for in evaluation of model results (e.g. wind shear stresses acting on the free surface may generate significant near shore circulation in nature that would be absent in any model which included only mechanical wave generation) (Hughes, 1993).
- Physical models are undeniably more expensive to operate than numerical models; and in situations where the numerical model gives reliable results with engineering accuracy, the numerical model is the tool of choice (Hughes, 1993).

### 3.2 Scaling requirements (for short-wave models)

#### 3.2.1 Scaling laws

The scale of the model is determined by geometric, dynamic and kinematic similarity.

- Geometric similarity of a model is given when all geometric lengths  $L_p$  in prototype have a constant relation to the corresponding lengths in the model  $L_m$ :

$$n_l = L_p/L_m \quad (3.2)$$

- Kinematic similarity says that time-dependent processes in the model  $t_m$  have a constant time relation to the processes in nature  $t_p$ :

$$n_t = t_p/t_m \quad (3.3)$$

- Dynamic similarity entails that the forces in nature  $F_p$  and model  $F_m$  have a constant relation:

$$n_f = F_p/F_m \quad (3.4)$$

Dynamic similarity is the premise that in geometrically similar models time dependent processes have kinematic similarity.

Thus for a geometrically similar model the key to a correct representation is dynamic similarity. This leads to the typically used scaling laws. Dependent on the importance of the individual attacking forces various scaling numbers have been introduced, e.g. Froude (Fr), Reynolds (Re), Weber (We), Cauchy (Ca).

$$Fr = \frac{u}{\sqrt{gL}} = \sqrt{\frac{\text{inertial force}}{\text{gravity force}}} = \sqrt{\frac{\rho L^2 u^2}{\rho L^3 g}} \quad (3.5)$$

$$Re = \frac{uL}{\vartheta} \text{ or } Re_D = \frac{\sqrt{gH_s D_n}}{\vartheta} \text{ (for flow conditions in the armour layer)} \quad (3.6)$$

$$We = \frac{\rho_w u^2 L}{\sigma} \quad (3.7)$$

$$Ca = \frac{\rho_w u^2}{E} \quad (3.8)$$

In which,  $u$  is particle velocity (m/s),  $g$  gravitational acceleration ( $\text{m/s}^2$ ),  $\vartheta$  kinematic viscosity of water ( $10^{-6} \text{ m}^2/\text{s}$ ) ( $\text{m}^2/\text{s}$ ),  $\rho_w$  density of water ( $\text{kg/m}^3$ ),  $\sigma$  surface tension (N/m),  $L$  characteristic length (m),  $H_s$  significant wave height (m),  $D_n$  nominal diameter of the armour units (m),  $E$  modulus of elasticity ( $\text{N/m}^2$ ).

A physical interpretation of the Froude number is that it gives the relative importance of inertial forces acting on a fluid particle to the weight of the particle. Requiring that the Froude number be the same in the model as in the prototype, i.e.,

$$\left(\frac{u}{\sqrt{gL}}\right)_p = \left(\frac{u}{\sqrt{gL}}\right)_m \quad (3.9)$$

Reynolds number is the condition given also by eq.:

$$\left(\frac{u_w l_a}{\mu/\rho_w}\right)_p = \left(\frac{u_w l_a}{\mu/\rho_w}\right)_m \quad (3.10)$$

Where  $\mu$  is dynamic viscosity of water in vicinity of breakwater,  $u_w$  water velocity in the vicinity of the cover layer,  $l_a$  characteristic linear dimension of armour unit,  $\rho_w$  mass density of water in vicinity of breakwater.

It is based on the characteristic linear dimension of the armour units (usually the mean diameter for quarry stone). It is impossible to satisfy completely this criterion at reduced scale. However, if the model is conducted at a large enough scale to assure that the flow through the primary armour layer remains turbulent, and then this criterion is reasonably well satisfied. However if the flow velocities and the size of the units are small, viscous forces

may be greater in the model resulting in a scale effect; therefore, it is the best to operate at larger scales when possible. Effects of surface roughness of the armour units in the prototype must be the same in the model.

$$\left(\frac{\xi_a}{l_a}\right)_p = \left(\frac{\xi_a}{l_a}\right)_m \quad (3.11)$$

Where  $\xi_a$  is characteristic linear dimension of armour unit surface roughness and  $l_a$  characteristic linear dimension of armour unit.

The resistance to movement offered by surface roughness in prototype – scale quarry stone or armour units is considered negligible. In the model, attempts are made to decrease the relative roughness of the structural units by making their surfaces as smooth as possible. If there is appreciable friction between armour units in the model, then the model will show higher stability than its prototype equivalent. This could lead to potentially unsafe design.

The condition that states that the relative mass density relationship between armour unit material and the prototype must be maintained in the scale model is:

$$\left(\frac{\rho_a}{\rho_a - \rho_w}\right)_p = \left(\frac{\rho_a}{\rho_a - \rho_w}\right)_m \quad (3.12)$$

Or more simply:

$$\left(\frac{\rho_a}{\rho_w}\right)_p = \left(\frac{\rho_a}{\rho_w}\right)_m \quad (3.13)$$

This Eq. 3.13 is useful for determining model armour unit mass density requirements to represent prototype salt-water breakwaters being tested in fresh-water model facilities.

The armour unit weight scale is obtained simply by taking the prototype-to-model ratio of the expression.

$$\gamma_a * v = W_a \quad (3.14)$$

Where  $\gamma_a$  is armour unit specific weight ( $=g*\rho_a$ ),  $v$  armour unit volume and  $W_a$  armour unit weight.

For true dynamic similarity the Fr, Re and We numbers must then be the same in model and prototype, but this is not always possible. The importance of friction is however often small since waves must propagate long distances before bottom friction seriously affects them and in the case of drag forces there are ranges of Reynolds numbers where the drag coefficient is constant (Wolters, 2007).

Commonly employed scales for physical breakwater models:

- Breakwater stability: 1:5 – 1:80 (typical 2D: 1:30 – 1:60, 3D: 1:30 – 1:80).
- Forces on solid bodies: 1:10 – 1:50.

### 3.2.1.1 Scaling laws for rubble mound breakwaters

For rubble mound breakwaters the following scaling criteria have to be fulfilled:

- a) Overall structural dimensions must be scaled geometrically undistorted in length-scale.
- b) Flow hydrodynamics (waves) need to conform to the Froude criterion. The Froude criterion states that inertial forces relative to gravity forces scale, form drag relative to gravity forces scale nearly correctly (depends on the form of armour unit, its weight, and the size of wave).
- c) Turbulent flow conditions have to exist throughout the primary armour layer (satisfied reasonably by the  $Re_D > 30000$ ).
- d) It is best to operate at larger scales when possible (since viscous forces can be greater if flow velocities and units are small).
- e) The geometric scaling of the model extends to providing a reasonable approximation of the shape and size distribution of the primary and underlayer armour units (Wolters, 2007).

From the Froude law the following typically used scaling relationships, expressed in terms of the length scale factor  $n_L$ , can be derived:

Table 11: Typically used scaling relationships (Wolters, 2007).

Wave height [m]	$n_H = n_L$
Time [s]	$n_T = n_L^{0.5}$
Velocity [m/s]	$n_U = n_L$
Acceleration [m/s <sup>2</sup> ]	$n_a = 1$
Mass [kg]	$n_M = n_p * n_L^3$
Pressure [kN/m <sup>2</sup> ]	$n_p = n_p * n_L$
Force [kN]	$n_F = n_p * n_L^3$
Discharge [l/s/m]	$n_q = n_L^{1.5}$

### 3.2.1.2 Permeability scaling

In the underlayers and core of model breakwaters, geometric scaling of the material sizes may lead to viscous effects because these layers can become less permeable (in our case core layer), thus limiting wave-driven flows into the inner layers and increasing the flow effects in the armour. Geometric scaling of underlayers and core material could thus be regarded as a conservative estimate of armour stability (larger damage and overtopping in the model). However, geometric scaling of the material sizes will lead to different values of transmission

and reflection from what occurs at prototype scale (more energy reflected and less transmitted).

Where the size grading of the underlayer and core materials are not well-established and cannot be assured in the construction, a distorted material size might give over-optimistic results for the stability analysis, so that it may be unsafe to apply such a permeability correction (Wolters, 2007).

### 3.2.1.3 Relative densities

When strict geometrical scaling is applied to the armour, the ratio of fluid mass density to the immersed mass density of the armour unit mass should be the same both in model and prototype.

$$\Delta = \left( \frac{\rho_a}{\rho_w} \right) - 1 \quad (3.15)$$

Where  $\rho_a$  is armour unit density and  $\rho_w$  is water density.

A method for compensating for the increased buoyancy of the salt water relative to the fresh water used in most scale models is to adjust the weight of the model armour units. The scaling requirement is based on preserving the value of a ‘stability parameter’ between prototype and model (Hughes, 1993).

### 3.2.1.4 Stability scaling

In stability scaling, it is ensured that the stability number  $N_s$  (Hudson) is the same in model and in nature. Stability scaling is of relevance for the toe material and the armour layers. The differences in water density (salt water in nature and fresh water in the model) and in the armour unit density are accounted for in this parameter. The stability number is defined as:

$$N_s = \frac{H_s}{\Delta D_{n,50}} \quad (3.16)$$

Where  $\Delta$  is relative mass density (Eq. 3.15),  $\rho_a$  density of armour units ( $\text{kg/m}^3$ ),  $\rho_w$  density of water ( $\text{kg/m}^3$ ),  $D_{n,50}$  nominal diameter of the armour units, based on  $M_{50}$  (m),  $H_s$  significant wave height (m). Thus the stability of the armour units is modelled correctly when the stability number in the model is the same as the stability number in prototype. This is the case when:

$$n_D = \frac{n_L}{n_\Delta} = n_L \frac{\Delta_{model}}{\Delta_{prototype}} \quad (\text{scaling relationship for armour diameter } D) \quad (3.17)$$

$$n_D = n_\rho n_D^3 = n_\rho \left( \frac{n_L}{n_\Delta} \right)^3 \quad (\text{scaling relationship for armour weight } W) \quad (3.18)$$

Absolute geometric similarity of the dimensions (diameter) of the model armour units is not necessarily maintained. Small differences do not significantly affect the results of the model experiments (effects on stability and overtopping are generally less than 5-10%) if care is taken that the armour geometry is correctly reproduced e.g. the crest elevation should be correctly modelled to insure similarity in overtopping. It is however important to ensure that the outer envelope of the armour is at the correct level. This may require that the underlayer level is adjusted in the model to accommodate (slightly) thicker or thinner armour.

### **3.2.1.5 Wave overtopping**

Model and scale effects in wave overtopping at model scale are induced e.g. by varying slope roughness, structure permeability and by wind effects. For smaller armour units and low overtopping volumes ( $q < 1$  l/s/m) the combination of model, scale and wind effects can increase (Wolters, 2007).

### **3.2.1.6 Modelling limits**

Modelling limits are defined on the one hand by the (maximum) size of the available modelling facility and on the other hand by the similarity laws (minimum size). The lower limit for the model size is determined for example by the Reynolds number, which must always be large enough to guarantee fully turbulent conditions in the model if these are also found in prototype. Also the Weber number must be large enough to guarantee no influence of surface tension (wave damping) in the model.

## **3.3 Scale effects in laboratory**

Scale effects occur when the employed scaling law does not correctly reproduce the physical conditions from prototype at model scale. This can be due to an oversimplification or omission of the governing forces in the physical process. The most obvious effect is that boundaries in wave tanks constrain the hydrodynamics to be essentially two-dimensional. The nonsimilitude of viscous forces and surface tension forces in Froude scaled models can lead to scale effects involving wave reflection, wave transmission, wave energy frictional dissipation, and wave breaking dissipation. Therefore it is very important to clearly define the study objective and to recognize important scale effects to allow an intelligent analysis of a particular modelling problem.

To prevent model effects the following provisions should be taken in the layout of the model:

- The model positioning in the wave channel/basin should be such that boundary effects are minimized and that the given wave conditions are achieved over the appropriate test section(s) and produce the appropriately scaled responses.
- Wave walls can be applied where appropriate to control energy spreading/diffraction effects (due to insufficient wave crest length in the model). A minimum distance

between (the end of the) wave walls and the test sections should be guaranteed so that no adverse effects due to the wall are experienced on the test section.

- Wave dampers should be used to prevent that (re-) reflections from model boundaries distort the incident wave conditions at the structure.
- Structure and measurement equipment should be appropriately fixed to prevent that structural oscillations influence the test results.
- The model scale should be as large as possible (Wolters, 2007).

### **3.3.1 Wave reflection**

A not-so-obvious boundary effect is caused by reflection of waves by the wave board. Waves are generated and propagate down the wave tank until they reach either a structure or beach on the far end. Some wave energy is reflected seaward (toward the board), just as happens in nature. But in nature reflected waves continue out into the ocean, whereas in the wave tank, they are again reflected (Hughes, 1993).

### **3.3.2 Wave separation, wave transmission**

Incident waves are usually assessed by separating (spectrally) the incoming waves into incident and reflected waves. They are based on measuring the incoming waves at several closely spaced locations by wave gauges. Typically employed techniques for a near-horizontal bottom and waves in one direction are three-point for 2D models or more point techniques (5-9 points) for 3D models.

### **3.3.3 Wave breaking**

Typically, scale effects due to wave breaking are not specifically considered in physical stability modelling. They seem to be low for sufficiently sized models. Scale effects are due to the fact that in breaking waves entrained air bubbles are larger in the model because the size is determined by surface tension. Also the depth of air entrainment will be greater in the model. The total energy budget remains however in similitude (Wolters, 2007).

## ***3.4 Model set-up and model operation***

### **3.4.1 Layout of model**

Independent of the chosen model scale is the physical model affected by the artificially introduced partitioning of the prototype situation in the model. Often only a section of the

prototype situation is modelled. In general the model positioning in the wave channel/basin should minimize boundary effects and that the given wave conditions are achieved over the appropriate test section(s) and produce the appropriately scaled responses (Wolters, 2007).

### 3.4.2 Bathymetry (fixed bed)

A correctly reproduced bathymetry ensures realistic wave conditions, i.e. wave dispersion, wave refraction/diffraction, shoaling and wave breaking are correctly simulated. The bathymetry is usually not modelled in every detail; rather the main bottom contours (isobaths) are represented. Special attention should be paid to the bottom contours within 1-2 wavelengths ( $1L - 2L$ ) from the structure toe, since those have a paramount influence on the wave climate and loading conditions at the structure.

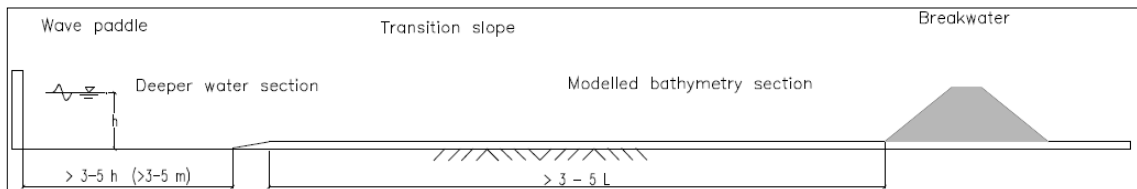


Figure 44: Bathymetry layout.

Source: Wolters, 2007.

Bathymetry changes can be expected during storms. Thus an alternative to the use of measured profiles in physical modelling could be the use of an adapted profile, based on scour and sediment transport estimations, which could present the bathymetry during a storm more accurately. Alternatively, as a conservative estimate, a larger water depth could be used (Wolters, 2007).

### 3.4.3 Structure

Rubble mounds are made of sieved or weighed quarry rock. Structural elements (e.g. when loading of crest elements is investigated) should be rigid enough to prevent or minimize unwanted structural oscillations. If unwanted structural oscillation cannot be prevented it should be in a frequency band outside the typical wave spectrum (usually  $f < 0.01 \text{ Hz}$  or  $f > 10 \text{ Hz}$ ).

#### 3.4.3.1 Crown walls

The modelling of breakwater crown wall stability (sliding or overturning failure) can be done by various methods:

- 1) Whole body forces can be measured on a section of crown wall using a force table or array of force elements.

- 2) Wave pressures on the front face and underside can be summed to determine the whole body forces and moments (as we did in our case).
- 3) The crown wall section can be reproduced at a reduced weight so that the friction forces between armour and crown wall are in similitude with the prototype forces.

### 3.4.4 Waves condition

Extreme water levels are not always the most critical design condition in stability testing. Design wave conditions are usually provided for different return periods (typically between 1 and 100 years return periods) including the significant wave height, the peak or mean wave period, the peak or mean wave direction and the duration of the storm (or a number of waves). Typically between 500-3000 waves are made to come up with a statistical reliable result test durations. Usually applied storm durations of 3-6 hours (in prototype) satisfy this condition. Storms are often also simulated as a series of test runs with fixed wave conditions, increasing in severity, depending on the likely storm profile.

Wave energy spectra in physical models are usually characterized by their spectral parameters. The most commonly used are the significant wave height  $H_{mo}$  and the peak period  $T_p$ . The most commonly employed wave spectra are JONSWAP (confined young seas) and Pierson- Moskowitz (PM, fully-developed open seas).

#### 3.4.4.1 Long and short crested waves

Both long and short crested waves are employed in physical modelling. Long crested waves are generally believed to give conservative results (larger energy input) for damage and wave overtopping. Short-crested waves are important if local wave characteristics/phenomena around the breakwater are to be investigated and may give more severe local effects.

### 3.5 Used materials

- Fluid

Fresh water is commonly used in most physical models.

- Armour

The rock gradation is usually provided by the designer. Otherwise, rock gradation and established rock sieving curves can be taken from the Rock Manual (CIRIA, CUR, CETMEF, 2007). Before the model testing the available rock material needs to be checked against the required grading curves using typical sieving/screening techniques or by weighing of the stone material. If hydraulic stability considerations dictate larger armour units, often surpassing the maximum stone sizes the quarry can produce, artificial concrete armour units

are used. These exist in various sizes and geometric configurations. Examples include Dolosse, Tribars, Tetrapods, CORE-LOCTM, ACCROPODETM, Xbloc®, hollow cube blocks (SHEDs or COBs), solid cubes and rectangular blocks etc.

Structural elements are often constructed of wood, metal, concrete or plastic. Stiff Perspex is used when it is important to get a view of current/wave behaviour inside the structure.

### ***3.6 Measurement equipment and measurement procedure***

#### **3.6.1 Instrumentation**

The employed instrumentation should provide adequate resolution, should be unsusceptible to soiling/dirt and be stable under varying temperatures. Current/wave induced structural oscillations should not affect the output of the instruments.

Employed instruments are:

- Wave probes (resistance or capacitance type).
- Directional wave gauges (to determine the wave direction; e.g. composed of a coupled velocity (u,v) and wave gauge ( $\eta$ )).
- Velocity meters (e.g. electromagnetic gauges, LDV, acoustic Doppler techniques or simple step/wave gauges).
- Pressure/force sensors (strain gauges, dynamometer).
- Profilers (for damage assessment; used are profilers of wheel type, acoustic type and 3D laser scanners).
- Photographic and video equipment.

Among the specified instrumentation, the photographic equipment is the most widely used and most versatile. It is used throughout the modelling process to document the model set-up, the model operation, the recording of damage and the assessment of wave conditions etc.

#### **3.6.2 Assessment techniques**

Depending on the area of instrument application the following assessment techniques are used:

- Damage

Is usually assessed using profilers and/or photographic techniques. Digital overlay techniques are employed to assess rock and concrete unit movement. Photographs (taken before and after the test) and videos are also used to assess structural/toe stability.

- Wave overtopping

Is usually assessed by collecting the overtopping water in overtopping trays or tanks and measuring the overtopped water volume or mass. The number of overtopping events can be assessed by a wave gauge at the crest of the breakwater or by continuous water level measurements (volume or mass) within the overtopping tray or tank.



Figure 45: Measurement of wave overtopping using an overtopping tank.

Source: Wolters, 2007.

- Wave run-up

Is usually assessed using resistance type wave gauges or step-gauges (pressure sensors embedded in the mound slope) and photographic techniques.

- Wave loading

Pressures are usually measured using pressure sensors installed within the structure. Force measurements (and moments) are usually conducted by strain gauges or by averaging pressure sensor readings over the given area. For force measurements it is often necessary to use suspended/independently anchored sensors or sensor arrays (force frames) to produce reliable force estimates. Force sensors are usually only able to resolve global or quasi-static forces. Peak loads arising from wave impacts are not measured with this system, as the force frame cannot respond quickly enough to peaks of very short durations. Information on wave impact loads can generally only be obtained by detailed pressure measurements on the front face of the structure (e.g. caisson). Particular attention needs to be taken when uplift forces/pressures are measured. Pressure and force sensors can be fragile and are often restricted in their applicability (pressure range, temperature, eigen frequency range).



Figure 46: Pressure sensors installed inside the wave wall.

- Velocity

Velocities can be measured by propeller, electromagnetically or using standard wave gauge techniques. The entrained air often causes unreliable measurements. In these cases conventional techniques, e.g. a series of wave gauges, is a better solution to determine the wave celerity.

### ***3.7 Analysis procedures***

#### **3.7.1 Data handling**

- Usually test results are presented in dimensional form and prototype values in design studies. Dimensionless analysis of the most important parameters as basis for interpretation of results and their presentation can however give valuable insights into the model behaviour. This is especially useful if compared with other relevant tests or design guidelines or if data is exchanged between varying partners/facilities.
- Depending on the analysis requirements, filtering of data after acquisition can facilitate correct data interpretation. For example, short waves can thus be separated from long ones or turbulent fluctuations in the surf zone can be filtered out.
- Statistic/probabilistic analyses are rarely used in physical modelling practice, partly due to the limited number of tests performed (and generally no repeat tests). However, they become constantly more important in research since many hydraulic (random) processes can be best described in this fashion.

#### **3.7.2 Removal of spurious data**

The removal of spurious data is an important prerequisite for an accurate data analysis/interpretation. This includes the removal from the data of the following:

- ‘Spikes’ due to instrument problems or data acquisition methods.

- Offsets due to the instrument or analogue/digital conversion.
- Slowly varying trends due to instrument drift and changes in water level.

### 3.7.3 Damage assessment

Two methods are commonly used for quantifying damage in rubble-mound structure models:

- Counting the number of individual armour units that have been dislodged, or
- Determining the volumetric change in areas where armour units have been displaced.

The method of counting displaced armour units requires some way of identifying those armour units that have moved. A common technique is to construct the model structure with differently coloured (painted) armour units placed in patterns. Dislodged units will then move into a region of a different colour and be easily recognized. The movement can be observed and noted, or more conveniently, video and photographic documentation can be used to record test results.

Quantifying damage by volumetric change requires that pre-test and post-test profiles of the armour slope be measured in a consistent manner for comparison. The test section should be surveyed over a set grid with sufficient resolution to determine profile change with reasonable accuracy. A ‘damage’ percentage can be defined in a number of different ways. For example, damage is defined as the percentage of dislodged armour units to the total number of armour units:

$$N_d = \frac{N_{displaced}}{N_{total}} \times 100\% \quad (3.19)$$

In which:

$N_{displaced}$  (-) is the number of displaced stones and  $N_{total}$  (-) is the total number of stones in that layer (section).

The damage percentage is typically calculated for individual sections. Typically displaced stones are stones which are displaced by more than one unit diameter ( $D_{n50}$ ).

### 3.7.4 Overtopping and wave transmission

The maximum permissible values for wave overtopping and wave transmission depend on structure type and the requirements of the designer. They vary with use of the structure, exposure etc. The Rock Manual (CIRIA, CUR, CETMEF, 2007), the Coastal Engineering Manual (CEM 2006) and the British Standards (BS 6349, 1991) provide possible guideline values. For dikes also the TAW (2002) guidelines can be recommended (see Chapter 2.6.5.3).

## 4 LABORATORY TESTING PROCEDURES

### 4.1 Introduction and Motivations

The use of physical model is particularly useful when assessing wave overtopping, as overtopping is affected by several factors whose individual and combined influences are still largely unknown and difficult to predict.

Wave overtopping at harbour breakwaters transfers wave energy into supposedly protected waters, causing larger waves and possible damage or loss of moored boats. Wave walls are areas frequently used by people/vehicles and overtopping waves may present a significant safety hazard. Many coastal wave walls are designed for a (tolerable) mean discharge to overtop the structure over a storm event. Prediction of mean overtopping discharge rates are based on empirical formulae fitted to laboratory measurements.

#### 4.1.1 Main objectives

The main objectives of this laboratory research are as follows:

- To measure the WO (Wave Overtopping) and wave-induced pressures on the wave wall.
- To study the influence of various design parameters, crest freeboard ( $R_c$ ) and length of overspill basin (OB) on overtopping discharges.
- To study the influence of various wave parameters ( $H_{m0}$ ,  $T_0$ ,  $\gamma$ ) on overtopping discharges;

The activities conducted in preparation for this thesis were:

1. Design of experiments.
2. Realization of a physical model and its configurations to be tested.
3. Conducting experiments aimed at measuring the wave overtopping and wave-induced pressures.
4. Post processing analysis and reporting.

### 4.2 Laboratory description

Physical model was installed and tested in the wave flume at the Maritime Engineering Laboratory (CoastLab, [www.unifi.it/labima](http://www.unifi.it/labima)) at the Department of Civil and Environmental Engineering of Florence University in Italy. The laboratory is operating since 1980 in the field

of Maritime and Coastal Engineering. The present work was conducted during the spring 2012 (Fig. 47).



Figure 47: Left: Firenze situated on a map. Right: Top view at the Faculty of Engineering of Florence.

Source: [www.googlemap.com](http://www.googlemap.com), 25. 06. 2012.

#### 4.2.1 Wave flume

Wave flume is made entirely of steel and glass with dimensions 47.0 m \* 0.8 m \* 0.8 m (length \* width \* height). It consists of 39 sectors of size 1.2 m \* 0.8 m \* 0.8 m (the first 37 made in glass and steel, the last two in concrete). The bottom, lifted from the floor for 0.5 m, is made up of fiber-reinforced prestressed concrete panels with dimensions 1.2 m \* 0.8 m \* 0.02 m, one for each sector, easily modifiable in order to reconstruct different profiles of the bottom (Fig. 49).



Figure 48: CoastLab wave flume at the Maritime Engineering Laboratory of Florence University.

At one end of the wave flume the wave generator is placed, which consists of a metal structure which supports and assists the movement of a wave paddle area, with dimensions equal to the internal section of the channel. At the other side a diffuser which performs a

curve at  $180^\circ$  and collects the water from the last sector is installed, sending it to a pipe below the channel which contains the water in the head to it.



Figure 49: Left: Diffuser at the bottom of the flume. Right: The bottom of the channel.

The wave flume is equipped with a system of generation of waves able to simulate real sea states with assigned spectral characteristics and a recirculation bi-directional system, with a maximum range of 25 l/s. A butterfly valve and an axial pump allow the operations of filling and emptying without any wastage of water due to the presence of an underground storage tank in the area in adjacent to the laboratory connected to the flume by means of a steel pipe.

#### 4.2.2 Wave generator

The generator consists of a mechanical paddle whose movement is controlled by electronic hydraulic system connected by a servo-hydraulic valve and used to assist the movement according to a principle of feedback. It reproduces waves with wave heights up to 0.35 m. The wave motion is controlled by software based on the technique Deterministic Spectral Amplitude Method which allows generating both the sine waves, with time period and altitude, which are assigned with wave motion energy spectrum equal to theoretical selected e.g.: JONSWAP, Pierson-Moskowitz, Scott-Neuman, Bretschneider, Ochi-Hubble.

The generated signal from digital to analogue conversion is sent to the hydraulic system that controls the generator, while the analog capture in real time the level of the free surface is performed through the provision of resistive probes along the channel. Random signal generated by the generator of the wave motion can be stored and reused to reproduce the same state of the sea more than once; once acquired, the signal is analyzed both in the frequency domain (spectral analysis) as in the time domain (zero-crossing analysis) to obtain all the wave's characteristic parameters including:  $H_{m0}$ ,  $H_{1/3}$ ,  $T_{1/10}$ ,  $H_{max}$ ,  $H_{rms}$ ,  $T_m$ ,  $T_{1/3}$ ,  $T_p$ ,  $T_{m0,-1}$ ,  $T_{m-1,0}$ .



Figure 50: Front perspective of the mechanical part of the wave maker.

#### 4.2.3 Recirculation pump

The wave flume is equipped with a bidirectional recirculation system. A centrifugal pump is connected to the pipe located under the channel and four open/closed valves allow to govern the system in terms to flow direction and magnitude.

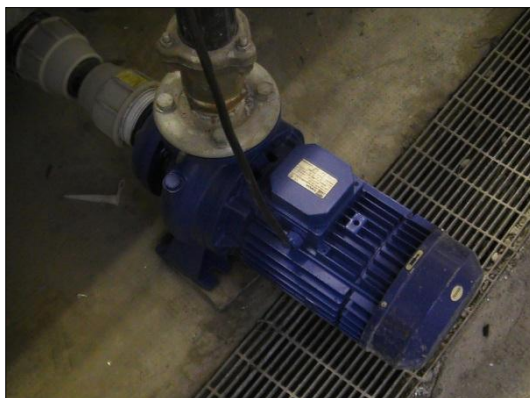


Figure 51: Recirculation pump.

#### 4.2.4 Back paddle pump

To allow emptying the portion of the water positioned behind the wave maker in wave flume, a centrifugal pump is used, which sucks the water from the back blade putting it in front of it. The pump suction discharge can be adjusted by a valve in order to fix the aquatic swing behind the blade.

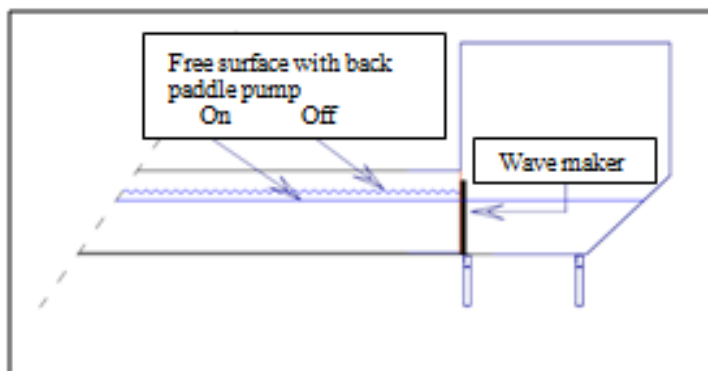


Figure 52: Back paddle pump effects.

#### 4.2.5 Wave flume refilling pump

Wave flume is connected by steel pipe to an underground storage tank in the area next to the laboratory: a gate valve and an axial pump allow the operations of filling and emptying without any waste of water.

#### 4.3 Used instruments

##### 4.3.1 Wave gauges (WG)

Water level measurements through wave flume are defined by resistive wave gauges (WG). These instruments are mounted so that their wires are vertical and piercing the water surface downward to the lowest wave trough point (i.e. some part of the wire must remain submerged at all times). WG are constituted by a current generator, whose ends are connected to two wires, not in contact with each other (the circuit is open); when the WG is immersed in water, the closure of the circuit and the establishment of a potential difference occurs ( $\Delta V = R \cdot i$ ) proportional to the water level in the flume, measured by a voltmeter placed in the top box of the WG (see Fig. 53). Together with the water level variations due to the wave motion also the potential difference of the WG varies, which reveals with sampling frequency equal to 20 Hz, i.e. every five hundredths of a second; the value acquired and provided by the WG in Volts must be converted to metric units using the calibration procedure.

Technical notes:

- Parallel wire:  $\varnothing = 0.3$  mm,
- Oscillator of 4 kHz,
- Output 0 to 10 V,
- Power:  $\pm 15$  V,

- Support insulator.

Five capacitive wave gauges are used to measure water surface elevation in the presented wave flume. They were used in ascending numerical order starting from the wave maker. The first wave gauge (WG 1) has been positioned at a distance 7.72 m from the wave generator, at the depth 56 cm (in model scale) to calculate the generated wave, while the remaining four WG (WG 2, 3, 4 and 5) were placed in front of the breakwater, at the distance of 28.6 m to 28.91 m from the wave maker and at the depth from 23 cm to 21 cm (in model scale) to calculate characteristic parameters of the incident wave and measurements of reflection parameters (see Table 12).

WG measures of wave motion provide a measure in Volts, which are converted to metric units through a linear relationship of the type:

$$\eta = V_0 + kV \quad (4.1)$$

Where  $\eta$  is measure of the oscillation of the free surface [cm],  $V$  is the measure of the oscillation of the free surface [Volt],  $V_0$  is the intercept of the linear relationship of conversion [Volt], and  $k$  is the angular coefficient of the linear relationship of conversion. The calibration of the wave gauges was checked daily, before starting the tests, using always the same calibration. Wave gauges linearity is ascertainable by calibration of the same operation performed daily for the whole duration of the tests and described by the following phases:

- Bring the water level at the SWL in advance for the test.
- Set your PC GANIMEDE for the calibration for each sensor input channel and associated acquisition parameters: acquisition range, depth and distance from wave maker (see Table 12).
- Bring the WG to the maximum level, wait until the water level has stabilized and acquire data.
- Bring WG to a minimum level, wait until the water level has stabilized and acquire data.
- Center WG, allow the water level has stabilized and acquire data.

The instruments acquire the level of the free surface with a nominal resolution of 0.1 mm. So the calibration of the WG must be repeated if the average error is greater than 0.2 cm, and the correlation coefficient of the interpolating straight line is not 1, converting the acquired signal from centimetres to volts for three noted levels, we obtain slightly different values from those expected. The average of the three differences between expected and calculated values, taken in absolute value, is defined as the average error. The immersion depth of WG was determined according to the depth of the flume at each gauge and so that the higher wave also fits into its range of acquisition and prevent the water level would not be acquired. In fact, if the maximum wave is too large a partial signal would be acquired. After setting the range of optimum calibration for each WG, these parameters were maintained for all the tests. After obtaining the calibration parameters for each WG, the conversion coefficients Volt-cm for the

signal acquired by the WG were processed with Matlab software into signals in cm, with a frequency of 20 Hz.

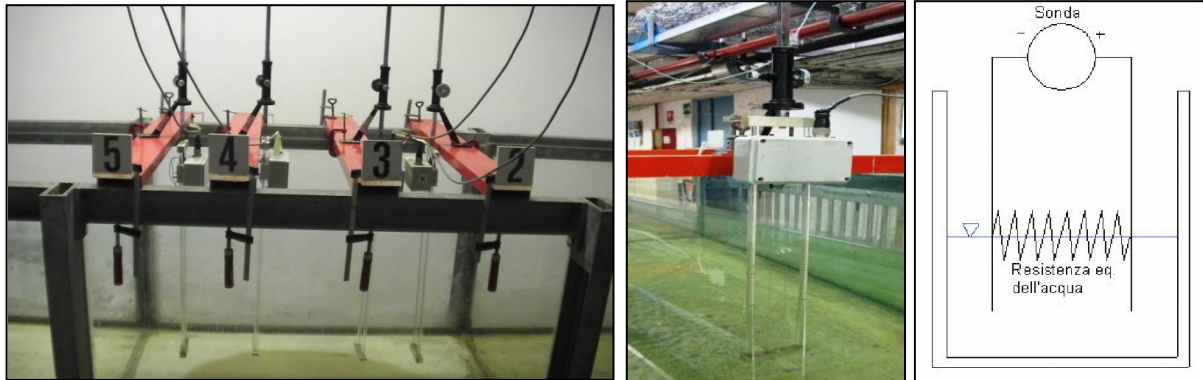


Figure 53: Wave gauges and their electric scheme.

Table 12 : Correspondence between WG and channel, calibration range, depth and distance from wave maker (in model scale).

Wave gauges	Channel	Range [mm]	Distance from wave maker [mm]	Depth (in the first calm 30'') [mm]
1	9	200	7718	560
2	2	100	28062	231
3	3	100	28362	226
4	4	100	28662	219
5	10	100	28912	212

#### 4.3.2 Load cells

Average flow rate of overflow and single wave-by-wave overtopping volumes behind the wave wall are measured by collecting the water in a special overtopping tank suspended in 4 load cells, which acquire the weight of the individual volume of overflow wave, with a total resolution of 4 g (500 kg in the prototype). They are type of model TCA load cells, manufactured by AEP transducers SRL, of Cognento, Modena, Italy. Overtopping tank has been emptied after each launched wave test.

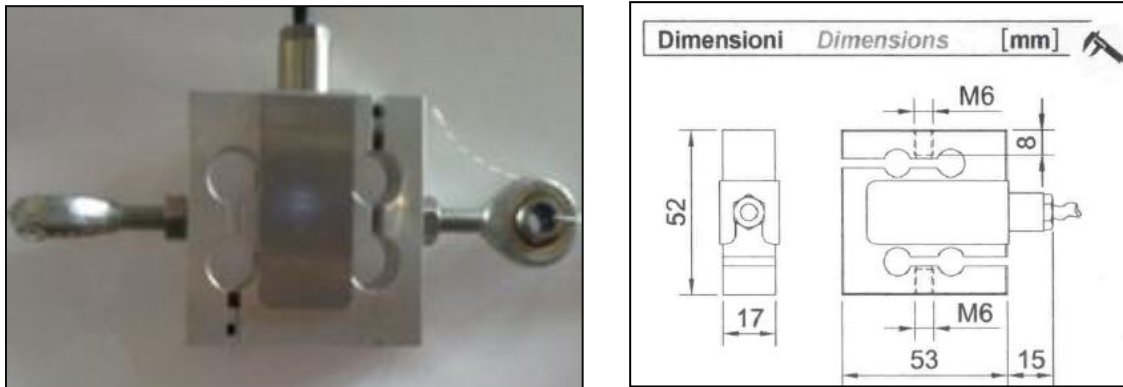


Figure 54: Load cell.

### 4.3.3 Pressure transducers

The measurement of pressures acting along the center line section of the wave wall were carried out using five pressure transducers placed inside the wave wall (Fig. 55), which acquire with the nominal resolution of  $0,01 \text{ kg/cm}^2$  ( $10 \text{ g/cm}^2$ , in prototype  $0,5 \text{ kg/cm}^2$ ) to measure the pressures frontally. They are type of the model series 46 X, manufactured by Keller, Winterthur, Germany. Metal frame connects the cable with the outside pressure transducer surface, where pressures are determined due to wave attacks caused by wave maker. Measurement values were acquired and reprogrammed by a PC.



Figure 55: Pressure transducer.

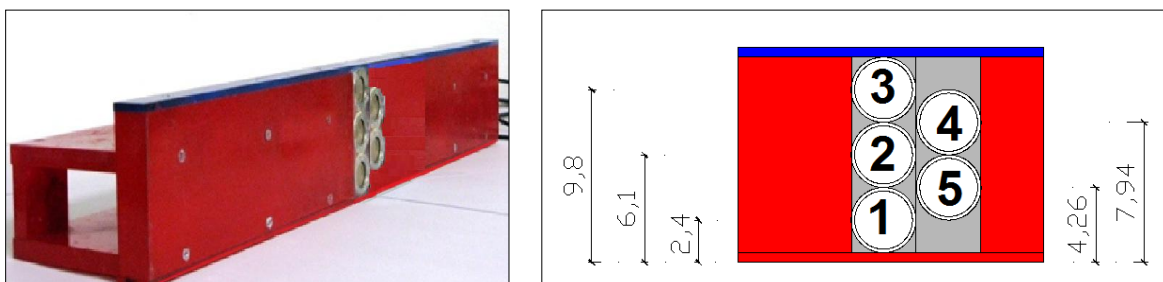


Figure 56: Disposition of the pressure transducers on the wave wall (in model scale, cm).

#### 4.3.4 Hydrometric tip at nonius

The water levels during the charging and emptying wave flume were determined using a hydrometric tip, located at the end of wave flume, at the distance 39.06 m from the wave maker (see Fig. 66). The tip is connected to nonius, which guarantees that measured water level has error less than 0.05 mm. The measures of water levels were made by sliding hydrometric tip along the vertical until the surface of water was not touching the tip, without penetrating the surface.

The accuracy of the water level in a wave flume with respect to the target level is important for two factors:

- Correspondence between the model project geometry and the one actually tested.
- Wave attack repetitions at different water levels, may lead to various wave characteristics of wave motion, even though we generate always the same wave (input signal).

During the calibration phase the water surface must be motionless, and this is possible only when the pumping system of back blade is turn off. The back blade pump, in fact, serves for emptying the tank at the back of the generator of wave motion; the water sucked is introduced forward into the flume and this creates a parasite wave and an increase of water level in the flume. Tests were conducted to estimate the magnitude of this parasite wave and increased water level in the preliminary phase that proceeded the first session of tests. A signal (of wave motion) lasting 20 or 10 minutes was acquired first with the back blade pump turned off, and then turned on. This type of test was repeated several times and has allowed us to estimate the average differences in level, united with a spectral analysis that has enabled us to evaluate the maximum frequency obtained with the various WG and the peak of time period of the unwanted wave.



Figure 57: Hydrometric tip at the nonius.

### 4.3.5 Overtopping tank

Capture system of overtopping water, consists of a tank made out of a yellow rectangular plastic tank, with dimensions 40.0 \* 35.0 \* 10.0 cm (length \* width \* height) and thickness of 0.2 cm, hanged on 4 wires which connect overtopping tank with 4 load cells (see Fig. 58).

Overtopping tank has been positioned as a continuation of the sampler (side), at the back of the wave wall. At the installation it was important that the overtopping tank did not touched the water surface, as this would contribute to wrong overtopping graphs, as a consequence of Archimed force, which could push up the tank and so the exact measurements would be smaller than the real one. Overtopping graphs made by Matlab software are summing each wave-by-wave overtopping volume and if the tank is acted by Archimed force, this force counteracts the sum.

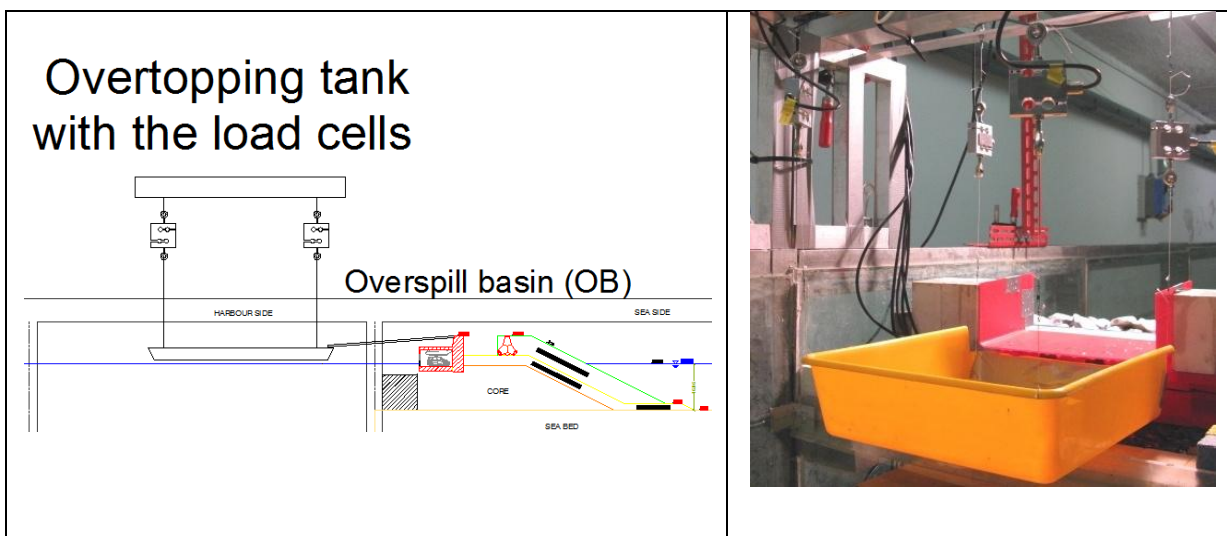


Figure 58: Overtopping tank for overtopping measurement.

### 4.3.6 Photo, video

For the realization of photos and video recordings during the execution of tests the following equipment was used:

- a) Compact digital camera, Canon Powershot G9

Technical notes:

- 12.1 megapixel sensor 1/1, 7 "
- 6x optical zoom with optical Image Stabilizer
- RAW image recording
- DIGIC III and iSAPS

- Face Detection AF / AE / FE
- 9-point AiAF and FlexiZone AF / AE
- PureColor LCD II 3.0 "
- ISO 1600 and Auto ISO Shift
- 25 shooting modes
- Canon Waterproof Case WP-DC21

b) Video camera, JVC GZ-MG77E

Technical notes:

- Dimensions: (W x H x D): 68.0 mm \* 69.0 mm \* 109.0 mm
- Weight: ~ 370 g (without battery)
- Motorized zoom lens with F 1.2 to 2.0, f = 3.8 to 38.0 mm, with a 10:1 zoom factor
- Filter diameter 30.5 mm
- CCD sensor 1/3.9 "(2.18 million pixels)
- Panel LCD TFT 2.7 "measured diagonally
- Monaural Speaker
- Flash within 2 m
- 11 V DC power supply (using the AC adapter), DC 7.2 V (using battery)
- Consumption 4.6 W



Figure 59: a) Camera (left); b) Video camera (right).

## 4.4 Scaling requirements

### 4.4.1 Froude similarity

A geometrical undistorted scale was adopted for the model  $n_L$  ( $n_L = \lambda_m / \lambda_p$ , where  $\lambda_m$  and  $\lambda_p$  are respectively the linear dimensions of the model and prototype) of:

$$n_L = \frac{\lambda_m}{\lambda_p} = \frac{1}{50} \quad (4.2)$$

Consequently, the time scale, according to Froude,  $n_T = T_m / T_p$  and the velocities  $n_V = V_m / V_p$  are equal to:

$$n_T = n_V = \sqrt{n_L} = \sqrt{\frac{1}{50}} = \frac{1}{7.07} \quad (4.3)$$

According to dimensional analysis, assuming the valid Froude similarity, there are valid scale relations for the other variables that intervene in the studied phenomenon. Table 13 lists the various steps taken to reduce in the physical model.

Table 13: Scales used for reducing the model.

Size	Dimension	Scale reducing
Length	L	$n_L$
Wave height	L	$n_H = n_L$
Period	T	$n_T = n_L^{1/2}$
Velocity	L/T	$n_V = n_L^{1/2}$
Discharge	$L^3/LT$	$n_Q = n_L^{3/2}$
Force (weight)	F	$n_P = n_L^3$

### 4.4.2 Dimensioning breakwater layers

Two-dimensional coastal structure model was constructed in wave flume respect to Froude scale law. The blade of wave maker with a water level of 56.3 cm (with a pump on), in front of it, can generate a regular wave with maximum height, equal to 30 cm, which is propagating on the other side of the flume, dissipates its energy, thus decreasing its wave height to the friction with the walls of glass and with the bottom of the channel.

To calculate the maximum height, where the waves are breaking on themselves in relation to water depth in front of the structure we use a simplified formula with a general validity:

$$H_b = \gamma * h_b \quad (4.4)$$

Where  $h_b$  is the average depth at wave breaking,  $\gamma$  is the wave breaking index and  $H_b$  is the breaking height; approximating to first order using the value of  $\gamma = 0.78$ , when the ratio between height and depth exceeds this index, the wave breaks.

The choice of the scaling factor has been performed taking into account the constraints of the laboratory wave flume and wave characteristics relating to wave motion found in Ligurian sea, as follows:

- The scale factor for optimal construction of the model has been identified in 1:50.
- The maximum water level in the flume in front of the generator is 56.3 cm.
- The maximum significant wave height that was generated with wave maker is equal to 15 cm ( $H_2$ ), with time periods from 1.20 to 1.77 seconds (in model scale).
- Toe of harbour breakwater was located at the depth of -16.06 cm (in model scale).
- Sea bed with a slope 1:38 in front of the harbour breakwater, it changes from a depth of approximately -16.06 to - 41.59 cm on a distance of 9.7 m.
- Harbour breakwater berm with a slope of 1:2.

This value is well represented also in guidelines given for international measures to ensure technically actual values that would occur in prototype.

#### 4.4.2.1 Selection parameters

For realization of the harbour breakwater model several materials found in the laboratory were used. For material selection and definition of following characteristic parameters of rocks granulometric analysis was carried out.

- Nominal diameter is defined as the diameter of a cube that has the same volume as the particle and gives us an idea of the physical size of the particle.
- Mean (average), is defined as the average size of the grains of a granulometric distribution.

$$\bar{X} = \sum_{i=1}^n x_i \quad (4.5)$$

- Standard deviation shows how much variation or "dispersion" exists from the average (mean, or expected value). A low standard deviation indicates that the data points tend to be very close to the mean, whereas high standard deviation indicates that the data points are spread out over a large range of values.

$$\sigma = \sqrt{\frac{\sum_{i=1}^n M_{2,i}}{100}}, \text{ where } M_2 \text{ is Moment } 2^\circ \quad (4.6)$$

- Skewness, is a measure of the asymmetry of the probability distribution of a real-valued random variable. It is sensitive to the presence of queues of finer or bigger material.

$$\sigma^{-3} * \frac{\sum_{i=1}^n M_{3,i}}{100}, \text{ where } M_3 \text{ is Moment } 3^\circ \quad (4.7)$$

- Kurtosis, is a descriptor of the shape, compares ranges of extremes of the distribution with the central part.

$$\sigma^{-4} * \frac{\sum_{i=1}^n M_{4,i}}{100}, \text{ where } M_4 \text{ is Moment } 4^\circ \quad (4.8)$$

- Characteristic diameters ( $D_x$ ) are defined as the values of the diameter on the abscissa axis, corresponding to the weight percentage (x). E.g.  $D_{10}$  is characteristic diameter for the weight equal to 10%.
- Coefficient of uniformity (U) is defined as the ratio between the characteristic diameters  $D_{60}$  and  $D_{10}$ . Particle sizes are defined monotone for  $U < 2$  and variable for  $U > 2$ .

$$U = \frac{D_{60}}{D_{10}} \quad (4.9)$$

- V coefficient is defined as the ratio between the difference of the characteristic diameters  $D_{85}$  and  $D_{15}$  and divided with  $D_{85}$ .

$$V = \frac{(D_{85} - D_{15})}{D_{85}} \quad (4.10)$$

The specific gravity of the available material in the laboratory has been preliminary determined, which has the same mineralogical characteristics as the rocks, which are (could) be actually used for the construction of the breakwater, using the following procedure:

Specific weight:

- Weighting individual rocks.
- Placing them in a graduated container with a known volume of water.

- Placing single rocks in graduated container and measuring the final registered volume:

$$V_{\text{final}} = V_{\text{H}_2\text{O}} + V_{\text{rock}} \quad (4.11)$$

- Evaluating variation of volumes:

$$\Delta V = V_{\text{start}} - V_{\text{final}} \quad (4.12)$$

- Density of the material (mass per unit volume), is defined as the ratio between weight (W) and volume change:

$$\rho_s = W / \Delta V \quad \left[ \text{Kg} / \text{m}^3 \right] \quad (4.13)$$

Average (mean) of all individual weights (see Table 14).

Table 14: Average of  $\rho_s$  for all rocks.

Rocks	Weight [gr]	Weight [Kg]	Initial Vol. [ml]	Final Vol. [ml]	$\Delta V$ [ml]	$\Delta V$ [l]	$\Delta V$ [m <sup>3</sup> ]	$\rho_s$ [Kg/m <sup>3</sup> ]
1	120	0,120	400	445	45	0,045	0,000045	2667
2	175	0,175	400	475	75	0,075	0,000075	2333
3	168	0,168	400	455	55	0,055	0,000055	3055
4	189	0,189	400	470	70	0,070	0,000070	2700
5	128	0,128	400	450	50	0,050	0,000050	2560
6	203	0,203	400	475	75	0,075	0,000075	2707
7	174	0,174	400	465	65	0,065	0,000065	2677
8	239	0,239	400	490	90	0,090	0,000090	2656
9	225	0,225	400	480	80	0,080	0,000080	2813
10	182	0,182	400	470	70	0,070	0,000070	2600
11	263	0,263	400	500	100	0,100	0,000100	2630
12	155	0,155	400	460	60	0,060	0,000060	2583
13	180	0,180	400	470	70	0,070	0,000070	2571
14	235	0,235	400	485	85	0,085	0,000085	2765
15	201	0,201	400	475	75	0,075	0,000075	2680
16	215	0,215	400	475	75	0,075	0,000075	2867
17	205	0,205	400	475	75	0,075	0,000075	2733
18	190	0,190	400	465	65	0,065	0,000065	2923
19	175	0,175	400	470	70	0,070	0,000070	2500
20	197	0,197	400	475	75	0,075	0,000075	2627
							<b>AVERAGE</b>	<b>2682</b>

For each type of material the porosity with laboratory measurements has also been defined. Hereinafter used procedure is reported:

Porosity:

- Tank with given volume  $V_{\text{tot}}$ .
- Fill the container with rocks until the border line.
- Determination of the voids volume  $V_v$  by measuring required volume of water, which reaches to the level of the border line.

- Determination of porosity with the relation:

$$n = \frac{V_v}{V_{tot}} * 100 \quad (4.14)$$

#### 4.4.2.2 Recommended scaling procedure of core material in rubble mound breakwater model test

For the tests on the breakwater section, with the necessity to measure the under stresses on the up – structure, the characteristic diameter of the core material in models ( $d_{50}$ ) is chosen in such a way that the Froude scale law holds for a characteristic pore velocity. According to the criterion used by Burcharth et al. (1999), this velocity can be chosen as the average velocity of the 6 points (see Figure 60). It is important to note that the characteristic pore velocity is averaged with respect to time (one wave period) and space (6 points).

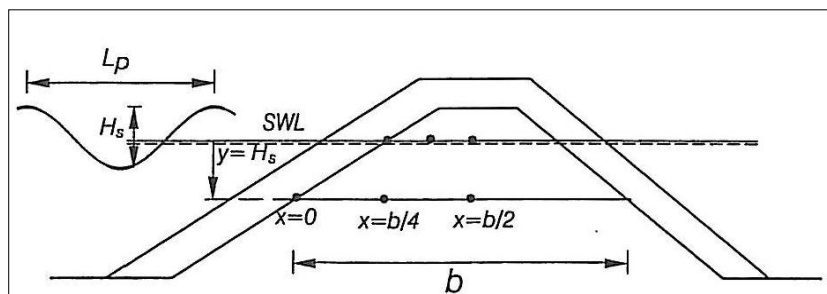


Figure 60: Location for characteristic velocity in the core.  
Source: Burcharth et al., 1999.

For the average diameter of the core material in model scale 1:50, we calculated the filter velocity characteristic of the prototype from the following data.

Table 15: Prototype data of the model.

IN PROTOTYPE
$H_s = 7.5$ m maximum significant wave height on the seabed in front of the harbour (about 8 m)
$T_p = 11.5$ s period
$L_p = 98$ m incident wavelength
$d_{50} = 0.58$ m nominal diameter of the core
$n = 0.36$ core porosity

From the equations 4.15 and 4.16 the reference pressure  $p_{0,max}$  at the interface filter-core and the damping coefficient  $\delta$  were calculated.

$$p_{0,max} = \rho_w g \frac{H_s}{2} \quad (4.15)$$

$$\delta = 0.0141 \frac{n^{1/2} L_p^2}{H_s b} \quad (4.16)$$

Where  $n$  is the porosity of the core material,  $L_p$  is the wave length in the vicinity of the structure and  $\rho_w$  is the sea water density, the vertical distance below the mean sea level is denoted by  $y$ .

Table 16: Vertical distances from MWL (in prototype scale).

y [m]	b[m]	$P_{0,max}$ [kPa]	$\delta$
0	<b>11</b>	38,00	<b>0,98</b>
7,5	<b>33,00</b>	38,00	<b>0,33</b>

For the researching model that does not have any existing prototype we used coefficients  $\alpha = 0$  and  $\beta = 3.6$  seconds Burchart et al. (1999).

The wavelength within the nucleus is:

$$L' = L_p / \sqrt{1.45} = 81.38 \text{ m} \quad (4.17)$$

The pressure gradient and the filtration rate at different points and at different times were calculated from the equations 4.18 and 4.19.

$$I_x = \frac{1}{\rho g} \frac{dp(x,t)}{dx} = -\frac{\pi H_s}{L'} e^{-\delta \frac{2\pi}{L'} x} [\delta \cos\left(\frac{2\pi}{L'} x + \frac{2\pi}{T_p} t\right) + \sin\left(\frac{2\pi}{L'} x + \frac{2\pi}{T_p} t\right)] \quad (4.18)$$

$$I_x = \alpha \left(\frac{1-n}{n}\right)^2 \frac{\vartheta}{g d_{50}^2} \left(\frac{U}{n}\right) + \beta \frac{1-n}{n} \frac{1}{g d_{50}^2} \left(\frac{U}{n}\right)^2 \quad (4.19)$$

Table 17: Characteristic pore velocity in the prototype.

At the point  $x=0, y=0, \Delta t_1$ 

t	0	0,1Tp	0,2Tp	0,3Tp	0,4Tp	0,5Tp	
t	0	1,150	2,300	3,450	4,600	5,750	
$l_x$	-0,285	-0,401	-0,363	-0,187	0,060	0,285	AVERAGE
U1  [m/s]	0,181	0,215	0,205	0,147	0,083	0,181	0,169
U2  [m/s]	-0,181	-0,215	-0,205	-0,147	-0,083	-0,181	-0,169

Solution of equation	$-lx+bU+aU^2=0$	$ax^2+bx+c=0$				
b	0,000					
a	8,68					
D	-9,894	-13,908	-12,615	-6,509	2,082	9,878
sqrt D	3,145	3,729	3,552	2,551	1,443	3,143
c=-lx	0,285	0,401	0,363	0,187	-0,060	-0,285

At the point  $x=0,055, y=0$ 

t	0	0,1Tp	0,2Tp	0,3Tp	0,4Tp	0,5Tp	
t	0	1,150	2,300	3,450	4,600	5,750	
$l_x$	-0,276	-0,329	-0,257	-0,087	0,116	0,275	AVERAGE
U1  [m/s]	0,178	0,195	0,172	0,100	0,116	0,178	0,157
U2  [m/s]	-0,178	-0,195	-0,172	-0,100	-0,116	-0,178	-0,157

Solution of equation	$-lx+bU+aU^2=0$	$ax^2+bx+c=0$				
b	0,000					
a	8,68					
D	-9,564	-11,428	-8,931	-3,025	4,034	9,554
sqrt D	3,093	3,381	2,988	1,739	2,009	3,091
c=-lx	0,276	0,329	0,257	0,087	-0,116	-0,275

At the point  $x=0,11, y=0$ 

t	0	0,1Tp	0,2Tp	0,3Tp	0,4Tp	0,5Tp	
t	0	1,150	2,300	3,450	4,600	5,750	
$l_x$	-0,249	-0,258	-0,169	-0,015	0,145	0,249	AVERAGE
U1  [m/s]	0,170	0,173	0,139	0,041	0,129	0,169	0,137
U2  [m/s]	-0,17	-0,17	-0,14	-0,04	-0,13	-0,17	-0,14

Solution of equation	$-lx+bU+aU^2=0$	$ax^2+bx+c=0$				
b	-6,509					
a	2,55					
D	-8,659	-8,972	-5,862	-0,514	5,030	8,654
sqrt D	2,943	2,995	2,421	0,717	2,243	2,942
c=-lx	0,249	0,258	0,169	0,015	-0,145	-0,249

At the point  $x=0, y=0,15$

t	0	0,1Tp	0,2Tp	0,3Tp	0,4Tp	0,5Tp	
t	0	1,150	2,300	3,450	4,600	5,750	
$l_x$	-0,094	-0,246	-0,304	-0,246	-0,094	0,094	AVERAGE
$ U1 $ [m/s]	0,104	0,168	0,187	0,168	0,104	0,104	0,139
$ U2 $ [m/s]	-0,10	-0,17	-0,19	-0,17	-0,10	-0,10	-0,14

Solution of equation	$-lx+bU+aU^2=0$	$ax^2+bx+c=0$				
b	0,000					
a	8,68					
D	-3,274	-8,552	-10,566	-8,548	-3,268	3,258
sqrt D	1,810	2,924	3,251	2,924	1,808	1,805
$c=-lx$	0,094	0,246	0,304	0,246	0,094	-0,094

At the point  $x=0,165, y=0,15$

t	0	0,1Tp	0,2Tp	0,3Tp	0,4Tp	0,5Tp	
t	0	1,150	2,300	3,450	4,600	5,750	
$l_x$	-0,201	-0,247	-0,199	-0,074	0,078	0,201	AVERAGE
$ U1 $ [m/s]	0,152	0,169	0,151	0,093	0,095	0,152	0,135
$ U2 $ [m/s]	-0,15	-0,17	-0,15	-0,09	-0,09	-0,15	-0,14

Solution of equation	$-lx+bU+aU^2=0$	$ax^2+bx+c=0$				
b	0,000					
a	8,68					
D	-6,993	-8,586	-6,903	-2,586	2,718	6,985
sqrt D	2,644	2,930	2,627	1,608	1,649	2,643
$c=-lx$	0,201	0,247	0,199	0,074	-0,078	-0,201

At the point  $x=0,33, y=0,15$

t	0	0,1Tp	0,2Tp	0,3Tp	0,4Tp	0,5Tp	
t	0	1,150	2,300	3,450	4,600	5,750	
$l_x$	-0,201	-0,161	-0,059	0,065	0,164	0,201	AVERAGE
$ U1 $ [m/s]	0,152	0,136	0,082	0,087	0,138	0,152	0,125
$ U2 $ [m/s]	-0,15	-0,14	-0,08	-0,09	-0,14	-0,15	-0,12

Solution of equation	$-lx+bU+aU^2=0$	$ax^2+bx+c=0$				
b	0,000					
a	8,68					
D	-6,976	-5,573	-2,044	2,266	5,710	6,976
sqrt D	2,641	2,361	1,430	1,505	2,390	2,641
$c=-lx$	0,201	0,161	0,059	-0,065	-0,164	-0,201

AVERAGE 0,144

Re 75698,88

So the average characteristic pore velocity in the prototype is:  $\bar{U}_p = 0.144$  m/s and the Reynolds number, which is given by :

$$Re^p = \frac{\bar{U}^p d_{50}}{\nu} = 75699 \quad (4.20)$$

The Reynolds number justifies the choice of the coefficients  $\alpha$  and  $\beta$ . In accordance with the Froude scale law, the characteristic speed in the filter of the model will be given by:

$$\bar{U}^m = \bar{U}^p / \sqrt{50} = 0.020 \text{ m/s} \quad (4.21)$$

Trying to use  $d_{50} = 0.0116 \text{ m}$ , for the core material in the model, by performing the same calculations for the prototype, and using the correct coefficients  $\alpha$  and  $\beta$  estimated by Burchart et al. (1999), the filtration velocity was found to  $\bar{U}^m = 0.013 \text{ m/s}$ , which is smaller than the previously obtained target by using the similarity of Froude, i.e.  $0.020 \text{ m/s}$ . Finally, the iterative method obtain the value of the characteristic diameter of the core components boulders, which respects the Froude similarity, and this value is equal to a diameter of  $d_{50} = 0.016 \text{ m}$ , i.e. elements from about 11 g. Thus the ratio of scale to be used for the core material will be given by:  $d_{50}^m / d_{50}^p = 0.016 / 0.580 = 1:36.3$ , which results to be larger than the ratio 1:50 used for the scale of the lengths in the model.

Table 18: Results from iterative method to obtain the characteristic core diameter (in model scale).

$d_{50}^m \text{ [m]}$	0,0116	Characteristic pore velocity in model [m/s]	0,013	Re	133,72
$d_{50}^m \text{ [m]}$	0,012	Characteristic pore velocity in model [m/s]	0,014	Re	147,54
$d_{50}^m \text{ [m]}$	0,014	Characteristic pore velocity in model [m/s]	0,017	Re	218,77
$d_{50}^m \text{ [m]}$	0,017	Characteristic pore velocity in model [m/s]	0,022	Re	334,78
$d_{50}^m \text{ [m]}$	0,016	Characteristic pore velocity in model [m/s]	0,020	Re	249,19

#### 4.4.3 Used materials

The materials used for the reproduction of various layers constituting the breakwater have been selected as a function of the respective scale factors used.

##### 4.4.3.1 Armour layer

The armour layer of the berm is constituted of natural rocks of IV category, with a weight variation from 7 to 12 tons (in prototype scale), arranged in two layers with a porosity of 37% and thickness of 6.6 cm.

Data for scaling rocks in smaller scale factor were taken from a port in Liguria, more precisely Pietra Ligure port (Cappiotti et. al, 2012). And so the following procedure was necessary:

$$\text{Model weight} = \left( \frac{V_m}{V_p^3} \right) * \left( \frac{(\rho_r - \rho_{w,s})}{(\rho_r - \rho_w)} \right) * \text{Prototype weight}, \quad (4.22)$$

$$\text{Model weight} = \left( \frac{1}{50^3} \right) * \left( \frac{(2682 - 1033)}{(2682 - 1000)} \right) * 7 * 10^6 = 57.12 \text{ g} \cong 60 \text{ g} \quad (4.23)$$

$$Model\ weight = \left(\frac{1}{50^3}\right) * \left(\frac{2682-1033}{2682-1000}\right) * 12 * 10^6 = 97.92\ g \cong 100\ g \quad (4.24)$$

Where  $\rho_r$  rock density,  $\rho_w$  water density,  $\rho_{w,s}$  density of sea water.

For chosen scale factor 1:50 selected material is included in the range  $60 \div 100$  gr, which corresponds to rocks characterized by  $D_{n,50}$  between  $27 \div 34$  mm.



Figure 61: Rocks used for armour layer.

Table 19: Calculations for granulometric analysis - Armour Layer.

	Ranges of the classes - Armour Layer						
	[27 ÷ 28]	[28 ÷ 29]	[29 ÷ 30]	[30 ÷ 31]	[31 ÷ 32]	[32 ÷ 33]	[33 ÷ 34]
<b>D [mm]</b>	27,5	28,5	29,5	30,5	31,5	32,5	33,5
<b><math>\phi</math></b>	-4,78	-4,83	-4,88	-4,93	-4,98	-5,02	-5,07
<b>Frequency</b>	1	70	86	107	121	120	66
<b>Frequency %</b>	0,2	12,3	15,1	18,7	21,2	21,0	11,6
<b>Cumulative Freq.</b>	0,2	12,4	27,5	46,2	67,4	88,4	100,0
<b>Moment 1°</b>	-0,84	-59,25	-73,54	-92,40	-105,47	-105,55	-58,56
<b>Moment 2°</b>	0,005	0,186	0,081	0,012	0,010	0,093	0,140
<b>Moment 3°</b>	9,3E-04	2,3E-02	5,9E-03	3,0E-04	-2,0E-04	-6,1E-03	-1,5E-02
<b>Moment 4°</b>	1,6E-04	2,8E-03	4,4E-04	7,6E-06	4,3E-06	4,1E-04	1,7E-03

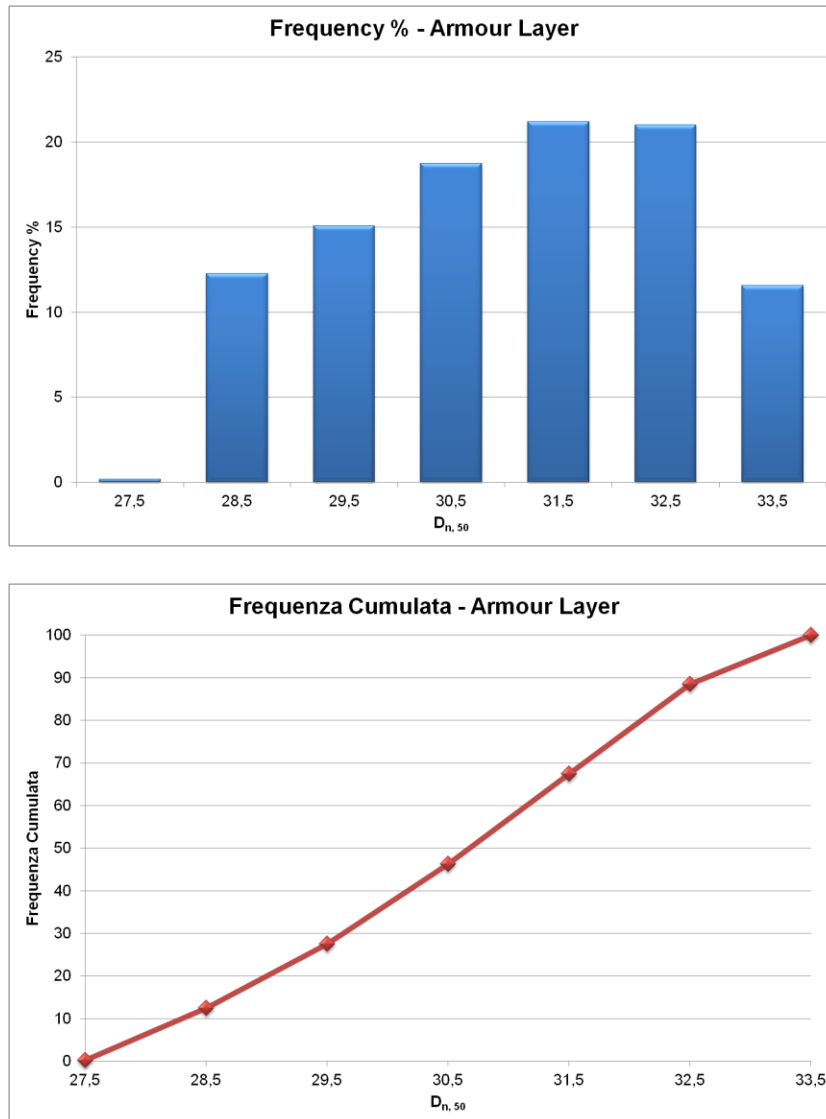
Table 20: Characteristic parameters determined by granulometric analysis - Armour layer.

Mean $\phi$	Mean [mm]	Standard Dev.	Skewness	Kurtosis
-5,0	31,0	0,0726	0,217	1,997

$D_{10}$ [mm]	$D_{15}$ [mm]	$D_{60}$ [mm]	$D_{85}$ [mm]	$D_{50}$ [mm]	$U = D_{60}/D_{10}$ [mm]	$V = D_{85}-D_{15}/D_{85}$ [mm]
28,5	28,7	31,1	32,3	31	1,09	0,11

Hereinafter are reported graphs of granulometric analysis, performed on a sample of approximately 1051 random taken stones, which were used in the model.



Graph 1: Granulometric analysis for the material constructing the armour layer.

#### 4.4.3.2 Filter layer

The filter layer of the berm is constituted under the main armour layer of smaller natural rocks of II category, with a weight variation from 1 to 3 tons (in prototype scale), size between 0.7 and 1.0 m (in prototype scale) formed in two layers of stones with a porosity of 37% and thickness of 4.0 cm (in model scale). This layer builds also berm toe, which is established on -13.84 cm deep.

$$Model\ weight = \left(\frac{1}{50^3}\right) * \left(\frac{(2682-1033)}{(2682-1000)}\right) * 1 * 10^6 = 8.16\ g \cong 9\ g \quad (4.25)$$

$$Model\ weight = \left(\frac{1}{50^3}\right) * \left(\frac{(2682-1033)}{(2682-1000)}\right) * 3 * 10^6 = 24.48\ g \cong 25\ g \quad (4.26)$$

For chosen scale factor 1:50 selected material is included in the range 9 ÷ 25 g, which corresponds to rocks characterized by  $D_{n,50}$  between 14 ÷ 22 mm.



Figure 62: Rocks used for filter layer.

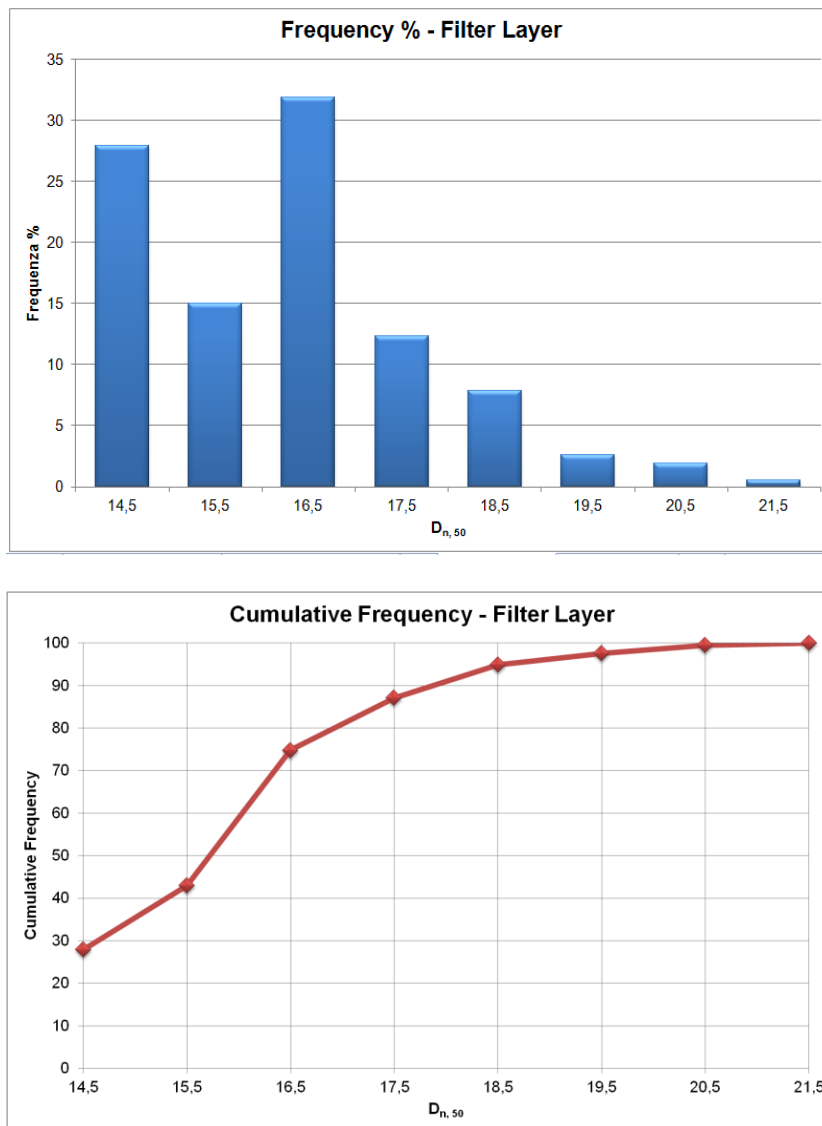
Table 21: Calculations for granulometric analysis - Filter Layer.

	Ranges of the classes - Armour Layer							
	[14 ÷ 15]	[15 ÷ 16]	[16 ÷ 17]	[17 ÷ 18]	[18 ÷ 19]	[19 ÷ 20]	[20 ÷ 21]	[21 ÷ 22]
<b>D[mm]</b>	14,5	15,5	16,5	17,5	18,5	19,5	20,5	21,5
<b>φ</b>	-3,86	-3,95	-4,04	-4,13	-4,21	-4,29	-4,36	-4,43
<b>Frequency</b>	352	189	402	155	99	33	24	7
<b>Frequency %</b>	27,9	15,0	31,9	12,3	7,9	2,6	1,9	0,6
<b>Cumulative Freq.</b>	27,9	42,9	74,8	87,1	94,9	97,5	99,4	100,0
<b>Moment 1°</b>	-107,69	-59,27	-128,93	-50,76	-33,05	-11,21	-8,29	-2,46
<b>Moment 2°</b>	0,702	0,058	0,025	0,156	0,292	0,189	0,221	0,093
<b>Moment 3°</b>	1,1E-01	3,6E-03	-6,8E-04	-1,8E-02	-5,6E-02	-5,1E-02	-7,5E-02	-3,8E-02
<b>Moment 4°</b>	1,8E-02	2,3E-04	1,9E-05	2,0E-03	1,1E-02	1,4E-02	2,6E-02	1,6E-02

Table 22: Characteristic parameters determined by granulometric analysis – Filter layer.

Mean φ	Mean [mm]	Standard Dev.	Skewness	Kurtosis
-4,0	16,2	0,1318	-0,541	2,843

Hereinafter graphs of granulometric analysis are reported, performed on a sample of approximately 1000 random taken stones from among those used.



Graph 2: Granulometric analysis for material constructing the filter.

#### 4.4.3.3 Core

For chosen scale factor 1:36.3 selected material is included in the range  $9 \div 13$  gr, which corresponds to rocks characterized by  $D_{n,50}$  between  $15 \div 17$  mm.

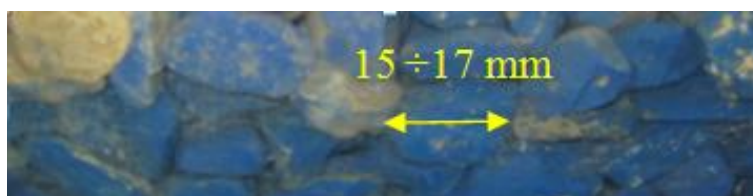


Figure 63: Rocks used for core.

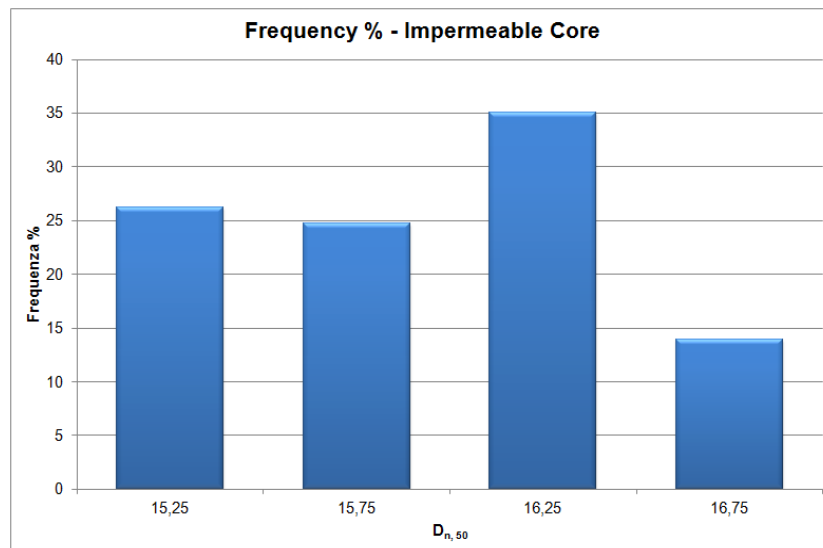
Table 23: Calculations for granulometric analysis – Core.

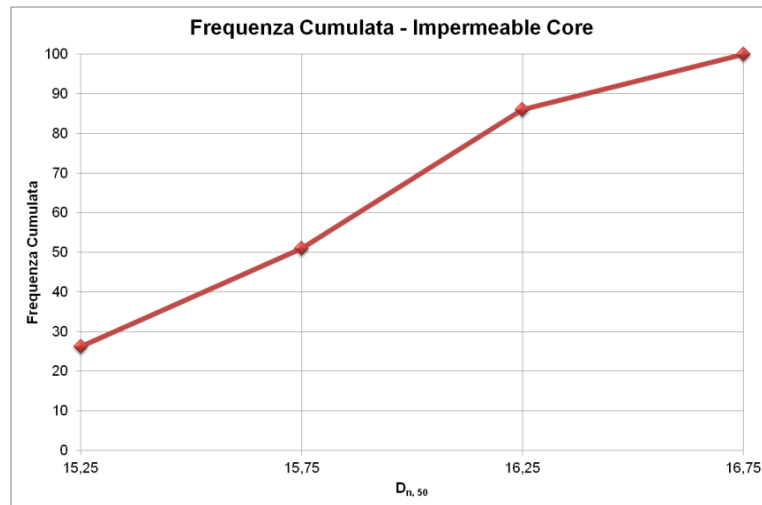
	Ranges of the classes -Core			
	[15 ÷ 15.5]	[15.5 ÷ 16]	[16 ÷ 16.5]	[16.5 ÷ 17]
<b>D[mm]</b>	15,25	15,75	16,25	16,75
<b>φ</b>	-3,93	-3,98	-4,02	-4,07
<b>Frequency</b>	294	277	393	156
<b>Frequency %</b>	26,3	24,7	35,1	13,9
<b>Cumulative Freq.</b>	26,3	51,0	86,1	100,0
<b>Moment 1°</b>	-103,18	-98,37	-141,14	-56,63
<b>Moment 2°</b>	0,103	0,006	0,030	0,074
<b>Moment 3°</b>	6,4E-03	1,0E-04	-8,7E-04	-5,4E-03
<b>Moment 4°</b>	4,0E-04	1,6E-06	2,5E-05	3,9E-04

Table 24: Characteristic parameters determined by granulometric analysis – Core.

Mean φ	Mean [mm]	Standard Dev.	Skewness	Kurtosis
-3,99	15,93	0,0461	0,027	1,815

Hereinafter are reported graphs of granulometric analysis, performed on a sample of approximately 1000 random taken stones from among those used.





Graph 3: Granulometric analysis for the material constructing core.

#### 4.4.3.4 Overspill basin (OB)

For chosen scale factor 1:50 selected tetrapods with all dimensions equal to 7 cm are included. Tetrapod is a four-legged concrete structure used as armour unit. We used them to stabilize OB. The Tetrapod's shape is designed to dissipate the force of incoming waves by allowing water to flow around rather than against it, and to reduce displacement. We place them into two lines (see Fig. 64), in the first line tetrapods were placed standing with three legs leaning down on a filter layer and in the second line, three-legs were in front of wave wall to ensure the stability of rocks form armour layer behind. Of course in nature it would be difficult to place them exactly like this, due to their weight and sea bed conditions.



Figure 64: Placing tetrapods into the model.

#### 4.4.3.5 Wave wall

For configurations C4 and C5 we used sticks with dimensions 2.0 cm \* 80.0 cm \* 3.0 cm (height \* length \* width) in C4 and 1.1 cm \* 80.0 cm \* 0.4 cm (height \* length \* width) in C5 made out of plexiglass to raise the wave wall.



Figure 65: Raising the wave wall in configurations C4 and C5.

#### 4.5 Harbour breakwater design and construction

After establishing the scale factor and selection of the material, we proceeded to the construction of the physical model in the wave flume. A principal design objective is to determine the size and layout of the components of the cross-section. Special attention was paid to the construction of the model sections in order to ensure the highest possible accuracy, especially by positioning the right elevation of the wave wall crest, from which the number and amount of overflowing waves depends in a decisive way.

Harbour breakwater berm toe (see Fig. 66) has been positioned at the distance 32.63 m from the wave maker. We have tested 6 different configurations of a model, from those; all have been subjected on a single range of sea state.

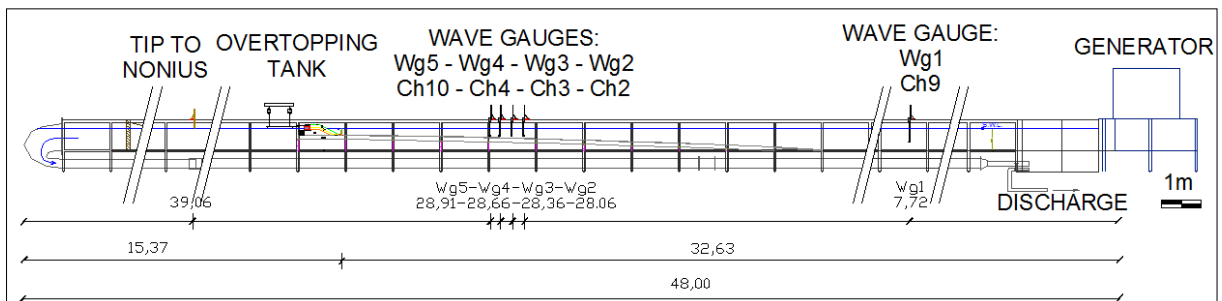


Figure 66: Side view of the wave flume with locations of analysed structures (in model scale).

### 4.5.1 Slope angle

Side slopes are generally as steep as possible to minimise the volume of core material and to reduce the reach of cranes working from the crest (Palmer et al. 1998). However it may be possible to develop a less steep slope if the cranes operate from a barge. In our case the slope angle for all the configurations was 2:1 facing to the sea side.

### 4.5.2 Layer thickness

Armour stability generally increases with an increase in armour layer thickness. Also the energy dissipation is better on thicker layer, so overtopping phenomenon would be less frequent. Values of thickness remain the same during the tests and are represented in the table below.

Table 25: Layer thickness in the model.

Layer thickness ( in cm, model scale)	C0	C1	C2	C3	C4	C5
Armour layer	6,6	6,6	6,6	6,6	6,6	6,6
Filter	4,0	4,0	4,0	4,0	4,0	4,0
Core	15,0	15,0	15,0	15,0	15,0	15,0
Berm toe	2,0	2,0	2,0	2,0	2,0	2,0

### 4.5.3 Configuration of cross sections

The configurations (C0, C1, C2, C3, C4 and C5) of the harbour breakwater provided for this thesis research have a concrete wave wall with 3 different crown heights and 3 different overspill basin widths. For the first 4 configurations C0, C1, C2 and C3 the crown height was constant + 9.60 cm, crown height for C4 was 11.6 cm and for C5 10.7 cm (in model scale) above the sea level. Overspill basin was added to configurations C1, C2 and C3, with lengths form 6.0 cm, 12.0 cm to 18.0 cm.

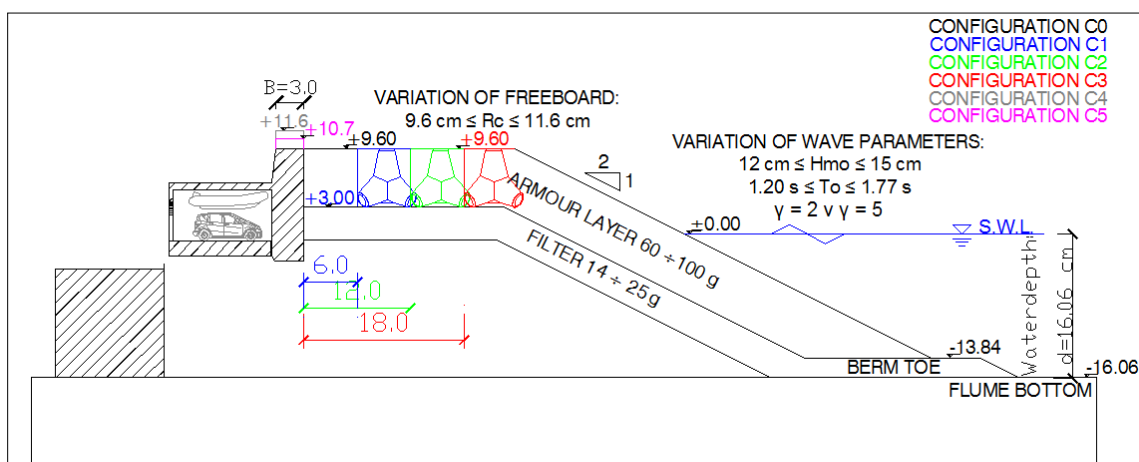


Figure 67: Schematic illustration of experiment (in model scale).

Table 26: Cross section heights at all configurations.

Height (m.a.s.l. in model scale)	C0	C1	C2	C3	C4	C5
Berm fullfilment to a wave wall	9,6	9,6	9,6	9,6	9,6	9,6
Wave wall crest	9,6	9,6	9,6	9,6	11,6	10,7
Toe of the structure from SWL	-13,84	-13,84	-13,84	-13,84	-13,84	-13,84
Flume (sea) bottom from SWL	-16,06	-16,06	-16,06	-16,06	-16,06	-16,06
Overspill basin (OB) added	0	6,0	12,0	18,0	0,0	0,0

The heights of the wave wall crest emerged and submerged berm and berm toe were measured by bringing the surface of the water in the wave flume tangential. We have made this in four points (as shown in upper Table 26) and measured them by the tip to nonius, with the 0.05 mm accuracy. It is possible to note that the height measurements in the model are affected by strong surface irregularities due to rock setting and shapes.

Hereinafter the photographic documentation during phases of model is shown and is so representing different stages for constructing starting configuration C0.





Figure 68: Construction phases of the harbour breakwater in the wave flume.

All conducted model configurations are presented below in continuous order, like they were carried out in our research during spring 2012.

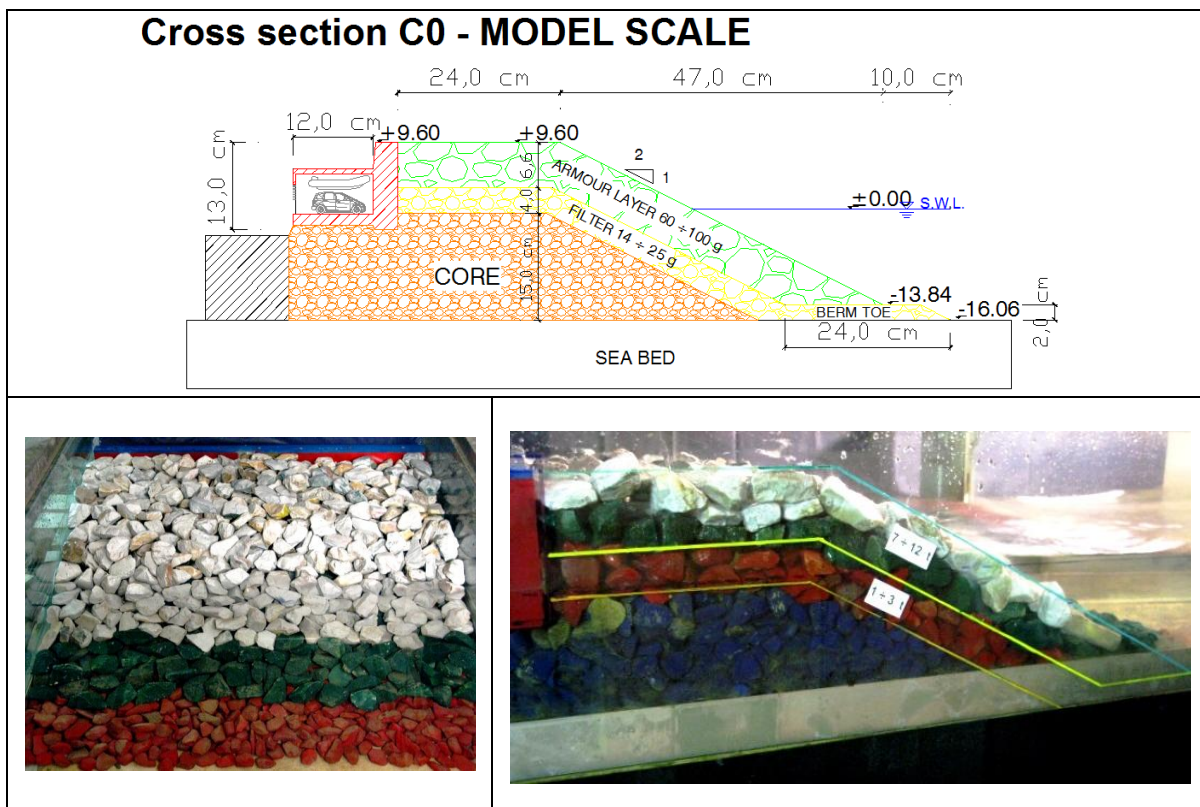


Figure 69: Configuration C0.

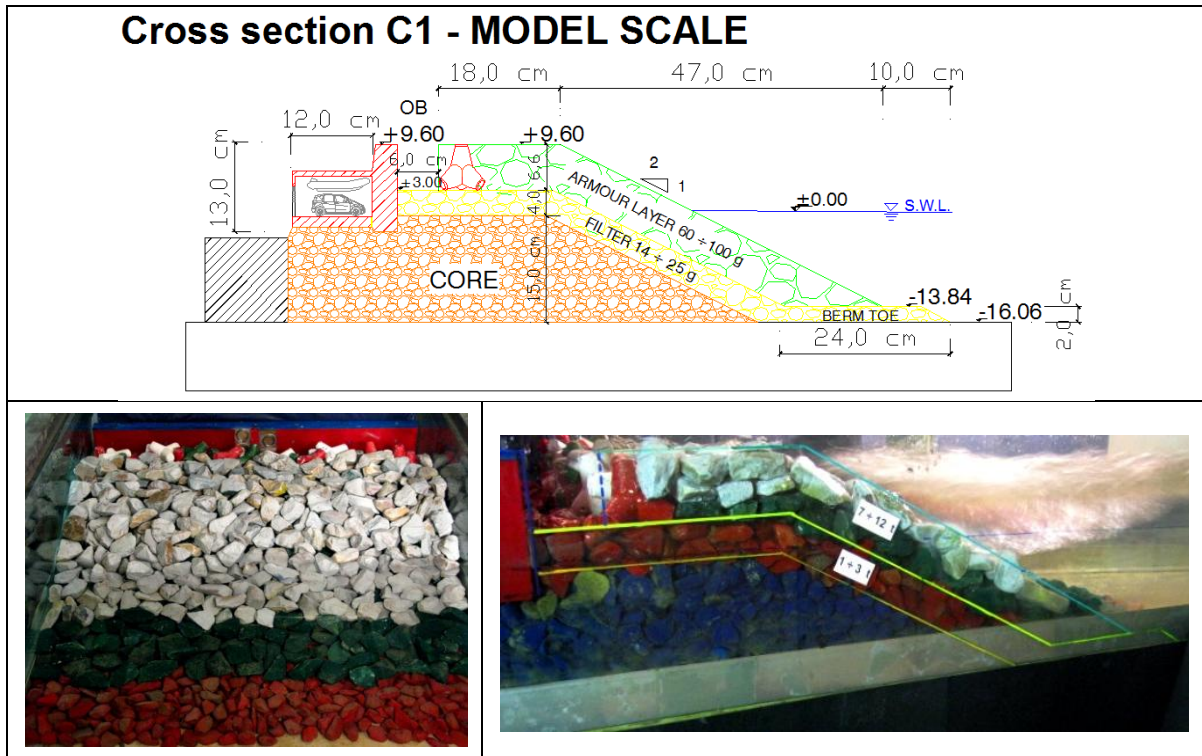


Figure 70: Configuration C1.

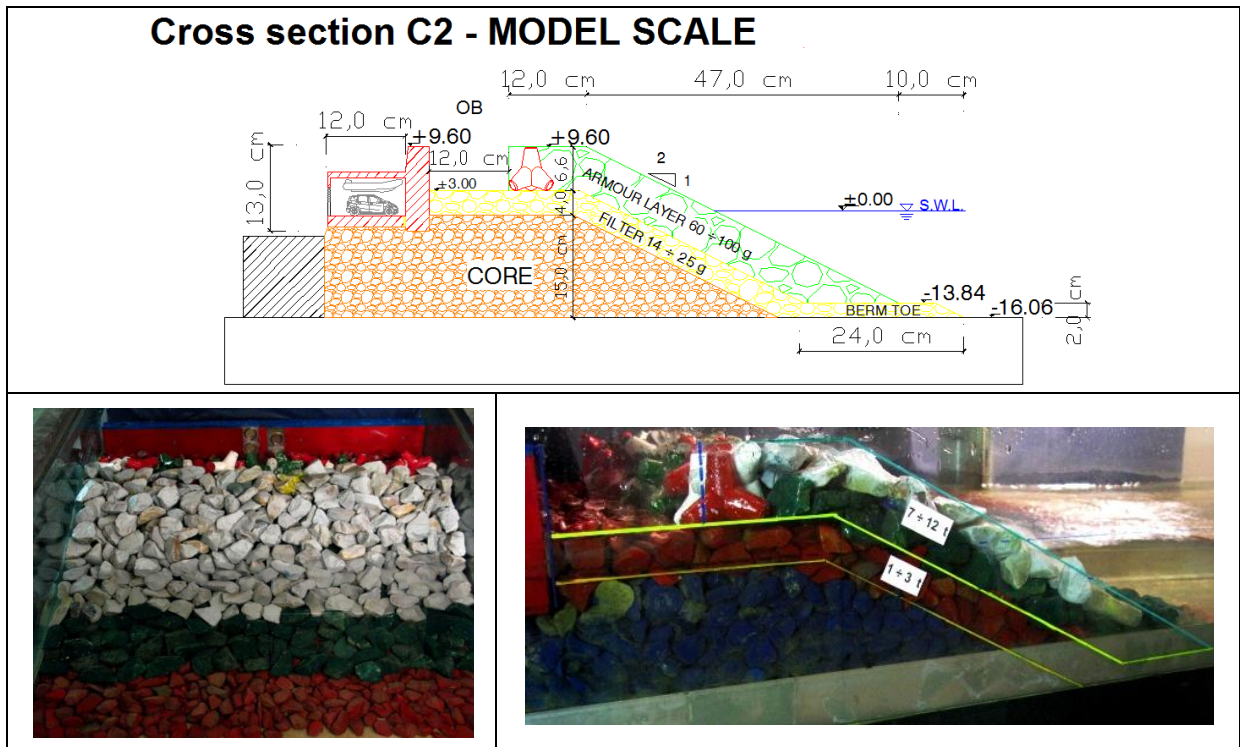


Figure 71: Configuration C2.

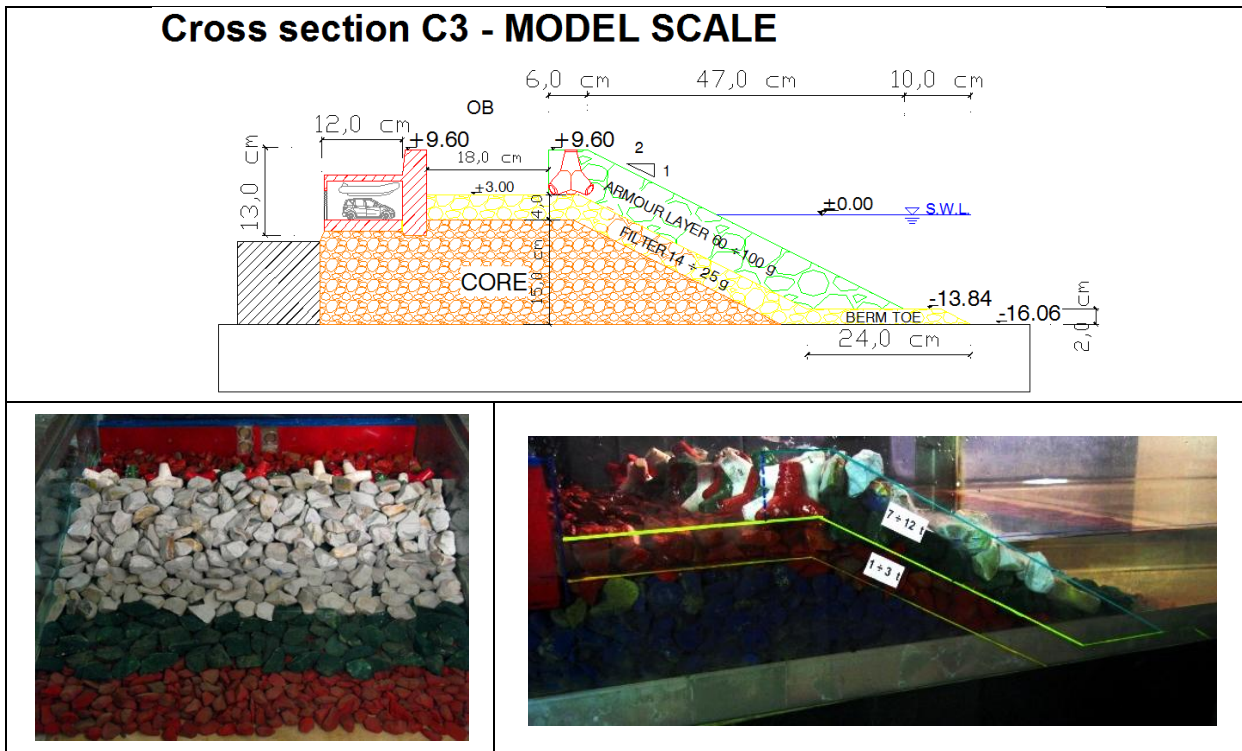


Figure 72: Configuration C3.

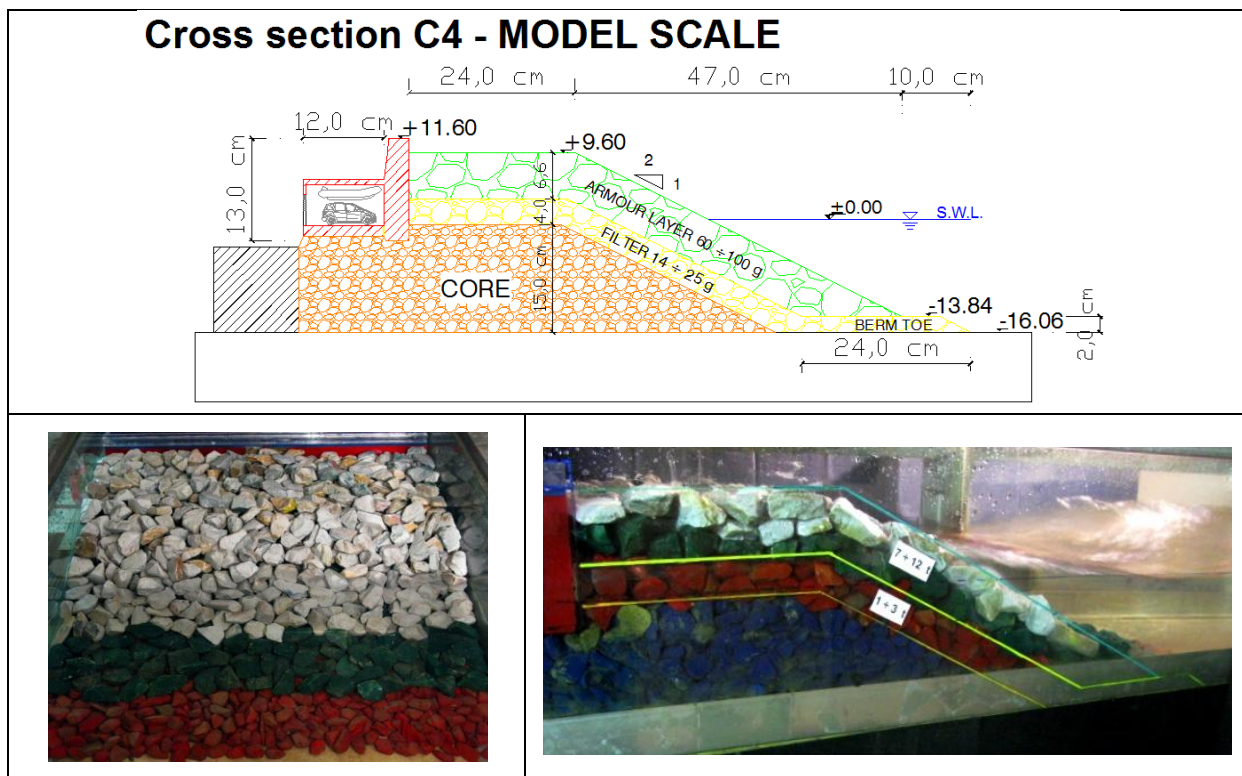


Figure 73: Configuration C4.

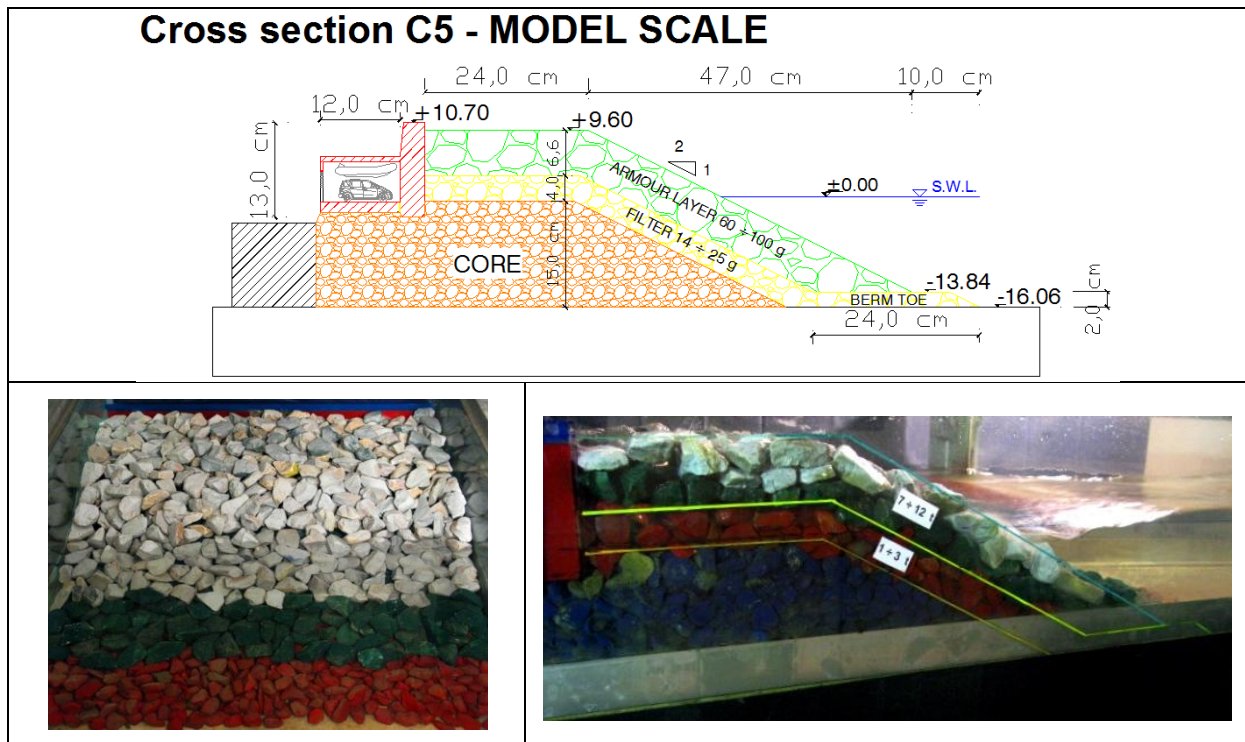


Figure 74: Configuration C5.

#### 4.6 Water levels and wave conditions

##### 4.6.1 Water levels

During the tests water level in wave flume (SWL) remained the same. It was 0.8 cm higher respect to the initial level with the pump off. SWL on the upper schemes (from Fig. 69 to Fig. 74) regards to calibrated water level at the beginning of each test, which could sometimes be lower than actual SWL, because of the possible loss of the wave flume.

Table 27: Water levels in the wave flume at back blade pump on or off.

Water levels (WL) in the wave flume		
Back blade pump	WL at the nonius tip [cm]	Depth at the wave maker blade [cm]
On	14,4	56,3
Off	15,2	55,5

##### 4.6.2 Wave conditions

Wave attacks were chosen in particular to those wave characteristics found in Ligurian sea, since University of Florence is often involved in designing Ligurian ports, which are found in Italian region Liguria. Wave attacks were random and characterized by a JONSWAP

spectrum, with peak incremental factor  $\gamma$  of 2 or 5. We tested 8 types of different waves on 5 different constructions. In total we have performed 40 tests.

The breaker parameter is defined as:

$$\xi_{m-1,0} = \frac{\tan\alpha}{\left(\frac{H_{m0}}{L_{m-1,0}}\right)^{1/2}} \quad (4.29)$$

Where  $\alpha$  is the slope of the front face of the structure and  $L_{m-1,0}$  being the deep water wave length  $gT_{m-1,0}^2/2\pi$  and  $H_{m0}$  is wave height.

In first approximation the values of  $\xi_{m-1,0} \leq 3$  are linked to the plunging waves. But we can note that attacks in the waves shown are both plunging and surging. Breaking process is influenced by the porosity and friction of the wave flume bottom.

#### 4.6.2.1 Preliminary tests

The preliminary tests were carried out between 28<sup>th</sup> and 30<sup>th</sup> of March 2012, in order to identify and evaluate behaviour of selected waves and improve them if necessary for further definitive tests.

The most important objectives of preliminary tests are:

- To assess functioning of laboratory instruments, particularly overtopping measurements.
- To evaluate and define wave parameters (and their transformation) from preliminary tests for the main tests to execute.
- Identification of main phases of work in order to prepare Check-List that will be followed during definite tests.

Experiments carried out during preliminary tests were not the same as definitive tests, there are differences as follow:

- Tests had a duration of 5 minutes.
- Between two followed tests there was not a pause of 20 min completed, to stabilize the water level in the flume.
- There were not data of the first 2 minutes of standing water level acquired.
- Only starting configuration, called C0 of a model has been tested.

After execution of tests was done, registered data (from WG) was analyzed by Matlab program. By analysing each of them, assessment of optimal characteristic parameters ( $H_{m0}$ ,  $H_{1/3}$ ,  $H_{max}$ ,  $T_{m0}$ ,  $T_{1/3}$ ,  $T_p$  ...) for the definitive tests has been done.

Hereinafter the preliminary wave attack parameters are shown, as they were assumed and actually measured by WG1 on the starting configuration C0.

Table 28: Assumed and generated parameters of preliminary wave attacks, registered by the WG1, for the starting configuration C0.

Date	Wave	Repetition	H_generated [cm]	T_generated [s]	$\gamma$ JONSWAP	Duration [min]	H_target [cm]	T_target [s]
28.3.2012	H10T99G2	A	7,68	0,90	2	5	10	0,99
28.3.2012	H11T99G2	A	7,77	1,00	2	5	11	0,99
28.3.2012	H12T99G2	A	10,16	1,10	2	5	12	0,99
28.3.2012	H12T99G2	B	9,54	1,00	2	5	12	0,99
28.3.2012	H12T99G2	C	10,49	1,00	2	5	12	0,99
28.3.2012	H115T9G2	A	10,41	1,00	2	5	11,5	0,9
28.3.2012	H115T9G2	B	9,83	1,10	2	5	11,5	0,9
29.3.2012	H115T127G2	A	9,30	1,20	2	5	11,5	1,27
29.3.2012	H115T156G2	A	9,62	1,60	2	5	11,5	1,56
29.3.2012	H18T163G5	A	17,04	1,60	5	5	18	1,63
29.3.2012	H17T163G5	A	15,15	1,60	5	5	17	1,63
29.3.2012	H17T163G5	B	15,44	1,60	5	5	17	1,63
29.3.2012	H17T163G5	C	15,48	1,60	5	5	17	1,63
29.3.2012	H17T163G5	A1	15,38	1,60	5	5	17	1,63
29.3.2012	H17T163G5	A2	15,41	1,60	5	5	17	1,63
29.3.2012	H17T163G5	A3	14,99	1,60	5	5	17	1,63
29.3.2012	H12T99G2	A	10,42	1,00	2	5	12	0,99
29.3.2012	H13T99G2	A	10,53	0,90	2	5	13	0,99
29.3.2012	H14T99G2	A	10,63	1,00	2	5	14	0,99
29.3.2012	H16T99G2	A	12,47	1,00	2	5	16	0,99
29.3.2012	H15T106G2	A	11,30	1,10	2	5	15	1,06
29.3.2012	H145T106G2	A	11,30	1,00	2	5	14,5	1,06
29.3.2012	H14T106G2	A	11,77	1,00	2	5	14	1,06
29.3.2012	H14T127G2	A	13,08	1,20	2	5	14	1,27
29.3.2012	H14T156G2	A	14,09	1,60	2	5	14	1,56
30.3.2012	H13T113G2	A	10,20	1,10	2	5	13	1,13
30.3.2012	H14T113G2	A	9,65	1,10	2	5	14	1,13
30.3.2012	H145T12G2	A	13,00	1,20	2	5	14,5	1,2
30.3.2012	H14T12G2	A	12,07	1,20	2	5	14	1,2
30.3.2012	H14T148G2	A	12,59	1,60	2	5	14	1,48
30.3.2012	H135T148G2	A	12,10	1,50	2	5	13,5	1,48
30.3.2012	H14T177G2	A	13,50	1,80	2	5	14	1,77
30.3.2012	H13T177G2	A	12,03	1,70	2	5	13	1,77
30.3.2012	H17T163G5	A	15,06	1,60	5	5	17	1,63

Waves attacks marked in orange were selected for the final definitive tests.

Table 29: Assumed wave attacks for definitive tests.

	Model		
	Hmo [cm]	Tp [sec]	Gamma
H1T85G2	12	1,2	2
H1T85G5	12	1,2	5
H1T105G2	12	1,48	2
H1T105G5	12	1,48	5
H1T125G2	12	1,77	2
H1T125G5	12	1,77	5
H2T115G2	15	1,63	2
H2T115G5	15	1,63	5

#### 4.7 Instrument placement

Instrumentation used along the flume for the execution of the tests is as follows:

- 1 tip with nonius, with precision of 1/10 of a millimetre,
- 5 resistive wave gauges with the sampling frequency of 20 Hz,
- 1 overtopping tank,
- 2 samplers (chute) which lead each wave-by-wave overtopping volume to the overtopping tank,
- 5 pressure transducers for measuring the pressures inside the wave wall,
- 1 measuring cylinder for measuring volume from overtopping tank,
- 4 load cells.

Table 30: Distances of single tools from the wave maker.

Tool	Distance from wave maker [m]
WG 1	7,02
WG 2	28,06
WG 3	28,36
WG 4	28,66
WG 5	28,91
Pressure tran.	33,43
Sampler	33,43
Overtopping tank	33,7
Load cells 1 and 2	33,9
Load cells 3 and 4	34,43
Tip at nonius	39,06

Please refer this Table 30 also together with an Attachment A which represents wave flume dimensions and instrumentation used.

## 4.8 Test conditions

### 4.8.1 Definition of wave attacks

Test conditions for the research are characterized by an irregular wave motion, representing the sea state with a return period of fifty-years, which must be reproduced for a single value of the sea state (water level F1). Definition of the waves (W1, W2, W3 ... W8) reported in the previous chapter, has served us to generate wave attacks in the tests.

Each wave attack lasted for an hour, which in nature (in prototype scale) would mean 7 hours, since the time in the wave flume is 7 times faster (Froude law). Further on wave attacks differed for waves with wave height H1 from those with wave height of H2. So each wave attack with a wave height H1 has been divided into 3 wave attacks with the duration of 20.5 minute, while wave attacks with a wave height H2 has been divided into 6, 10.5 minute long attacks. All repetitions of wave attacks have duration of 30 additional seconds, as in the first half a minute wave motion is stopped by generator and WG record the zero levels of the free surface. In both cases there was always a wave attack with a total duration of about 1 hour, characterized by a JONSWAP spectrum with the peak elevation factor gamma 2 or 5 for all the waves.

Table 31: Definition of wave attacks.

Wave	Repetition	H [cm]	T [s]	$\gamma_{\text{JONSWAP}}$	Duration [s]
W1	A	12	8,5	2	20+0,5
	B	12	8,5	2	20+0,5
	C	12	8,5	2	20+0,5
W2	A	12	8,5	5	20+0,5
	B	12	8,5	5	20+0,5
	C	12	8,5	5	20+0,5
W3	A	12	10,5	2	20+0,5
	B	12	10,5	2	20+0,5
	C	12	10,5	2	20+0,5
W4	A	12	10,5	5	20+0,5
	B	12	10,5	5	20+0,5
	C	12	10,5	5	20+0,5
W5	A	12	12,5	2	20+0,5
	B	12	12,5	2	20+0,5
	C	12	12,5	2	20+0,5
W6	A	12	12,5	5	20+0,5
	B	12	12,5	5	20+0,5
	C	12	12,5	5	20+0,5
W7	A	15	11,5	2	10+0,5
	B	15	11,5	2	10+0,5
	C	15	11,5	2	10+0,5
	D	15	11,5	2	10+0,5
	E	15	11,5	2	10+0,5
	F	15	11,5	2	10+0,5
W8	A	15	11,5	5	10+0,5
	B	15	11,5	5	10+0,5
	C	15	11,5	5	10+0,5
	D	15	11,5	5	10+0,5
	E	15	11,5	5	10+0,5
	F	15	11,5	5	10+0,5

### 4.8.2 Test methodology

There were special types of waves tested in order to get better knowledge about parameters in which we were interested:

#### 1. Wave overtopping

Wave overtopping is affected by many factors: geometry of a structure (model), model position in the flume, wave parameters (wave heights, wave periods...). For a good statistical analysis it is necessary to have number of events (wave-by-wave overtopping) big enough. It is recommended to extend tests to have minimum of 2000 wave periods (Esposito, 2011). The wave period which is provided in the experiments is about 2 s (in model scale) which means that the measures of WO must be conducted for at least about 4000 s. Therefore tests duration of 60 min = 3600 s is suitable for our purposes. Wave overtopping flow rate is captured by the overtopping tank connected to the wave wall by sampler (slide).

Sampler had 2 different entrance widths, 30 cm width for tests with wave height H1 and width of 20 cm for tests with wave height H2. The reason to do this were preliminary tests, which showed us, that in case of higher waves (H2) the quantity of water that overflowed the wave wall crown was too big for load cells capacity and overtopping tank to receive it. The same argument explain us also decision why have we chosen 2 different durations of the tests, 20 and 10 min. Preliminary tests lasted for 5 min and were made on C0 configuration, which in comparison to the others should be the least harmful, so when dimensioning the others we consider this fact very carefully.

#### 2. Pressures at the surface of wave wall

The measurement of pressures installed along the center line section of the wave wall were carried out using five pressure transducers placed inside the wave wall, which acquire with the nominal resolution of 0,01 kg/cm<sup>2</sup> (10 g/cm<sup>2</sup>, in prototype 0,5 kg/cm<sup>2</sup>) to measure the pressures frontally in different points. Graphs recorded distribution of pressures at each pressure transducer (in bar) during the test. Measures are in bars, 1 bar is 100000 Pa, which is 100000 N/m<sup>2</sup>, a measure of force (load) per unit area.

#### 3. Reflection

Wave gauge data with the sampling frequency of 20Hz have calculated wave reflection coefficients (Hi, Hr, Kr), which are important measures of the effectiveness of wave wall protection.

### 4.8.3 Test nomenclature

Each test done was identified with a code constructed according to different variables of the test.

For example: **H1T085G2AF1C0**

Where:

- H1 indicates wave height ( $H1 > H_{m0} = 12.0$  cm,  $H2 > H_{m0} = 15.0$  cm),
- T085 indicates wave period ( $T_{p,085} = 1.2$  s,  $T_{p,105} = 1.48$  s,  $T_{p,115} = 1.63$  s  $T_{p,125} = 1.77$  s),
- G2 peak elevation factor of JONSWAP spectrum ( $\gamma_{G2} = 2.0$ ,  $\gamma_{G5} = 5.0$ ),
- A repetition of the test (A, B, C or A, B, C, D, E, F),
- F1 water level in the wave flume at the nonius tip equal to 14.4 cm (pump on),
- C0 configuration of the model (C0, C1, C2, C3, C4, C5).

## 5 ANALYSIS AND RESULTS

### 5.1 Analysis structure

Table 32: Analysis procedure.

Structure of the experimental data										
<p>1. Experimental Launch wave attacks, check whether experiments were accurate. In case of correct experiment, continue with analysis as shown bellow, otherwise repeat the experiment.</p> <p>2. I. Level analysis Put testing data in chronological order in “Esperimenti” in subfolder of the day: “11-04-12”, “12-04-12”... “02-05-12”.</p> <p style="text-align: center;">↓ INPUT</p> <p style="text-align: center;">Run Matlab from “FileMatLabPerAnalisiDati”: FILE.mat</p> <p style="text-align: center;">↓ OUTPUT</p> <p>OUTPUT data saved again in Folder of the day in Subfolders: “Figure” and “Dati Calibrati”</p> <p style="text-align: center;">↓</p> <p style="text-align: center;">OUTPUT Analysis</p>	<p>3. II. Level analysis — Study of processes “INPUT” folder: All data taken from I. Level Analysis from Folder of the day: “H1T085G2AF1C0.dat”, “H1T085G2BF1C0.dat” (for Cells, Pressure transducer and Calibration dates) ...</p> <table border="1" style="width: 100%; border-collapse: collapse;"> <tr> <td style="font-size: small;">H1T085G2AF1C0_Celle</td> <td style="font-size: small;">4.4.2012 19:07</td> <td style="font-size: small;">Datoteka DAT</td> </tr> <tr> <td style="font-size: small;">H1T085G2AF1C0_Trasd</td> <td style="font-size: small;">4.4.2012 19:07</td> <td style="font-size: small;">Datoteka DAT</td> </tr> <tr> <td style="font-size: small;">H1T085G2AF1C0-Calibrata</td> <td style="font-size: small;">2.5.2012 15:37</td> <td style="font-size: small;">Datoteka DAT</td> </tr> </table> <p style="text-align: center;">↓ INPUT</p> <p style="text-align: center;">Run Matlab from “FileMatLabPerAnalisiDati”: FILE.mat</p> <p style="text-align: center;">↓ OUTPUT</p> <p>OUTPUT data saved in Subfolder “Figure”, “H1T085G2F1C0-Riflessione”.dat, “H1T085G2F1C0Overtopping”.dat and “H1T085G2F1C0ParametriCaratteristiche”.dat</p> <p style="text-align: center;">↓</p> <p style="text-align: center;">OUTPUT Analysis</p>	H1T085G2AF1C0_Celle	4.4.2012 19:07	Datoteka DAT	H1T085G2AF1C0_Trasd	4.4.2012 19:07	Datoteka DAT	H1T085G2AF1C0-Calibrata	2.5.2012 15:37	Datoteka DAT
H1T085G2AF1C0_Celle	4.4.2012 19:07	Datoteka DAT								
H1T085G2AF1C0_Trasd	4.4.2012 19:07	Datoteka DAT								
H1T085G2AF1C0-Calibrata	2.5.2012 15:37	Datoteka DAT								

A series of tests were executed in a wave flume (described in Chapter 4.2.1) after water level stabilization in the flume and calibration of wave gauges were made. Sample of Check-list (see Attachment C) with a special procedure for executing tests has been followed each day.

Brief description of test procedure:

- Turn on computers (PC GENERATORE and GANIMEDE), load cells and pressure transducers.
- Create the folder of the day, folders figures and calibrated data on computer GANIMEDE, while on PC GENERATORE create only folder of the day.

- Place the nonius hydrometric tip on the depth position F1 with the pump off, wait and check that the free surface in the channel is tangent to the hydrometric tip, otherwise input or output the water.
- Calibration procedure of wave gauges.
- Turn on the pump at the back blade, connect overtopping tank to the load cells, put 500 ml of water inside and wait for the time necessary for the stabilization of the water level in the flume.
- Start the program of load cells and pressure transducers then perform calibration for both.
- Launch wave attack, start the acquisition of load cells and pressure transducers, turn on the spotlight and start filming the video.
- At the end of each repetition: stop recording the video, stop load cells and pressure transducers program, register accumulated overtopping volume from overtopping tank, and transfer the file that has just been acquired.
- Analyze transferred file by Matlab software and complete data base and report (see Attachment E) in the meantime.
- Analyze the graph of overtopping volume and create a table showing corresponding cumulative wave-by-wave overtopping volumes.
- Wait for stabilization of the water level inside the wave flume before launching the next wave attack.
- Always control the water level, in case of any changes repeat the calibration.

Table 33: Scheme of wave attacks performed in laboratory from 03.04. – 02.05.2012.

Date	Wave	Rep.	Structure	Date	Wave	Rep.	Structure
3.4.2012	H1T85G2	A, B, C	C0	17.4.2012	H2T115G5	B, C, D, E, F	C3
3.4.2012	H1T105G2	A, B, C	C0	17.4.2012	H1T125G2	A, B, C	C3
4.4.2012	H1T85G2	A	C0	17.4.2012	H1T125G5	A, B, C	C3
4.4.2012	H1T125G2	A, B, C	C0	17.4.2012	H1T105G2	A	C3
4.4.2012	H1T85G5	A, B, C	C0	18.4.2012	H1T105G2	B, C	C3
4.4.2012	H1T105G5	A, B, C	C0	18.4.2012	H1T105G5	A, B, C	C3
4.4.2012	H1T125G5	A, B, C	C0	19.4.2012	H1T85G2	A, B, C	C3
5.4.2012	H2T115G2	A, B, C, D, E, F	C0	19.4.2012	H1T85G5	A, B, C	C3
5.4.2012	H2T115G5	A, B, C, D, E, F	C0	19.4.2012	H1T85G2	A, B, C	C4
10.4.2012	H2T115G2	A, B, C, D, E, F	C1	19.4.2012	H1T85G5	A, B	C4
10.4.2012	H2T115G5	A, B, C, D, E, F	C1	20.4.2012	H1T85G5	C	C4
10.4.2012	H1T125G5	A, B, C	C1	20.4.2012	H1T105G2	A, B, C	C4
10.4.2012	H1T125G2	A	C1	20.4.2012	H1T105G5	A, B, C	C4
11.4.2012	H1T125G2	B, C	C1	23.4.2012	H1T125G2	A, B, C	C4
11.4.2012	H1T105G5	A, B, C	C1	23.4.2012	H1T125G2	A, B, C	C4
11.4.2012	H1T105G2	A, B, C	C1	23.4.2012	H1T125G5	A, B, C	C4
11.4.2012	H1T85G5	A, B, C	C1	23.4.2012	H2T115G2	A, B, C, D	C4
11.4.2012	H1T85G2	A, B, C	C1	24.4.2012	H2T115G2	E, F	C4
12.4.2012	H1T85G2	A, B, C	C2	24.4.2012	H2T115G5	A, B, C, D, E, F	C4
12.4.2012	H1T85G5	A, B, C	C2	24.4.2012	H2T115G2	A, B	C5
12.4.2012	H1T105G2	A, B, C	C2	26.4.2012	H2T115G2	C, D, E, F	C5
12.4.2012	H1T105G5	A, B, C	C2	26.4.2012	H2T115G5	A, B, C, D, E, F	C5
12.4.2012	H1T125G2	A, B	C2	26.4.2012	H1T125G2	A, B	C5
13.4.2012	H1T125G2	C	C2	27.4.2012	H1T125G2	C	C5
13.4.2012	H1T125G5	A, B, C	C2	27.4.2012	H1T125G5	A, B, C	C5
13.4.2012	H2T115G2	A, B, C, D, E, F	C2	27.4.2012	H1T105G2	A, B, C	C5
13.4.2012	H2T115G5	A, B, C	C2	27.4.2012	H1T105G5	A, B, C	C5
16.4.2012	H2T115G5	D, E, F	C2	27.4.2012	H1T85G2	A	C5
16.4.2012	H2T115G2	A, B, C, D, E, F	C3	2.5.2012	H1T85G2	B, C	C5
16.4.2012	H2T115G5	A	C3	2.5.2012	H1T85G5	A, B, C	C5

### 5.2 I. level analysis

I. level analysis was carried out to investigate the wave performance, by calculating its characteristic parameters, wave-by-wave overtopping volumes and pressure stresses through analysis of data acquired with different instruments immediately after each test execution. Due to this fact, three measuring systems have been deployed:

1. Wave measuring system,
2. Overtopping measuring system and

### 3. Pressure measuring system.

I. level analysis estimated also whether working of measuring instruments is properly. The results of this analysis were summarized in the Daily report of the tests.

Results of one daily report from 18<sup>th</sup> April 2012 of the test H1T105G2CF1C3 will be represented in the following subchapters (see Attachment E).

#### 5.2.1 Calibration procedure

At the beginning of daily experiments, calibration procedure of WG has been made. Water level depth at the back blade (with the pump switched off) must be 55.50 cm (15.20 cm at the nonius tip) before calibration procedure can be started. This procedure allows verifying both the accuracy of the calibration and the existence of any possible error in measuring instruments. Detailed WG calibration process is described in Check list in Attachment C.

Brief description of calibration procedure:

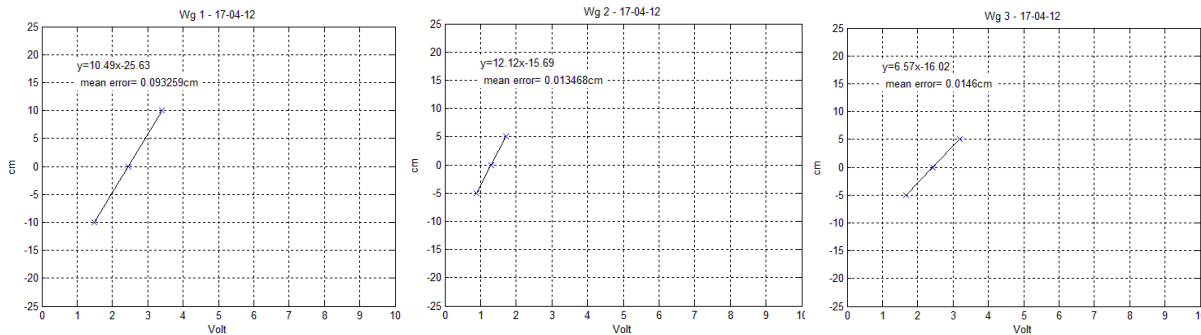
- Run the calibration program from PC GENERATOR.
- Select corresponding wave gauges channels to calibrate from 1 to 10.
- Enter range of calibration, distance from back blade and depth for each of five WG.
- Bring WG to maximum level, minimum level and finally centre them, after each movement wait for stabilization of the water level and then register levels.
- Analyze the calibration file by Matlab's program and note possible deviations found during calibration.
- Matlab program "VerificaCalibrazione" loads the file of calibration levels in correspondence between wave gauges and channels, than execute calibration of each WG and turns results as seen in Table 34 and graphs in Graph 4 and 5.

Hereinafter results obtained from calibration of wave gauges for the day 18<sup>th</sup> of April 2012 is shown.

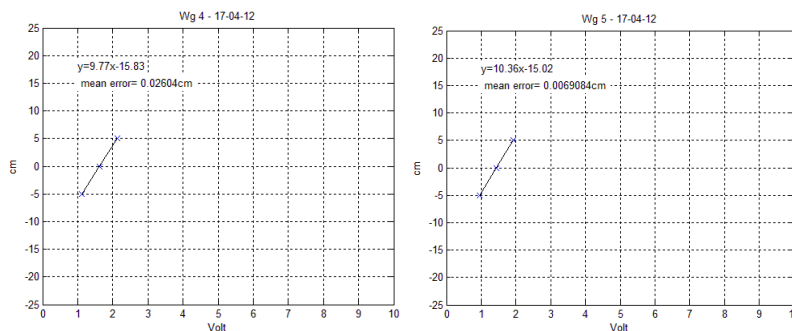
Table 34: Calibration parameters for each wave gauge [cm] = [Volt] A + B.

Position	A [cm/volt]	B [cm]	Error [cm]
1	10.49	-25.63	0.09
2	12.12	-15.69	0.01
3	6.57	-16.02	0.01
4	9.77	-15.83	0.03
5	10.36	-15.02	0.01

Five wave gauges have been set up to return the same tension value corresponding to equal water level. With this procedure the linearity should also be ensured throughout all acquisition range. Calibration of the WG must be repeated if the average error is greater than 0.2 cm. Since the correlation coefficient of the interpolation line is not 1 (in centimeters), acquired signal is converted in Volts for three known levels then slightly different values from those expected are obtained. Average of three differences between expected and calculated values, taken in absolute value, is defined as an average error.



Graph 4: Results for WG1, WG2 and WG3 calibrations on 18<sup>th</sup> of April 2012.



Graph 5: Results for WG4 and WG5 calibrations on 18<sup>th</sup> of April 2012.

## 5.2.2 Wave gauges registration

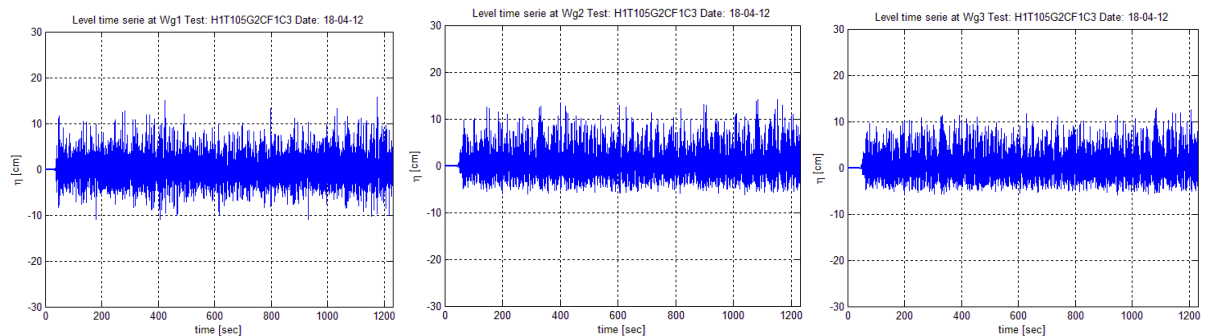
Wave gauges immersion depth was determined according to the wave flume depth, at each WG location and in such a way that the wave heights fall within the acquisition range.

### 5.2.2.1 Time level series

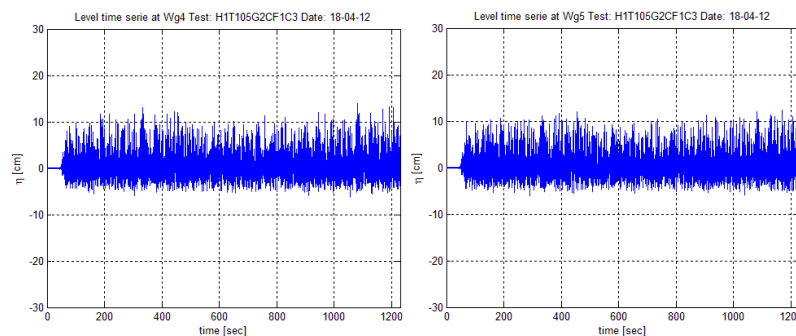
Program “Labview” has been set during experimental session to acquire water level in the wave flume for the first 30 sec of the test (10 + 0.5 min or 20 + 0.5 min) with a stopped wave maker. That is how water level elevation respect to previously determined water level from calibration was recorded. Water level elevation appeared due to ignition of the back blade pump. The signal acquired during the first 30 seconds was analyzed by Matlab program,

which returned a string with values of “new” zero and a string with the standard deviation of the recorded signal during the acquisition for the first 30 seconds for each WG. These data reveal both proper functioning of WG and the actual calm sea state in the wave flume, which is necessary to perform accurately desired wave attacks.

Hereinafter examples of graphs relating to acquired time - elevation signals by each WG for test H1T105G2CF1C3 are reported.



Graph 6: Time level series at WG1, WG2 and WG3 for the test H1T105G2CF1C3.

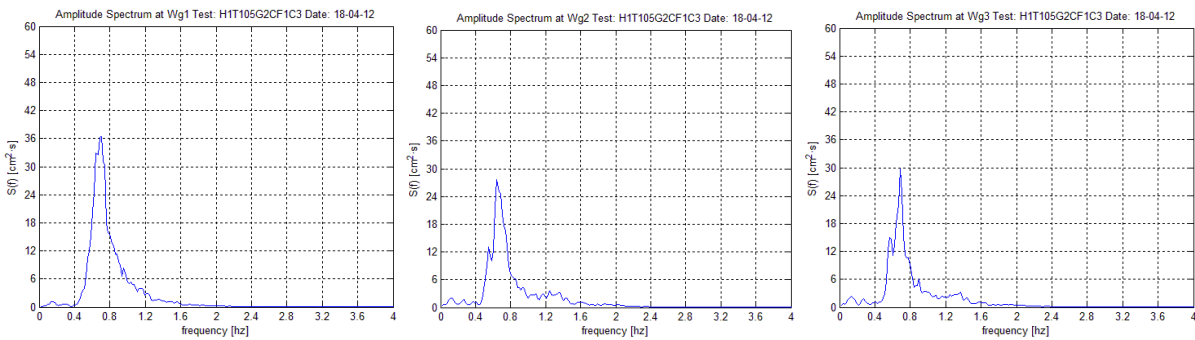


Graph 7: Time level series at WG4 and WG5 for the test H1T105G2CF1C3.

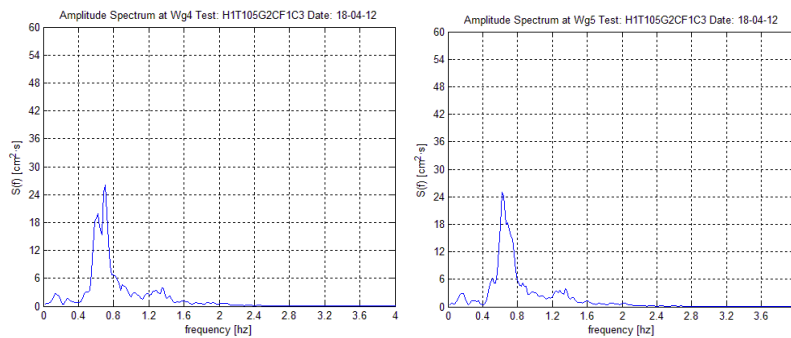
### 5.2.2.2 Amplitude spectrum

Spectral analysis was conducted by mean spectral measurements of 21 samples with 1024 elements and frequency resolution equal to 0.0010 Hz.

Hereinafter examples of graphs for amplitude spectrums at each WG for test H1T105G2CF1C3 are reported.



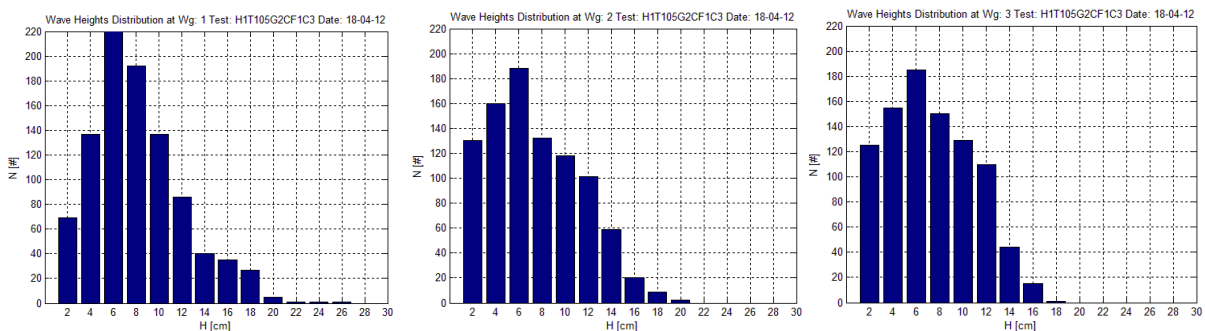
Graph 8: Amplitude spectrum at WG1, WG2 and WG3 for the test H1T105G2CF1C3.



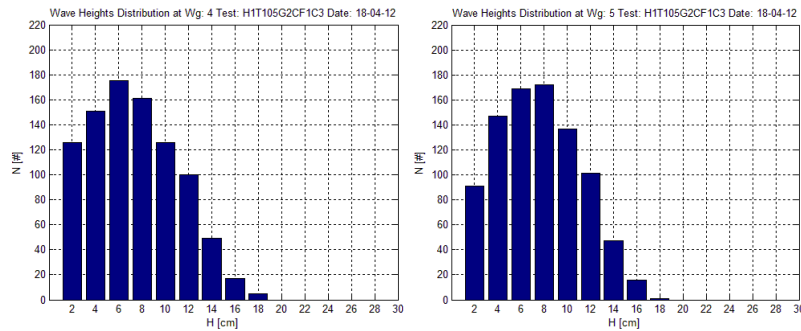
Graph 5.6: Amplitude spectrum at WG4 and WG5 for the test H1T105G2CF1C3.

Wave spectrums with a second smaller peak are characteristic for breaking waves. Some values of  $S(f)$  for amplitude spectrum graphs were bigger than the limit  $60 \text{ cm}^2 \cdot \text{s}$ , so in the II. level analysis the axis  $S(f)$  has been extended.

### 5.2.2.3 Wave heights zero crossing distribution



Graph 9: Wave heights distribution at WG1, WG2 and WG3 for the test H1T105G2CF1C3.



Graph 10: Wave heights distribution at WG4 and WG5 for the test HIT105G2CF1C3.

### 5.2.2.4 Reflection analysis

Parameters used in reflection analysis:

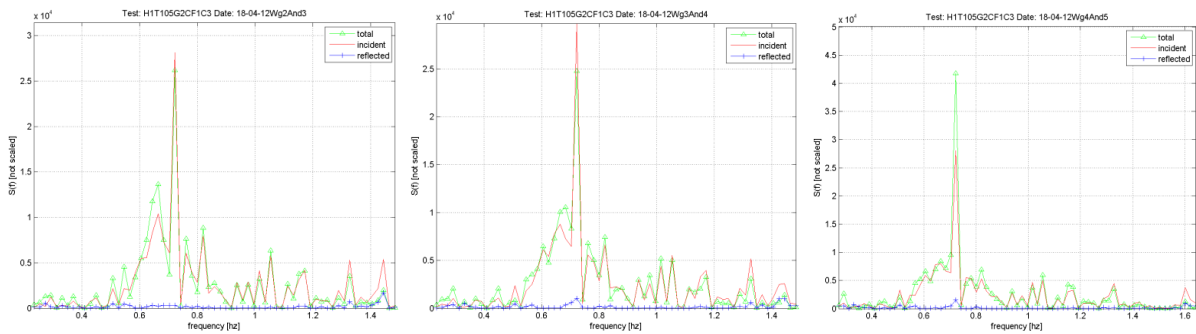
- $K_r$  - reflection coefficient of the incident wave at the harbour breakwater's toe, measured by WG2, WG3, WG4 and WG5,
- $H_i$  – incident wave height [cm] measured by WG2, WG3, WG4 and WG5,
- $H_r$  – reflected wave height [cm] measured by WG2, WG3, WG4 and WG5.

Hereinafter examples of reflection parameters, graphs of total effective spectrum, incident spectrum and the reflected spectrum extracted from wave attack HIT105G2CF1C3 are shown.

Reflection parameters were obtained between pairs of WG2 – WG3, WG3 – WG4 and WG4 – WG5.

Table 35: Reflection coefficients analysis according to Goda and Suzuki (1976).

$H_i$ (2-3) [cm]	$H_r$ (2-3) [cm]	$K_r$ (2-3) [cm]	$H_i$ (3-4) [cm]	$H_r$ (3-4) [cm]	$K_r$ (3-4) [cm]	$H_i$ (4-5) [cm]	$H_r$ (4-5) [cm]	$K_r$ (4-5) [cm]
10.61	2.78	0.26	10.50	2.73	0.26	10.47	2.88	0.27



Graph 11: Graphs for total effective spectrum, incident spectrum and the reflected spectrum extracted from the wave attack H1T105G2CF1C3.

### 5.2.2.5 Wave characteristic parameters

Wave characteristic parameters:

- $H_{m0}$  – incident wave height at harbour breakwater's toe, measured by WG2, WG3, WG4 and WG5 [cm],
- $T_p$  – peak wave period recorded in front of harbour breakwater, measured by WG2, WG3, WG4 and WG5 [s],
- $H_{1-3}$  – significant wave height [cm],
- $H_{max}$  – maximum wave height [cm],
- $H_m$  – mean wave height [cm],
- $T_m$  – mean wave period recorded in front of harbour breakwater, measured by WG2, WG3, WG4 and WG5 [s],
- $N$  – number of zero crossing waves.

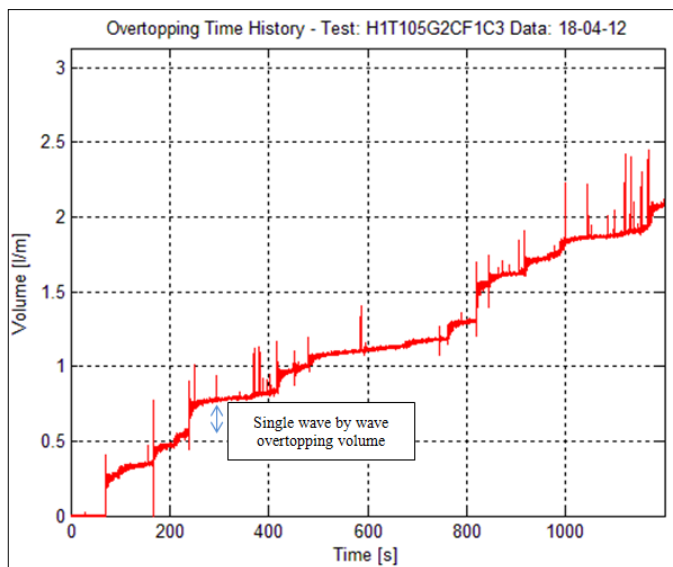
Table 36: Characteristic wave parameters for 20 + 0.5 min long wave attack H1T105G2CF1C3.

Date	Wave	Rep.	Level	Structure	WG	Zero Level [cm]	Stand. Dev [cm]	Hmo [cm]	Tp [sec]	Tm_10 [sec]	Tm01 [sec]	Mean Level [cm]	H1_3 [cm]	Hmax [cm]	Hm [cm]	TL_3 [s]	Tm [s]	N
18/04/2012	H1T105G2	C	F1	C3	1	0.50	0.03	12.97	1.4	1.4	1.2	-0.21	12.60	25.48	8.10	1.36	1.3	953
18/04/2012	H1T105G2	C	F1	C3	2	0.56	0.03	11.28	1.5	1.6	1.2	-0.15	12.10	19.74	7.38	1.44	1.3	920
18/04/2012	H1T105G2	C	F1	C3	3	0.57	0.02	10.93	1.5	1.7	1.2	-0.17	11.50	18.14	7.25	1.45	1.3	915
18/04/2012	H1T105G2	C	F1	C3	4	0.60	0.03	11.06	1.4	1.7	1.2	-0.14	11.70	18.24	7.33	1.45	1.3	911
18/04/2012	H1T105G2	C	F1	C3	5	0.57	0.03	10.9	1.6	1.7	1.1	-0.16	11.6	17.35	7.51	1.46	1.3	882

### 5.2.3 Wave overtopping analysis

For accurate measurements of overtopping volumes 500 ml of water inside the overtopping tank before calibration of the load cells at the beginning of each test was put, that meant the zero value for load signal acquisition. Load signal has been acquired with a precision of 0.02 g. When test was finished accumulated overtopping volume from overtopping tank (in litres), without the starting 500 ml has been measured and registered in Data base and Daily report (see Attachment E).

Furthermore Matlab’s program “Overtopping” has been launched and then overtopping graph in time history has been analysed by creating a table with 2 columns, one showing serial number of overtopping events and the other corresponding accumulated volumes read from the graph. Finally accumulated volume measured from overtopping tank was transformed into discharge in prototype scale and mean discharge was calculated.



n.°	Session	Steps wave by wave o. v. [l/m]	Single wave by wave o. v. [l/m]
1	<b>C</b>	0,01	0,01
2		0,27	0,26
3		0,36	0,09
4		0,47	0,11
5		0,54	0,07
6		0,58	0,04
7		0,79	0,21
8		0,84	0,05
9		0,97	0,13
10		1,01	0,04
11		1,15	0,14
12		1,18	0,03
13		1,19	0,01
14		1,31	0,12
15		1,56	0,25
16		1,63	0,07
17		1,73	0,10
18		1,87	0,14
19		1,94	0,07
20		2,08	0,14

Graph 12: Graph Overtopping time history for the test H1T105G2CF1C3 (left). Table of wave-by-wave overtopping volumes for the same wave attack (right).

Overtopping graph has some irregularities, such as long vertical lines, which occur due to fast and big wave-by-wave overtopping events and are caused by Archimedes force on overtopping tank, which leans on the water surface.

Measured accumulated overtopping volume from overtopping tank without the starting 500 ml for this wave attack was 0.67 l with approximately 20 wave-by-wave overtopping events. With the following formula prototype discharge has been calculated:

$$\text{Prototype discharge} [l * m/s] = \frac{\text{Model Volume [l]} * \text{Sampler width [m]}}{(\text{Test duration [min]} - 2[\text{min}]) * 60 [s]} * \text{Model scale}^{\frac{3}{2}} \quad (5.1)$$

Where:

— Sampler width has values of 0.3 or 0.2 m.

- Test duration is 20 or 10 min.
- Model scale is 1:50.

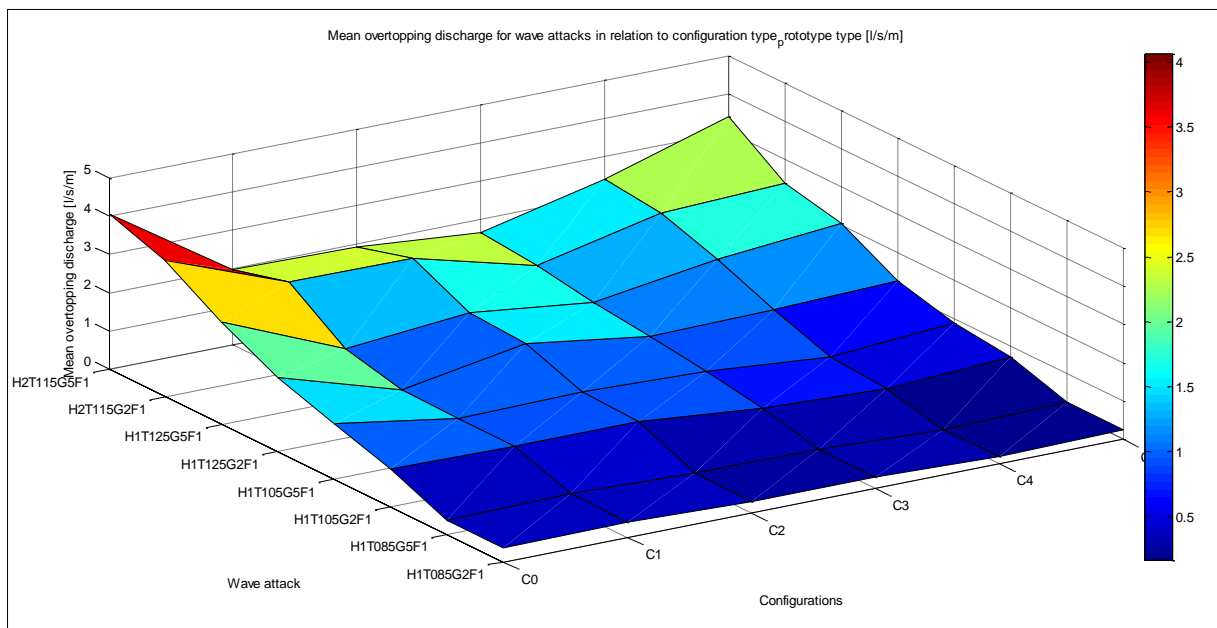
Table 37: Accumulated overtopping volume in model and prototype scale for H1T105G2F1C3.

Volume model (from overtopping tank) [l]	Prototype capacity [l/s/m]	Volume model (from cells) [l]
0,67	0,71	0,64

Accumulated volume recorded by load cells was always smaller than the one measured. The reason for this is that the load cells time acquisition finishes before waves stop attacking the harbour, since even after back blade stops, waves are still travelling towards the construction. In this example overtopping volume measured from overtopping tank was 0.67 l and volume measured by load cells was 0.64 l.

Table 38: Overtopping discharges with mean values measured directly from overtopping tank (in prototype scale).

Wave	Discharge prototype [l/s/m]	Configuration					
		C0	C1	C2	C3	C4	C5
H1T85G2	A	0,36	0,38	0,21	0,23	0,19	0,29
	B	0,32	0,41	0,37	0,36	0,18	0,22
	C	0,40	0,39	0,28	0,29	0,22	0,23
	Mean	0,36	0,39	0,28	0,29	0,19	0,25
H1T85G5	A	0,32	0,34	0,16	0,27	0,14	0,23
	B	0,34	0,45	0,33	0,24	0,19	0,18
	C	0,42	0,51	0,44	0,40	0,18	0,34
	Mean	0,36	0,43	0,31	0,30	0,17	0,25
H1T105G2	A	1,53	1,26	1,26	0,88	0,50	0,88
	B	0,69	0,64	0,72	0,38	0,45	0,56
	C	0,75	0,91	0,88	0,71	0,59	0,67
	Mean	0,99	0,94	0,95	0,65	0,51	0,70
H1T105G5	A	1,71	1,30	1,14	0,94	0,56	0,82
	B	1,25	0,86	0,86	1,01	0,79	1,05
	C	1,42	0,72	1,04	0,77	0,53	0,81
	Mean	1,46	0,96	1,01	0,91	0,63	0,89
H1T125G2	A	1,80	0,99	1,43	1,09	0,78	1,29
	B	2,01	0,74	1,55	1,11	1,11	1,49
	C	2,05	1,25	1,68	1,11	1,57	1,02
	Mean	1,95	0,99	1,56	1,11	1,15	1,27
H1T125G5	A	2,38	1,32	1,95	1,30	1,66	1,61
	B	2,39	1,18	1,25	0,84	1,51	1,18
	C	3,25	1,51	1,69	1,69	2,07	3,32
	Mean	2,67	1,33	1,63	1,28	1,75	2,04
H2T115G2	A	2,29	2,25	2,32	1,30	2,74	4,02
	B	3,78	1,91	2,37	1,56	1,92	2,32
	C	2,60	1,28	1,27	0,90	2,11	1,91
	D	2,70	2,34	1,84	1,25	2,34	1,73
	E	3,85	3,43	3,90	2,77	1,98	2,06
	F	6,24	2,98	2,39	1,33	2,39	2,25
Mean	3,58	2,37	2,35	1,52	2,25	2,38	
H2T115G5	A	3,60	2,51	2,08	1,04	2,69	2,95
	B	4,89	2,25	1,73	1,66	3,29	3,90
	C	3,33	1,20	2,70	1,79	0,97	1,99
	D	5,06	2,69	2,32	2,08	3,80	6,85
	E	4,94	1,32	1,59	1,91	2,36	3,21
	F	2,53	1,77	1,09	1,39	1,33	1,46
Mean	4,06	1,96	1,92	1,64	2,41	3,39	



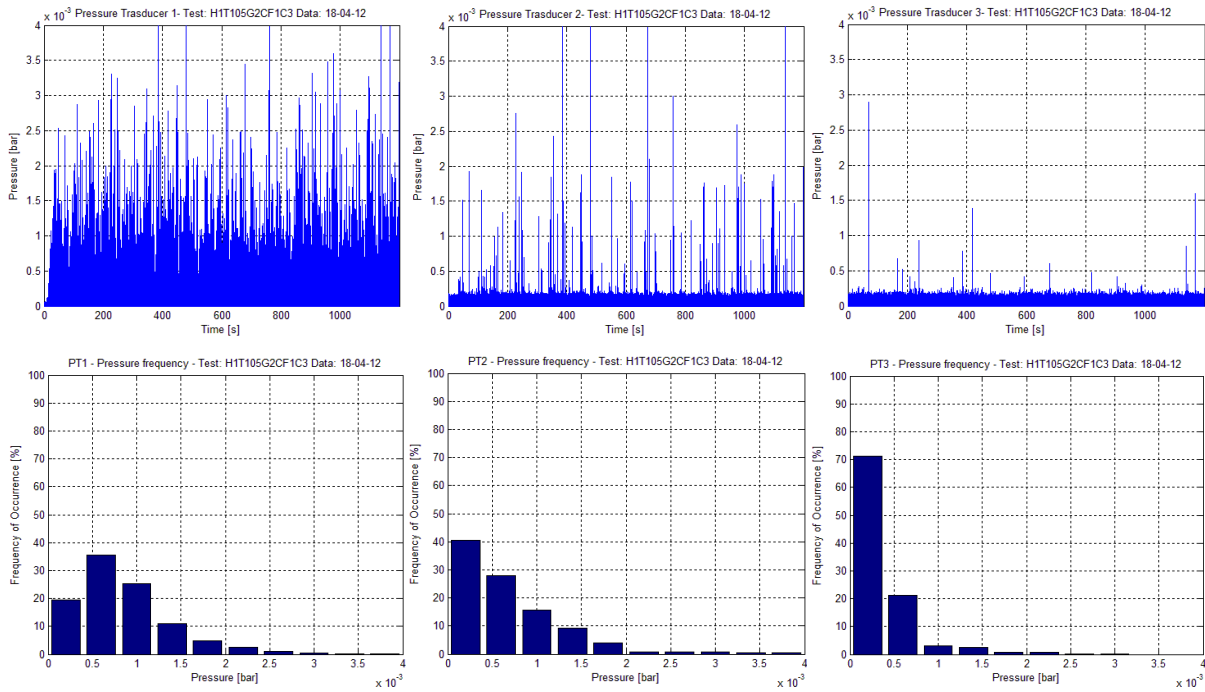
Graph 13: Mean overtopping discharges for all tests depending on configuration type in prototype scale.

In general, larger wave-by-wave overtopping discharges for all wave attacks are typical for the starting configuration C0, regarding to the graph legend, which is defining the highest values of overtopping discharges there. The most effective for wave attacks H1T125G5F1, H2T115G2F1 and H2T115G5F1 is configuration C3, with overspill basin of 18.0 cm width (in model scale) before the wave wall, where energy dissipates and so smaller quantity of water overflow the wall crown. On the other hand for wave attacks H1T085G2F1, H1T085G5F1, H1T105G2F1 and H1T105G5F1 the most effective configuration is C4 with an elevated wave wall of 2 cm (in model scale) respect to starting configuration and full berm, which has positive effect on reducing overtopping discharges. For wave attack H1T125G2F1 the most effective construction is C1 with overspill basin of 6 cm (in model scale).

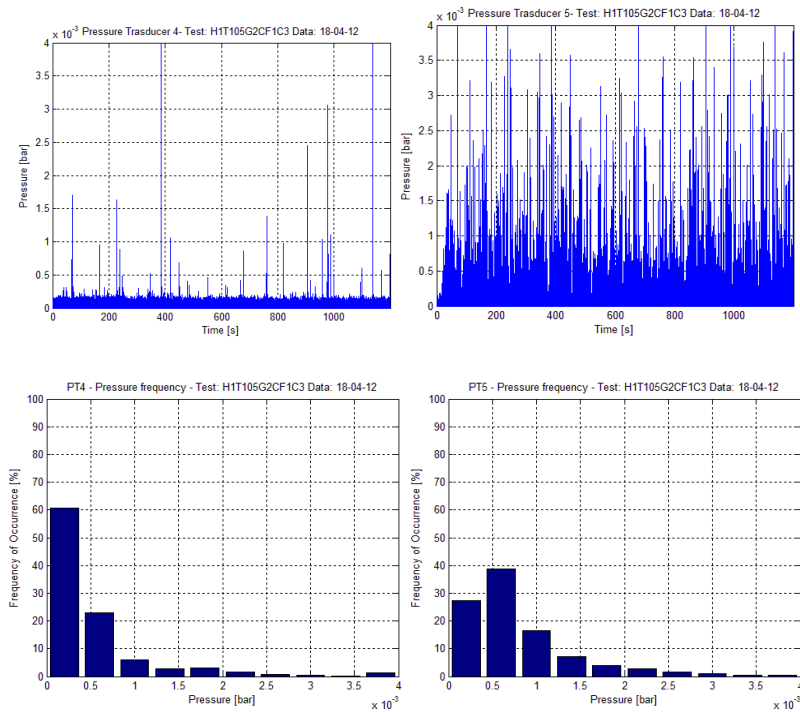
#### 5.2.4 Wave pressure of impact

The pressures acting along the centre of wave wall were measured by five pressure transducers with a nominal resolution of 0.2 g/cm (0.01 kg/cm<sup>2</sup> in prototype scale) on an impact area of 4.5 cm<sup>2</sup> (1.13 m<sup>2</sup> in prototype scale). The frequency of acquisition for all tests was set to be equal 1 kHz.

Pressure stresses have been analysed by Matlab program "Trasduttori". Mean value of the frequency ( $f_s$ ) acquired in the first 30 sec was set for zero starting value on the graph Time – Pressure. In order to get clearer graph there were not pressure less than 0.0002 bar considered.



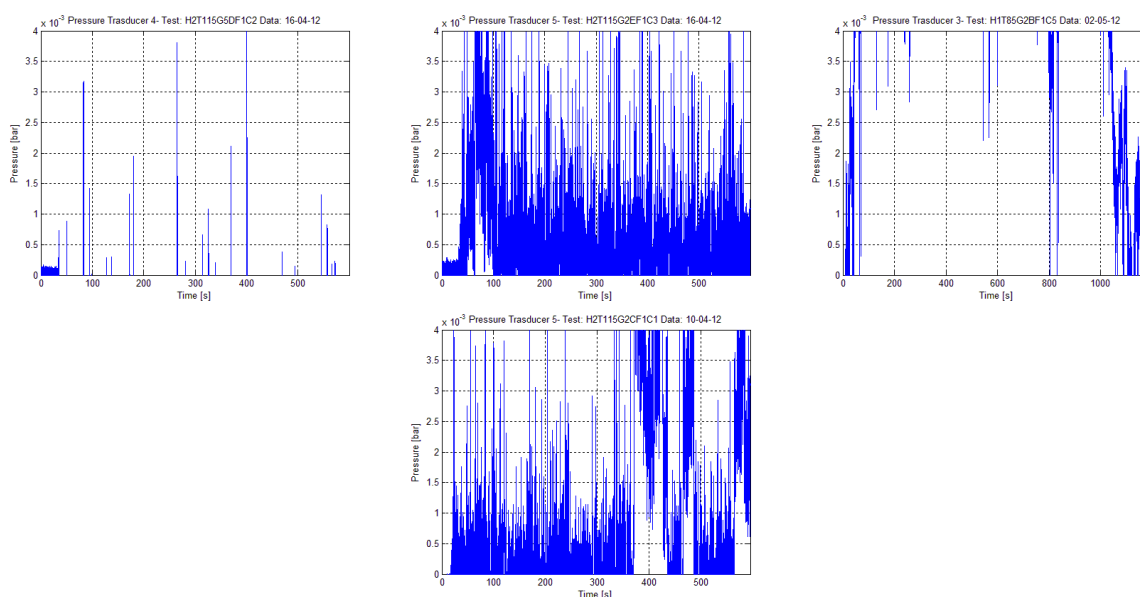
Graph 14: Wave pressures acquired by pressure transducers 1, 2 and 3 (top). Pressure distribution in frequency of occurrence for transducers 1, 2 and 3 (bottom).



Graph 15: Wave pressure stresses acquired by pressure transducers 4 and 5 (top). Pressure distribution in frequency of occurrence for transducers 4 and 5 (bottom).

Pressure transducers 1, 2 and 3 were positioned on the left centre side, in a descending order from a wave wall crown, while pressure transducers 4 and 5 were positioned on the right centre side in an increasing order. In general and also for example H1T105G2F1C3, bigger pressures are found on transducers positioned at the bottom 5 and 1, since wave forces increase with water depth (hydrostatic pressure) and effect of overspill basin is obvious and are smaller for other transducers lying above.

In some cases malfunctioning of pressure transducers was noted, due to moving of stones in front of them or electric shock and therefore bad measurements were acquired. Hereinafter example of malfunctioning of pressure transducers can be seen.



Graph 16: Different types of malfunctioning of pressure transducers offset.

### 5.2.5 Effective and target values of wave parameters

When the experimental part was done a table with mean effective values of wave parameters was made in order to estimate deviations between target and effective values of wave parameters.

Table 39: Effective values of  $H_{m0}$  and  $T_p$  for configurations C0, C1 and C3.

Name	Gamma	C0		C1		C2	
		Effective		Effective		Effective	
		Hmo,eff [cm]	Tp,eff [sec]	Hmo,eff [cm]	Tp,eff [sec]	Hmo,eff [cm]	Tp,eff [sec]
H1T85	2	9,80	1,27	10,80	1,27	10,00	1,25
	5	10,68	1,23	11,17	1,24	10,75	1,23
H1T105	2	11,08	1,50	11,73	1,50	11,51	1,50
	5	11,54	1,49	11,72	1,49	11,67	1,49
H1T125	2	11,47	1,74	11,24	1,74	11,60	1,75
	5	11,60	1,75	12,05	1,75	11,45	1,75
H2T115	2	13,09	1,68	13,16	1,68	13,00	1,70
	5	13,33	1,65	13,37	1,65	12,97	1,65

Table 40: Effective values of  $H_{m0}$  and  $T_p$  for configurations C4, C5 and C6.

Name	Gamma	C3		C4		C5	
		Effective		Effective		Effective	
		Hmo,eff [cm]	Tp,eff [sec]	Hmo,eff [cm]	Tp,eff [sec]	Hmo,eff [cm]	Tp,eff [sec]
H1T85	2	10,39	1,25	10,55	1,26	10,48	1,26
	5	10,97	1,25	10,91	1,24	10,85	1,24
H1T105	2	11,17	1,50	11,65	1,50	11,41	1,50
	5	11,66	1,49	11,95	1,48	11,70	1,48
H1T125	2	11,67	1,74	11,61	1,78	11,66	1,78
	5	11,76	1,77	11,82	1,76	11,80	1,77
H2T115	2	13,00	1,67	13,17	1,71	13,27	1,70
	5	13,04	1,66	13,33	1,66	13,14	1,65

Effective values of wave height read from WG 2, 3, 4 and 5 are always smaller than target one. Assumed value for wave height H1 was 12.0 cm and for H2 was 15.0 cm. On the other hand the differences between target and effective values for time period are smaller, in most cases effective wave period is bigger or the same as assumed value. Assumed values for time period T85 was 1.2 s, T105 was 1.48 s, T125 1.77s and for T115 was 1.63 s.

### 5.2.6 Problems at I. level analysis

- During I. level analysis one subtest H1T105G2BF1C4 from the day 20<sup>th</sup> April 2012 has been lost after already executed analysis.
- As previously mentioned some axes in graphs were too short and therefore all values were not included into the graph (Amplitude spectrum, Wave heights distribution and Pressure).
- Wave gauges have suffered offset upwards or downwards in some cases (see Attachment D – Diary).
- Malfunctioning of pressure transducers was noted, due to moving of stones in front of them or electric shock and therefore bad measurements were acquired.
- During executing wave attacks on configurations C1, C2 and C3 with an overspill basin, deepening and dislodging of filter stones was noted, since they were directly exposed to loads of the waves.

### 5.3 II. Level analysis

II. level analysis is based on I. level analysis, since parameters obtained in I. level analysis are used in developing this one. II. level analysis aims on a research and representation of data acquired during the experimental session of wave overtopping phenomenon, pressure measurements and reflection.

For this analysis following procedure has been used:

- Output data taken from I. level analysis for cells, pressure transducers and calibration parameters and put into folder “Input”.
- Prepare folder “Output” and subfolder “Figure”.
- Development of Matlab program (from I. level analysis) by joining all wave attack sessions (3 or 6) into one completed unit for each wave attack.
- Running of Matlab program.
- Analysing output data.

Before launching Matlab program there were some problems regarding to lost file for the test H1T105G2BF1C4 from the day 20<sup>th</sup> April 2012. In order to be able to run the program without report of an error, I replaced it with a copy of data from section A and rename it by B. Doing this kind of analysis of course is not allowed, since sea wave attacks are random processes and as so this kind of data in nature is not possible.

Some axes of the graphs were extended:

- Pressure - Time, pressure axis was extended from 4 to 8 mbar,
- Amplitude spectrum, axis  $S(f)$  has been extended from -15 to -20  $\text{cm}^2 \cdot \text{s}$ .

### 5.3.1 Overtopping analysis

Wave-by-wave overtopping masses achieved with this laboratory experiments are analyzed in order to:

- To determine the distribution of individual wave-by-wave overtopping masses for different configurations and wave attacks.
- To set up the relationship between continuously sampled signal of the overtopping detection system and measures taken directly from overtopping tank.

Second level overtopping analysis was carried out in the following steps:

- Definition of strings names for all tests.
- Data files to be analyzed for each test were created or simply a joining combination of measurements for sub tests was made.
- Combination of 3 (or 6) sub tests was made by adding second (and forward) sub test to the last value (summed) of the preliminary sub test and so on. In addition first 2 minutes of acquisition in the second and all subsequent sub tests forward were taken away since no overtopping events were present there (waves at that time are still

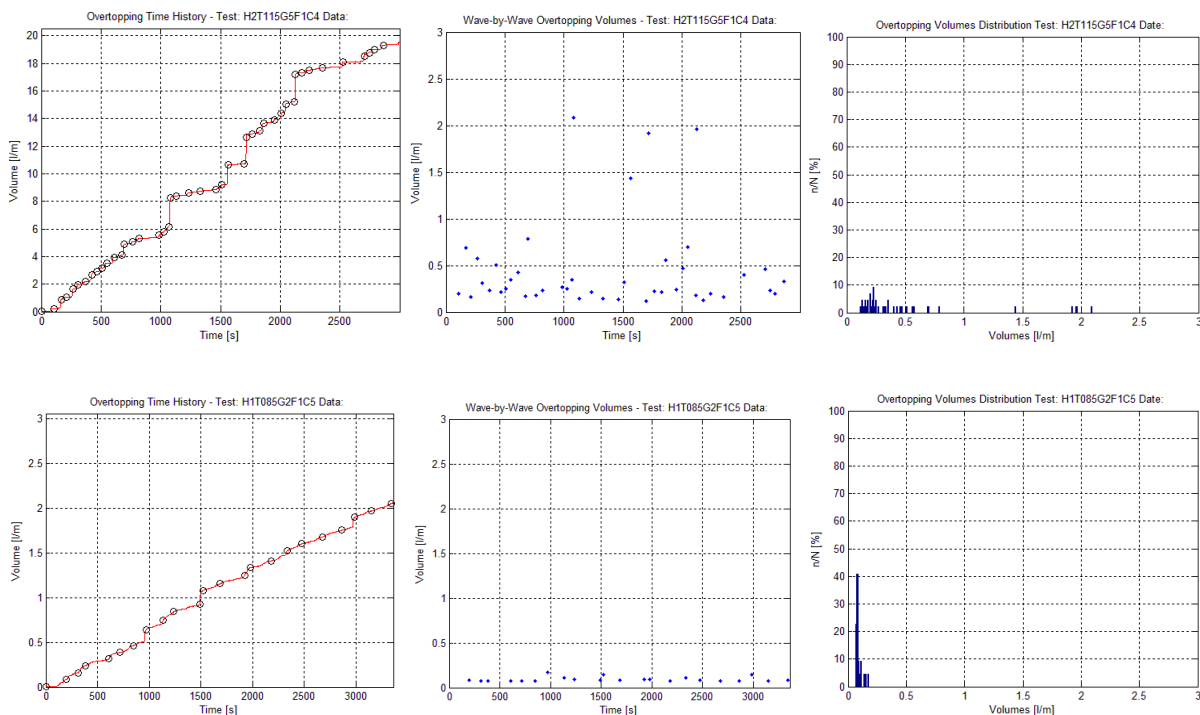
arriving towards the harbour breakwater). New overtopping graphs have duration of 55.5 min for tests with wave height H1 and 51.0 min for H2.

- Filtration of an overtopping graph was made in order to get a smooth curve with steps that will indicate overtopping events.

Result of overtopping analysis is three graphs:

- Overtopping time history,
- Wave-by-wave overtopping volumes,
- Overtopping volumes distribution.

For easier comparison between volumes in “Overtopping volumes distribution” the same number and range of intervals was used, that is 20 classes of range  $1/20 * V_{max}$ . A study of maximum overtopping volume from I. level analysis has been made in order to decide ranges of intervals and length of x axis in “Overtopping volumes distribution” and “Wave-by-wave overtopping volumes”. Maximum value of 3 l/m for single wave-by-wave overtopping volume has been established.



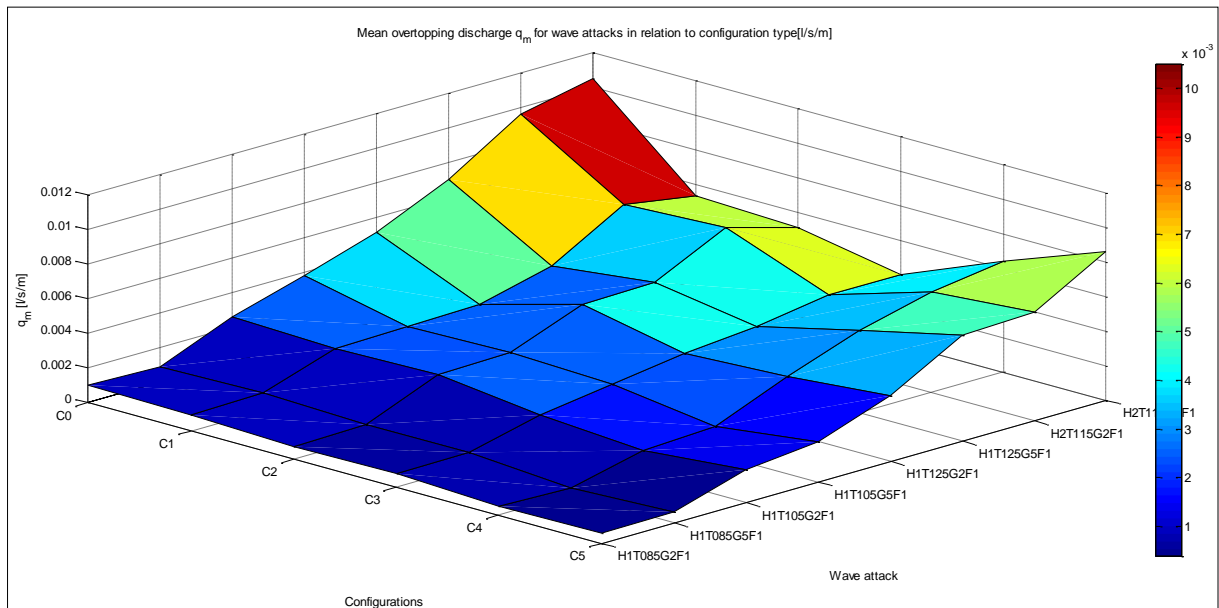
Graph 17: Typical output of overtopping analysis for the test H2T115G5F1C4 (up) and H1T085G2F1C5 (down) is showed.

### 5.3.1.1 Mean overtopping discharges

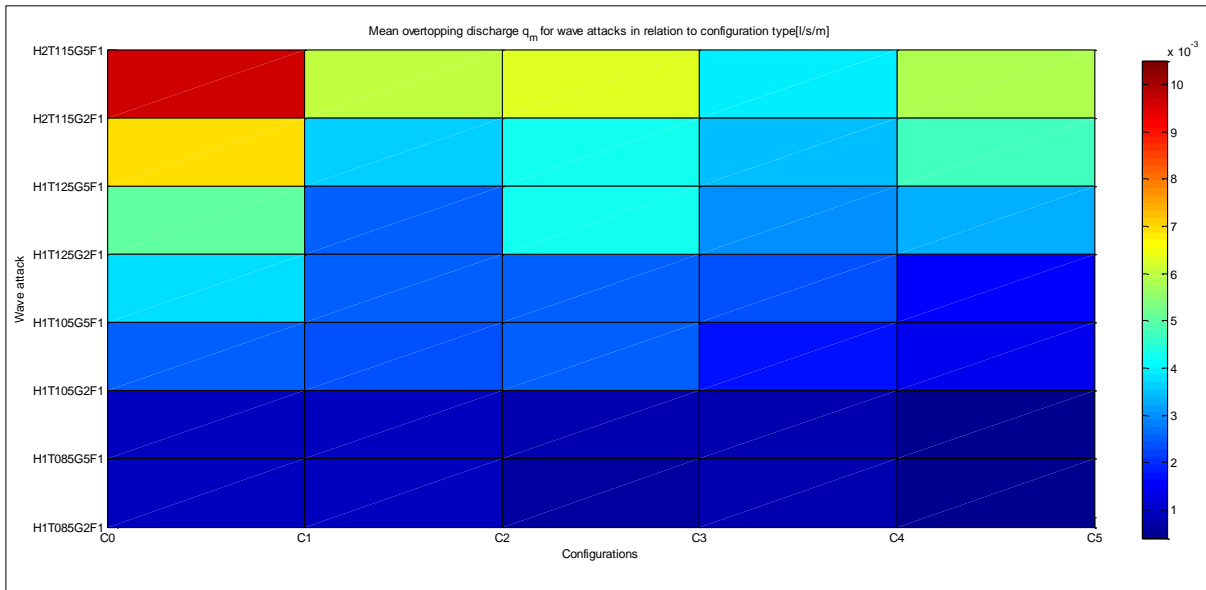
Table 41: Mean overtopping discharges  $q_m$  calculated by Matlab program (in prototype scale).

$\%q_m$ [l/s/m]	C0	C1	C2	C3	C4	C5
<b>H1T085G2F1</b>	0.0010	0.0009	0.0007	0.0008	0.0005	0.0006
<b>H1T085G5F1</b>	0.0009	0.0010	0.0008	0.0008	0.0004	0.0006
<b>H1T105G2F1</b>	0.0026	0.0024	0.0025	0.0018	0.0014	0.0019
<b>H1T105G5F1</b>	0.0038	0.0025	0.0026	0.0024	0.0016	0.0023
<b>H1T125G2F1</b>	0.0051	0.0026	0.0042	0.0030	0.0033	0.0038
<b>H1T125G5F1</b>	0.0070	0.0036	0.0043	0.0034	0.0048	0.0061
<b>H2T115G2F1</b>	0.0096	0.0060	0.0063	0.0040	0.0058	0.0063
<b>H2T115G5F1</b>	0.0105	0.0053	0.0051	0.0040	0.0064	0.0086

Values in green squares represent minimum of mean overtopping discharge  $q_m$  for each wave attack.



Graph 18: Mean overtopping discharge  $q_m$  for all wave attacks in relation to configurations.



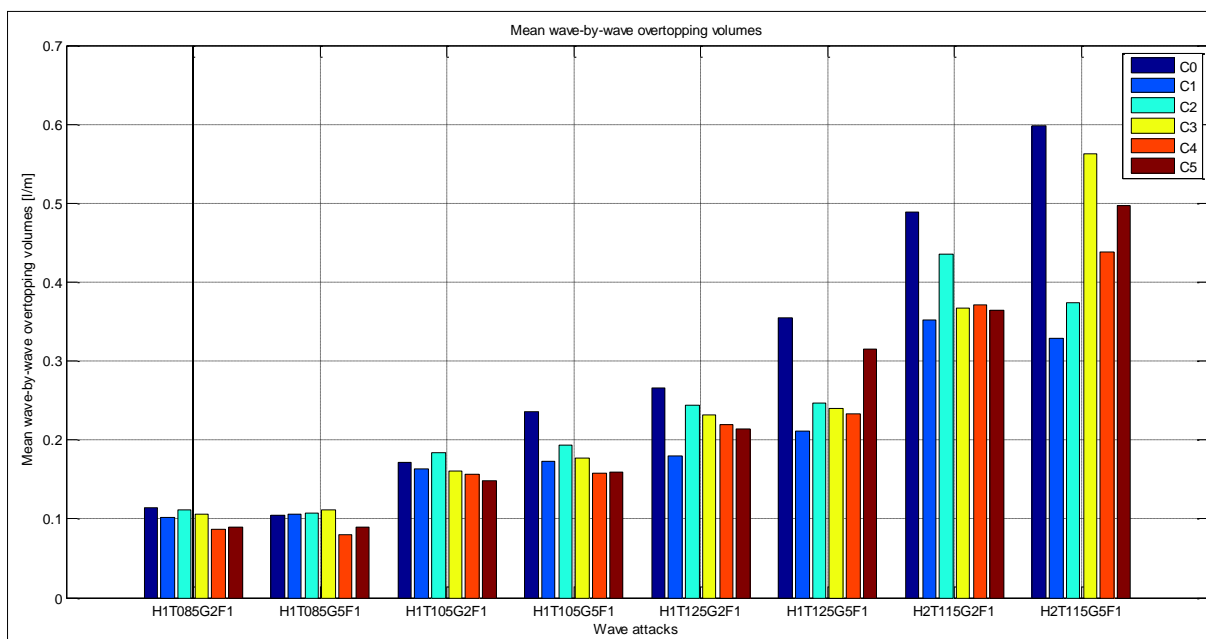
Graph 19: Ground plan of mean overtopping discharge graph.

It can be observed that for a smaller wave height H1 where wave periods are increasing from T085 to T125 mean overtopping discharges are increasing too. The relationship between peak elevation factors of JONSWAP spectrum  $\gamma_{G2}$  and  $\gamma_{G5}$  in most of the cases, for wave attack with the same wave height and period but different peak elevation factor, there is bigger mean overtopping discharge for bigger peak elevation factor, for example in wave attack H2T115G2F1C0  $q_m$  is 0.0096 l/s/m and in H2T115G5F1C0  $q_m$  is 0.0105 l/s/m.

Table 42: Mean wave-by-wave overtopping volumes calculated by Matlab program (in prototype scale).

MEAN Wave-by-wave o.v. [l/m]	C0	C1	C2	C3	C4	C5
H1T085G2F1	0,114	0,102	0,112	0,106	0,087	0,089
H1T085G5F1	0,105	0,106	0,108	0,111	0,081	0,090
H1T105G2F1	0,172	0,163	0,183	0,160	0,156	0,148
H1T105G5F1	0,236	0,173	0,194	0,177	0,158	0,159
H1T125G2F1	0,267	0,180	0,244	0,231	0,219	0,215
H1T125G5F1	0,355	0,212	0,247	0,241	0,233	0,315
H2T115G2F1	0,489	0,353	0,435	0,368	0,372	0,364
H2T115G5F1	0,598	0,329	0,374	0,563	0,439	0,497

Values in green squares represent minimum value of mean wave-by-wave overtopping volume for each wave attack.



Graph 20: Mean wave-by-wave overtopping volume.

Different wave attacks show many similarities in mean wave-by-wave overtopping volumes. In general, bigger wave-by-wave overtopping volumes for all wave attacks are typical for the starting configuration C0.

The biggest mean values of overtopping at configuration C0 were acquired for wave attacks H1T105G5F1, H1T125G2F1, H1T125G5F1, H2T115G2F1 and H2T115G5F1, which means that in most cases configuration C0 does not represent the most appropriate harbour breakwater. The most effective for wave attacks H1T085G2F1, H1T085G5F1, H1T105G2F1 and H1T105G5F1 is configuration C4, with an elevated wave wall of 2 cm (in model scale), which often stop the stream of water that would continue the path across the wall crest. The most effective for wave attacks H1T125G2F1, H1T125G5F1, H2T115G2F1 and H2T115G5F1 is configuration C1, with overspill basin of 9.0 cm width (in model scale) before the wave wall, where energy dissipates and so smaller quantity of water overtop the wall crown.

There are differences between mean overtopping values from I. level analysis and II. level analysis noted. In case of wave attacks H1T125G5F1, H2T115G2F1 and H2T115G5F1 the most effective in I. level analysis was configuration C3, here as mentioned before for the same wave attacks the most effective is configuration C1. Still both configurations have overspill basin which is the reason for reduction of overtopping discharge into the tank, due to dissipation of wave energy. Results regarding to configurations C1, C2 and C3 (all with OB) demonstrate that the less efficient is configuration C2 with an OB of 12 cm. For all wave attacks, except for H2T115G5F, the biggest mean wave-by-wave overtopping discharge is acquired for C2 configuration. Differences in mean overtopping discharge between configurations C4 and C5 (both with extended wall crest) in wave attacks with smaller wave heights are almost negligible (except in case of H1T125G5F1), which brings us to conclusion

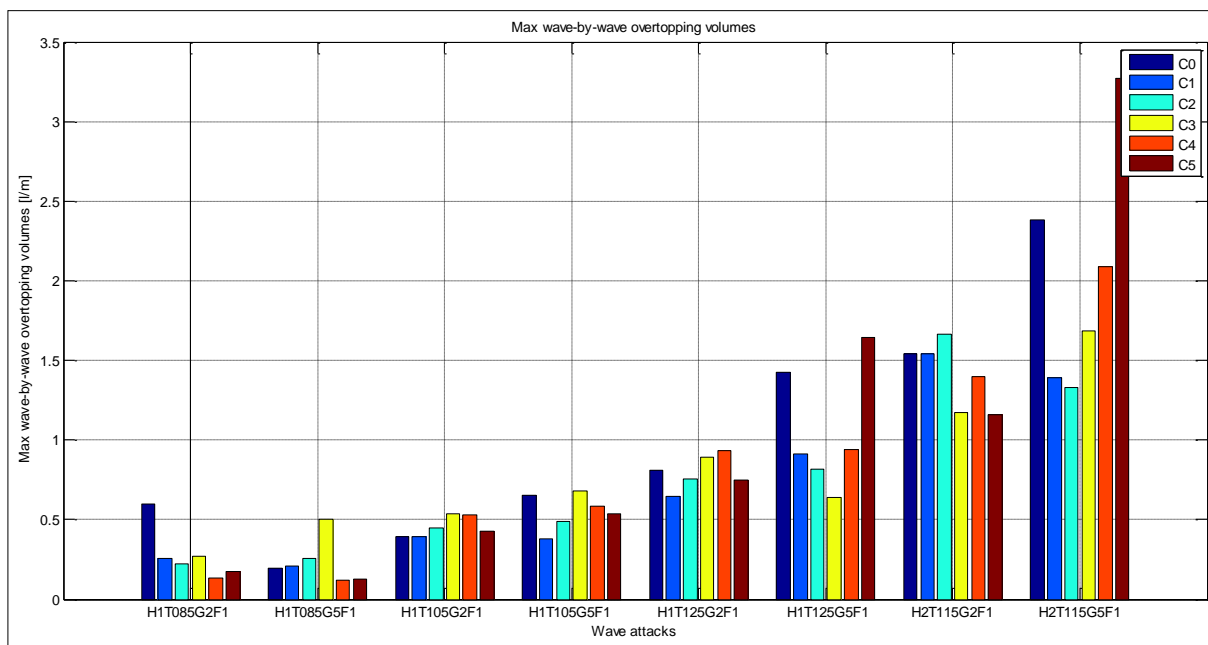
that when there are small founds, smaller wave wall could be realised. The difference between C4 and C5 for H1T125G5F1 is 0.082 l/m, where configuration C4 is more efficient.

### 5.3.1.2 Maximum overtopping discharge

Table 43: Max wave-by-wave overtopping volume calculated by Matlab program (in prototype scale).

MAX Wave-by-wave o.v. [l/m]	C0	C1	C2	C3	C4	C5
H1T085G2F1	0,598	0,253	0,225	0,271	0,132	0,172
H1T085G5F1	0,193	0,210	0,258	0,505	0,121	0,129
H1T105G2F1	0,393	0,393	0,448	0,537	0,529	0,428
H1T105G5F1	0,650	0,381	0,492	0,681	0,584	0,536
H1T125G2F1	0,809	0,645	0,754	0,892	0,935	0,750
H1T125G5F1	1,427	0,914	0,817	0,636	0,942	1,646
H2T115G2F1	1,539	1,544	1,664	1,174	1,401	1,157
H2T115G5F1	2,380	1,389	1,331	1,684	2,085	3,27

Values in orange squares represent extreme value of max wave-by-wave overtopping volume for each wave attack.



Graph 21: Max wave-by-wave overtopping volume.

In general, maximum wave-by-wave overtopping discharges for different wave attacks are achieved on different configurations. Maximum wave-by-wave overtopping volume was acquired for wave attack H2T115G5F1 at C5 configuration and has a value of 3.27 l/m.

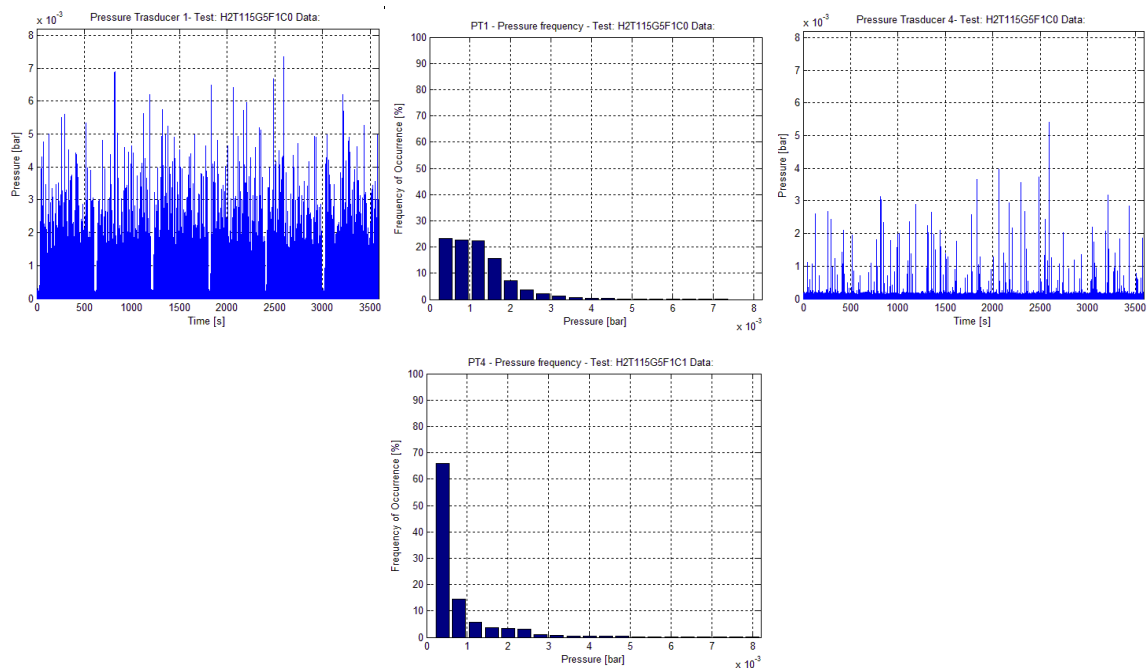
Maximum overtopping volume for this wave attack was assumed in advance, since it has the biggest wave height. There is also another wave attack H1T125G5F1 that acquire its maximum value on the same configuration C5, with a value of 1.65 l/m. Wave attacks H1T085G5F1, H1T105G2F1 and H1T105G5F1 reach their maximum on breakwater configuration C3 with an overspill basin of 18.0 cm (in model scale). Wave attacks H1T085G2F1 acquire its maximum wave-by-wave overtopping volume at C0 configuration and H2T115G2F1 on configuration C1.

Since sea waves follow random behaviour at the next execution of the same wave attacks at the same laboratory conditions, there could be maximum values of overtopping for wave attacks (with smaller wave heights) reached on any other configurations.

### 5.3.2 Maximum wave pressure of impact

After review of first level analysis was done, we noticed all pressure data were not included in the graph window, so we extended y axis for pressures from 4 to 8 mbar, since most of the values are smaller than 8 mbar.

Combination of 3 (or 6) sub tests was made by putting second (and forward) sub test to the last value of the preliminary sub test and so on. In addition first 2 minutes of acquisition in the second and all subsequent sub test forward were taken away, since waves at that time are still arriving towards the breakwater and no wave pressure are present. New graph for single pressure transducer has duration of 55.5 min for tests with wave height H1 and 51.0 min for H2.



Graph 22: Typical output results after joining all sub tests of wave pressures for the test H2T115G5F1C0 at transducers 1 and 4 is showed.

There are still gaps between sub tests data after joining in some cases. Since the time for waves to arrive to the wave wall sometimes is still bigger than 2 minutes.

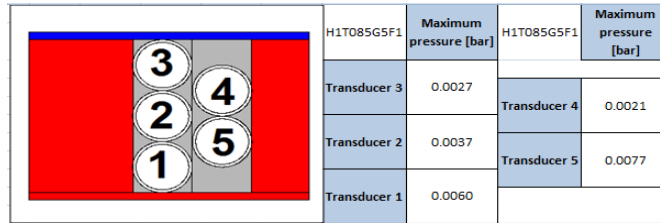
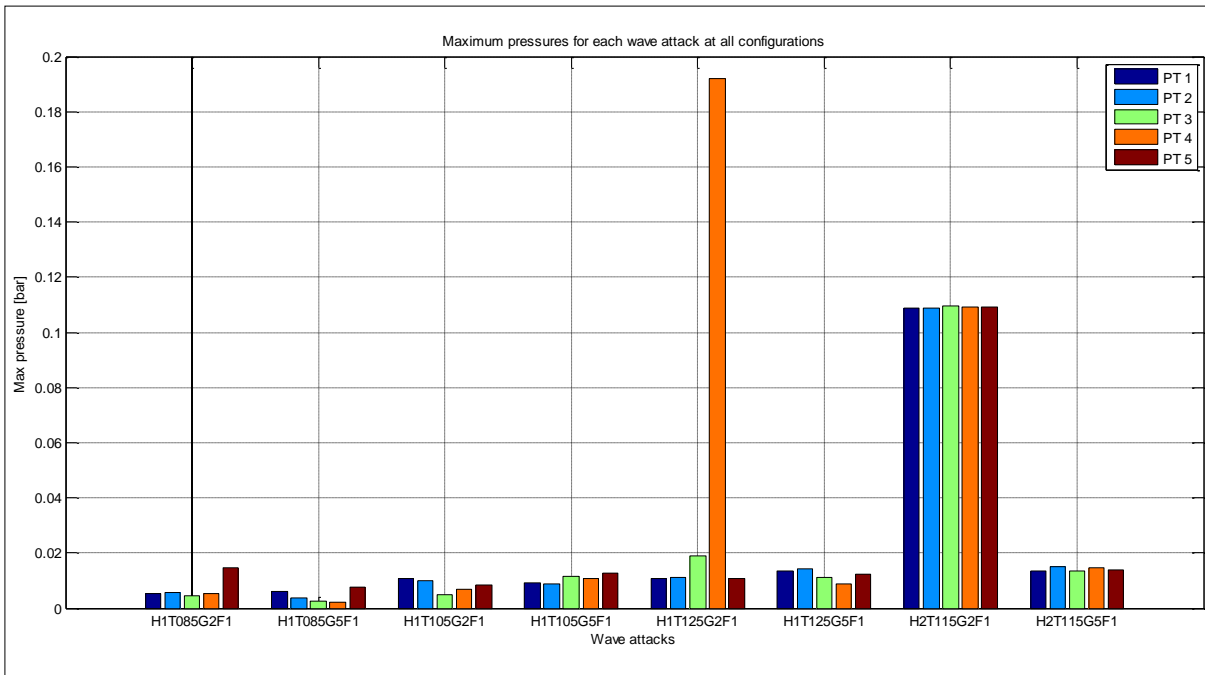


Figure 75: Maximum pressure stresses for each pressure transducer, attacked by wave H1T085G5F1.

Table 44: Maximum pressures for each wave attack at all configurations.

For all configurations	Trasd. 1 [bar]	Trasd. 2 [bar]	Trasd. 3 [bar]	Trasd. 4 [bar]	Trasd. 5 [bar]
H1T085G2F1	0.0054	0.0055	0.0043	0.0051	0.0148
H1T085G5F1	0.0059	0.0037	0.0027	0.0021	0.0077
H1T105G2F1	0.0108	0.0098	0.0047	0.0068	0.0083
H1T105G5F1	0.0093	0.0089	0.0114	0.0108	0.0128
H1T125G2F1	0.0106	0.0111	0.0188	0.192	0.0107
H1T125G5F1	0.0136	0.0143	0.0112	0.0086	0.0122
H2T115G2F1	0.1088	0.1089	0.1094	0.1092	0.1090
H2T115G5F1	0.0136	0.0149	0.0135	0.0147	0.0139

Maximum pressures were achieved for wave attacks H1T125G2F1 and H2T115G2F1 as seen from the Table 44 above.



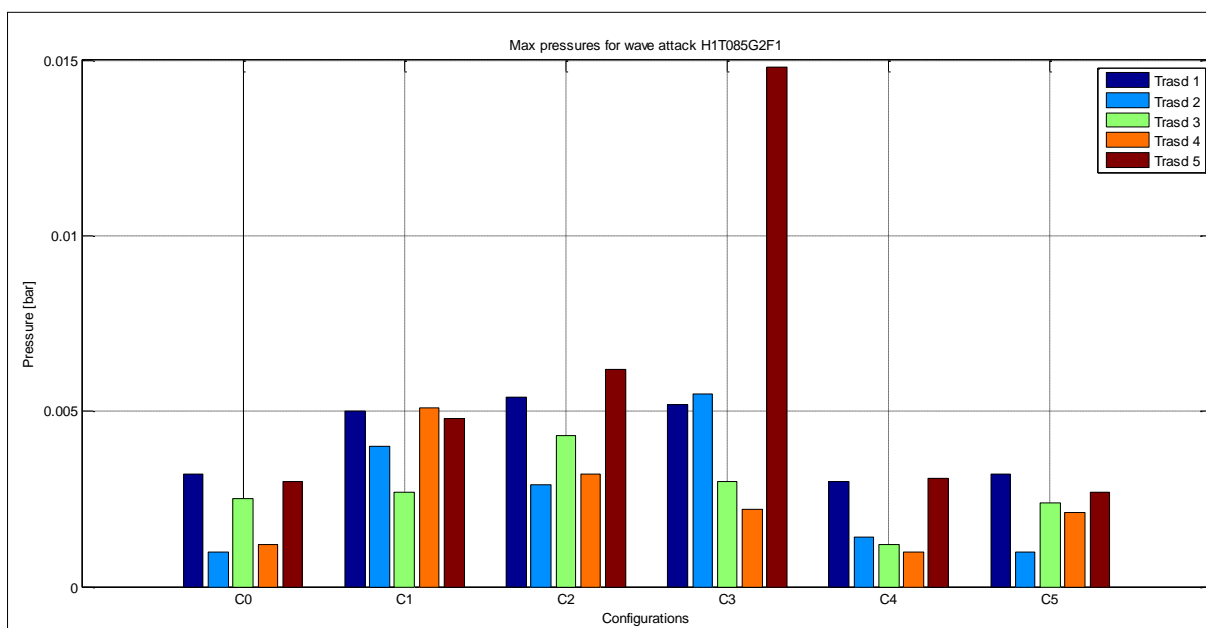
Graph 23: Maximum pressures for each wave attack.

The biggest wave force has acted on lower lying pressure transducers 1 and 5. These values were achieved for configurations (C3 and C1) with an overspill basin, since wave wall there is less protected from direct waves. There are extremely high pressures seen from results for wave attack H2T115G2F1 and max pressure at transducer n. 4 for wave attack H1T125G2F1. Maximum value for H2T115G2F1 was achieved at transducer n. 3 of 0.1094 bar, it is not excluded the possibility that the transducers did not work properly.

Furthermore maximum pressures for each wave attack and all model constructions are being represented.

Table 45: Maximum pressure values for wave attack H1T085G2F1.

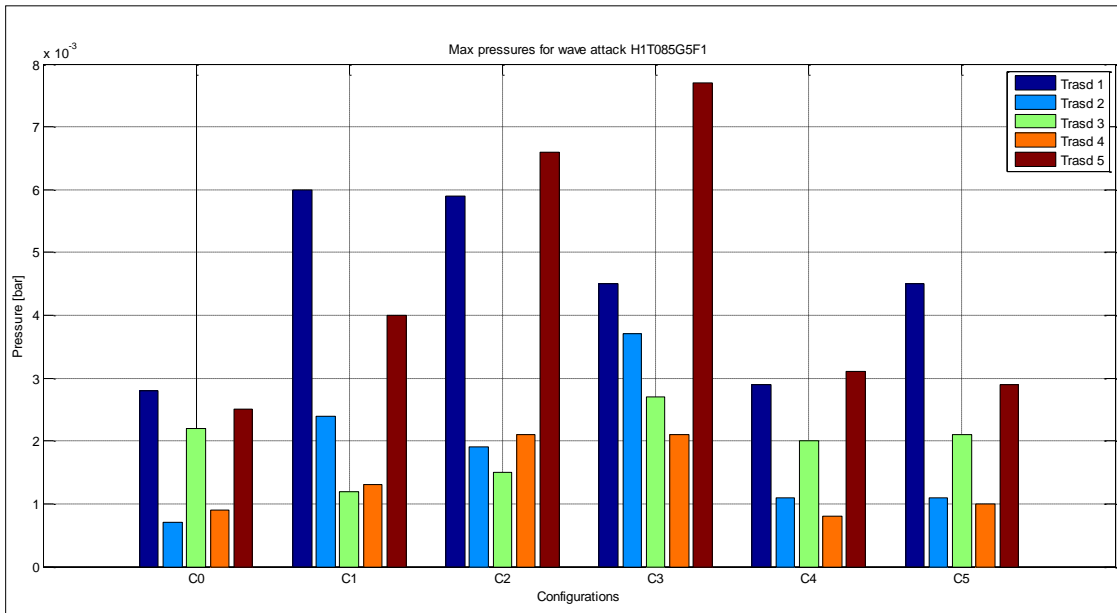
		Trasd. 1 [bar]	Trasd. 2 [bar]	Trasd. 3 [bar]	Trasd. 4 [bar]	Trasd. 5 [bar]
H1T085G2F1	C0	0.0032	0.0010	0.0025	0.0012	0.0030
	C1	0.0050	0.0040	0.0027	0.0051	0.0048
	C2	0.0054	0.0029	0.0043	0.0032	0.0062
	C3	0.0052	0.0055	0.0030	0.0022	0.0148
	C4	0.0030	0.0014	0.0012	0.0010	0.0031
	C5	0.0032	0.0010	0.0024	0.0021	0.0027



Graph 24: Max pressures for wave attack H1T085G2F1.

Table 46: Maximum pressure values for wave attack H1T085G5F1.

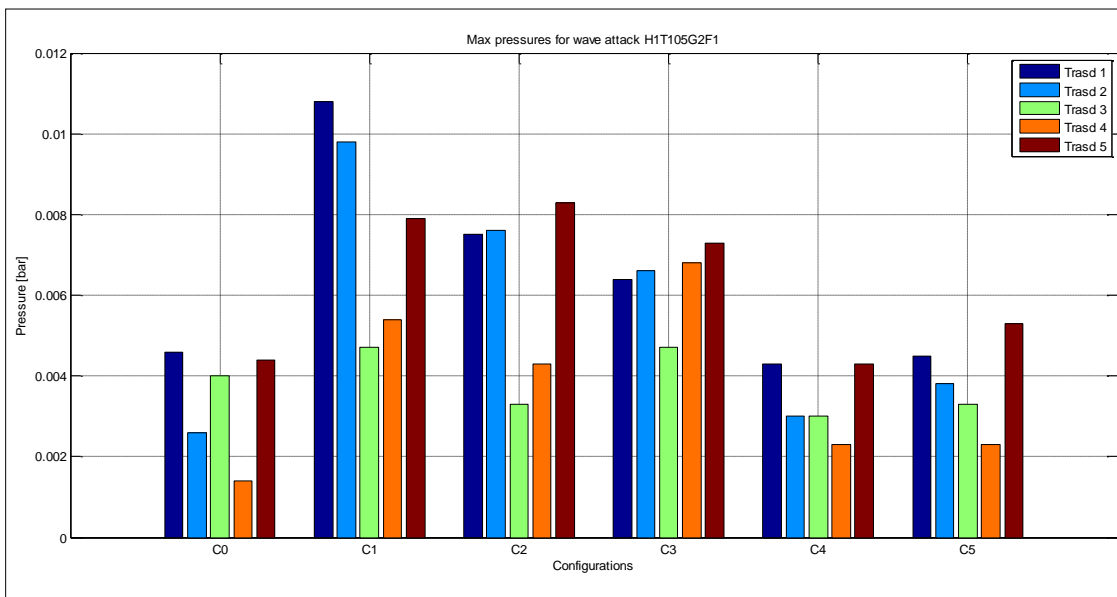
		Trasd. 1 [bar]	Trasd. 2 [bar]	Trasd. 3 [bar]	Trasd. 4 [bar]	Trasd. 5 [bar]
H1T085G5F1	C0	0.0028	0.0007	0.0022	0.0009	0.0025
	C1	0.0060	0.0024	0.0012	0.0013	0.0040
	C2	0.0059	0.0019	0.0015	0.0021	0.0066
	C3	0.0045	0.0037	0.0027	0.0021	0.0077
	C4	0.0029	0.0011	0.0020	0.0008	0.0031
	C5	0.0045	0.0011	0.0021	0.001	0.0029



Graph 25: Max pressures for wave attack H1T085G5F.

Table 47: Maximum pressure values for wave attack H1T105G2F1.

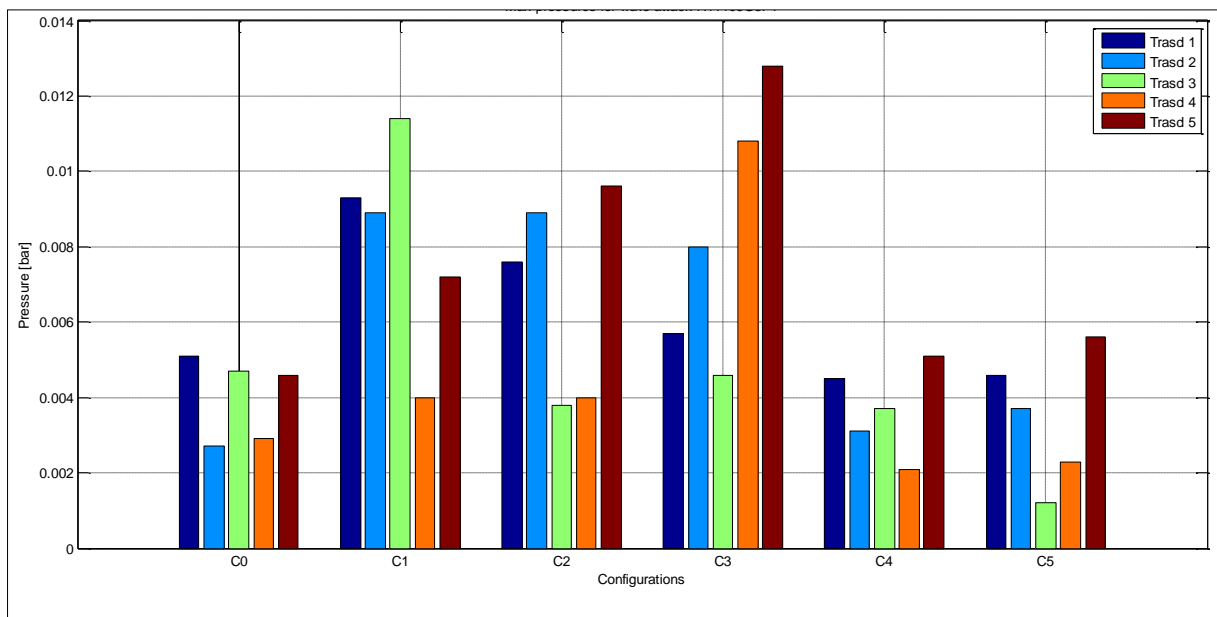
		Trasd. 1 [bar]	Trasd. 2 [bar]	Trasd. 3 [bar]	Trasd. 4 [bar]	Trasd. 5 [bar]
H1T105G2F1	C0	0.0046	0.0026	0.0040	0.0014	0.0044
	C1	0.0108	0.0098	0.0047	0.0054	0.0079
	C2	0.0075	0.0076	0.0033	0.0043	0.0083
	C3	0.0064	0.0066	0.0047	0.0068	0.0073
	C4	0.0043	0.0030	0.0030	0.0023	0.0043
	C5	0.0045	0.0038	0.0033	0.0023	0.0053



Graph 26: Max pressures for wave attack H1T105G2F1.

Table 48: Maximum pressure values for wave attack H1T105G5F1.

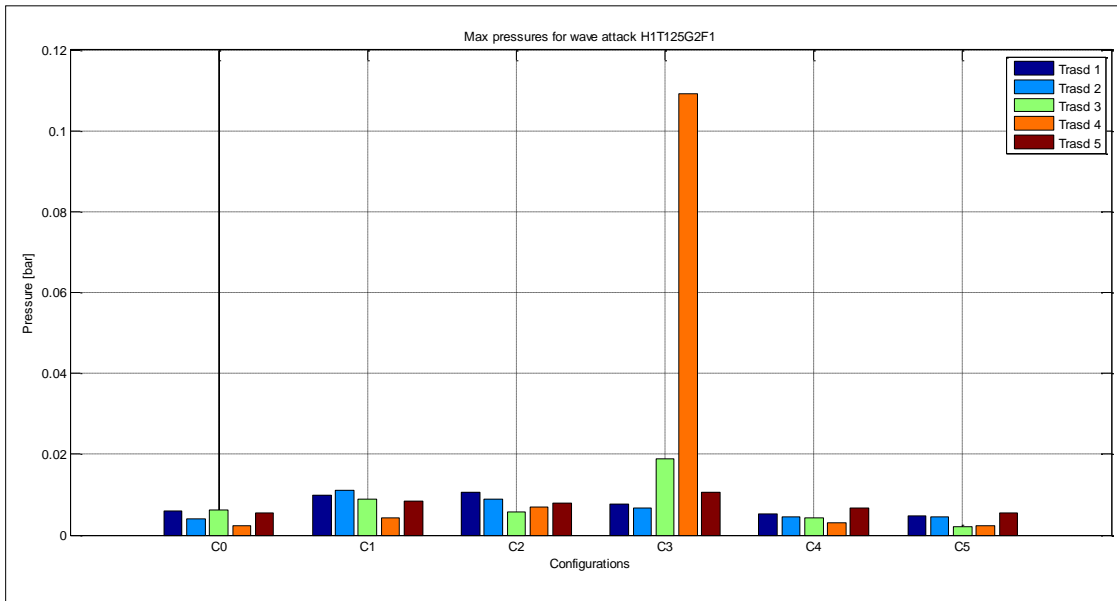
		Trasd. 1 [bar]	Trasd. 2 [bar]	Trasd. 3 [bar]	Trasd. 4 [bar]	Trasd. 5 [bar]
H1T105G5F1	C0	0.0051	0.0027	0.0047	0.0029	0.0046
	C1	0.0093	0.0089	0.0114	0.0040	0.0072
	C2	0.0076	0.0089	0.0038	0.0040	0.0096
	C3	0.0057	0.0080	0.0046	0.0108	0.0128
	C4	0.0045	0.0031	0.0037	0.0021	0.0051
	C5	0.0046	0.0037	0.0012	0.0023	0.0056



Graph 27: Max pressures for wave attack H1T105G5F1.

Table 49: Maximum pressure values for wave attack H1T125G2F1.

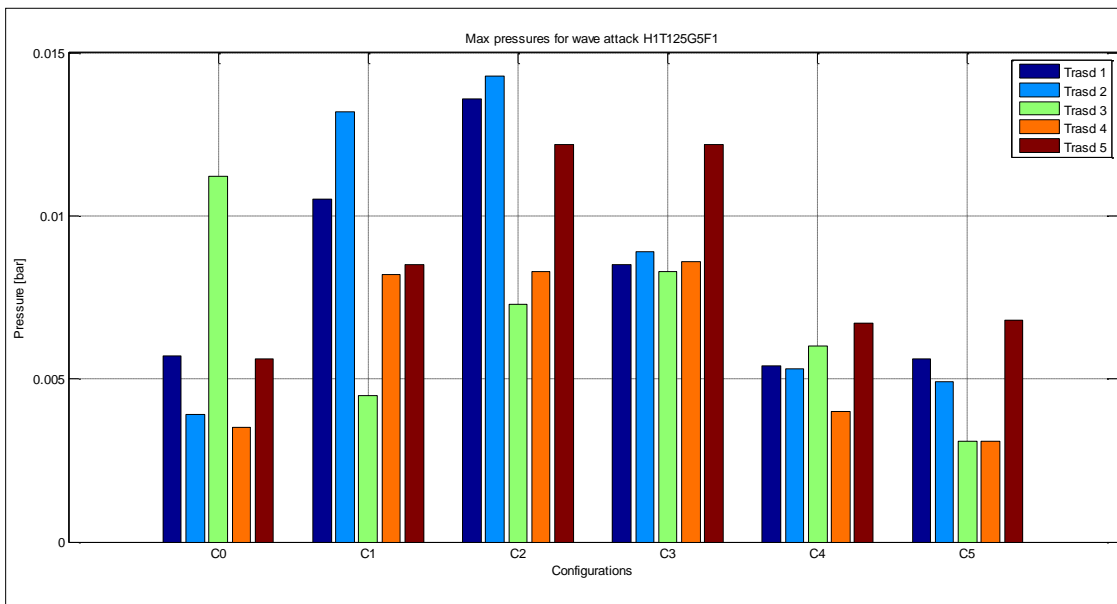
		Trasd. 1 [bar]	Trasd. 2 [bar]	Trasd. 3 [bar]	Trasd. 4 [bar]	Trasd. 5 [bar]
H1T125G2F1	C0	0.0060	0.0039	0.0063	0.0024	0.0054
	C1	0.0099	0.0111	0.0090	0.0043	0.0084
	C2	0.0106	0.0088	0.0056	0.0069	0.0079
	C3	0.0077	0.0067	0.0188	0.1092	0.0107
	C4	0.0052	0.0046	0.0042	0.0030	0.0066
	C5	0.0048	0.0046	0.0020	0.0022	0.0055



Graph 28: Max pressures for wave attack H1T125G2F1.

Table 50: Maximum pressure values for wave attack H1T125G5F1.

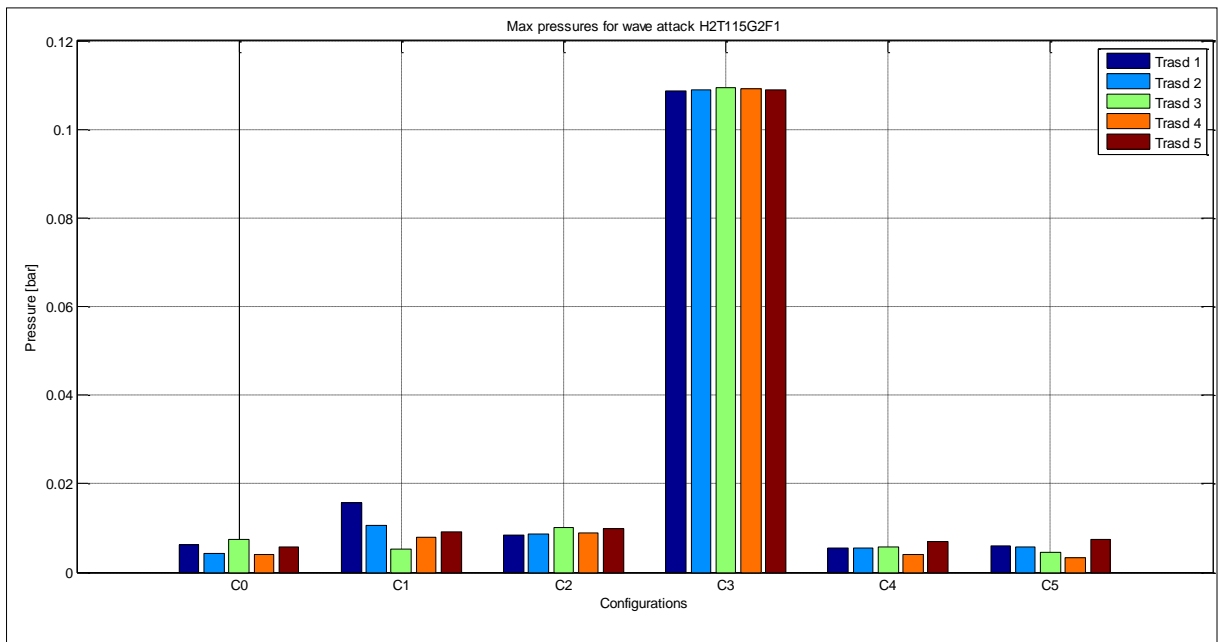
		Trasd. 1 [bar]	Trasd. 2 [bar]	Trasd. 3 [bar]	Trasd. 4 [bar]	Trasd. 5 [bar]
H1T125G5F1	C0	0.0057	0.0039	0.0112	0.0035	0.0056
	C1	0.0105	0.0132	0.0045	0.0082	0.0085
	C2	0.0136	0.0143	0.0073	0.0083	0.0122
	C3	0.0085	0.0089	0.0083	0.0086	0.0122
	C4	0.0054	0.0053	0.0060	0.0040	0.0067
	C5	0.0056	0.0049	0.0031	0.0031	0.0068



Graph 29: Max pressures for wave attack H1T125G5F1.

Table 51: Maximum pressure values for wave attack H2T115G2F1.

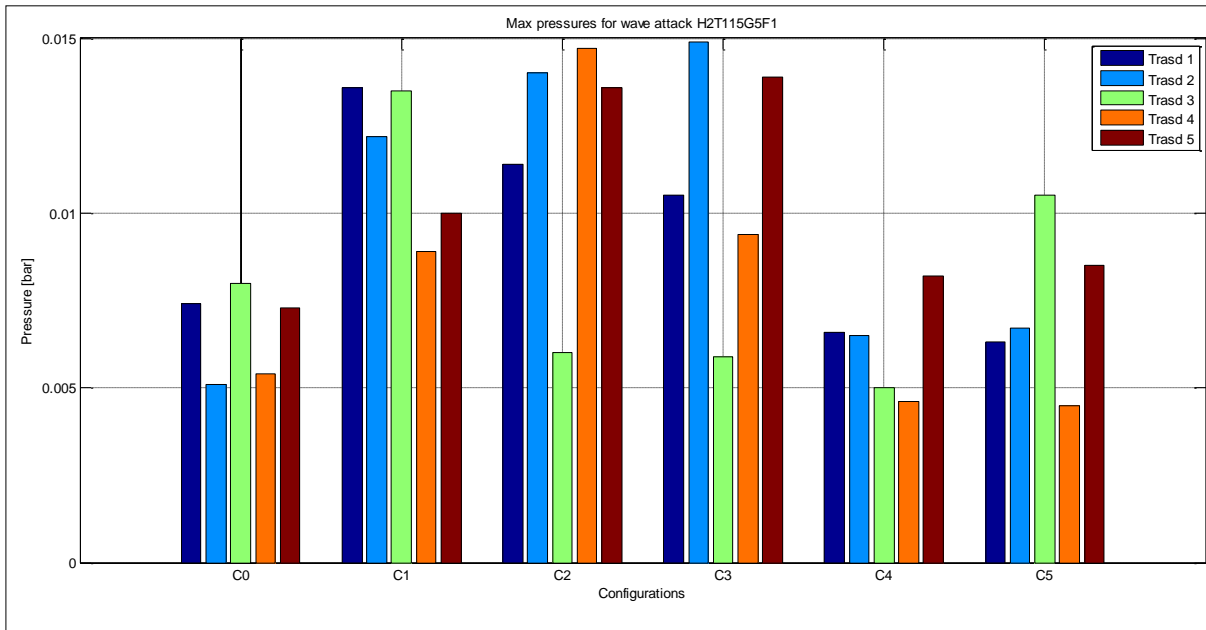
		Trasd. 1 [bar]	Trasd. 2 [bar]	Trasd. 3 [bar]	Trasd. 4 [bar]	Trasd. 5 [bar]
H2T115G2F1	C0	0.0062	0.0043	0.0074	0.0041	0.0057
	C1	0.0157	0.0107	0.0053	0.0078	0.0091
	C2	0.0083	0.0086	0.0100	0.0088	0.0098
	C3	0.1088	0.1089	0.1094	0.1092	0.1090
	C4	0.0055	0.0054	0.0057	0.0040	0.0069
	C5	0.0059	0.0057	0.0044	0.0034	0.0074



Graph 30: Max pressures for wave attack H2T115G2F1.

Table 52: Maximum pressure values for wave attack H2T115G5F1.

		Trasd. 1 [bar]	Trasd. 2 [bar]	Trasd. 3 [bar]	Trasd. 4 [bar]	Trasd. 5 [bar]
H2T115G5F1	C0	0.0074	0.0051	0.0080	0.0054	0.0073
	C1	0.0136	0.0122	0.0135	0.0089	0.0100
	C2	0.0114	0.0140	0.0060	0.0147	0.0136
	C3	0.0105	0.0149	0.0059	0.0094	0.0139
	C4	0.0066	0.0065	0.0050	0.0046	0.0082
	C5	0.0063	0.0067	0.0105	0.0045	0.0085



Graph 31: Max pressures for wave attack H2T115G5F1.

Values in orange squares in tables above are representing max value for each pressure transducer. In general, extreme wave impact pressures are achieved on transducers 1 and 5 for configurations with an overspill basin (C1, C2 and C3) and the smallest on transducer 3 for C4 and C5 configurations in most of the cases. Seeing on graphs above, configuration C3 with the largest overspill basin of 18.0 cm (in model scale) causes in comparison with the others, the highest wave pressures on wave wall, due to “missing” material in berm and small dissipation of wave energy. Extreme wave impact pressures were achieved on most of constructions for wave attack H2T115G5F1.

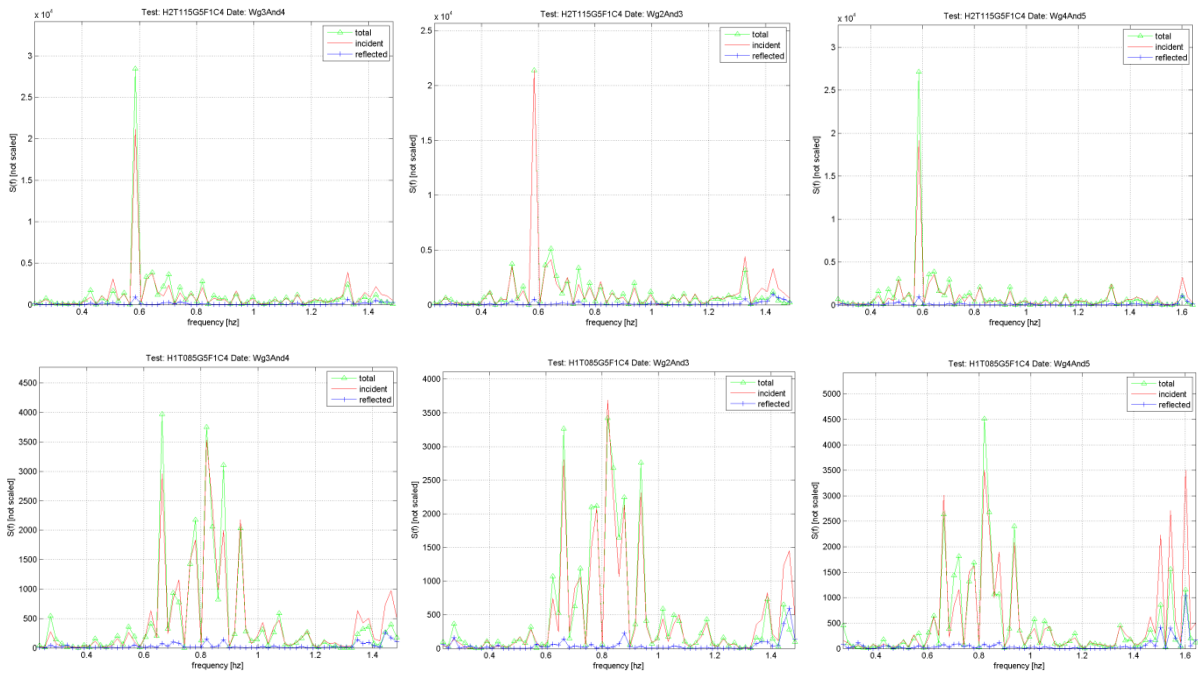
It can be observed that for wave height H1 where wave periods are increasing from T085 to T125 maximum pressure together with wave periods are increasing too. The relationship between peak elevation factors of JONSWAP spectrum ( $\gamma_{G2}$  and  $\gamma_{G5}$ ) in most of the cases is similar than for wave heights and periods. For wave attacks with the same wave height and period but different peak elevation factors, bigger wave pressure impacts are found for bigger peak elevation factor, for example in wave attack H1T105G2F1C3 at transducer n. 5 pressure is 0.0073 bar and in H1T105G5F1C3 at the same transducer, pressure is 0.0128 bar. The smallest wave impact pressures regarding to all wave attacks are found to be on C4 and C5 model configuration, which were proved to be the most effective also for wave-by-wave overtopping analysis.

### 5.3.3 Reflection analysis

Reflection analysis provides the components of the incident and reflected wave heights by Goda and Suzuki method, which is based on measurements carried out with the wave gauges in position 2, 3, 4 and 5 (see Attachment A).

Table 53: Results from reflection analysis.

Wave	Config.	%Hi_23 [cm]	Hr_23 [cm]	kr_23	Hi_34 [cm]	Hr_34 [cm]	kr_34	Hi_45 [cm]	Hr_45 [cm]	kr_45
H1T085G2F1	C0	9,17	2,85	0,31	9,06	2,79	0,31	9,78	2,58	0,26
	C1	10,64	2,44	0,23	10,50	2,57	0,25	10,38	2,91	0,28
	C2	9,82	2,15	0,22	9,69	2,24	0,23	9,56	2,56	0,27
	C3	10,21	2,38	0,23	10,06	2,50	0,25	9,92	2,80	0,28
	C4	10,39	2,37	0,23	10,26	2,49	0,24	10,10	2,82	0,28
	C5	10,32	2,24	0,22	10,14	2,43	0,24	10,05	2,63	0,26
H1T085G5F1	C0	10,42	2,90	0,28	10,27	2,79	0,27	10,18	2,98	0,29
	C1	10,85	3,20	0,29	10,77	2,90	0,27	10,64	3,30	0,31
	C2	10,44	3,23	0,31	10,39	2,83	0,27	10,22	3,20	0,31
	C3	10,73	2,86	0,27	10,64	2,53	0,24	10,45	3,12	0,30
	C4	10,58	3,27	0,31	10,54	2,85	0,27	10,31	3,49	0,34
	C5	10,54	3,25	0,31	10,47	2,73	0,26	10,27	3,18	0,31
H1T105G2F1	C0	10,87	2,52	0,23	10,80	2,41	0,22	10,80	2,56	0,24
	C1	11,64	2,78	0,24	11,51	2,86	0,25	11,57	2,90	0,25
	C2	11,45	2,73	0,24	11,39	2,62	0,23	11,37	2,83	0,25
	C3	11,13	2,69	0,24	11,04	2,71	0,24	11,01	3,01	0,27
	C4	11,54	2,89	0,25	11,44	2,84	0,25	11,48	2,96	0,26
	C5	11,40	2,75	0,24	11,23	2,69	0,24	11,26	2,90	0,26
H1T105G5F1	C0	11,40	3,03	0,27	11,24	2,97	0,26	11,21	2,86	0,26
	C1	11,56	3,06	0,27	11,41	2,93	0,26	11,38	2,85	0,25
	C2	11,56	3,05	0,26	11,43	2,87	0,25	11,28	3,05	0,27
	C3	11,54	3,14	0,27	11,39	2,99	0,26	11,28	3,06	0,27
	C4	11,77	3,37	0,29	11,68	2,96	0,25	11,60	2,98	0,26
	C5	11,58	3,25	0,28	11,32	3,15	0,28	11,33	2,98	0,26
H1T125G2F1	C0	11,27	2,62	0,23	11,25	2,46	0,22	11,08	2,93	0,26
	C1	11,05	2,90	0,26	11,04	2,68	0,24	10,91	2,84	0,26
	C2	11,36	2,73	0,24	11,35	2,63	0,23	11,22	2,85	0,25
	C3	11,47	2,76	0,24	11,45	2,59	0,23	11,29	2,85	0,25
	C4	11,58	2,81	0,24	11,52	2,69	0,23	11,40	2,98	0,26
	C5	11,47	2,77	0,24	11,40	2,64	0,23	11,26	2,87	0,26
H1T125G5F1	C0	11,29	2,87	0,25	11,22	2,94	0,26	10,99	3,39	0,31
	C1	11,76	3,11	0,26	11,67	3,05	0,26	11,36	3,46	0,30
	C2	11,04	3,08	0,28	11,05	2,95	0,27	10,89	3,26	0,30
	C3	11,33	3,31	0,29	11,35	3,04	0,27	11,12	3,50	0,31
	C4	11,40	3,18	0,28	11,39	2,95	0,26	11,21	3,42	0,31
	C5	11,40	3,23	0,28	11,34	2,98	0,26	11,19	3,39	0,30
H2T115G2F1	C0	12,84	3,54	0,28	12,56	3,67	0,29	12,48	3,47	0,28
	C1	13,09	3,59	0,27	12,84	3,57	0,28	12,61	3,55	0,28
	C2	12,72	3,57	0,28	12,50	3,74	0,30	12,38	3,76	0,30
	C3	12,77	3,66	0,29	12,52	3,74	0,30	12,36	3,70	0,30
	C4	12,89	3,73	0,29	12,61	3,87	0,31	12,50	3,83	0,31
	C5	12,99	3,77	0,29	12,72	3,89	0,31	12,59	3,92	0,31
H2T115G5F1	C0	12,93	3,52	0,27	12,72	3,79	0,30	12,56	3,87	0,31
	C1	13,05	3,54	0,27	12,82	3,78	0,29	12,56	3,68	0,29
	C2	12,55	3,44	0,27	12,42	3,63	0,29	12,15	3,93	0,32
	C3	12,46	3,64	0,29	12,28	3,89	0,32	12,16	3,67	0,30
	C4	12,80	3,89	0,30	12,63	3,86	0,31	12,46	4,01	0,32
	C5	12,70	3,78	0,30	12,51	3,79	0,30	12,30	3,90	0,32



Graph 32: Typical output results for reflection analysis for two wave attacks H1T085G5F1C4 and H2T115G5F1C4.

It can be observed that reflected wave heights and reflection coefficients ( $k_r$ ) increase together with increasing wave height, wave period and peak elevation factor in most of the cases.

## 6 CONCLUSIONS

Natural sea states have irregular wave characteristics which makes difficult to predict effects of studied processes even for known wave attacks and constructions. Sea defence structures as harbour breakwaters with wave walls are constructed primarily to limit overtopping volumes that might cause flooding, or other potential hazards at harbours. On average, approximately 2 - 5 people are killed each year of Italy and United Kingdom through wave action, chiefly on seawalls and similar structures.

Two dimensional physical model for this thesis research was installed and tested in the wave flume at the Maritime Engineering Laboratory (CoastLab, [www.unifi.it/labima](http://www.unifi.it/labima)) at the Department of Civil and Environmental Engineering of Florence University in Italy. This research is part of the international exchange ERASMUS between University of Ljubljana and University of Florence, which lasted during spring 2012.

The objectives of this laboratory research were to measure wave overtopping (WO) and extreme wave-induced pressures on the wave wall, obtained by testing various design parameters, such as crest freeboard height ( $R_c$ ), overspill basin length (OB) and various wave parameters ( $H_{m0}$ ,  $T_0$ ,  $\gamma$ ) on harbour breakwater. Finally the main aim was to study the differences between various constructions and to find the most effective harbour breakwater construction that would totally protect people and potential traffic from harmful consequences of overtopping waves.

A series of tests were executed in a wave flume after water level stabilization in the flume and calibration of wave gauges was made. Wave attacks were chosen in particular to those wave characteristics found in Ligurian Sea. Conducted tests give us very wide range of overtopping discharges and wave pressures of impact due to the large number of wave conditions and geometries tested.

Capture system of overtopping water, consists of a plastic overtopping tank, hanged on 4 wires which connect overtopping tank with 4 load cells, measuring cylinder and a sloping chute of two different widths (sampler) by which water pass inside the tank. The pressures acting along the centre of wave wall were measured by five pressure transducers. Pressure transducers 1, 2 and 3 were positioned on the left centre side, in a descending order from a wave wall crown, while pressure transducers 4 and 5 were positioned on the right centre side in an increasing order from a wave wall crown. This concept of acquiring signal is very reliable and gives us good results on which detailed II. level analysis is based. There was also measuring cylinder used in order to compare measurements (volumes) between volume recorded by load cells and volume collected inside the overtopping tank. Accumulated volume recorded by load cells was always smaller than the one measured.

In II. level analysis Matlab program was updated (see Attachment F - Overtopping program), which analyzed individual wave-by-wave overtopping volumes, unless a few overtopping waves come in one wave group. The overtopping graphs in Chapter 5 (Analysis and Results), clearly show the irregularity of wave overtopping volumes.

It can be summarized that by increasing wave height, period and peak elevation factor of JONSWAP spectrum wave overtopping is increasing too. In general, larger wave-by-wave overtopping discharges for all wave attacks are typical for the starting configuration C0. The most effective in decreasing overtopping discharges for wave attacks H1T125G5F1, H2T115G2F1 and H2T115G5F1 is configuration C3, with an overspill basin of 18.0 cm (in model scale) before the wave wall, where energy can be dissipated and so smaller quantity of water overflow the wall crown. On the other hand for wave attacks H1T085G2F1, H1T085G5F1, H1T105G2F1 and H1T105G5F1 the most effective configuration is C4 with an elevated wave wall of 2.0 cm (in model scale) respect to starting configuration C0, which has also positive effects on reducing overtopping discharges. For wave attack H1T125G2F1 the most effective construction is C1 with an overspill basin of 6.0 cm (in model scale).

In general, extreme wave impact pressures are achieved on transducers 1 and 5 for configurations with an overspill basin (C1, C2 and C3) and the smallest on transducer 3 for C4 and C5 configurations in most of the cases. Configuration C3 with the largest overspill basin of 18.0 cm (in model scale) causes the highest wave pressures on wave wall, due to “missing” berm material and small dissipation of wave energy. Extreme wave impact pressures were achieved on most of constructions for wave attack H2T115G5F1.

To conclude the smallest wave impact pressures are found to be on C4 and C5 model configuration (for most of wave attacks), which were proved to be the most effective also in wave-by-wave overtopping analysis. Differences in mean overtopping discharge between C4 and C5 are almost negligible, so C5 construction from financial point of view seems to be the best option, since extension of wave wall respect to starting C0 is smaller and so less expensive.

In general if we consider increasing of mean sea level due to global warming by 2050 of + 0.2 to more than + 1.0 m, already established sea defence constructions in harbours against overtopping and other hazards will have to be rebuilt to ensure the highest possible security. Most convenient for small wave heights (H1) would be elevation of wave wall, since in this research positive results in decreasing wave overtopping were shown. Problem here is that most of the people do not see it as a nice solution, since elevation of wave wall does not provide an open sea view. On the other hand the most convenient for greater wave heights (H2) is construction C3 with the largest overspill basin, also from economic point of view, since less material is necessary to fill the berm.

Another interesting issue in future of this research could be testing three dimensional model, use of other material combination in the berm (such as artificial armour units) and a repetition of all the experiments. Sea waves follow random behaviour, so at the next execution of the same wave attacks at the same laboratory conditions, mean and maximum overtopping discharges could be different.

This research could be very important also for Slovenia, despite the fact that it only has 46.6 km of sea side and that wave characteristics from Ligurian sea are not the same as for Adriatic sea. There are few small harbours and a leading harbour of Koper, which has an important role in North Adriatic Sea not just for our small country but also for the countries of Central and Eastern Europe. Koper's climate is dominated by the Bora wind, which occurs anytime

during the year, however the peak frequency occurs in the cold season (November – March) (Naval research Laboratory, 2003) and that effects port of Koper to stormy weather with high waves and wave overtopping.

## 7 SLOVENSKI POVZETEK

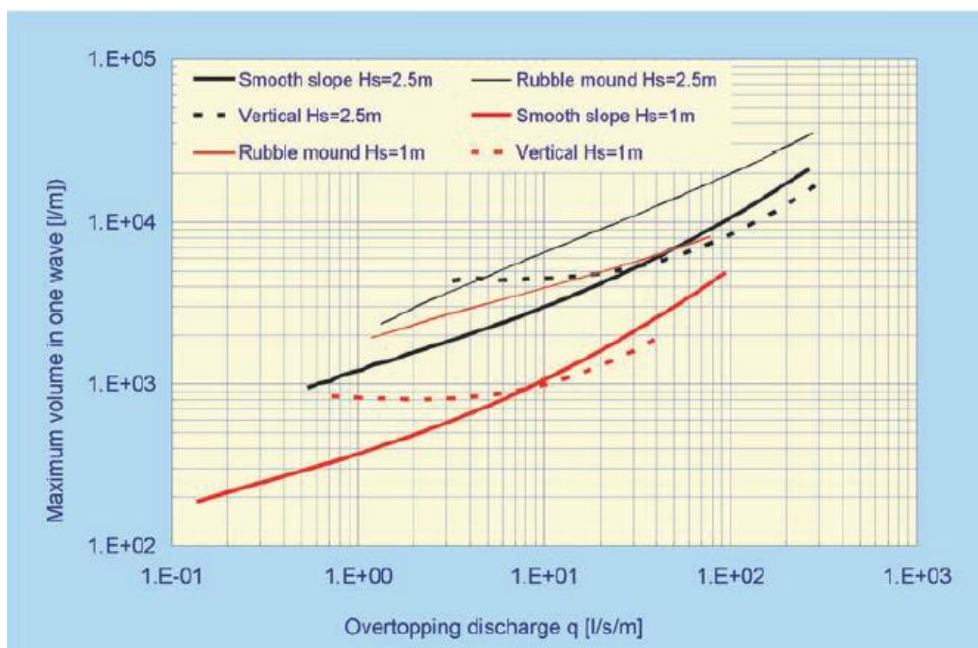
### 7.1 Pojav prelivanja valov (ang. Overtopping)

Naravno stanje morja je ob močnejših vetrovih zelo zapleteno, zato je predvidevanje obnašanja posameznih valovno-nevihtnih procesov kljub že znanim valovnim pogojem in geometriji konstrukcije zelo oteženo. Pojav prelivanja valov preko pristaniških valobranov je eden izmed glavnih vzrokov pri povzročanju škode na privezanih plovilih v pristaniščih in na obali. Vsako leto v Italiji in Veliki Britaniji umre približno 2 do 5 ljudi zaradi nevarnih prelivanj valov čez stene valobranov in drugih konstrukcije.

Znan proces prelivanja valov se pojavi zaradi razlivanja vala navzgor po (in čez) steni konstrukcije in je odvisen od številnih dejavnikov (nekateri so bili preizkušeni tudi v sklopu te raziskave). Že majhne spremembe geometrije konstrukcije močno spremenijo obnašanje in količino prelivanja valov (Wai et al., 2003). Obalne konstrukcije, kot so pristaniški valobrani (ang. harbour breakwater) z vgrajenim zidom (ang. wave wall) zmanjšujejo prelivanje valov, ki bi povzročili škodo v pristaniščih ali poplave na zavetrni strani.

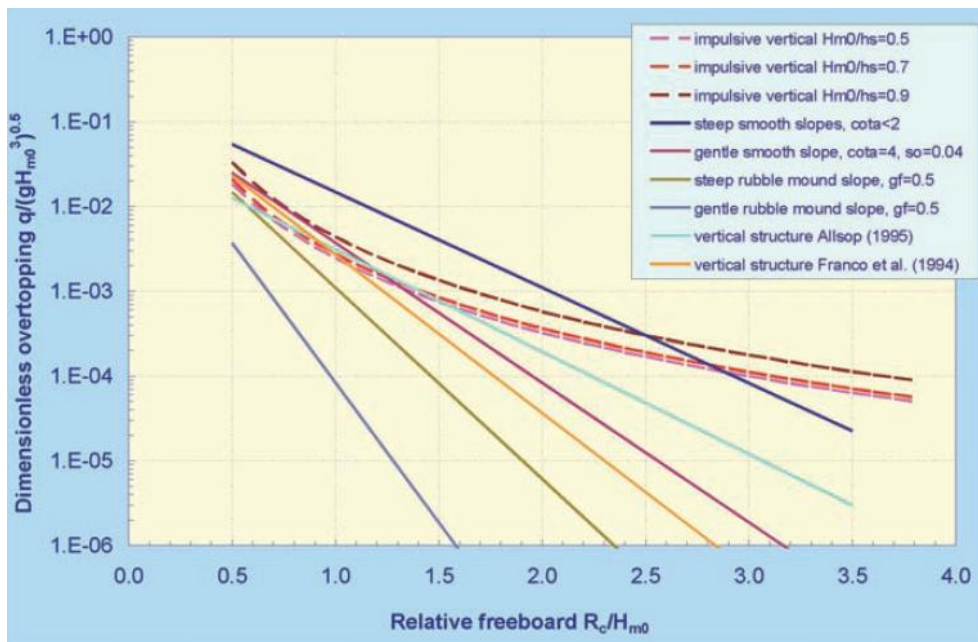
#### 7.1.1 Dopustni srednji pretoki $q$ in maksimalni volumen $V_{\max}$ prelivanja

Glavni parameter procesa prelivanja je srednji pretok prelivanja  $q$  ( $m^3/s$  na  $m$  širine ali bolj praktično uporabno  $l/s$  na  $m$  širine) (ang. mean overtopping discharge), ki ga je enostavno izmeriti v laboratorijskem kanalu ali bazenu. Na obseg prelivanja in pretok vpliva tudi način lomljenja valov (Pullen et al., 2007). Informacija o srednjem pretoku prelivanja pa ni vedno najbolj zanesljiv indikator varnosti za ljudi v določenih razmerah. Mogočo povzročeno škodo bolje opiše parameter maksimalnega prelitega volumna (pljuska) vala  $V_{\max}$  (Pullen et al., 2007). Pljusk (ang. wave-by-wave overtopping volume) je volumen vode, ki se prelije čez steno valobrana v posameznem prelivajočem se valu.



Slika 1: Razmerje med srednjim pretokom  $q$  in maksimalnim volumnom pljuska  $V_{max}$  na gladki, nasuti (ang. rubble mound) in navpični konstrukciji, pri srednji valovni višini med 1.0 in 2.5 m.

Vir: Pullen et al., 2007.



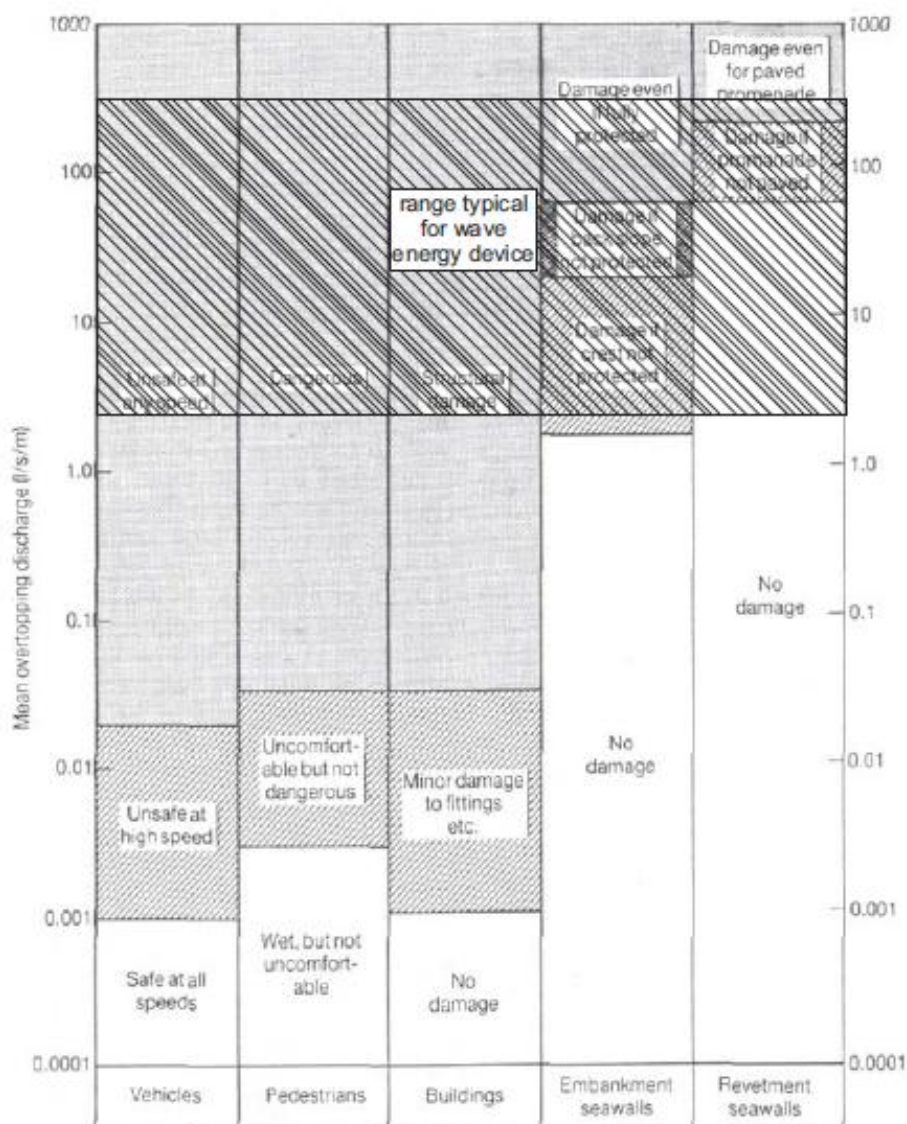
Slika 2: Primerjava različnih konstrukcij glede na brezdimenzijski obseg prelivanja.

Vir: Pullen et al., 2007.

Na zgornjih slikah je prikazano, da strma pobočja povzročajo večje prelivanje, ta pa se zmanjša z upadom naklona. Bolj navpična hrapava pobočja pa vseeno prelivajo manj, kot podobna strma pobočja z gladko oblogo, razen v primerih visokih navpičnih konstrukcij z

zelo impulzivnimi valovnimi pogoji. Obseg (in hitrost) prelivanja se lahko bistveno spremeni s spremembo valovnih in geometrijskih pogojev konstrukcije, tudi za že dani srednji pretok prelivanja (Pullen et al., 2007).

Daljše nevihte povzročijo več prelivanja in statistično gledano tudi pljuske večjih dimenzij. Več manjših prelivajočih valov (ti so značilni za rečne nasute pregrade) lahko ustvari podobne srednje pretoke kot malo število ekstremno velikih valov na nemirnem morju. V splošnem je večina prelivajočih valov dokaj majhnih, vendar že nekaj valov lahko povzroči izdatnejše prelive. Zelo veliki dogodki prelivanja so značilni pri visokem valovanju na morju (Pullen et al., 2007).



Slika 3: Povzročena nevarnost prelivnih pretokov za vozila, pešce, zgradbe, nasipane in zaščitne valobrane.

Vir: Kofoed, 2002.

Prelivanje valov čez pristaniške valobrane povzroči prenos energije vala v mirno zavetrno območje, kar lahko privede do povzročitve večjih valov znotraj pristanišča in morebitno škodo ali izgubo privezanih plovil.

Krone valobranov so območja, ki jih pogosto uporabljajo ljudje skupaj s prevoznimi sredstvi, kar lahko v primeru zelo valovitega morja predstavlja veliko tveganje za varnost. Veliko obalnih konstrukcij (valobranov itd.) je načrtovanih za prelivanje sprejemljivih srednjih pretokov pri visokem valovanju morja. Predvidevanje prelivanja srednjih pretokov temelji na empiričnih formulah določenih v skladu z laboratorijskimi meritvami. Nevaren vpliv prelivanja lahko zmanjšamo z odmaknjenostjo od obrambne črte (ang. defence line). Efektiven pretok prelivanja  $q_{effective}$  je tako približno podan z naslednjo enačbo v odvisnosti od razdalje  $x$  (od 5 do 25 m):

$$q_{effective} = q_{seawall} x \quad (2.1)$$

Kjer je  $q_{seawall}$  nevarni prelivni pretok preko stene valobrana.

Laboratorijski eksperimenti na fizičnem modelu so nujno potrebni za natančnejšo oceno obnašanja prelivajočih se valov (Wai et al., 2003), saj je ta proces slučajen, nanj vpliva veliko parametrov (posameznih ali povezanih) in ga je težko vnaprej napovedati.

## 7.2 Cilji diplomske naloge

Ta diplomska naloga je bila narejena v sodelovanju med Univerzo v Ljubljani in Univerzo v Firencah v okviru mednarodne študijske izmenjave ERASMUS, z namenom preučevanja procesa prelivanja in tlakov valov na fizičnem modelu pristaniškega valobrana v odprtem kanalu v Laboratoriju za morsko hidravliko v Firencah.

Glavni motivi testiranja modela valobrana so bili:

- Merjenje pretoka in volumna prelitih valov čez krono valobrana, sil na osrednji del vgrajenega betonskega zidu in parametrov odboja valov.
- Študija vpliva različnih projektnih parametrov: višine krone zidu nad normalno gladino  $R_c$  in dolžine umirjevalne ploščadi (ang. overspill basin OB) na prelivanje in velikost tlakov na vgrajeno steno.
- Študija obnašanja različnih karakteristik valov (srednja valovna višina  $H_{m0}$ , valovna perioda  $T_0$ , gama faktor stopnje vrha vala JONSWAP energijskega spektra  $\gamma$ ).

Končni cilj te raziskave je bil preučiti obnašanje različnih konstrukcij valobrana in najti najvarnejšo konstrukcijo, ki štiti ljudi in plovila v pristaniščih pred visokimi valovi. Obdelava podatkov in analiza rezultatov sta bili izvedeni s pomočjo računalniškega programa Matlab.

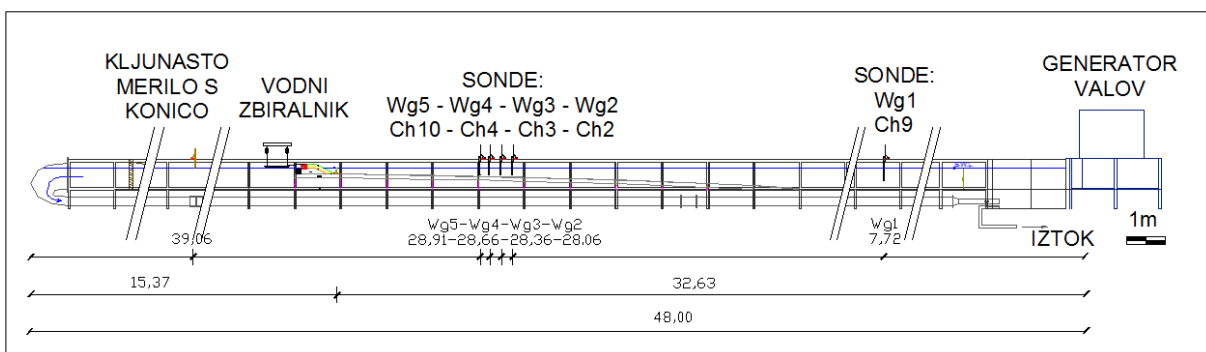
V sklopu priprave in izvajanja testov za to diplomsko nalogo so bile izvedene naslednje dejavnosti:

- Priprava programa testiranja.
- Priprava in oprema kanala, postavitev fizičnega modela in njegovih konfiguracij.
- Testiranje in merjenje parametrov.
- Analiza in obdelava rezultatov, pridobljenih iz meritev.

### 7.3 Opis laboratorija

Fizični hidravlični model je bil nameščen in testiran v odprtem kanalu Laboratorija za morsko hidravliko (CoastLab) na oddelku za gradbeništvo in okoljsko gradbeništvo na Univerzi v Firencah v Italiji. Laboratorij obratuje od leta 1980 na področju pomorskega in obalnega inženirstva. Testiranje za diplomsko nalogo je bilo izvedeno v obdobju med marcem in junijem 2012.

Laboratorijski hidravlični kanal je narejen iz železa in steklenih plošč z dimenzijami 47,0 m \* 0,8 m \* 0,8 m (dolžina \* širina \* višina). Sestavljen je iz 39 podsektorjev z dimenzijami 1,2 m \* 0,8 m \* 0,8 m (prvih 37 podsektorjev je iz stekla in železa zadnja 2 pa iz betona). Dno kanala je od tal dvignjeno za 0,5 m in narejeno iz vlakenskih prednapetih betonskih plošč dimenzij 1,2 m \* 0,8 m \* 0,02 m, ki so lahko prestavljive in prilagojene zahtevam po spreminjanju profila (slika 48 v angleškem tekstu zgoraj, prerez na sliki 4 v slovenskem povzetku).



Slika 4: Vzdolžni prerez kanala z modelom in merilno opremo (v merilu modela).

### 7.4 Načrtovanje in izdelava valobrana

Osnovne značilnosti kanala in testiranega hidravličnega modela so naslednje:

- Merilo modela v kanalu 1:50.
- Globina vode pred loputo generatorja valov (ang. wave maker) 56,3 cm.
- Dno kanala z naklonom 1:38.
- Pobočje berme valobrana z naklonom 1:2.
- Material v jedru v merilu 1:36,3.
- Peta valobrana na globini – 16,06 cm.
- Material za filter in skalometno oblogo v merilu 1:50.
- Izbrana največja višina valov za testiranje je 15 cm (H2) z valovno periodo od 1,20 do 1,77 sekund (na modelu).

Po mednarodnih smernicah fizični model valobrana, narejen v merilu 1:50, zagotavlja tehnično dovolj dobre rezultate meritev, ki jih lahko prenesemo na dejansko konstrukcijo.

V splošnem so nakloni valobrana kar se da strmi, saj se na ta način zmanjša količina potrebnega materiala v jedru in žerjav pri vgradnji materiala (skal, tetrapodov...) lahko deluje na manjšem delovnem radiju od krone valobrana (Palmer et al., 1998). Naklon pobočja na privetni strani valobrana v našem modelu je bil enak za vse konfiguracije in znaša, kot je navedeno zgoraj, 1:2.

Izbor materiala za skalometno oblogo in filter je v istem merilu kot model sam, tj. 1:50. Za določitev velikosti in merila materiala v jedru pa smo sledili posebnemu postopku po Burcharth-u et al. (1999) za laboratorijski model valobrana. Ta pravi, da se za potrebe testiranja valobrana in natančne meritve tlakov merilo karakterističnega premera jedra  $d_{50}$  izbere na podlagi Froudovega zakona za hitrost vode v porah jedra. Račun te hitrosti se izvede v 6 točkah. Nato se poišče srednjo vrednost hitrosti vseh točk, ki mora biti enaka porni hitrosti v jedru dejanske konstrukcije za predpostavljen karakterističen polmer v merilu 1:50 (glej poglavje 4.4.2.2, slika 60 v angleškem tekstu zgoraj). Po daljšem iteracijskem izračunu dobimo, da je potrebno merilo za kamne v jedru 1: 36,3.

Če bi se ravnali po določitvi karakterističnega premera kamna za jedro po enotnem merilu za valobran, bi zaradi učinkov viskoznosti (ang. viscous effect) ta sloj postal premalo propusten (in voda ne bi pronicala skozenj). Posledica tega bi bile netočne meritve na modelu, prevelike količine prelite vode, napačni učinki delovanja na konstrukcijo in tudi preveliki sile na samo steno valobrana, kot bi se to dejansko zgodilo v naravi. Ta način izbire materiala modela pa nam na drugi strani vrne drugačne vrednosti od pričakovanih za odboj (ang. reflection) in prenos energije (ang. transmission) (Wolters, 2007).

Absolutno geometrijsko ujemanje med izračunanim (premer  $d_{50}$ ) in dejansko vgrajenim materialom v konstrukcijo valobrana ni potrebno. Majhne razlike ne vplivajo v veliki meri na rezultate testov. V splošnem je napaka pri rezultatih učinkov prelivanja in stabilnosti manjša

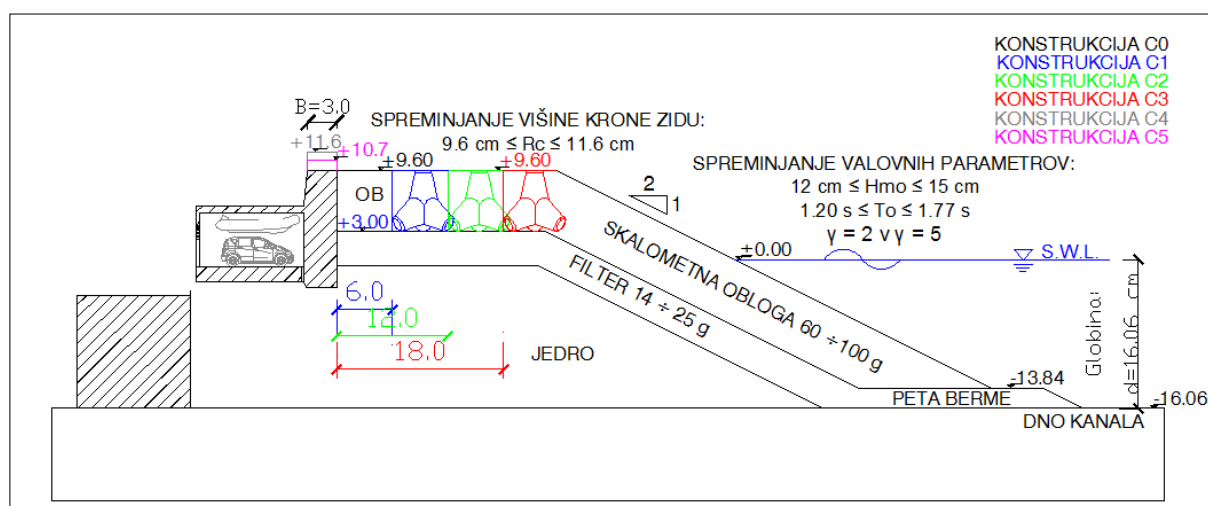
od 5-10 %. Bolj pomembna za točne meritve prelivanja je krona zidu, ki pa mora biti kar se da natančno izvedena, saj je od te najbolj odvisno število in količina prelitih valov. Pri dimenzioniranju kamnov za posamezne sloje Wolters (2007) pravi še, da je zelo pomembno zagotoviti pravi nivo zunanje skalometne obloge. Ta lahko v določenih primerih tudi zahteva, da se spodnji sloji temu primerno prilagodijo in so zaradi tega lahko tanjši ali debelejši.

Stabilnost konstrukcije in disipacija energije valov se povečuje z večanjem debeline obloge valobrana, tako je na debelejših slojih prelivanje manj pogosto in izdatno. Debeline slojev so v celotnem testu ostajale enake in so prikazane v spodnji tabeli. V konstrukcijah C1, C2 in C3 smo vgradili z odvzemom materiala iz berme pred betonsko steno (natančneje skalometne obloge) umirjevalno ploščad, za disipiranje energije valov (ang. overspill basin OB) različnih dolžin. Vse debeline slojev so prikazane v naslednji preglednici.

Preglednica 1: Debeline posameznih slojev valobrana.

Sloj	Debelina [cm]
Skalometna obloga	6,6
Filter	4,0
Jedro	15,0
Peta berme	2,0

Testirali smo 6 različnih konfiguracij modela valobrana, od tega se morska globina v kanalu ni spreminjala. Konstrukcije modela (C0, C1, C2, C3, C4 in C5) valobrana v pristanišču imajo vgrajeno betonsko steno s tremi različnimi višinami krone in tremi različno dolgimi umirjevalnimi ploščadmi pred steno. V prvih štirih konstrukcijah je bila višina krone modela konstantna, to je + 9,60 cm, nato smo jo v konstrukciji C4 povišali za 2 cm, na + 11,60 cm in nazadnje v konstrukciji C5 znižali na + 10,7 cm. Vse višine so merjene od prostega nivoja gladine. Umirjevalna ploščad se pojavi v konstrukcijah C1, C2 in C3, in imajo dolžino od 6,0 cm za C1, 12,0 cm za C2 in 18,0 cm za model C3.



Slika 5: Shematični prikaz vzdolžnega prereza vseh različic modela valobrana.

Preglednica 2: Geometrijske karakteristike posameznih konfiguracij modela valobrana.

Geom. karakteristike [cm n.v.]	C0	C1	C2	C3	C4	C5
<b>Berma</b>	9,6	9,6	9,6	9,6	9,6	9,6
<b>Krona valovne stene</b>	9,6	9,6	9,6	9,6	11,6	10,7
<b>Peta valobrana dolvodno</b>	-13,84	-13,84	-13,84	-13,84	-13,84	-13,84
<b>Dno kanala</b>	-16,06	-16,06	-16,06	-16,06	-16,06	-16,06
<b>Umirjevalna ploščad (OB)</b>	0	6,0	12,0	18,0	0,0	0,0

V merilu modela 1:50 smo za utrditev materiala za umirjevalno ploščadjo izbrali tetrapode višine 7,0 cm. Tetrapodi so štirinožne umetno oblikovane betonske enote, ki se pogosto uporabljajo za oblogo valobranov v pristaniščih, kjer naravnega materiala večjih dimenzij primanjkuje. Oblika tetrapodov naravno disipira energijo valov, ko se le ti približujejo konstrukciji in jim onemogoča večje premike materiala v bermi (slika 64 v angleškem tekstu zgoraj). V modelu so postavljeni v dveh vrstah, v prvi slonijo na treh nogah stabilno na sloju filtra, v naslednji vrsti pa so s tremi nogami obrnjeni proti vgrajeni betonski steni valobrana in tako stabilizirajo material za njim. V naravi ni vedno mogoče doseči tako natančne postavitve, saj je ta odvisna od naravnih pogojev dna.

Za modela C4 in C5 smo za nadvišanje vgrajenega zidu uporabili pravokotni palici iz pleksi stekla z dimenzijami 2,0 cm \* 80,0 cm \* 3,0 cm (višina \* dolžina \* širina) za C4 in 1.1 cm \* 80.0 cm \* 0.4 cm za konstrukcijo C5 (slika 65 v angleškem tekstu zgoraj).

### 7.5 Valovni pogoji

Parametri testiranega valovanja so značilni za Ligurijsko morje, ki se nahaja na SZ Italije v regiji Ligurija. Univerza v Firencah namreč pogosto sodeluje pri projektiranju pristaniških valobranov v tej regiji. Morsko valovanje je nelinearno in ima značilnosti JONSWAP energijskega spektra valovanja na razburkanem morju z gama ("stopnja faktorja vrha", ang. "peak incremental factor") parametrom 2 ali 5. Pogoji testiranega valovanja predstavljajo stanje morja s povratno dobo petdesetih let.

Vseh šest konstrukcij modela smo testirali na 8 različnih tipov razburkanega morja. Skupno smo izvedli 40 testov, od katerih smo predhodno posamezne teste razdelili na podteste. Tako smo teste razburkanega morja z manjšo srednjo valovno višino (ang. wave height) H1 razdelili na 3 podteste s trajanjem 20 + 0,5 min in teste z večjo srednjo valovno višino H2 na 6, 10+ 0,5 min trajajočih podtestov. Oboji skupaj predstavljajo 1 urno nevihto, v realnosti pa 7 urno. Čas v laboratoriju je namreč sedemkrat počasnejši od tega v realnosti (Froudov zakon, poglavje 4.4 v angleškem tekstu zgoraj).

Preglednica 3: Testirani valovni pogoji.

Val	Ponovitev	H [cm]	T [s]	$\gamma_{\text{JONSWAP}}$	Trajanje [s]
W1	A	12	8,5	2	20 + 0,5
	B	12	8,5	2	20 + 0,5
	C	12	8,5	2	20 + 0,5
W2	A	12	8,5	5	20 + 0,5
	B	12	8,5	5	20 + 0,5
	C	12	8,5	5	20 + 0,5
W3	A	12	10,5	2	20 + 0,5
	B	12	10,5	2	20 + 0,5
	C	12	10,5	2	20 + 0,5
W4	A	12	10,5	5	20 + 0,5
	B	12	10,5	5	20 + 0,5
	C	12	10,5	5	20 + 0,5
W5	A	12	12,5	2	20 + 0,5
	B	12	12,5	2	20 + 0,5
	C	12	12,5	2	20 + 0,5
W6	A	12	12,5	5	20 + 0,5
	B	12	12,5	5	20 + 0,5
	C	12	12,5	5	20 + 0,5
W7	A	15	11,5	2	10 + 0,5
	B	15	11,5	2	10 + 0,5
	C	15	11,5	2	10 + 0,5
	D	15	11,5	2	10 + 0,5
	E	15	11,5	2	10 + 0,5
	F	15	11,5	2	10 + 0,5
W8	A	15	11,5	5	10 + 0,5
	B	15	11,5	5	10 + 0,5
	C	15	11,5	5	10 + 0,5
	D	15	11,5	5	10 + 0,5
	E	15	11,5	5	10 + 0,5
	F	15	11,5	5	10 + 0,5

Vsak valovni podtest ima svoje ime, ki se od drugih razlikuje glede na karakteristike posameznega vala.

Na primer: **H1T085G2AF1C0**

Kjer:

- H1 označuje srednjo višino vala ( $H1 > H_{m0} = 12,0$  cm,  $H2 > H_{m0} = 15,0$  cm),
- T085 označuje valovno periodo ( $T_{p,085} = 1,2$  s,  $T_{p,105} = 1,48$  s,  $T_{p,115} = 1,63$  s,  $T_{p,125} = 1,77$  s),

- G2 stopnja faktorja vrha (ang. »peak elevation factor«) JONSWAP spektra ( $\gamma_{G2} = 2,0$ ,  $\gamma_{G5} = 5,0$ ),
- A ponovitev podtesta (A, B, C or A, B, C, D, E, F),
- F1 nivo gladine pri loputi generatorja valov, v kanalu s prižganim generatorjem (ang. pump on) je enaka 56,3 cm in 55,5 cm pri ugasnjenem (ang. pump off),
- C0 različica modela (C0, C1, C2, C3, C4, C5).

Vsi podtesti imajo dodanih 30 sekund v katerih loputa generatorja valov miruje, merilne sonde pa takrat izmerijo začetni nivo gladine v kanalu. Pomembno je tudi, da smo med posameznimi test počakali dovolj dolgo, da se je nivo vode stabiliziral, tj. vsaj 15 min.

## 7.6 Preučevani parametri

Naše zanimanje med in po testiranju valovnih prehodov je bilo osredotočeno na pojave in parametre:

### 1. Prelivanje

Za dobro statistično analizo je pomembno, da imamo dovolj veliko število prelivnih pljuskov. Priporočljivo je, da se posamezne poskuse podaljša na minimalno število 2000 valovnih period. Valovna perioda, predvidena v testih, znaša približno 2 sekundi (v merilu modela), kar pomeni, da izmeri prelivanje valov za najmanj 4000 s. Dolžina testa, ki temu ustreza, je tako 60 min = 3600 s. Prelivanje valov ujamemo v zbiralnik za krono valobrana preko drče, nastanjene na sredini krone. Drča ima 2 vstopni širini in sicer se razlikuje za teste z višino valov H1, kjer znaša 30 cm od testov z višino valov H2, kjer znaša 20 cm. Razlog za tako odločitev je, da valovi z višino H2 prinašajo veliko večje pljuske in smo zaradi omejene kapacitete vodnega zbiralnika in celic, ki merijo obtežbo vode, zmanjšali širino in s tem zmanjšali tudi sam dotok zbiralnika. To je bilo razvidno iz predhodno opravljenih testov (s trajanjem 5 min na začetni konfiguraciji C0), ki smo jih opravili v času med 28. in 30. marcem 2012. Z zgornjo utemeljitvijo upravičimo tudi uporabo 2 različnih dolžin testiranja posameznih podtestov, za valove z višino H1 in H2.

### 2. Valovni tlaki

Meritve tlakov valov smo opravili v osrednjem delu vgrajenega betonskega zidu (slika 56 v angleškem tekstu zgoraj) s 5 tlačnimi pretvorniki, vgrajenimi v sredino stene s frekvenco vzorčenja  $0,01 \text{ kg/cm}^2$  ( $10 \text{ g/cm}^2$ , v prototipu  $0,5 \text{ kg/cm}^2$ ). Po sprejemu signala in obdelavi podatkov smo v vsakem posameznem tlačnem pretvorniku grafično, preko programa Matlab (»Trasduttori«) dobili porazdelitev tlakov po času in frekvenci pojavljanja. Tlaki so v bar-ih, 1 bar je  $100000 \text{ Pa}$ , kar je  $100000 \text{ N/m}^2$  in pomeni silo na enoto površine.

### 3. Refleksija ali odboj (ang. reflection)

Merilne sonde (2, 3, 4 in 5) z vzorčno frekvenco 20 Hz so izmerile podatke o koeficientih valovne refleksije ( $H_i$ ,  $H_r$ ,  $K_r$ ). Ti parametri so pomembni pri presoji učinkovitosti zaščite vgrajenega zidu v valobranu.

## 7.7 ANALIZA

### 7.7.1 Analiza prelivanja

Sistem zajemanja in zbiranja pljuskov je sestavljen iz plastičnega zbiralnika, obešenega na 4 nitkah z merilnimi celicami, merilnega valja in nagnjene drče (dveh), po kateri voda steče v zbiralnik. Pri analiziranju prelite količine vode je bil uporabljen tudi merilni valj, s katerim smo takoj po zaključenem testu izmerili volumen vode v zbiralniku in ga primerjali s tistim, ki je bil izmerjen s celicami, ki so merile obtežbo. V vseh primerih so meritve volumna z merilnim valjem dale večje vrednosti od meritev z merilnimi celicami. Merilne celice namreč predčasno prenehajo beležiti signal, v tem času pa zadnji valovi še vedno prihajajo do valobrana.

Za natančno sledenje signalu (tj. obtežbe celic) v zbiralniku, je bilo v sam zbiralnik dodano 0,5 l vode pred začetkom vsakega poskusa. Merilne celice smo umerili na to vrednost, kar je pomenilo začetno vrednost beleženja obtežbe, z natančnostjo 0,02 g. Po vsakem končanem podtestu smo v analizi I. stopnje izmerili volumen vode iz zbiralnika, brez začetnih 500 ml in vpisom volumna v podatkovno bazo ter Dnevno poročilo (Priloga E v angleškem tekstu). Sledila je obdelava zabeleženega signala obtežbe merilnih celic z Matlabovim programom »Overtopping«. Dobili smo graf seštevka obtežbe posameznih pljuskov v času trajanja podtesta, vrednost srednjega prelivnega pretoka ter celoten obseg volumna. Izmerjen volumen z merilnim valjem smo prav tako zabeležili in ga s pomočjo enačbe 5.1 (v angleškem tekstu zgoraj) pretvorili v srednji prelivni pretok v merilo realne konstrukcije. Z analizo I. stopnje ocenimo ali so merilni instrumenti delovali pravilno in izračunamo karakteristike valov, velikost pljuskov in tlakov. Nato nadaljujemo z analizo II. stopnje.

Za vrednotenje rezultatov analize II. stopnje je najprej narejena primerjava med srednjim pretokom prelivanja in maksimalnimi volumni pljuskov, nato pa še presoja maksimalnih tlakov in analiza odboja valov na vgrajeno betonsko steno za posamezen tip konstrukcije in valovanja.

Potek analize II. stopnje za prelivanje valov:

- Definicija imen zank za vse teste,
- Združitev podtestov v en sam test in s tem ustvariti podatke testa za analizo,
- Kombinacija 3 ali 6 podtestov je bila v analizi prelivanja narejena z seštevanjem posameznih podtestov k predhodnemu podtestu. Prvo vrednost naslednjega grafa smo

prišteli zadnji vrednosti predhodnega grafa. Pri tem sta bili vsakemu naslednjemu grafu podtesta od A naprej odvzeti prvi 2 minuti, v katerih valovi še ne prihajajo v zbiralnik in merilne celice še ne zabeležijo obtežbe (na grafu se to pozna kot ravna črta). Novi test ima tako trajanje 55,5 min za teste z višino valov H1 in trajanje 51,0 min za teste z višino valov H2.

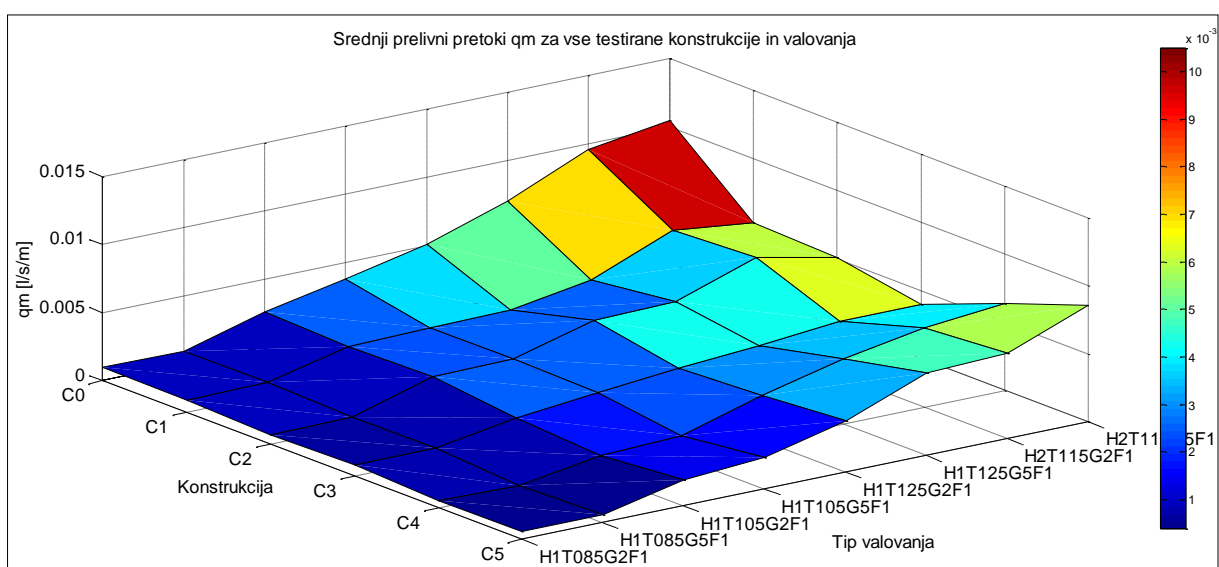
- Sledila je filtracija krivulje grafa prelivanja v stopničasto krivuljo, kjer vsaka stopnica prikazuje posamezen pljusk ter analiza pogostosti in razporeditve le teh.

Rezultati analize prelivanja II. stopnje so trije tipi grafov (glej Graf 17 v angleškem tekstu zgoraj):

- Stopničast graf prelivanja valov po času s krogci, ki označujejo dogodke prelivajočih pljuskov (ang. wave-by-wave overtopping volumes).
- Velikost pljuskov v trajanju nevihtnega dogodka.
- Porazdelitev vseh pljuskov danega valovanja.

Za lažjo primerjavo med volumni pljuskov v grafu porazdelitev prelivajočih dogodkov je bilo za vse teste narejenih 20 razredov enotne velikosti  $1/20 * V_{max}$ . S pomočjo analize I. stopnje smo določili  $V_{max}$  pljuska prelivanja, ki znaša 3 l/m. Drugostopenjska analiza z nadgrajenim programom Matlab (Priloga G – Overtopping program) je pod drobnogled vzela posamezne pljuske, kadar je bilo to seveda možno. V primeru, da več visokih valov skupaj v zelo kratkem časovnem obdobju pljusne čez vgrajeno steno, jih ni mogoče razločiti in smo privzeli, da gre za en sam večji pljusk.

Grafi prelivanja (overtopping) v 5. poglavju angleškega teksta z imenom Analiza in rezultati jasno pokažejo, da gre pri pojavu prelivanja za zelo nepravilen in slučajen proces.



Graf 1: Srednji pretoki prelivanja  $q_m$  za vse valove v povezavi s konstrukcijami modela.

Zgornji graf prikazuje, da so za valove z manjšo višino  $H_1$  značilni manjši srednji pretoki prelivanja kot za tiste z večjo. Z naraščanjem valovne periode  $T_{085}$  do  $T_{125}$  za valove z višino  $H_1$  narašča tudi srednji pretok  $q_m$ . Prav tako je iz grafa razvidno, da pri valovih z enako višino in periodo, a višjim faktorjem JONSWAP spektra  $\gamma_{G5}$ , nastopa večji srednji pretok preliva kot v primerljivem valu s faktorjem  $\gamma_{G2}$ . Na primer za val  $H2T115G2F1C0$   $q_m$  znaša 0,0096 l/s/m, za val  $H2T115G5F1C0$  pa je  $q_m$  enak 0,0105 l/s/m. Povzamemo lahko, da se z naraščanjem višine vala, periode in faktorja JONSWAP spektra povečuje tudi količina prelitih valov. V splošnem so večji pretoki prelivanja doseženi za večino tipov valov v začetni konstrukciji C0. Najučinkovitejša v zmanjševanju prelivanja valov  $H1T125G5F1$ ,  $H2T115G2F1$  in  $H2T115G5F1$  je konstrukcija C3 z najdaljšo umirjevalno ploščadjo, ki znaša 18,0 cm (v merilu modela) pred vgrajenim zidom. Tu se vodni tok umiri in energija valov zmanjša preden doseže sam zid. Za valove  $H1T085G2F1$ ,  $H1T085G5F1$ ,  $H1T105G2F1$  in  $H1T105G5F1$  da najmanjše prelivanje konstrukcija C4 z nadvišanjem zidu za 2,0 cm, glede na prvotno konstrukcijo C0. Za val  $H1T125G2F1$  pa je najmanj prelite vode v zbiralniku pri konstrukciji C1 z umirjevalno ploščadjo dolgo 6,0 cm.

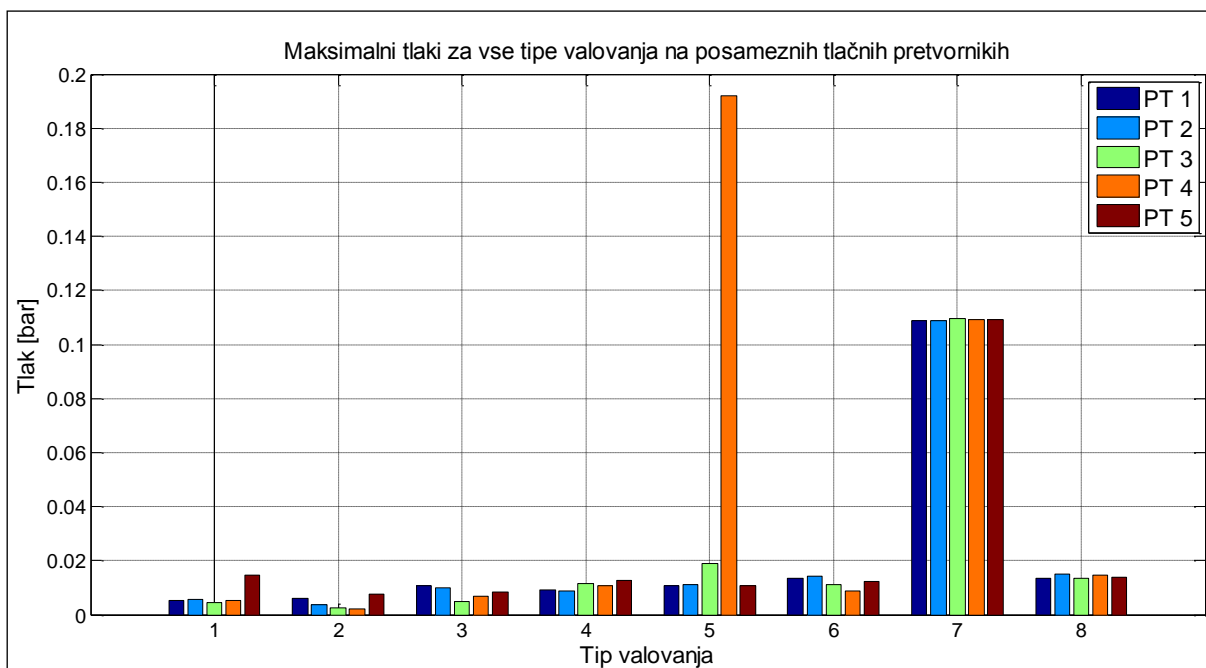
### 7.7.2 Maksimalni tlaki na vgrajeni zid v valobranu

Tlaki so merjeni s 5 tlačnimi pretvorniki. Tlačni pretvorniki 1, 2 in 3 so bili nameščeni levo od sredine zidu v padajočem vrstnem redu od krone zidu, medtem ko sta bila tlačna pretvornika 4 in 5 nameščena v naraščajočem zaporedju od krone zidu desno od sredine. Ta način vzorčenja signala je zelo zanesljiv in nam je dal dobre rezultate, na osnovi katerih je bila razvita drugostopenjska analiza obdelave podatkov.

Potek analize II. stopnje za maksimalne tlake je bil naslednji:

- Definicija imen zank za vse teste.
- Združitev podtestov v en sam test z namenom ustvariti podatke za analizo.
- Združitev 3 ali 6 podtestov je narejena z zaporednim dodajanje posameznih podtestov (grafov) k predhodnemu podtestu. Prvo vrednost naslednjega grafa smo dodali zadnji vrednosti predhodnega grafa. Tudi tu smo odvzeli prvi 2 minuti zabeleženega signala sil na steno, zaradi istega razloga kot pri analizi prelivanja (graf 22 v angleškem tekstu zgoraj).
- Rezultat analize sta 2 grafa: tlaki v času in porazdelitev vrednosti tlakov po razredih.

V nekaterih grafih lahko opazimo presledke med posameznimi podtesti, kar pomeni, da je ponekod začetni val od lopute generatorja valov potreboval tudi več kot 2 minuti.



Graf 2: Največji tlaki na steno valobrana po vseh testih.

V večini poskusov so največji tlaki doseženi na najnižje nameščenih tlačnih pretvornikih na valovni steni, pri konstrukcijah z umirjevalno ploščadjo (tj. C1, C2 in C3), najmanjši pa na zgornjem tlačnem pretvorniku 3 za konstrukciji C4 in C5. Konstrukcija C3 z najdaljšo umirjevalno ploščadjo 18,0 cm (v merilu modela) povzroči največje sile na steno valobrana. Razlog za take rezultate je odvzet material iz berme oz. ploščad, ki služi disipaciji oz. uničenju valovne energije, preden doseže zid in vodni zbiralnik. V primeru umirjevalne ploščadi pa je bil kljub dobri rezultatom v zmanjšanju prelivne količine opazen tudi nastajajoč »tolmun«. Zgornja skalometna obloga je bila odstranjena in tako so močni valovi pričeli spodjedati ploščad. V tej diplomski nalogi se na to nismo posebej osredotočili, smo pa zaznali ta pojav. Največje tlake je na vseh tipih konstrukcije povzročal tip vala H2T115G5F1.

Najmanjše vrednosti tlakov na vgrajeni zid kažeta konstrukciji modela C4 in C5 (za večino valovnih dogodkov). Ti dve različici modela sta se izkazali za najugodnejši tudi pri analizi pljuskov valov. Razlika med srednjima prelivnima pretokoma med omenjenima konstrukcijama je skoraj zanemarljiva, zato se iz finančnega vidika zdi boljša rešitev optimizacija konstrukcije modela valobrana C5. Ta ima za 0,5 m nižjo krono zidu od C4, a je vseeno zelo učinkovita in cenejša.

### 7.7.3 Refleksija ali odboj

Robni pogoji v valobranu povzročajo pojav refleksije oz. odboje valov od sten kanala. Valovi potujejo navzdol po kanalu, dokler na koncu ne dosežejo valobrana. Nekaj energije valov se odbije v nasprotni smeri prihajanja valov, kar se dogaja tudi v naravi. Razlika je le v tem, da se odbiti valovi v naravi vračajo nazaj v ocean, v kanalu, pa so ponovno odbiti itn. (Hughes, 1993). Analiza odboja omogoča izračun komponent vpadnih (ang. incident) in odbitih

valovnih višin po metodi Goda in Suzuki (1976). Račun je bil izveden na podlagi meritev, pridobljenih s sond 2, 3, 4 in 5 nameščenih v kanalu (Priloga A v angleškem tekstu).

Analiza odboja je pokazala, da za večino primerov odbite višine valov in refleksijski koeficienti ( $k_r$ ) naraščajo skupaj z naraščanjem valovnih parametrov (višina valov, valovna perioda in faktor gama JONSWAP spektra).

## **7.8 Zaključek**

To diplomsko delo obsega v 7 poglavij, ki si vsebinsko sledijo v naslednjem zaporedju: v 2. poglavju so predstavljena pomembna teoretična izhodišča o valovih, standardne tehnike za določanje le-teh, pristaniška hidrodinamika, valobrani in pojav prelivanja. V 3. poglavju so opisane karakteristike hidravličnih fizičnih modelov, slabosti in prednosti testiranja modela v laboratoriju, materiali in merilna oprema. V poglavju 4 sledi opis laboratorija v Firencah in postopek testiranja in izdelave valobrana pristanišča. V poglavju 5 je predstavljena obdelava podatkov in rezultati. Pred slovenskim povzetkom pa so v poglavju 6 navedeni še zaključki o prelivanju valov na valobranu v pristaniščih.

Če privzamemo, da se bo morska gladina zaradi globalnega segrevanja do leta 2050 dvignila med 0,2 m pa vse do 1,0 m, bodo konstrukcije valobranov za zaščito obale in pristanišč pred visokimi valovi potrebne obnovitve. Najbolj primerna rešitev za male srednje višine valov ( $H_1$ ) bi bilo nadvišanje vgrajene betonske stene, saj rezultati analize tu prikažejo najmanjše prelivanje čez krono stene. Vendar pa to ni vedno najboljša rešitev, saj imamo vsi povsod radi pogled na odprto morje, ki pa nam bi ga povišan zid zakrival. Na drugi strani pa je najbolj primerna rešitev za valove z višino  $H_2$  konstrukcija valobrana C3 z najdaljšim umirjevalno ploščadjo. Ta je tudi iz finančnega vidika zelo ugodna, saj je potrebnega manj materiala za zapolnitev skalometne obloge berme.

Pri prihodnjem delu bi lahko poskusili s testiranjem podobnega modela v 3D bazenu in preizkusili obnašanje kombinacije drugih materialov v valobranu kot so npr. umetno narejene betonske enote (ang. artificial armour units). Ker pa gre v primeru pojava prelivanja morskih valov za slučajen in nenapovedljiv pojav, bi bilo zanimivo celotno testiranje ponoviti in primerjati rezultate novih testov s predhodnimi.

Rezultati te raziskave bi lahko bili zelo pomembni tudi za Slovenijo in to kljub dejstvu da nimamo veliko obale in da so karakteristike valovanja v Jadranskem morju drugačne od teh v Ligurijskem morju. Močna burja pogosto povzroča preglavice v obratovanju največjega slovenskega pristanišča Koper tako v zimskih mesecih kot občasno tudi čez leto. Učinki burje pa povzročajo visoke valove in posledično prelivanje valov preko valobranov.

## BIBLIOGRAPHY

Burcharth, H. et al. 1999. Scaling of core material in rubble mound breakwater model tests. Proceedings of the 5th International Conference on Coastal and Port Engineering in Developing Countries (COP.EDEC V), Cape Town, South Africa: pg. 1518-1528.

Breakwater.

[http://coastal.wru.edu.vn/Thu\\_vien/Mon\\_hoc/CTBVB/Chuong12%20-%20de%20chan%20song.pdf](http://coastal.wru.edu.vn/Thu_vien/Mon_hoc/CTBVB/Chuong12%20-%20de%20chan%20song.pdf), (20. 08. 2012).

Cappiotti, L., Crema, I., Esposito, A., 2012, Studio su modello per il porto di Pietra Ligure progetto, costruzione e strumentazione del modello in scala, Study of the physical model, Firenze, Università degli studi di Firenze, Dipartimento di ingegneria civile e ambientale: 58 f.

Coastal Engineering Manual, 2002, Chapter 1, Water wave mechanics, Washington, Department of the army, U.S. Army Corps of Engineers: pg. II-1-5, II-1-4, II-1-17, II-1-65, II-1-89.

[http://140.194.76.129/publications/eng-manuals/EM\\_1110-2-1100\\_vol/PartII/Part\\_II-Chap\\_1.pdf](http://140.194.76.129/publications/eng-manuals/EM_1110-2-1100_vol/PartII/Part_II-Chap_1.pdf) (18.04.2012).

CoastLab.

<http://www.unifi.it/diceals/CMpro-v-p-92.html> (22. 05. 2012).

Esposito, A. 2011, Misure su modello fisico dei flussi indotti a tergo di scogliere frangiflutti a cresta bassa, Graduation thesis, Firenze, Università degli Studi di Firenze, Dipartimento di ingegneria civile e ambientale: 256 f.

Goda, Y. and Suzuki, Y. 1976, Estimation of incident and reflected waves in random wave experiments, Proc. of 15th Int. Conf. Coastal Engineering, Hawaii, ASCE: pg. 828-845.

Goda, Y. 2000. Random seas and design of maritime structures, 2<sup>nd</sup> Edition, Advanced Series on Ocean Engineering, Vol. 15, Tokyo, Yokohama National University, World scientific: pg. 12-15, 39-42.

Googlemap.

<https://maps.google.it/maps?hl=sl> (25. 06. 2012).

Harbour of Rotterdam.

<http://www.rnw.nl/africa/bulletin/new-rotterdam-docks-change-dutch-coastlineIII> (16.06.2012).

Hasselmann et al. 1973, Measurements of wind-wave growth and swell decay during the Joint North Sea Wave Project (JONSWAP), Universität Hamburg, Germany: 93, pg.

Cappiotti, L. 2011. La modellistica sperimentale per la progettazione delle dighe marittime, Firenze, Università degli studi di Firenze, Dipartimento di ingegneria Civile e Ambientale: 84 f.

Holthuijsen, H. L. 2007. Waves in Oceanic and Coastal Waters, Cambridge, Delft, Delft University of Technology and UNESCO – IHE: 405: pg. 1-7, 10-15, 31-41, 122.

Hughes, S. A. 1993. Physical models and laboratory techniques in coastal engineering, Singapore, World Scientific: 568 pg., pg. 1-16, 80-119, 169-174, 176-178.

Hughes, S. A. et al. 2002. USAID/OAS/UWI Coastal Infrastructure Design, Construction and Maintenance Training, US Army Engineer Research and Development Center, Coastal and Hydraulics Laboratory.  
[http://www.oas.org/cdcm\\_train/](http://www.oas.org/cdcm_train/) (02.07.2012).

Infrastructure, tools and software for laboratory research.  
<http://www.unifi.it/diceals/CMpro-v-p-252.html> (23. 05.2012).

Kamphuis, J. W. 2000. Introduction to coastal engineering and management, Advanced Series on Ocean Engineering, Vol. 16, Singapore, World Scientific: pg. 211-212, 216, 218.

Kofoed, J. P. 2002. Wave Overtopping of Marine Structures – Utilization of wave energy, Aalborg University, Denmark: pg. 18.

Naval research Laboratory - Local Hazardous Weather Conditions for Koper, 2003  
<http://www.nrlmry.navy.mil/~cannon/medports/Koper/ihazcond.html> (19. 08. 2012).

Palmer, G. N. et al. 1998, Design and construction of rubble mound breakwaters, IPENZ Transactions, Vol. 25, No. 1/CE: pg. 22.

Pullen, T. et al. 2007. EurOtop Wave Overtopping of Sea Defences and Related Structures: Assessment manual (Overtopping Manual), Number 73, Hamburg, Die Kuste - Archive for research and technology on the North sea and Baltic coast: 193, pg.  
<http://www.overtopping-manual.com/eurotop.pdf> (03.04.2012).

Typical three-dimensional coastal structure model in wave basin.  
<http://www.wrl.unsw.edu.au/site/projects/3d-physical-modelling-of-dalrymple-bay-coal-terminal-apron-widening-queensland/> (20. 06. 2012).

User Manual of Load cells, Data sheet: TCA.315.R3:  
[http://www.aep.it/AEPtransducers/Data\\_Sheet/TCA.315.R3.pdf](http://www.aep.it/AEPtransducers/Data_Sheet/TCA.315.R3.pdf) (12. 05. 2012).

User Manual Submersible Capacitive Transmitters for water level measurements Keller Series 46 X, 46 X Ei , Winterthur, Germany:  
<http://www.unifi.it/diceals/upload/sub/Manuali/TrasduttoriDiPressioneKeller.pdf> (12. 05. 2012).

User Manual ML2x-UM-1.211.21 Type ML2x Theta Probe. 1999, Delta-T Devices, Cambridge:

<http://www.unifi.it/diceals/upload/sub/Manuali/ML2x%20ThetaProbe%20User%20Manual%20v1.21.pdf> (12. 05. 2012).

Violent wave overtopping.

<http://www.vows.ac.uk/> (12. 07. 2012).

Wolters, G., van Gent, M. 2007. Guidelines for physical model testing of breakwaters: Rubble mound breakwaters, Delft, Deltares Delft Hydraulics: pg. 10-27, 30-32.



## **APPENDIX**

Appendix A: Wave flume model with physical model at Maritime Engineering Laboratory

Appendix B: Granulometric Analysis Data

Appendix C: Check – List

Appendix D: Diary of laboratory activities

Appendix E: An example of a daily report

Appendix F: Matlab program for overtopping analysis

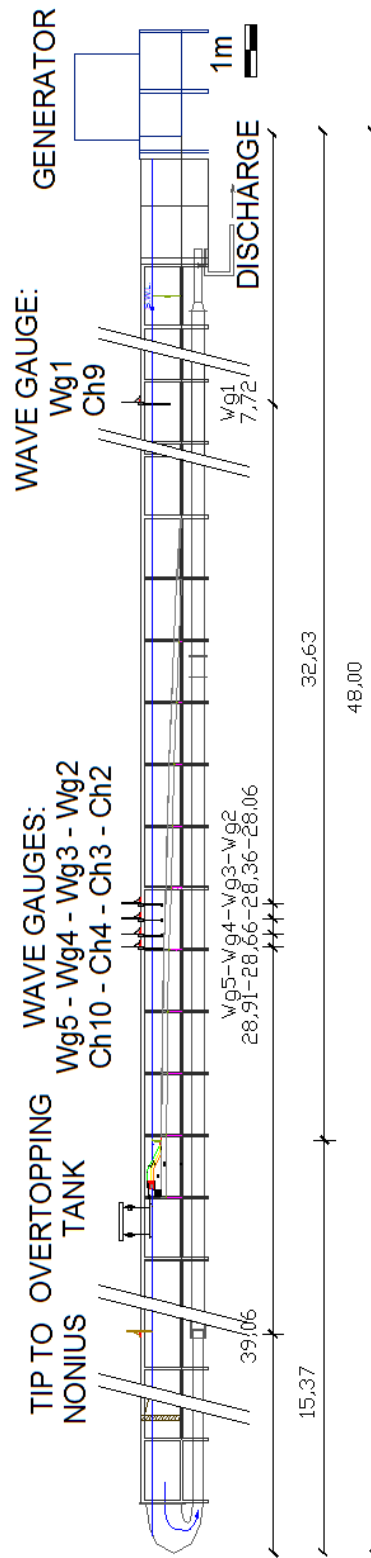
Appendix G: Matlab program for pressure analysis

Appendix H: Program Output

Appendix H.1: Output graphs for overtopping analysis

Appendix H.2: Output graphs for pressure analysis

# Appendix A: Wave flume with physical model at Maritime Engineering Laboratory



## Appendix B: Granulometric Analysis Data

Example of first 43 (of total 571) rocks for armour layer in range of 60 ÷ 100 g.

ARMOUR LAYER Range 60 ÷ 100g			$\rho$	2682,0	$\text{kg/m}^3$
Rock Number	Weight [g]	Weight [Kg]	$D_{n,50}$ [m]	$D_{n,50}$ [mm]	$\phi$
1	83	0,083	0,031	31,4	-4,97
2	75	0,075	0,030	30,4	-4,92
3	88	0,088	0,032	32,0	-5,00
4	84	0,084	0,032	31,5	-4,98
5	65	0,065	0,029	28,9	-4,85
6	60	0,06	0,028	28,2	-4,82
7	78	0,078	0,031	30,8	-4,94
8	100	0,1	0,033	33,4	-5,06
9	89	0,089	0,032	32,1	-5,01
10	60	0,06	0,028	28,2	-4,82
11	86	0,086	0,032	31,8	-4,99
12	83	0,083	0,031	31,4	-4,97
13	98	0,098	0,033	33,2	-5,05
14	82	0,082	0,031	31,3	-4,97
15	71	0,071	0,030	29,8	-4,90
16	91	0,091	0,032	32,4	-5,02
17	100	0,1	0,033	33,4	-5,06
18	84	0,084	0,032	31,5	-4,98
19	60	0,06	0,028	28,2	-4,82
20	85	0,085	0,032	31,6	-4,98
21	79	0,079	0,031	30,9	-4,95
22	73	0,073	0,030	30,1	-4,91
23	82	0,082	0,031	31,3	-4,97
24	95	0,095	0,033	32,8	-5,04
25	60	0,06	0,028	28,2	-4,82
26	67	0,067	0,029	29,2	-4,87
27	93	0,093	0,033	32,6	-5,03
28	88	0,088	0,032	32,0	-5,00
29	97	0,097	0,033	33,1	-5,05
30	86	0,086	0,032	31,8	-4,99
31	83	0,083	0,031	31,4	-4,97
32	100	0,1	0,033	33,4	-5,06
33	85	0,085	0,032	31,6	-4,98
34	73	0,073	0,030	30,1	-4,91
35	88	0,088	0,032	32,0	-5,00
36	99	0,099	0,033	33,3	-5,06
37	70	0,07	0,030	29,7	-4,89
38	69	0,069	0,030	29,5	-4,88
39	97	0,097	0,033	33,1	-5,05
40	80	0,08	0,031	31,0	-4,95
41	100	0,1	0,033	33,4	-5,06

Example of first 40 (of total 1261) rocks for filter layer in range of 14 ÷ 25 g.

FILTER Range 14 ÷ 25 g		ρ		2682,0	kg/m <sup>3</sup>
Rock Number	Weight [g]	Weight [Kg]	D <sub>n,50</sub> [m]	D <sub>n,50</sub> [mm]	φ
1	18	0,018	0,019	18,9	-4,24
2	9	0,009	0,015	15,0	-3,90
3	10	0,01	0,016	15,5	-3,95
4	25	0,025	0,021	21,0	-4,40
5	9	0,009	0,015	15,0	-3,90
6	14	0,014	0,017	17,3	-4,12
7	11	0,011	0,016	16,0	-4,00
8	9	0,009	0,015	15,0	-3,90
9	14	0,014	0,017	17,3	-4,12
10	12	0,012	0,016	16,5	-4,04
11	14	0,014	0,017	17,3	-4,12
12	14	0,014	0,017	17,3	-4,12
13	12	0,012	0,016	16,5	-4,04
14	8	0,008	0,014	14,4	-3,85
15	14	0,014	0,017	17,3	-4,12
16	12	0,012	0,016	16,5	-4,04
17	15	0,015	0,018	17,8	-4,15
18	9	0,009	0,015	15,0	-3,90
19	12	0,012	0,016	16,5	-4,04
20	9	0,009	0,015	15,0	-3,90
21	17	0,017	0,019	18,5	-4,21
22	10	0,01	0,016	15,5	-3,95
23	10	0,01	0,016	15,5	-3,95
24	9	0,009	0,015	15,0	-3,90
25	12	0,012	0,016	16,5	-4,04
26	21	0,021	0,020	19,9	-4,31
27	13	0,013	0,017	16,9	-4,08
28	12	0,012	0,016	16,5	-4,04
29	8	0,008	0,014	14,4	-3,85
30	9	0,009	0,015	15,0	-3,90
31	13	0,013	0,017	16,9	-4,08
32	8	0,008	0,014	14,4	-3,85
33	9	0,009	0,015	15,0	-3,90
34	8	0,008	0,014	14,4	-3,85
35	12	0,012	0,016	16,5	-4,04
36	11	0,011	0,016	16,0	-4,00
37	10	0,01	0,016	15,5	-3,95
38	12	0,012	0,016	16,5	-4,04
39	18	0,018	0,019	18,9	-4,24
40	24	0,024	0,021	20,8	-4,38

Example of first 41 (of total 1120) rocks for core in range of 9 ÷ 13 g.

CORE		$\rho$ 2682,0 kg/m <sup>3</sup>			
Range 9 ÷ 14 g					
Rock Number	Weight [g]	Weight [Kg]	D <sub>n,50</sub> [m]	D <sub>n,50</sub> [mm]	$\phi$
1	13	0,013	0,017	16,92	-4,08
2	10	0,01	0,016	15,51	-3,95
3	10	0,01	0,016	15,51	-3,95
4	11	0,011	0,016	16,01	-4,00
5	9	0,009	0,015	14,97	-3,90
6	13	0,013	0,017	16,92	-4,08
7	13	0,013	0,017	16,92	-4,08
8	11	0,011	0,016	16,01	-4,00
9	11	0,011	0,016	16,01	-4,00
10	9	0,009	0,015	14,97	-3,90
11	9	0,009	0,015	14,97	-3,90
12	11	0,011	0,016	16,01	-4,00
13	9	0,009	0,015	14,97	-3,90
14	10	0,01	0,016	15,51	-3,95
15	9	0,009	0,015	14,97	-3,90
16	13	0,013	0,017	16,92	-4,08
17	9	0,009	0,015	14,97	-3,90
18	11	0,011	0,016	16,01	-4,00
19	13	0,013	0,017	16,92	-4,08
20	9	0,009	0,015	14,97	-3,90
21	12	0,012	0,016	16,48	-4,04
22	11	0,011	0,016	16,01	-4,00
23	11	0,011	0,016	16,01	-4,00
24	12	0,012	0,016	16,48	-4,04
25	11	0,011	0,016	16,01	-4,00
26	9	0,009	0,015	14,97	-3,90
27	12	0,012	0,016	16,48	-4,04
28	11	0,011	0,016	16,01	-4,00
29	10	0,01	0,016	15,51	-3,95
30	13	0,013	0,017	16,92	-4,08
31	10	0,01	0,016	15,51	-3,95
32	12	0,012	0,016	16,48	-4,04
33	11	0,011	0,016	16,01	-4,00
34	9	0,009	0,015	14,97	-3,90
35	13	0,013	0,017	16,92	-4,08
36	9	0,009	0,015	14,97	-3,90
37	10	0,01	0,016	15,51	-3,95
38	11	0,011	0,016	16,01	-4,00
39	12	0,012	0,016	16,48	-4,04
40	11	0,011	0,016	16,01	-4,00
41	11	0,011	0,016	16,01	-4,00

## Appendix C: Check – List

Sample Check-list example of testing procedure for harbour breakwater model

<b><u>CHECK-LIST</u> - 2012 ICCE</b>		<b>Operator:</b>	<b>Date:</b>
<b>Executed tests:</b>			
<b>Step</b>	<b>Daily operations:</b>	<b>Notes:</b>	
<b>1</b>	Turn on the resistive wave gauges (No. 8 in the electrical cabinet) and the wave maker (No. 7 in the electrical cabinet).		
<b>2</b>	Turn on the PC GENERATORE, GANIMEDE, and power of the load cells and pressure transducers.		
<b>3</b>	Check the memory on PC GENERATORE (E:) and GANIMEDE (F:).		
<b>4</b>	Create folder of the day in the format dd-mm-yy in <u>GANIMEDE</u> <b>F:\ModelliFisiciInCondizione\2012_ICCE\Esperimenti</b> and folders Figure and DatiCalibrati always in <u>GANIMEDE</u> , on <u>PC GENERATORE</u> create <b>E:\2012_ICCE</b> only folder of the day in the format dd-mm-yy.		
<b>5</b>	Create text file in folder of the day in <u>GANIMEDE</u> (e.g. <b>c180112F10livelli.cal</b> ) with the following content: <b>WG CHANNEL TROUGH CREST ZERO</b> 1 9 -10 10 0 2 2 -5 5 0 3 3 -5 5 0 4 4 -5 5 0 5 10 -5 5 0 Copy in Ganimede's folder of the day in "DatiCalibrati" the Matlab file <b>IstogrammaVolumiOvertopping.m</b> and update items "name" and "saveas".		
<b>6</b>	Place the hydrometric tip on the right level position for the test, where pump is off <b>F1: 15.2 cm.</b>	* note: <b>Level F1:</b> Pomp on, at the nonius is <b>14.4 cm.</b>	
<b>7</b>	Check that the free surface in the channel is tangent to the hydrometric tip, wait for about <b>10 minutes</b> . If the level is less than requested, input water in the channel and wait that the level is tangent to the tip of the nonius.		
<b>8</b>	Start the <b><u>Calibration</u></b> procedure ( <b><u>Calibrazione</u></b> )(see further on the check-list wave gauges calibration).		
<b>9</b>	Turn on the pump of the back blade and wait for about 20 minutes.		
<b>10</b>	Connect the overtopping tank to the load cells, put 500 ml of water inside and wait for the time necessary for the stabilization.		
<b>11</b>	Perform <b><u>Load cells calibration</u></b> ( <b><u>Calibrazione delle celle di carico</u></b> )		

	<p>from PC GANIMEDE in  F:\ModelliFisiciInConduzione\2012_ICCE\Esperimenti start the program of the load cells and pressure transducers <b>ICCE.seproj</b></p> <ul style="list-style-type: none"> <li>- Stepsetup – Configuration;</li> <li>- Device – Strain Calibration for each sensor;</li> <li>- Select only “Enable Offset Nulling”;</li> <li>- Finally, click on <b>Calibrate</b> and then <b>Finish</b> and proceed for the other transducer</li> </ul>	
<b>12</b>	Before execution of the test, register at the back of the check-list the level at the hydrometric tip at the nonius.	
<b>13</b>	Launch the first 20 min wave attack from the PC-GENERATORE (start from the menu bar of Labview, the module of “esecuzione” example: <b>H1G2A*.pre</b> ), start <b>ICCE.seproj</b> by clicking "RUN" the acquisition of load cells and pressure transducers, turn on the two spotlights above the flume and start <b>filming the video</b> .	<p><b>*Note!!!</b>  The repetitions to do are three A, B, C of 20 min each, for waves with wave height H1 and six repetitions A, B, C, D, E, F of 10 minutes each, for waves with wave height H2.</p>
<b>14</b>	<p>At the end of <b>each repetition</b>:</p> <ul style="list-style-type: none"> <li>- Stop recording the video;</li> <li>- Empty the overtopping tank, which collects overflows and write down the <b>volume</b> in the check-list and in the Excel file;</li> <li>- End the recording of the load cells and pressure transducers, cut the file <u>Celle.txt</u> and <u>Trasd.txt</u> from the folder Esperimenti (Experiments) and put them in the folder of the day with the name of the test performed <b>H1G2A1F1C0_Celle.dat</b> and <b>H1G2A1F1C0_Trasd.dat</b>;</li> </ul>	
<b>15</b>	Transform the file you just obtained from the PC-GENERATORE ( <b>H1G2A.a01</b> ) from binary to ASCII (start from the menu bar of Labview the module form of “trasformazione” ("transformation")).	
<b>16</b>	Transfer the file that has been just acquired ( <b>binario.a01</b> ) in the folder of the day of PC-GENERATORE.	
<b>17</b>	Cut the transformed file from PC-GENERATORE ( <b>ASCII.t01</b> ) and copy it to GANIMEDE (in the folder of the day!) and rename it in the form like <b>H1G2A1F1C0.dat</b>	
<b>18</b>	Analyze the file you have just acquired it by Matlab 7.1 program using the program "Main".	
<b>19</b>	Analyze the graph of overtopping volume ( <b>H2G1A1F1C0-Overtopping.bmp</b> ) and create a text file with 2 columns, one showing the serial number of overtopping events and the other the corresponding cumulative volumes; save it into the form	

	<b>H1G2A1F1C0_VolumiOvertopping.dat</b>	
<b>20</b>	Analyze the file you have just created by software Matlab 7.1 with the program "IstogrammaVolumiOvertopping.m".	
<b>21</b>	Wait 10 minutes to stabilize the water level inside the wave flume and fill the <b>database</b> and the <b>daily report</b> .	
<b>22</b>	Repeat the operations from <b>step 9</b> until the end of the daily tests. <b>IN CASE OF THE CHANGES IN THE STUDIED LEVEL REPEAT THE CALIBRATION!!</b>	
<b>23</b>	When the daily tests are finished, turn off the computers, wave gauges, load cells, pressure transducers and close the door of PC GENERATORE's room.	
<b><u>CHECK-LIST</u></b> <b>Wave gauges calibration</b>		<b>Operator:</b>
		<b>Date:</b>
<b>Step</b>	<b>Tiered approach for wave gauges calibration</b>	<b>Notes</b>
<b>1</b>	Start the calibration procedure by opening the folder <b>2012_ICCE</b> from your PC GENERATORE's desktop.	
<b>2</b>	Launch the file idra11.vi.	
<b>3</b>	Launch the module "predisposizione" ("predisposition") from the menu bar and after that launch the module "taratura" ("calibration").	
<b>4</b>	Select channels of wave gauges to calibrate: wave gauges from 1-10.	
<b>5</b>	Enter the range of calibration for each wave gauge [mm].	
<b>6</b>	Enter the <u>distance</u> value for each wave gauge from the back blade [mm].	
<b>7</b>	Enter the depth value for each wave gauge [mm].	
<b>8</b>	Bring the wave gauges to the <b>maximum level</b> , firmly attach the nonius, wait until the water level stabilize and acquire data from GENERATORE (select the "taratura" ("calibration")).	
<b>9</b>	Bring the wave gauges to the <b>minimum level</b> , firmly attach the nonius, wait until the water level stabilize and acquire data from GENERATORE (select the "taratura" ("calibration")).	
<b>10</b>	<b>Center</b> the wave gauges, firmly attach the nonius, wait until the water level stabilize and acquire data from GENERATORE (select the "taratura" ("calibration")).	
<b>11</b>	Copy file idra11.son into the folder of the day of GENERATORE and connect it to GANIMEDE and GENERATORE network and copy it F:\ModelliFisiciInConduzione\2012_ICCE \Esperimenti\dd-mm-yy and rename into cddmmyzxx.cal (day month year level, number of calibration (e.g. <b>c040507F00.cal</b> )).	
<b>12</b>	Analyze the calibration file using the Matlab program "VerificaCalibrazione" by entering calibration instruction (' date ', level ', number of calibration).	
<b>13</b>	Write down in notes and in the diary any deviations found during calibration.	

**Notes:**

<b>Wave Code</b>	<b>Rep.</b>	<b>Config.</b>	<b>Level before the test execution (read on the nonius)</b>	<b>Volume of overtopping (liters)</b>
<b>H1G2</b>	<b>A1</b>	<b>C0</b>		
<b>H1G2</b>	<b>B1</b>	<b>C0</b>		
<b>H1G2</b>	<b>C1</b>	<b>C0</b>		

Appendix D: Diary of laboratory activities

Testing Schedule 2012 ICCE			
Date	Operator	Activity	NOTES
March 28, 2012	Andrea	<p><b><u>PRELIMINARY TESTS</u></b></p> <p><b><u>H1T7G2 – <math>H_{m0}=4.5m</math>, <math>T_p=7s</math>, <math>\gamma=2</math></u></b>            → Wave H10T99G2A (<math>H=10cm</math>, <math>T=0.99s</math>, <math>\gamma=2</math>)            → Wave H11T99G2A (<math>H=11cm</math>, <math>T=0.99s</math>, <math>\gamma=2</math>)            → Wave H12T99G2A (<math>H=12cm</math>, <math>T=0.99s</math>, <math>\gamma=2</math>)            → Wave H12T99G2B (<math>H=12cm</math>, <math>T=0.99s</math>, <math>\gamma=2</math>)            → Wave H12T99G2C (<math>H=12cm</math>, <math>T=0.99s</math>, <math>\gamma=2</math>)            → Wave H115T99G2A (<math>H=11.5cm</math>, <math>T=0.99s</math>, <math>\gamma=2</math>)            → Wave H115T99G2B (<math>H=11.5cm</math>, <math>T=0.99s</math>, <math>\gamma=2</math>)</p>	<p>Performed with a single calibration, there are not significant errors.</p> <p>Wave H115T99G2 (<math>H=11.5cm</math>, <math>T=0.99s</math>, <math>\gamma=2</math>) is the wave of the project H1T7G2</p>
March 29, 2012	Andrea Urška	<p><b><u>PRELIMINARY TESTS</u></b></p> <p><b><u>H1T9G2 – <math>H_{m0}=4.5m</math>, <math>T_p=9s</math>, <math>\gamma=2</math></u></b>            → Wave H115T127G2A (<math>H=11.5cm</math>, <math>T=1.27s</math>, <math>\gamma=2</math>)  <b><u>H1T11G2 – <math>H_{m0}=4.5m</math>, <math>T_p=11s</math>, <math>\gamma=2</math></u></b>            → Wave H115T156G2A (<math>H=11.5cm</math>, <math>T=1.56</math>, <math>\gamma=2</math>)  <b><u>H1T7G5 – <math>H_{m0}=4.5m</math>, <math>T_p=7s</math>, <math>\gamma=5</math></u></b>            → Wave H115T99G5A (<math>H=11.5cm</math>, <math>T=0.99s</math>, <math>\gamma=2</math>)  <b><u>H2T115G5 – <math>H_{m0}=7.5m</math>, <math>T_p=11.5s</math>, <math>\gamma=5</math></u></b>            → Wave H18T163G5 (<math>H=18cm</math>, <math>T=1.63s</math>, <math>\gamma=5</math>)            → Wave H17T163G5 (<math>H=17cm</math>, <math>T=1.63s</math>, <math>\gamma=5</math>)</p>	<p>Performed with a single calibration there are not significant errors.</p> <p>Wave H115T127G2 (<math>H=11.5cm</math>, <math>T=1.27s</math>, <math>\gamma=2</math>) is the wave of the project H1T9G2.</p> <p>Wave H115T156G2 (<math>H=11.5cm</math>, <math>T=1.56s</math>, <math>\gamma=2</math>) is the wave of the project H1T11G2.</p> <p>Wave H175T163G5 (<math>H=17cm</math>, <math>T=1.63s</math>, <math>\gamma=5</math>) is the wave of the project H2T115G5.</p>
		<b><u>PRELIMINARY TESTS</u></b>	Modification of characteristic

<p><b>March 30, 2012</b></p>	<p>Andrea Urška</p>	<p><u>H1T85G2 – H<sub>m0</sub>=6.0m, T<sub>p</sub>=8.5s, γ=2</u> → Wave H14T12G2 (H=14cm, T=1.20, γ=2)</p> <p><u>H1T105G2 – H<sub>m0</sub>=6.0m, T<sub>p</sub>=10.5s, γ=2</u> → Wave H135T148G2 (H=13.5cm, T=1.48, γ=2)</p> <p><u>H1T125G2 – H<sub>m0</sub>=6.0m, T<sub>p</sub>=12.5s, γ=2</u> → Wave H13T177G2 (H=13cm, T=1.77, γ=2)</p> <p><u>H1T85G5 – H<sub>m0</sub>=6.0m, T<sub>p</sub>=8.5s, γ=5</u> → Wave H14T12G5 (H=14cm, T=1.20, γ=5)</p> <p><u>H1T105G5 – H<sub>m0</sub>=6.0m, T<sub>p</sub>=10.5s, γ=5</u> → Wave H135T148G5 (H=13.5cm, T=1.48, γ=5)</p> <p><u>H1T125G5 – H<sub>m0</sub>=6.0m, T<sub>p</sub>=12.5s, γ=5</u> → Wave H13T177G5 (H=13cm, T=1.77, γ=5)</p> <p><u>H2T163G5 – H<sub>m0</sub>=7.5m, T<sub>p</sub>=11.5s, γ=5</u> → Wave H17T163G5 (H=17cm, T=1.63, γ=5)</p> <p><u>H2T163G2 – H<sub>m0</sub>=7.5m, T<sub>p</sub>=11.5s, γ=2</u> → Wave H17T163G2 (H=17cm, T=1.63, γ=2)</p>	<p>parameters of the waves; new search of the waves.</p> <p>Performed with a single calibration there are not significant errors.</p>
<p><b>April 03, 2012</b></p>	<p>Andrea Urška Deniz</p>	<p><b><u>DEFINITIVE TESTS</u></b></p> <p>→ Wave H1T85G2AF1C0 → Wave H1T85G2BF1C0 → Wave H1T85G2CF1C0</p> <p>→ Wave H1T105G2AF1C0 → Wave H1T105G2BF1C0 → Wave H1T105G2CF1C0</p>	<p>Performed with a single calibration there are not significant errors.</p> <p>In the test H1T85G2AF1C0 has been recorded an electric shock to the WG2 and WG3 and to the transducers during the first 30".</p> <p>Performed a second calibration before the execution of wave H1T105G2 because there has been an offset</p>

			towards the bottom of the WG 2, 3, 4 and 5.
<b>April 04, 2012</b>	Andrea Urška	<p><b><u>DEFINITIVE TESTS</u></b></p> <p>→ Wave H1T125G2AF1C0  → Wave H1T125G2BF1C0  → Wave H1T125G2CF1C0</p> <p>→ Wave H1T85G5AF1C0  → Wave H1T85G5BF1C0  → Wave H1T85G5CF1C0</p> <p>→ Wave H1T105G5AF1C0  → Wave H1T105G5BF1C0  → Wave H1T105G5CF1C0</p> <p>→ Wave H1T125G5AF1C0  → Wave H1T125G5BF1C0  → Wave H1T125G5CF1C0</p>	<p>Performed with a single calibration there are not significant errors</p> <p>From the tests H1T105G5 there is an offset upward of the WG1 equal to about 2-3 mm.</p>
<b>April 05, 2012</b>	Andrea Urška	<p><b><u>DEFINITIVE TESTS</u></b></p> <p>→ Wave H2T115G2AF1C0  → Wave H2T115G2BF1C0  → Wave H2T115G2CF1C0  → Wave H2T115G2DF1C0  → Wave H2T115G2EF1C0  → Wave H2T115G2FF1C0</p> <p>→ Wave H2T115G5AF1C0  → Wave H2T115G5BF1C0  → Wave H2T115G5CF1C0  → Wave H2T115G5DF1C0  → Wave H2T115G5EF1C0  → Wave H2T115G5FF1C0</p>	<p>Performed with a single calibration there are not significant errors  Recalibrated (with a pump on) before the test H2T115G2CF1C0 due to a power outage.</p> <p>The wave gauges have been subjected to an offset upwards of about 2 mm before the tests H2G5</p>
<b>April 10, 2012</b>	Andrea Urška	<p><b><u>DEFINITIVE TESTS</u></b></p> <p>→ Wave H2T115G2AF1C1  → Wave H2T115G2BF1C1  → Wave H2T115G2CF1C1  → Wave H2T115G2DF1C1  → Wave H2T115G2EF1C1  → Wave H2T115G2FF1C1</p>	<p>Performed with a single calibration there are not significant errors.</p> <p>In the test H2T115G2CF1C1 there has been a</p>

		<p>→ Wave H2T115G5AF1C1</p> <p>→ Wave H2T115G5BF1C1</p> <p>→ Wave H2T115G5CF1C1</p> <p>→ Wave H2T115G5DF1C1</p> <p>→ Wave H2T115G5EF1C1</p> <p>→ Wave H2T115G5FF1C1</p> <p>→ Wave H1T125G5AF1C1</p> <p>→ Wave H1T125G5BF1C1</p> <p>→ Wave H1T125G5CF1C1</p> <p>→ Wave H1T125G2AF1C1</p>	<p>wrong functioning of the pressure transducer 5 due to the presence of a stone close to the same transducer</p> <p>From the test H2T115G2CF1C1 there is an upward offset of the wave gauges of approximately 1-2 mm.</p> <p>In the test H2T115G5EF1C1 the wave gauge 3 has suffered an electric blackout (see the water zero levels)</p>
April 11, 2012	Andrea Urška Deniz	<p><b><u>DEFINITIVE TESTS</u></b></p> <p>→ Wave H1T125G2BF1C1</p> <p>→ Wave H1T125G2CF1C1</p> <p>→ Wave H1T105G5AF1C1</p> <p>→ Wave H1T105G5BF1C1</p> <p>→ Wave H1T105G5CF1C1</p> <p>→ Wave H1T105G2AF1C1</p> <p>→ Wave H1T105G2BF1C1</p> <p>→ Wave H1T105G2CF1C1</p> <p>→ Wave H1T85G5AF1C1</p> <p>→ Wave H1T85G5BF1C1</p> <p>→ Wave H1T85G5CF1C1</p> <p>→ Wave H1T85G2AF1C1</p> <p>→ Wave H1T85G2BF1C1</p> <p>→ Wave H1T85G2CF1C1</p>	<p>Performed with a single calibration there are not significant errors</p> <p>After the first test the WG1 has an upward offset of about 5 mm.</p> <p>From the test H1T85G5AF1C1 there is a further upward offset of all the wave gauges.</p>
April 12,	Andrea Urška	<b><u>DEFINITIVE TESTS</u></b>	

2012		<p>→ Wave H1T85G2AF1C2  → Wave H1T85G2BF1C2  → Wave H1T85G2CF1C2</p> <p>→ Wave H1T85G5AF1C2  → Wave H1T85G5BF1C2  → Wave H1T85G5CF1C2</p> <p>→ Wave H1T105G2AF1C2  → Wave H1T105G2BF1C2  → Wave H1T105G2CF1C2</p> <p>→ Wave H1T105G5AF1C2  → Wave H1T105G5BF1C2  → Wave H1T105G5CF1C2</p> <p>→ Wave H1T125G2AF1C2  → Wave H1T125G2BF1C2</p>	<p>Performed with a single calibration there are not significant errors</p> <p>The WG1 has an upward offset, which increases from test to test.</p>
April 13, 2012	Andrea Urška	<p><b><u>DEFINITIVE TESTS</u></b></p> <p>→ Wave H1T125G2CF1C2</p> <p>→ Wave H1T125G5AF1C2  → Wave H1T125G5BF1C2  → Wave H1T125G5CF1C2</p> <p>→ Wave H2T115G2AF1C2  → Wave H2T115G2BF1C2  → Wave H2T115G2CF1C2  → Wave H2T115G2DF1C2  → Wave H2T115G2EF1C2  → Wave H2T115G2FF1C2</p> <p>→ Wave H2T115G5AF1C2  → Wave H2T115G5BF1C2  → Wave H2T115G5CF1C2</p>	<p>Performed with a single calibration there are not significant errors.</p>
April 16, 2012	Andrea Urška	<p><b><u>DEFINITIVE TESTS</u></b></p> <p>→ Wave H2T115G5DF1C2  → Wave H2T115G5EF1C2  → Wave H2T115G5FF1C2</p> <p>→ Wave H2T115G2AF1C3  → Wave H2T115G2BF1C3  → Wave H2T115G2CF1C3</p>	<p>Performed with a single calibration there are not</p>

		<ul style="list-style-type: none"> <li>→ Wave H2T115G2DF1C3</li> <li>→ Wave H2T115G2EF1C3</li> <li>→ Wave H2T115G2FF1C3</li> <li>→ Wave H2T115G5AF1C3</li> </ul>	<p>significant errors.</p> <p>The WG has a downward offset, gets bigger from the second day test forward.</p>
April 17, 2012	Andrea Urška	<p><b><u>DEFINITIVE TESTS</u></b></p> <ul style="list-style-type: none"> <li>→ Wave H2T115G5BF1C3</li> <li>→ Wave H2T115G5CF1C3</li> <li>→ Wave H2T115G5DF1C2</li> <li>→ Wave H2T115G5EF1C2</li> <li>→ Wave H2T115G5FF1C2</li> <li>→ Wave H1T125G2AF1C3</li> <li>→ Wave H1T125G2BF1C3</li> <li>→ Wave H1T125G2CF1C3</li> <li>→ Wave H1T125G5AF1C3</li> <li>→ Wave H1T125G5BF1C3</li> <li>→ Wave H1T125G5CF1C3</li> <li>→ Wave H1T105G2AF1C3</li> </ul>	<p>Performed with a single calibration there are not significant errors.</p> <p>The WG1 has a downward offset of about 5.0 mm.</p>
April 18, 2012	Andrea Urška	<p><b><u>DEFINITIVE TESTS</u></b></p> <ul style="list-style-type: none"> <li>→ Wave H1T105G2BF1C3</li> <li>→ Wave H1T105G2CF1C3</li> <li>→ Wave H1T105G5AF1C3</li> <li>→ Wave H1T105G5BF1C3</li> <li>→ Wave H1T105G5CF1C3</li> </ul>	<p>Performed with a single calibration there are not significant errors.</p> <p>All the wave gauges are subjected to a downward offset.</p>
April 19, 2012	Andrea Urška	<p><b><u>DEFINITIVE TESTS</u></b></p> <ul style="list-style-type: none"> <li>→ Wave H1T85G2AF1C3</li> <li>→ Wave H1T85G2BF1C3</li> <li>→ Wave H1T85G2CF1C3</li> <li>→ Wave H1T85G5AF1C3</li> <li>→ Wave H1T85G5BF1C3</li> <li>→ Wave H1T85G5CF1C3</li> <li>→ Wave H1T85G2AF1C4</li> <li>→ Wave H1T85G2BF1C4</li> <li>→ Wave H1T85G2CF1C4</li> </ul>	<p>Performed with a single calibration there are not significant errors.</p> <p>The WG1 has by a downward offset of about 5.0 mm.</p>

		<ul style="list-style-type: none"> <li>→ Wave H1T85G5AF1C4</li> <li>→ Wave H1T85G5BF1C4</li> <li>→ Wave H1T85G5CF1C4</li> </ul>	
April 20, 2012	Andrea Urška	<p><b><u>DEFINITIVE TESTS</u></b></p> <ul style="list-style-type: none"> <li>→ Wave H1T85G5CF1C4</li> <li>→ Wave H1T105G2AF1C4</li> <li>→ Wave H1T105G2BF1C4</li> <li>→ Wave H1T105G2CF1C4</li> </ul>	Performed with a single calibration there are not significant errors.
April 23, 2012	Urška	<p><b><u>DEFINITIVE TESTS</u></b></p> <ul style="list-style-type: none"> <li>→ Wave H1T125G2AF1C4</li> <li>→ Wave H1T125G2BF1C4</li> <li>→ Wave H1T125G2CF1C4</li> <li>→ Wave H1T125G5AF1C4</li> <li>→ Wave H1T125G5BF1C4</li> <li>→ Wave H1T125G5CF1C4</li> <li>→ Wave H2T115G2AF1C4</li> <li>→ Wave H2T115G2BF1C4</li> <li>→ Wave H2T115G2CF1C4</li> <li>→ Wave H2T115G2DF1C4</li> </ul>	Performed with a single calibration there are not significant errors.
April 24, 2012	Andrea Urška	<p><b><u>DEFINITIVE TESTS</u></b></p> <ul style="list-style-type: none"> <li>→ Wave H2T115G2EF1C4</li> <li>→ Wave H2T115G2FF1C4</li> <li>→ Wave H2T115G5AF1C4</li> <li>→ Wave H2T115G5BF1C4</li> <li>→ Wave H2T115G5CF1C4</li> <li>→ Wave H2T115G5DF1C4</li> <li>→ Wave H2T115G5EF1C4</li> <li>→ Wave H2T115G5FF1C4</li> <li>→ Wave H2T115G2AF1C5</li> <li>→ Wave H2T115G2BF1C5</li> </ul>	Performed with a single calibration there are not significant errors.
April 26, 2012	Andrea Urška	<p><b><u>DEFINITIVE TESTS</u></b></p> <ul style="list-style-type: none"> <li>→ Wave H2T115G2CF1C5</li> <li>→ Wave H2T115G2DF1C5</li> <li>→ Wave H2T115G2EF1C5</li> </ul>	Performed with a single calibration there are not significant errors.

		<p>→ Wave H2T115G2FF1C5</p> <p>→ Wave H2T115G5AF1C5</p> <p>→ Wave H2T115G5BF1C5</p> <p>→ Wave H2T115G5CF1C5</p> <p>→ Wave H2T115G5DF1C5</p> <p>→ Wave H2T115G5EF1C5</p> <p>→ Wave H2T115G5FF1C5</p> <p>→ Wave H1T125G2AF1C5</p> <p>→ Wave H1T125G2BF1C5</p>	
<p><b>April 27, 2012</b></p>	<p>Andrea</p>	<p><b><u>DEFINITIVE TESTS</u></b></p> <p>→ Wave H1T125G2CF1C5</p> <p>→ Wave H1T125G5AF1C5</p> <p>→ Wave H1T125G5BF1C5</p> <p>→ Wave H1T125G5CF1C5</p> <p>→ Wave H1T105G2AF1C5</p> <p>→ Wave H1T105G2BF1C5</p> <p>→ Wave H1T105G2CF1C5</p> <p>→ Wave H1T105G5AF1C5</p> <p>→ Wave H1T105G5BF1C5</p> <p>→ Wave H1T105G5CF1C5</p> <p>→ Wave H1T85G2AF1C5</p>	<p>Performed with a single calibration there are not significant errors.</p>
<p><b>May 02, 2012</b></p>	<p>Andrea Urška</p>	<p><b><u>DEFINITIVE TESTS</u></b></p> <p>→ Wave H1T85G2BF1C5</p> <p>→ Wave H1T85G2CF1C5</p> <p>→ Wave H1T85G5AF1C5</p> <p>→ Wave H1T85G5BF1C5</p> <p>→ Wave H1T85G5CF1C5</p>	<p>Performed with a single calibration there are not significant errors.</p>

**Appendix E: Example of a daily report**

An example of a daily laboratory report of the day April 20, 2012 is shown.

**REPORT -- April 20, 2012**

Level F1 Configuration C0

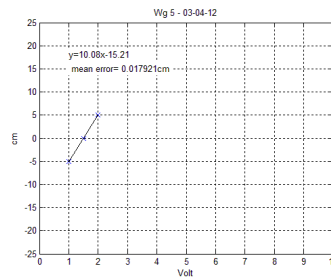
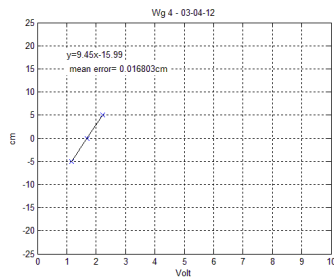
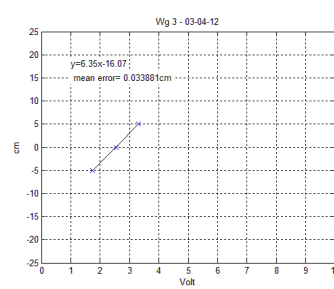
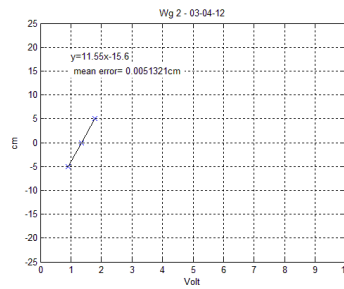
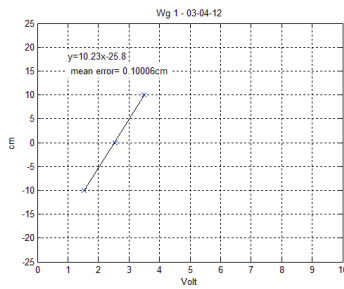
Depth at the blade with the pump off: 55.50 cm (15.2 cm at nonius)

Report of the calibration coefficients lines for the five wave gauges used in the wave flume:

Table 1: Calibration Parameters for each wave gauge [cm]=[Volt]A+B

Position	A [cm/volt]	B [cm]	Error [cm]
1	10.2337	-25.8	0.1
2	11.5473	-15.6	0.01
3	6.3527	-16.07	0.03
4	9.4516	-15.99	0.02
5	10.0804	-15.21	0.02

Hereinafter the graphs of each WG daily calibration are reported:



## Water levels in the wave flume

WAVE CODE	REPETITION	LEVEL	CONFIG.	READ WITH HYDROMETRIC TIP AT THE BLADE [cm]	VOLUME OVERTOPPING [liters]
H1T85G2	A	F1	C0	14.4	0.340
H1T85G2	B	F1	C0	14.4	0.300
H1T85G2	C	F1	C0	14.4	0.375
H1T105G2	A	F1	C0	14.4	1.440
H1T105G2	B	F1	C0	14.4	0.650
H1T105G2	C	F1	C0	14.4	0.710

### Acquisition made by back blade and generator on, for wave H1T85G2A $H_{m0}=12.0$ cm $T=1.2$ s $\gamma=2$ (duration 20 min)

Table 3: Characteristic Wave Parameters measured by each relative WG from the wave attack

Date	Wave	Rep.	Level	Structure	WG	Zero Level [cm]	Stand. Dev. [cm]	$H_{m0}$ [cm]	$T_p$ [sec]	$T_{m10}$ [sec]	$T_{m01}$ [sec]	Mean Level [cm]	$H_{1/3}$ [cm]	$H_{max}$ [cm]	$H_m$ [cm]	$T_{1/3}$ [s]	$T_m$ [s]	Number Of Zero Crossing waves
04/04/2012	H1T85G2	A	F1	C0	1	1.24	0.01	12.96	1.3	1.2	1.1	-0.20	12.90	20.51	8.30	1.2	1.1	1087
04/04/2012	H1T85G2	A	F1	C0	2	0.72	0.02	10.61	1.3	1.4	1.1	-0.07	11.00	16.36	7.12	1.3	1.2	1008
04/04/2012	H1T85G2	A	F1	C0	3	0.76	0.02	10.45	1.3	1.5	1.1	-0.09	10.80	15.97	7.02	1.3	1.2	1003
04/04/2012	H1T85G2	A	F1	C0	4	0.83	0.02	10.46	1.2	1.5	1.1	-0.06	10.60	17.62	6.93	1.3	1.2	1017
04/04/2012	H1T85G2	A	F1	C0	5	0.79	0.03	10.33	1.3	1.5	1.1	-0.08	10.60	15.40	6.97	1.3	1.2	1004

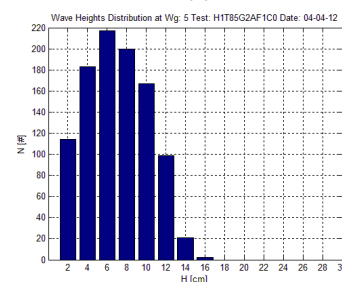
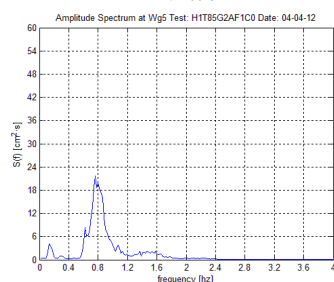
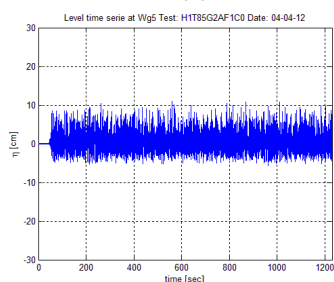
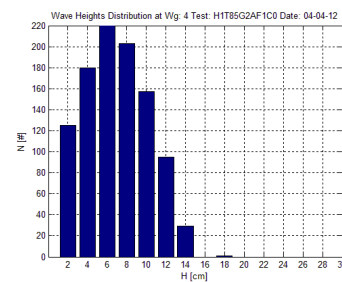
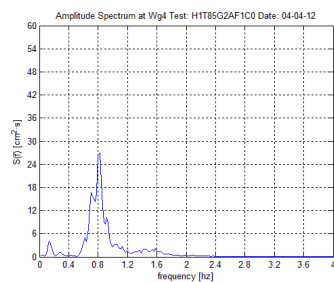
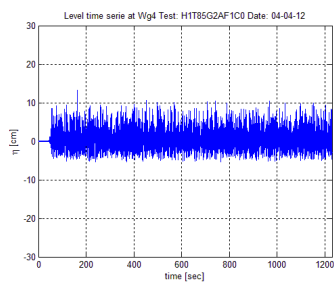
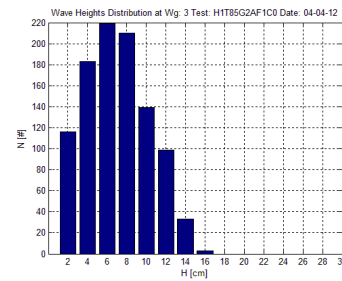
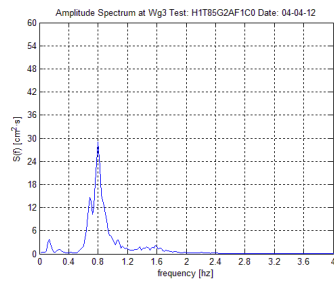
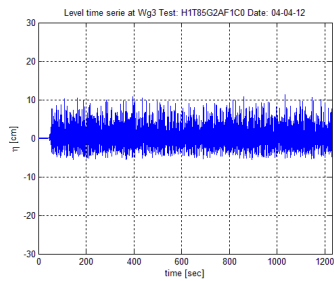
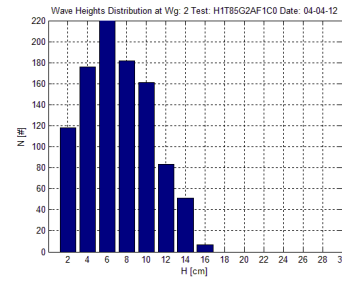
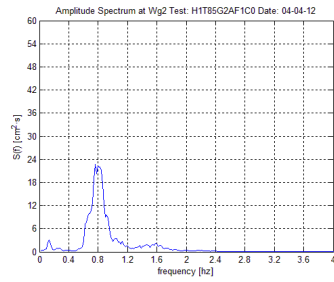
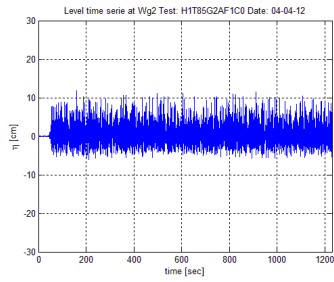
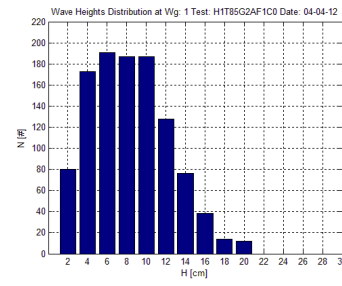
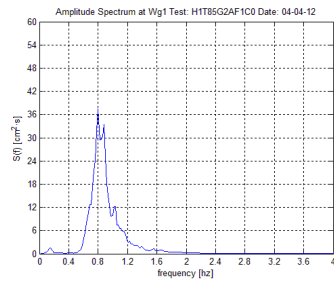
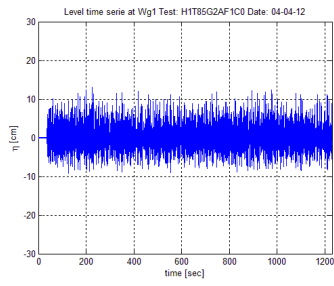
\*\* These values are computed by using the 30s long measurements before the activation of the wave maker.

Table 4: Reflection analysis according to Godo and Suzuki (1976)

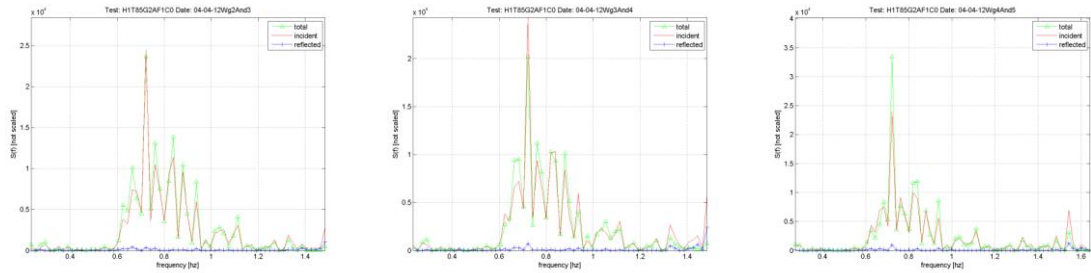
$H_i$ (2-3) [cm]	$H_r$ (2-3) [cm]	$K_r$ (2-3) [cm]	$H_i$ (3-4) [cm]	$H_r$ (3-4) [cm]	$K_r$ (3-4) [cm]	$H_i$ (4-5) [cm]	$H_r$ (4-5) [cm]	$K_r$ (4-5) [cm]
10.44	2.15	0.21	10.32	2.48	0.24	10.32	2.35	0.23

Hereinafter graphs for each WG are reported in terms of:

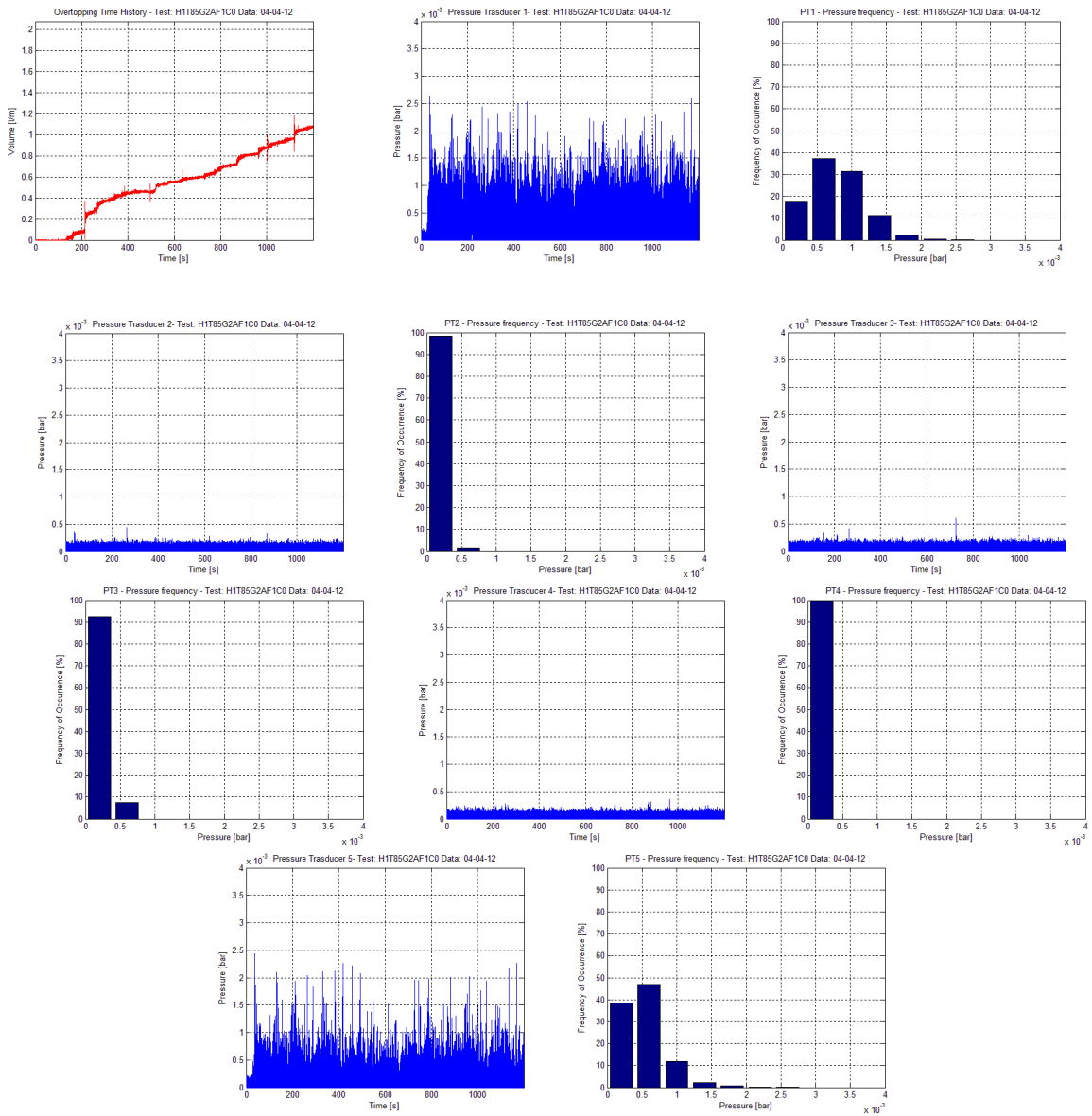
- i) Level time series
- ii) Spectrum in frequency
- iii) Zero crossing distribution of the wave heights



Hereinafter graphs of each reflection analysis after Goda and Suzuki (1976) are reported (See Table 4):



Hereinafter graphs of overtopping analysis obtained by the four load cells placed at the back of the wave wall and graphs of pressure analysis are reported:



## Appendix F: Matlab program for overtopping analysis

```
function [VolumeCumulato
qm]=Overtopping(LarghezzaCampionatore,TempoRiferimento,Celle,fs,Data,scala,
FileWg)
precisioneMisura=0.02; %kg
step = precisioneMisura/LarghezzaCampionatore;

%Celle=dati; %load(['..\input\' FileWg '_Celle.dat']);
VolumeCumulato=-sum(Celle(length(Celle),2:5)');
OvertoppingCumulato=-sum(Celle(:,2:5)')/LarghezzaCampionatore;
time=[0:1/fs:length(OvertoppingCumulato)/fs-1/fs];

OvertoppingCumulato_filt=OvertoppingCumulato;
intervallo=20;
for i=1:length(OvertoppingCumulato)
    if (i<=intervallo)

OvertoppingCumulato_filt(i)=mean(OvertoppingCumulato(1:i+intervallo));
        elseif i>=(length(OvertoppingCumulato)-intervallo)
            OvertoppingCumulato_filt(i)=mean(OvertoppingCumulato(i-
intervallo:length(OvertoppingCumulato)));
        else
            OvertoppingCumulato_filt(i)=mean(OvertoppingCumulato(i-
intervallo:i+intervallo));
        end
    end
end

j=1;
intervallo2=1000;
jumpIndex=[1];
for i=1+intervallo2:length(OvertoppingCumulato_filt)

    if mean(OvertoppingCumulato_filt(i-intervallo2:i))-
OvertoppingCumulato_filt(j)>step
        jumpIndex=[jumpIndex; i];
        j=i;
    else
        end
end

OvertoppingVolumes=[];

close all
plot(time,OvertoppingCumulato_filt,'-r')
hold on
plot(time(jumpIndex(1)),OvertoppingCumulato_filt(jumpIndex(1)),'ok');
for i=2:length(jumpIndex)
    plot(time(jumpIndex(i)),OvertoppingCumulato_filt(jumpIndex(i)),'ok');
    OvertoppingVolumes(i-1)=OvertoppingCumulato_filt(jumpIndex(i))-
OvertoppingCumulato_filt(jumpIndex(i-1));
end

%qm: mean discharge [l/s/m]
qm=OvertoppingCumulato(length(OvertoppingCumulato))/TempoRiferimento;
```

```

title(['Overtopping Time History - Test: ' FileWg ' Data: ' Data]);
xlabel(['Time [s]']);
ylabel(['Volume [l/m]']);
axis([0 time(length(time)) 0
OvertoppingCumulato(length(OvertoppingCumulato))+1]);
grid on;
saveas(gcf,['..\OutPut\Figure\' FileWg '-Overtopping.bmp']);
hold off;
close all;

plot(time(jumpIndex(2:length(jumpIndex))), OvertoppingVolumes, '.');
title(['Wave-by-Wave Overtopping Volumes - Test: ' FileWg ' Data: ' Data]);
xlabel(['Time [s]']);
ylabel(['Volume [l/m]']);
axis([0 time(length(time)) 0 3]);
grid on;
saveas(gcf,['..\OutPut\Figure\' FileWg '-WaveBywaveOvertopping.bmp']);
hold off;
close all

M=[0.01:3/300:3];
[pluto MM]=hist(OvertoppingVolumes,M);
bar(MM,pluto/sum(pluto)*100);
title(['Overtopping Volumes Distribution Test: ' FileWg ' Date: ' Data]);
grid on
axis([0 3 0 100]);
xlabel('Volumes [l/m]');
ylabel('n/N [%]');
saveas(gcf,['..\OutPut\Figure\' FileWg '-
OvertoppingVolumesDistribution.bmp']);
close all

risultati=fopen(['..\OutPut\' FileWg 'Overtopping.dat'],'w');
fprintf(risultati, ' %7.4f ',qm);
fprintf(risultati, ' %%q_m [l/s/m]\r\n ')
for i=1:length(OvertoppingVolumes)
    fprintf(risultati, ' %6.3f ',OvertoppingVolumes(i));
    fprintf(risultati, ['%%Volume N. ' num2str(i) ' [l/m]\r\n ']);
end
fclose(risultati);

```

## Appendix G: Matlab program for pressure analysis

```
function []=Trasduttori(Trasd,fs,Data,FileWg)

%Trasd=load(['..\Input\' FileWg '_Trasd.dat']);
Trasd(:,1)=[];
[n m]=size(Trasd);
time=[0:1:n-1]/fs;
Pzero=mean(Trasd(1:30*fs,:));

for i=1:m
    Trasd(:,i)=Trasd(:,i)-Pzero(i);

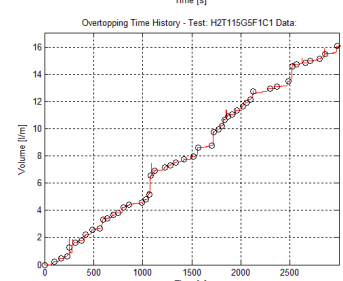
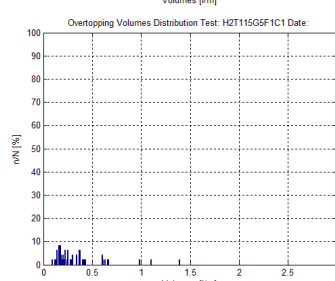
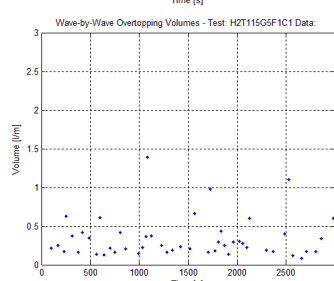
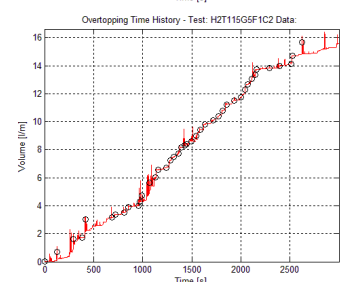
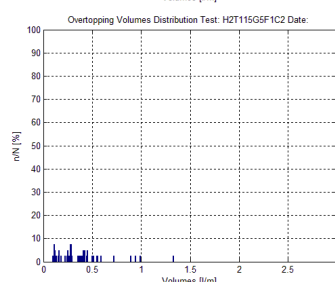
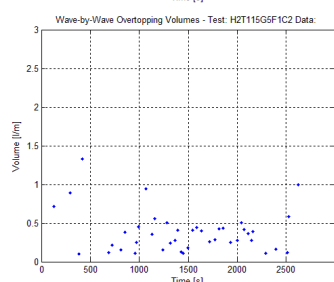
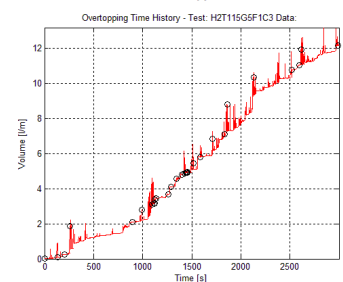
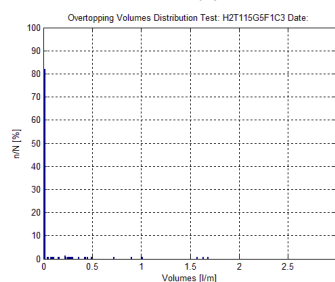
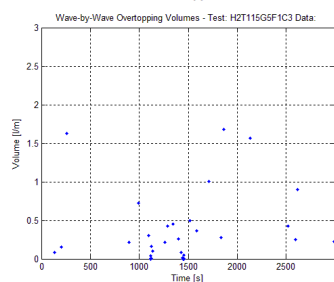
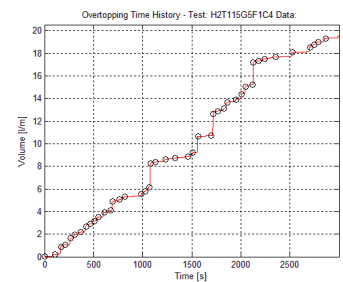
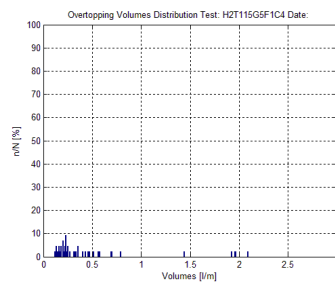
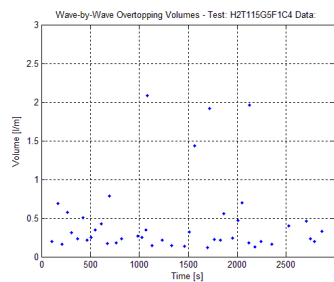
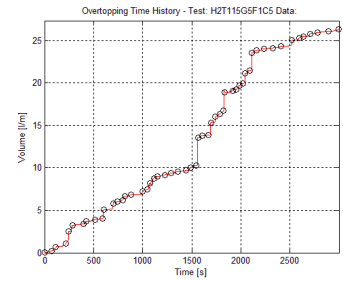
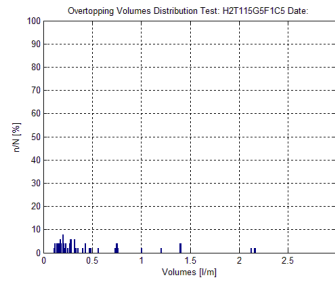
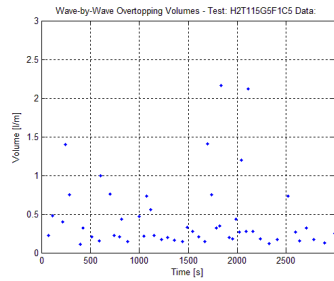
    plot(time, Trasd(:,i));
    title(['Pressure Transducer ' num2str(i) '- Test: ' FileWg ' Data: '
Data ], grid on;
    xlabel(['Time [s]']);
    ylabel(['Pressure [bar]']);
    axis([0 time(length(time)) 0 0.0082]);
    saveas(gcf,['..\OutPut\Figure\' FileWg '-Trasduttore' num2str(i)
'.bmp']);

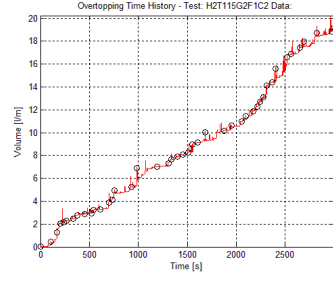
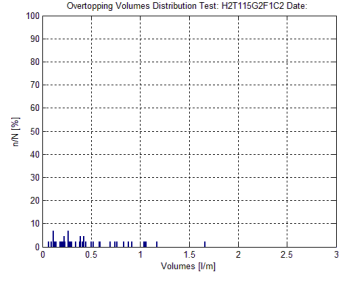
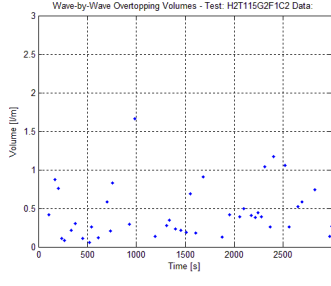
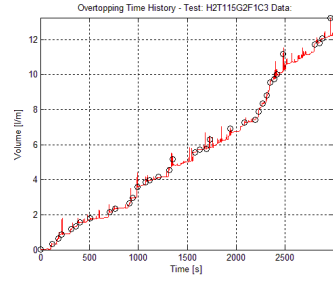
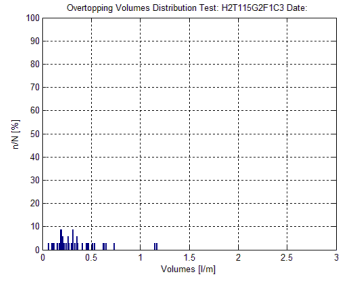
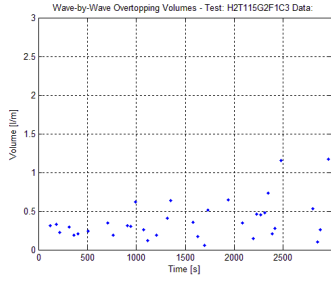
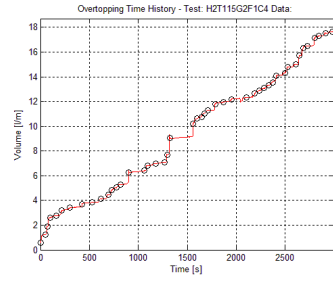
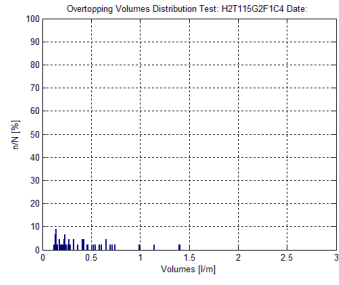
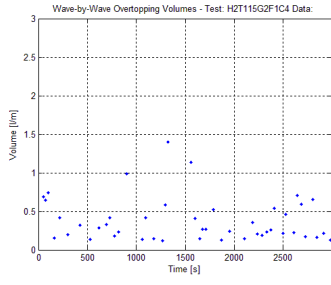
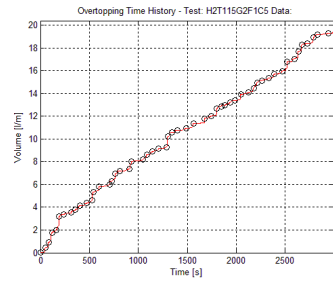
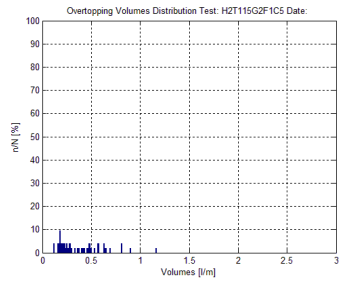
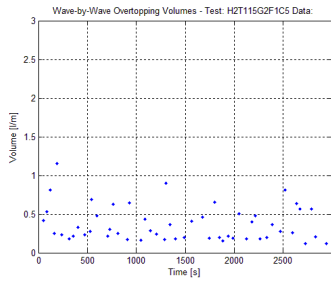
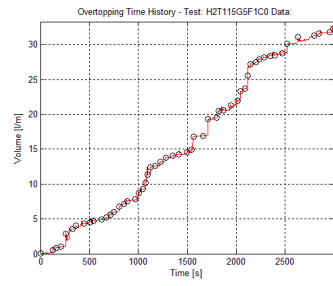
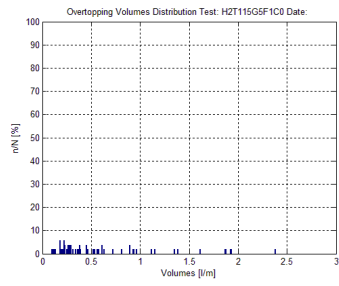
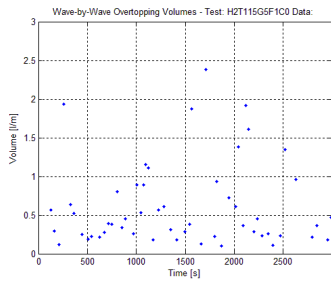
    I=find(Trasd(:,i)>0.0002); %tolgo il rumore
    X=[0.0004:0.0004:0.0082];
    [N1 XX]=hist(Trasd(I,i),X);
    Freq_1=N1/sum(N1)*100;
    bar(X,Freq_1);
    title(['PT' num2str(i) ' - Pressure frequency - Test: ' FileWg ' Data:
' Data ]);
    xlabel('Pressure [bar]');
    ylabel ('Frequency of Occurrence [%]')
    axis([0 0.0082 0 100]), grid on
    saveas(gcf,['..\OutPut\Figure\' FileWg '-PressureFrequency-PT'
num2str(i) '.bmp']);

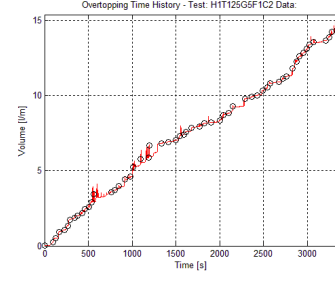
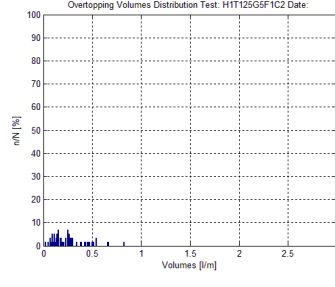
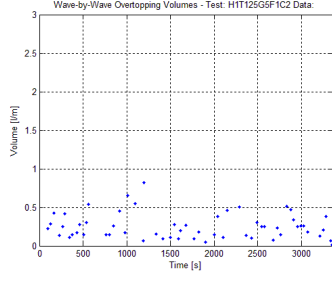
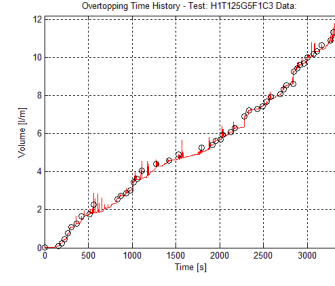
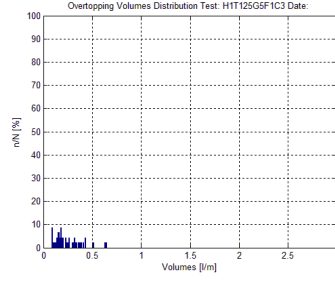
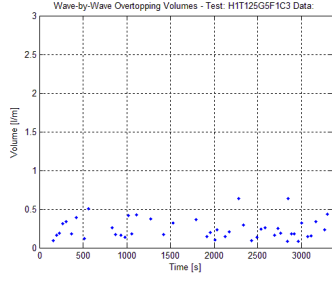
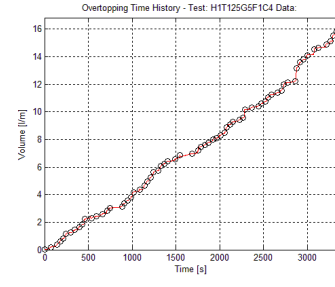
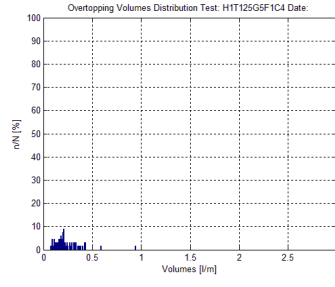
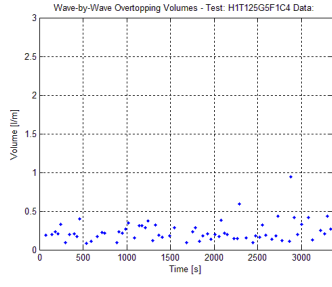
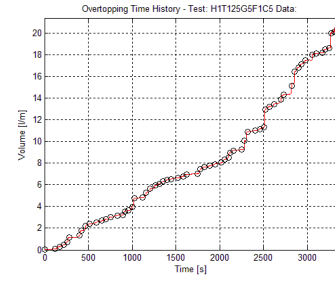
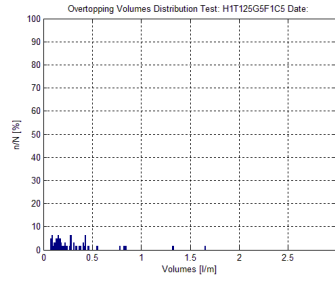
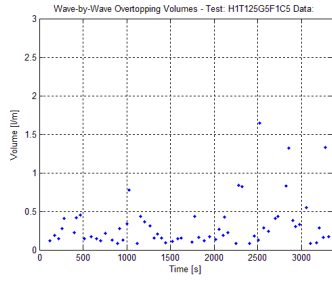
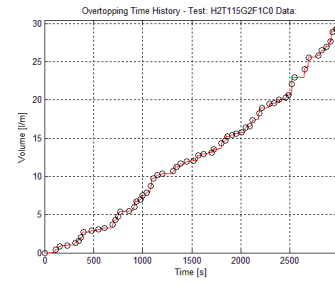
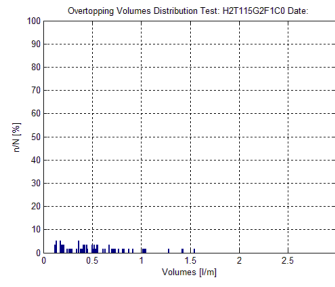
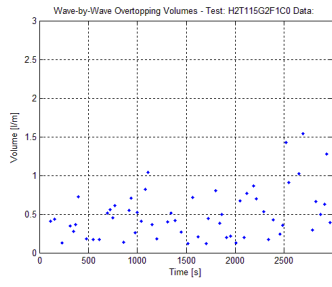
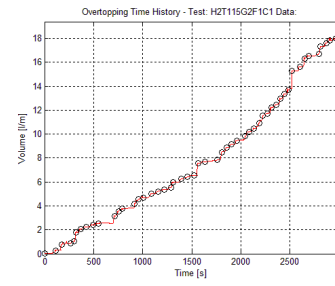
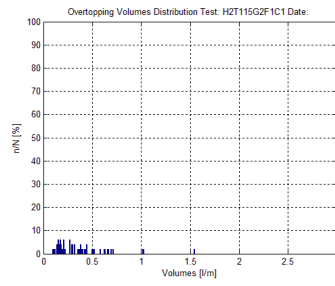
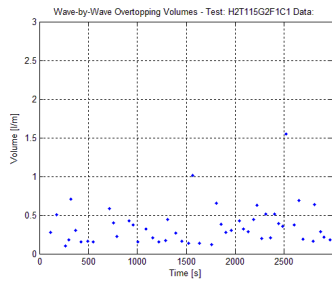
end
```

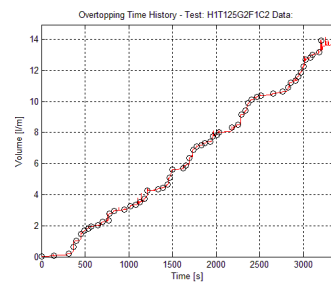
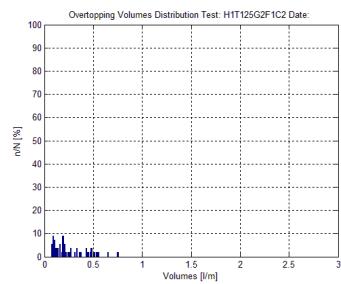
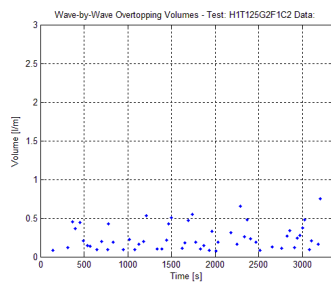
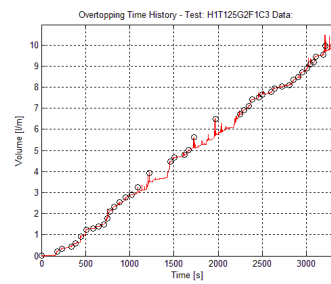
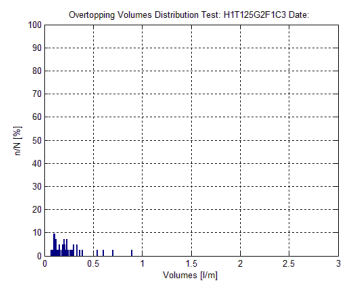
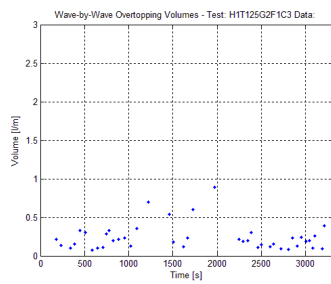
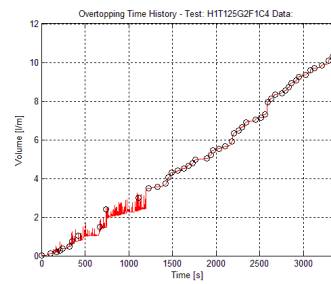
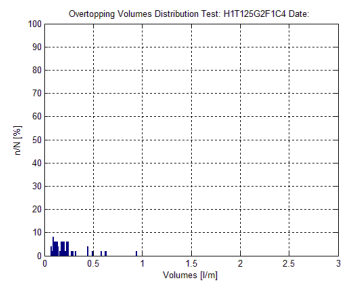
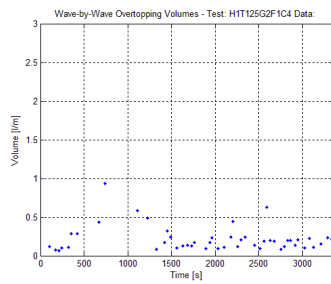
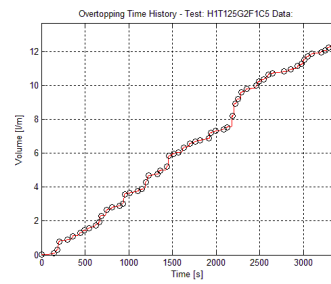
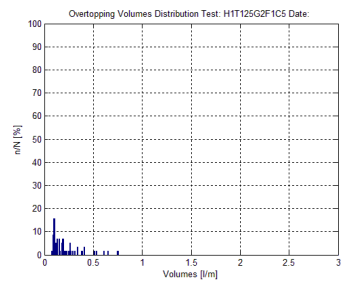
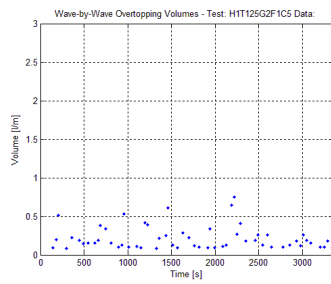
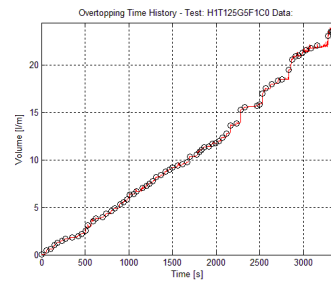
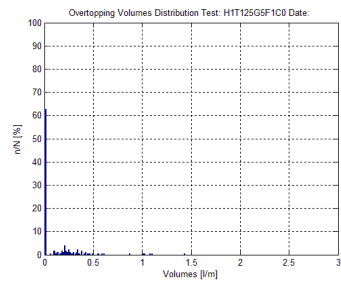
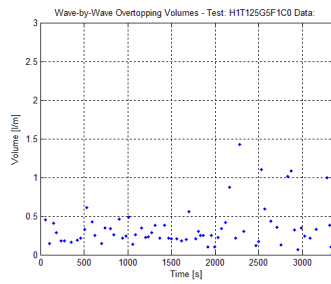
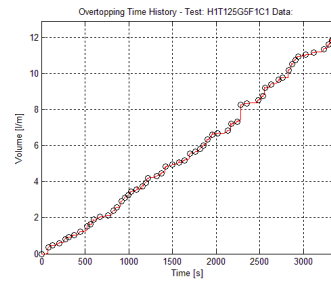
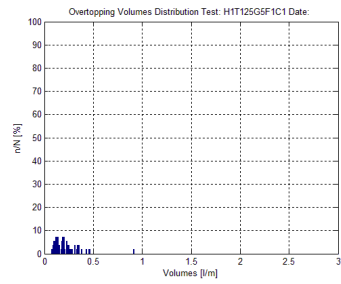
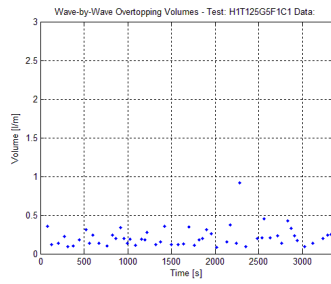
## Appendix H: Program output

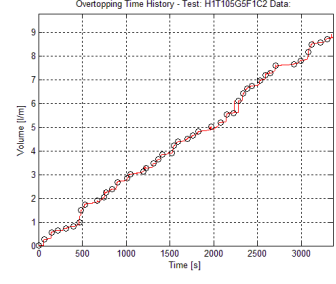
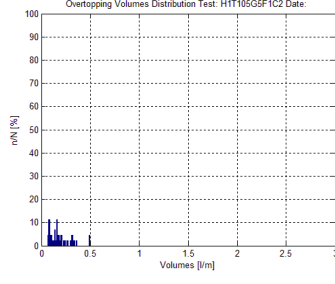
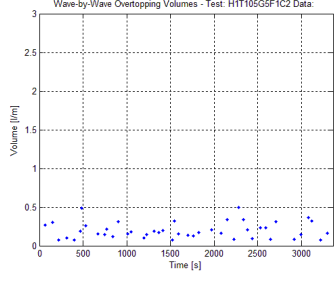
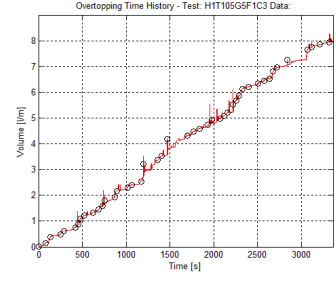
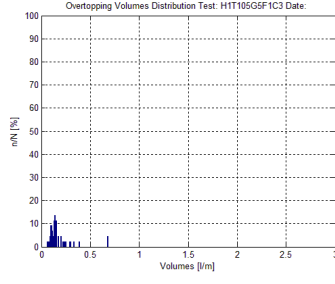
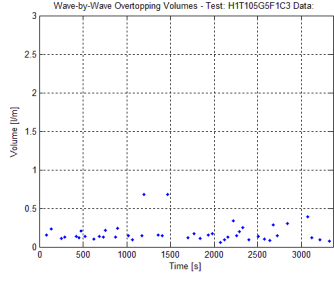
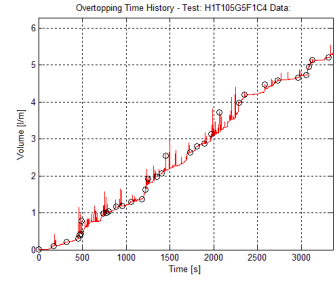
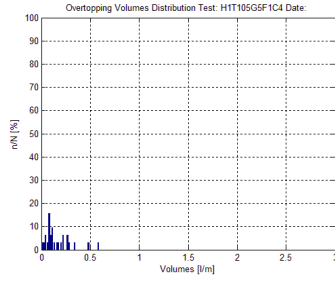
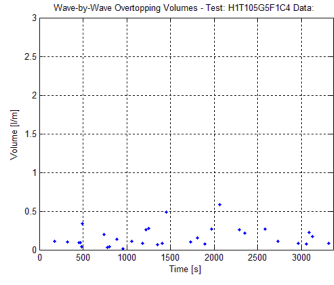
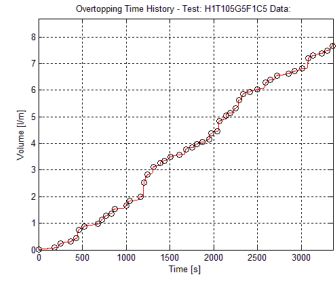
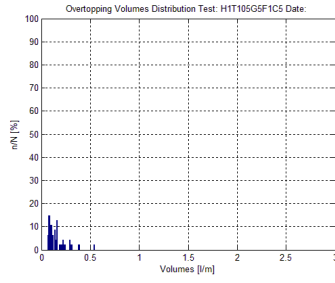
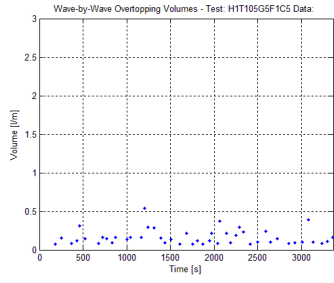
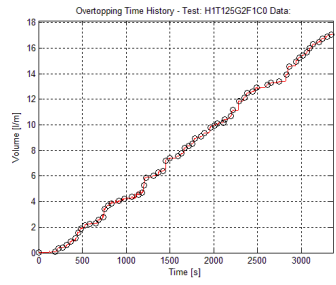
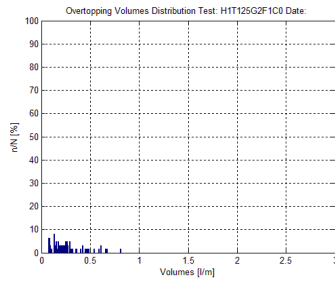
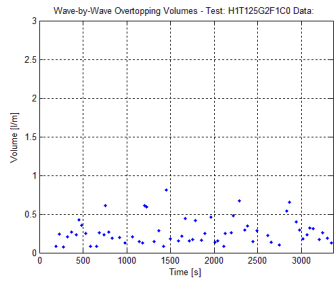
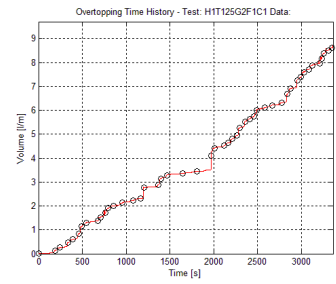
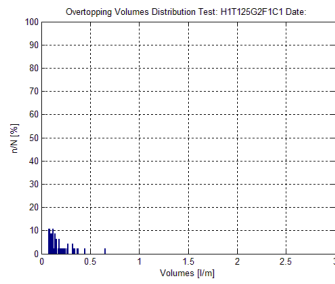
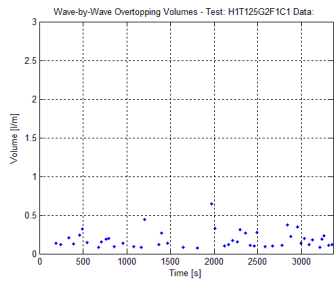
### Appendix H.1: Output graphs for overtopping analysis

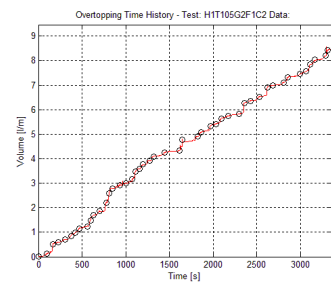
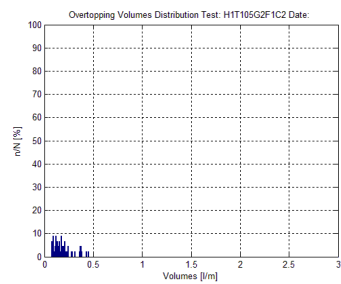
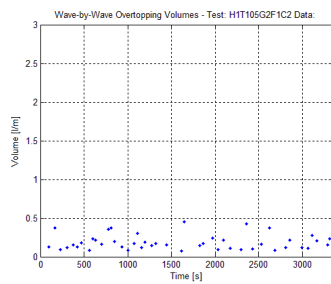
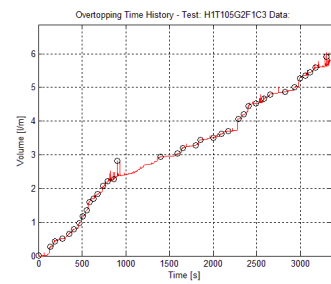
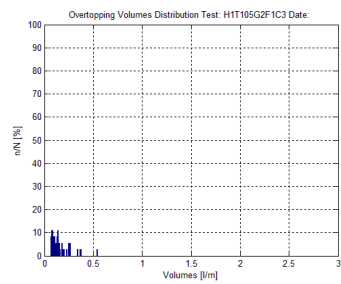
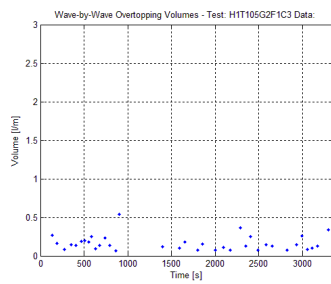
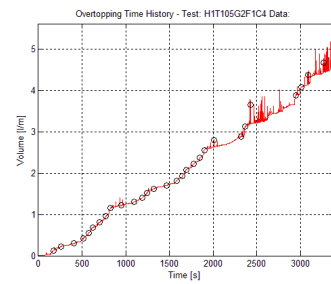
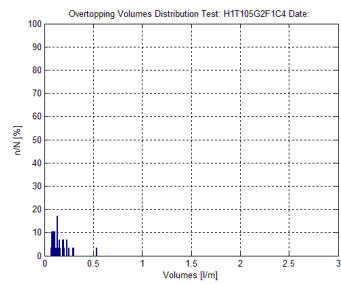
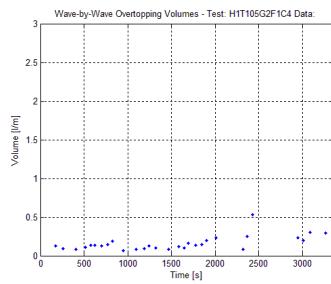
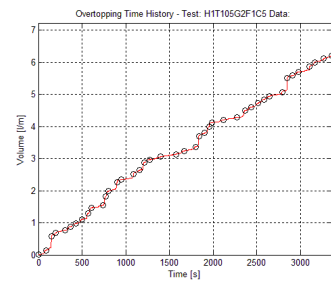
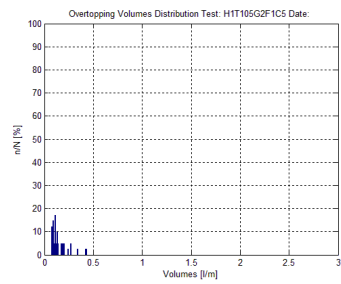
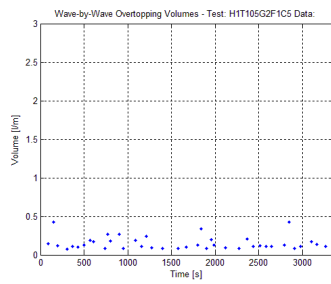
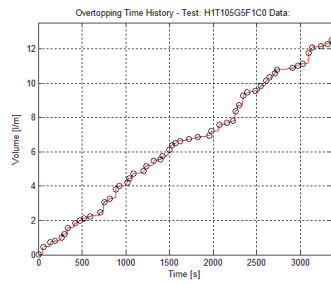
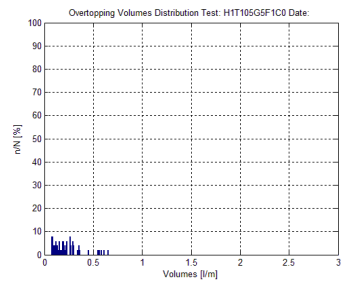
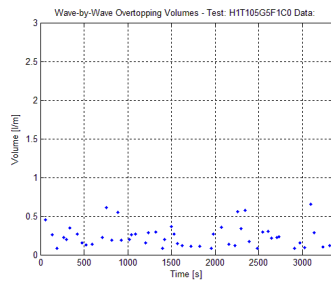
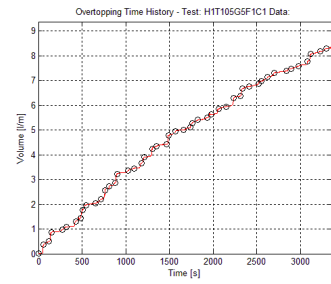
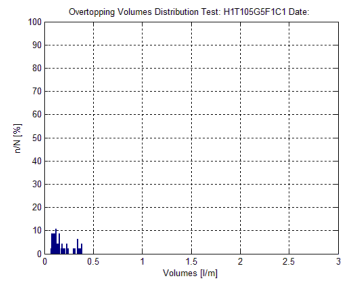
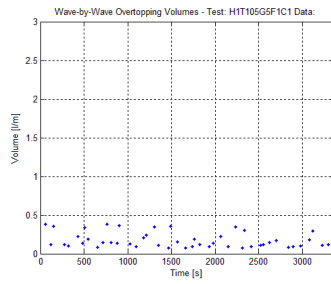


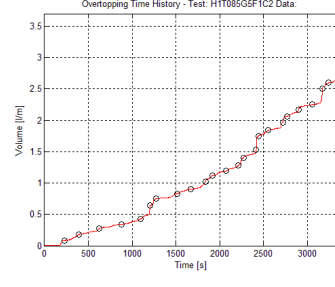
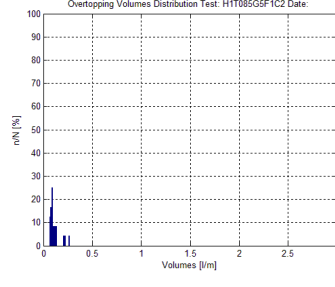
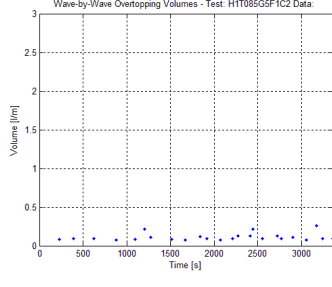
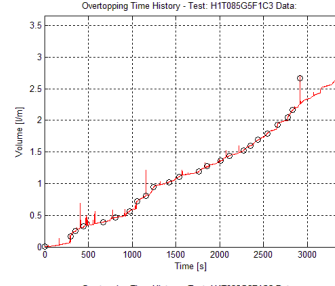
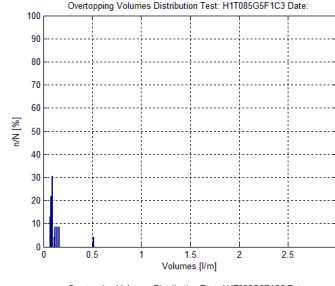
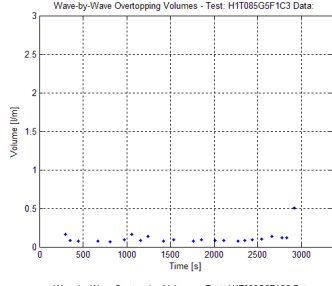
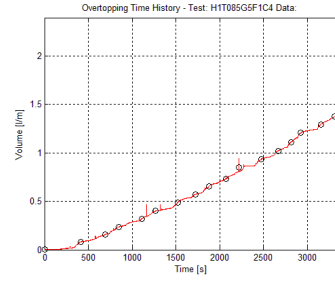
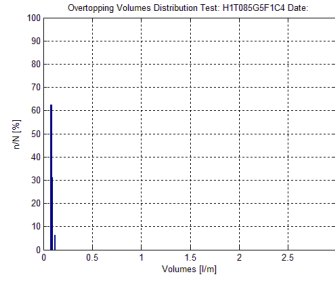
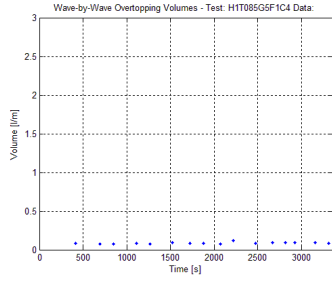
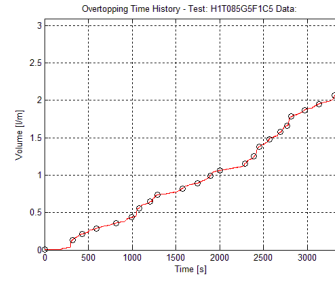
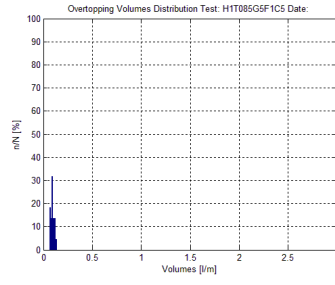
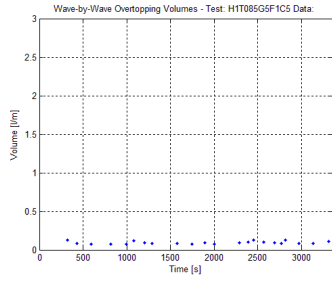
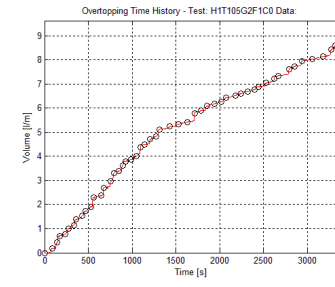
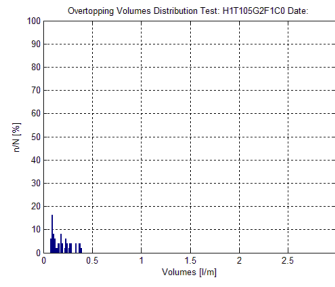
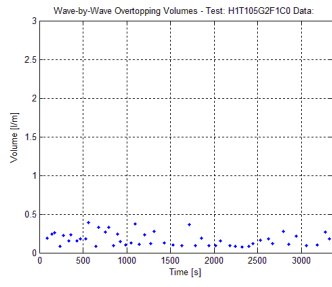
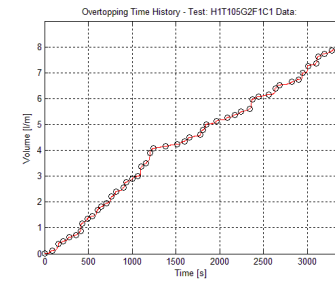
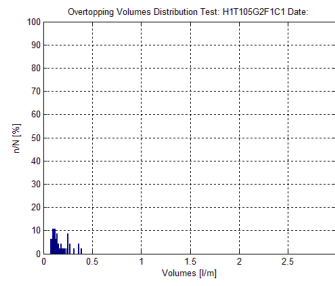
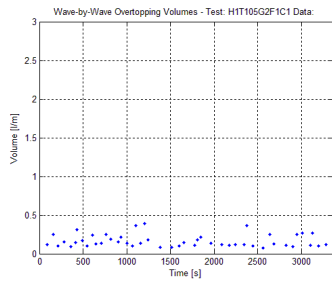


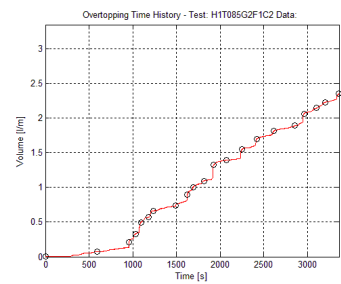
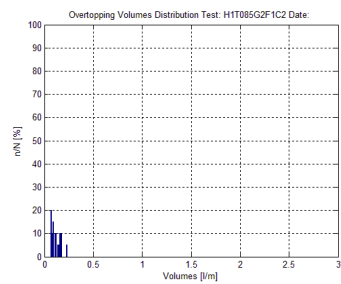
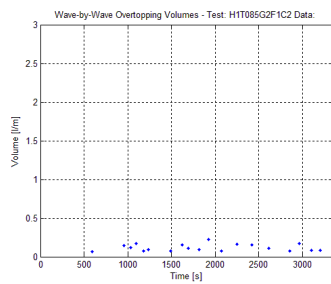
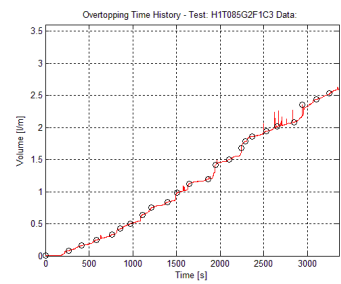
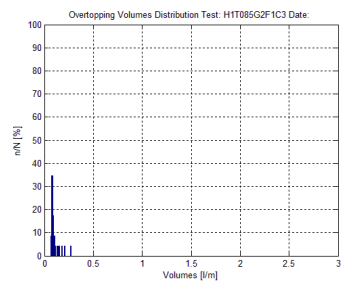
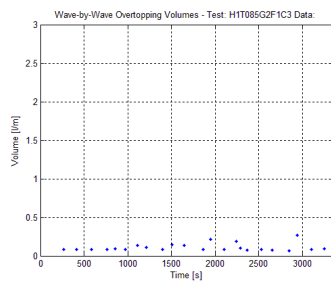
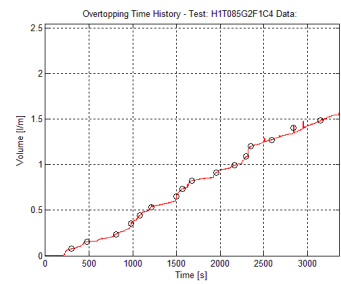
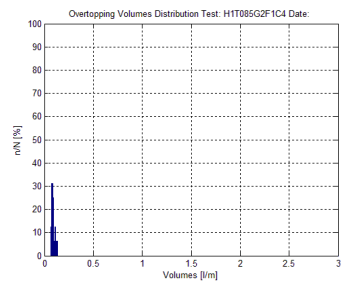
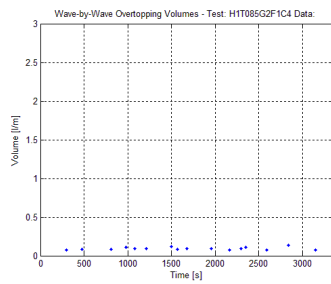
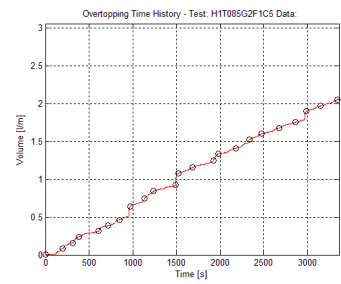
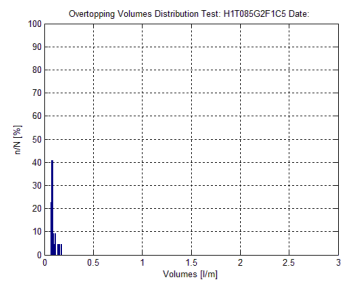
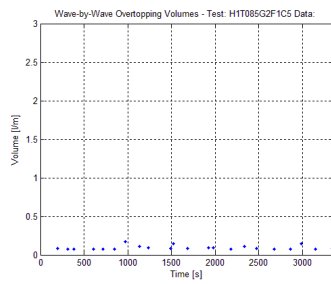
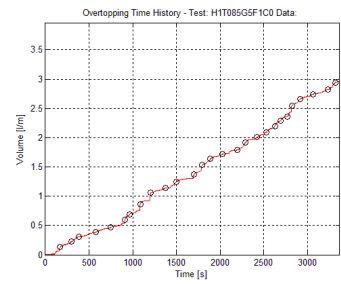
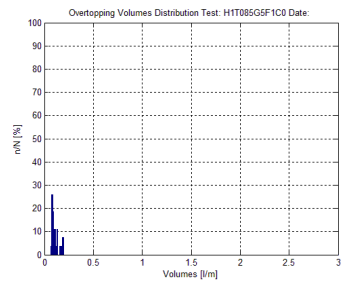
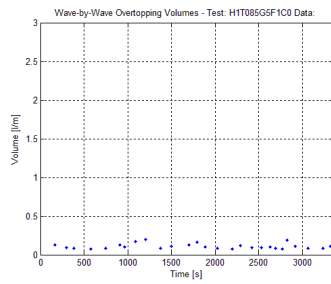
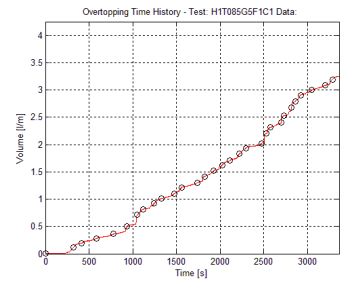
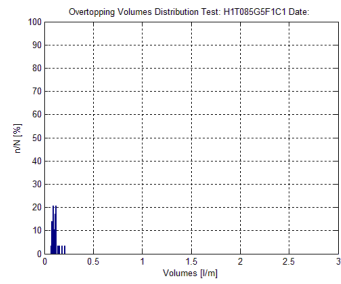
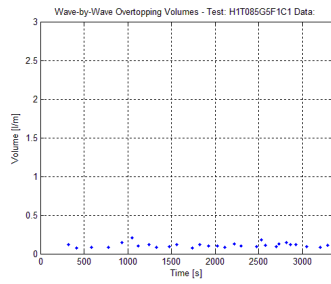












## Appendix H.2: Output graphs for pressure analysis

Hereinafter graphs of pressure distribution for pressure transducer 1 are reported. Graphs of pressure distribution for the other transducers are available on CD in the repository of UL FGG.

